FACULTY OF ENGINEERING
AND ARCHITECTURE

Alkali Activated Lightweight Aggregate as Bacterial Protector in Manufacturing Self-Healing Concrete

Puput Risdanareni

Doctoral dissertation submitted to obtain the academic degree of
Doctor of Civil Engineering

Supervisors
Prof. Nele De Belie, PhD* - Prof. Jianyun Wang, PhD**

* Department of Structural Engineering and Building Materials
Faculty of Engineering and Architecture, Ghent University

** Department of Civil Engineering
Faculty of Human Settlements and Civil Engineering, Xi'an Jiaotong University, China

October 2021

GHENT
UNIVERSITY

FACULTY OF ENGINEERING
AND ARCHITECTURE

Alkali Activated Lightweight Aggregate as Bacterial Protector in Manufacturing Self-Healing Concrete

Puput Risdanareni

Doctoral dissertation submitted to obtain the academic degree of
Doctor of Civil Engineering

Supervisors
Prof. Nele De Belie, PhD* - Prof. Jianyun Wang, PhD**

* Department of Structural Engineering and Building Materials
Faculty of Engineering and Architecture, Ghent University

** Department of Civil Engineering
Faculty of Human Settlements and Civil Engineering, Xi’an Jiaotong University, China

October 2021

GHENT
UNIVERSITY

ISBN 978-94-6355-531-9
NUR 955
Wettelijk depot: D/2021/10.500/79

Members of the Examination Board

Chair

Prof. Em. Luc Taerwe, PhD, Ghent University

Other members entitled to vote

Prof. Zeynep Basaran Bundur, PhD, Özyeğin Üniversitesi, Turkey
Prof. Nico Boon, PhD, Ghent University
Prof. Steffen Grünewald, PhD, Ghent University
Yury Villagran Zaccardi, PhD, Ghent University
Prof. Qingliang Yu, PhD, Technische Universiteit Eindhoven, the Netherlands

Supervisors

Prof. Nele De Belie, PhD, Ghent University
Prof. Jianyun Wang, PhD, Xi'an Jiaotong University, China

Acknowledgment

It felt like just yesterday when I arrived in Ghent, and now four years after that day, it comes to the day when I have to write my dissertation acknowledgment, an indication that soon I have to leave this rainy city. This PhD is indeed not an easy journey for me. But with the company and encouragement from my colleagues, friends and family, finally I can reach the finish line of this marathon journey. I might have thanked you many times during my PhD, yet I still want to express my sincere acknowledgment to all of you once more.

First of all, I would like to express my great thanks to my main supervisor Prof. Dr. Ir. Nele De Belie, who allowed me to join her excellent concrete and environmental research group. I still profoundly remember how grateful and happy I was when you accepted me as your student. Your letter of acceptance for sure changed my life at that moment. During my PhD, I also have learned a lot from you, not only from the scientific knowledge, but also from how to manage the research group and the laboratory. Thank you for always being patient in helping and guiding me whenever I needed your suggestions, even though you had a very busy schedule.

I also would like to thanks my co-supervisor / my best buddy, Prof. Dr. Ir Jianyun Wang. Thank you for patiently introducing me to the world of microbiology Jianyun. Even though we only worked in the same lab for 1 year, you were always available to be reached via WeChat. Thank you for the proof that you can be friends with your PhD promotor Jianyun.

My great appreciation also goes to the chair and the examination committee Prof. Em. Luc Taerwe, PhD (Ghent University), Prof. Zeynep Basaran Bundur, PhD, Özyeğin University (ÖzÜ, Turkey), Prof. Nico Boon, PhD, (Ghent University), Prof. Steffen Grünewald, PhD (Ghent University), Yury Villagran Zaccardi, PhD (Ghent University) and Prof. Qingliang Yu, PhD, (Eindhoven University of Technology, The Netherlands) for their valuable comments and suggestions which significantly improved the quality of this PhD dissertation. I would also like to send my special gratitude to Prof. Nico Boon for allowing me to work in CMET, giving me suggestions and guiding me during my PhD as if he were my supervisor.

A big word of thanks also goes to all the technicians of Magnel-Vandepitte Laboratory and CMET. For the rulers of the concrete room, Tom Stulemeijer, Nathan Lampens, and Stefan De Bock, making concrete will be far from fun without you guys. For Mr. full with ideas Dieter Hillewaere, thank you for making all the devices that I required come true. For Tommy and Brenda, who patiently arranged all my last minutes' work orders, thank you. I also would like to thank Sandra De Buck, Peter Lampaert, Peter Van den bussche, and the rest of the technicians in Magnel-Vandepitte Laboratory that I might have forgotten to mention. I also would like to thank Greet van de Velde, Sarah Steenbeke, Jana de Bodt, and Mike Taghon from CMET for all of their help during my stay in CMET.

My special thank also goes to Dr. Katrin Schollbach together with the research group of Prof. dr. ir. H.J.H. (Jos) Brouwers of TU Eindhoven that guided me during my research stay in TU Eindhoven in 2017.

Words of thanks also go to the secretary office of Magnel-Vandepitte Laboratory and CMET : Marijke Reuners, Christel Malfait, Jens Mortier, and Regine Haspeslagh, who always helped me deal with all the administrative work in both labs.

My specials thanks are extended to my office mates: Philip, Jianyun (again), Yu, Judy, Vanessa, Yasmina, and Pardis. I only have very good memories in that office, guys. Thanks for helping me to improve my crappy English, laughing at my stupidity, and understanding my crazy ideas. You are the best office mates I ever had.

Next, I would like to thank all my colleagues and friends in Magnel-Vandepitte lab: Kim, Natalia, Bjorn, Yury (again), Aneeta, Adelaide, Romy, Tim, Ali, Pithchai, Paula, Vincent, Zhiyuan, Didier, Laurence, Davide, Xuejiao, Jingbin, Franco, Dulce, Mert, Paula, Juan Manuel, Qiu, Kai, Mahzad, Chizya, Robin, Khadija, Metwally, Dengwu, Yaxin, Jolien, Carolina, Luiza, Weixi, Beibei, Manu, Ivana, Saeid, Shahryar, Rahul, Yubo and all the people that I might forget to mention here. Thanks for all the random chats we had during lunchtime downstairs, when we were busy doing all the lab experiments and our lovely activities outside the lab. I am going to miss all those moments, guys.

I also want to thank my CMET buddies, who made my time dealing with my lovely bacteria more fun: Laurenz, Funda, Myrsini, Antonin, Jose, Stanley, Taylor, Xiaona, and Barbara.

I also would like to thank Fanny Schepens and Isabelle Mrozowski, who were always helping me during my wonderful stay at OBSG. For sure, OBSG has successfully become a home far away from home for the International students in Ghent.

Ucapan terima kasih juga saya tujukan untuk para tetua, sahabat dan teman-teman PPI Ghent : Wa Ann, Wa Francis, Tante Lanny, Om Jul, Mami Lely, Pak Baktiar, mbak Oka sekeluarga, mami Fitri, mbak Ani, mas Radit sekeluarga, mbak Angga, Sastri & Arfah, Ratna, Annisa, Raka, Fathya, Nonik, Ojan, Fahreza, Hary, mbak Resi sekeluarga, mbak bro Agustina, mbak

Merry, mas Edo, mas Dimas, pak Bowo, Budhe Jenjang, Bu Nurul, Bu Uci, mbak Susan, Loka, mbak Anik, mbak Ayun sekeluarga, power puff girls beserta tuan muda (Nafi, Selly, Nabila, Devin), Irdanto, Ipit, Listia, Obby, Kevin dan semua teman PPI yang tidak bisa saya sebutkan namanya satu persatu, TERIMA KASIH sudah menjadi keluarga bagi saya selama 4 tahun ini.

Teruntuk Upi, Jeroen, Aurelia dan Laurentia di Hoofdorp, terima kasih sudah menjadi 'rumah' bagi ku selama 4 tahun ini.

Teruntuk Nuril dan mbak Astri, rekan sejawat yang selalu mendukung dan menerima segala keanehan ku, Suwun buk.

Teruntuk mbak terbaik di dunia mbak Evi, adik paling menggemaskan Mita aka Cipooh, mas ipar paling baik hati Mas Fajar dan keponakan kesayangan Adam, terima kasih tuk selalu menjadi sandaran dalam hidupku.

Yang terakhir, teruntuk kedua orang tua saya Bapak Tumardi dan Ibu Sri Sudjiati, yang tak hentinya berdoa dan mendukung semua keputusan penting yang saya buat dalam hidup, yang selalu mengalah dan tiada habisnya berkorban untuk kesuksesan putri-putri nya, gelar doctor ini saya persembahkan untuk bapak dan ibuk. Terima kasih pak buk, semoga Puput selalu bisa membuat bapak dan ibuk bangga.

Puput
Ghent, 30th September, 2021

Notation Index

LWA	Lightweight Aggregate
EC	Expanded Clay
FA	Fly Ash
XRF	X-ray Fluorescence
QXRD	Quantitative X-Ray Difraction
CR	Crushing Resistance
Lusi	Sidoarjo Volcanic Mud
MSWI BA	Municipal Solid Waste Incenerator
CCP	Coal combustion Product
ρ_a	Apparent density
ρ_{OD}	Oven dried density
ρ_{SSD}	Water saturated surface-dry density
WA_{24}	Water absorption over 24 hours
MIP	Mercury Intrusion Porosimetry
BSE	Back Scattered Electron
FESEM	Field Emission Scanning Electron Microscope
EDS	Energy Dispersive Spectroscopy
PSD	Particle Size Distribution
d_{th}	Threshold pore diameters
N-A-S-H	Sodium alumino silicate
C-A-S-H	Calcium alumino silicate
ITZ	Interfacial Transition Zone
D_{nssm}	Non-steady-state migration coefficient
WA	Water Absorption
AD	Apparent Density
OP	Open Porosity
MICP	Microbially Induced Calcium Carbonate Precipitation
DU	Decomposed Urea
TAN	Total Ammonium Nitrogen
Mr	Relative Molecule Mass
BS	*Bacillus sphaericus*
B	Bacteria
N	Nutrient

NB	Nutrient + Bacteria
NBE	Nutrient + Bacteria + Encapsulation
HR	Healing Ratio
C_{wi}	Crack width intitial
C_{wf}	Crack width final
SE	Sealing Efficiency
CRFP	Carbon Reinforcement Fiber Polymer
$q_{initial}$	Water flow rate initial (g/minutes)
q_{healed}	Water flow rate healed (g/minutes)
SIL	Sodium silicate
SAL	Sodium alginate
PVA	Polyvinyl alcohol

Summary

Concrete is the most used construction material worldwide as it is strong, durable, and affordable. However, the long lifespan of concrete could decrease drastically due to the occurrence of unavoidable cracks. The presence of cracks larger than 0.3 mm in concrete structures could shorten their service life span as cracks will allow water, chloride and CO_2 to penetrate concrete and induce corrosion of the embedded steel reinforcing bars. Thus, concrete repair becomes a necessary action to prevent further damage in concrete structures when cracks occur. Unfortunately, the concrete repairing cost has been reported to be quite expensive. In Europe, the estimated repair costs could reach half of the construction budget. To mitigate these forthcoming high maintenance costs, which are expected to increase even further with increasing concrete consumption, a new material that could solve this durability issue is self-healing concrete.

Among developed self-healing techniques, bacteria-based self-healing concrete using microbially-induced calcium carbonate precipitation (MICP), was reported to provide excellent performance for healing cracks in concrete. The basic principle of this technique is that microorganisms will provide a local micro-environment with conditions that allow the precipitation of calcium carbonates that could heal the crack.

The hydration process in concrete that leads to decreasing pore sizes of the hardened material could crush the bacteria, and the high shear forces during concrete mixing could harm the bacteria inside concrete. Thus, a carrier to protect the bacteria before crack occurrence is needed. Porous aggregates appear to be attractive carriers as they are compatible with the concrete matrix and affordable. Previous research has shown that by encapsulating spores or cells of *B. sphaericus, B. cohnii, B, alkalinitrilicus*, *S. pasteurii, B. pseudofirmus, Diaphorobacter nitroreducens* and *Pseudomonas aeruginosa* into various porous aggregates, by using urea hydrolysis, denitrification or conversion of organic compound metabolic pathways, after immersion in water up to 100 days, crack widths in the range of 0.20-0.79 mm could be entirely healed. However, from an environmental point of view, common porous aggregate carriers available on the market, such as expanded clay aggregates, are not so environmentally friendly because they require a high temperature for production.

Two important properties should be met for the LWA to be suitable as a bacteria carrier. First, the LWA should have enough pores with sizes 2 to 5 times the bacteria size. It also needs to have a high porosity to allow more bacterial cells to penetrate into the pores. The second requirement is that it

needs to be strong enough to survive concrete mixing. Revisiting all the basic requirements of a porous carrier, alkali activated LWA could be a suitable bacteria protector candidate. It was reported to have high water absorption and adequate crushing resistance (Illikainen, 2017). From an environmental point of view, utilising alkali activated LWA can avoid the use of a high sintering temperature needed to produce commercial porous LWA such as expanded clay.

The first aspect to investigate in the production of alkali activated LWA is the concentration of NaOH as the primary alkali activator besides sodium silicate. Three NaOH concentrations of 4, 6, and 8 molars were tested to activate fly ash in alkali activated LWA production in the first stage. A relatively low NaOH concentration was chosen to manufacture LWA, as high NaOH concentration would speed up the chemical reaction too much, which could disturb the agglomeration process in LWA production. Based on the results when investigating the properties of fly ash-based alkali activated LWA and its resulting mortar, a NaOH concentration of 6 molars is sufficient for the LWA production. A significant decrease in the amount of macropores was obtained with a NaOH concentration of 6 molars. Moreover, the major amount of pores in this LWA was in the size range that allows bacteria to penetrate (6-15 µm). In mortar application, replacing 16% volume of fine aggregates with fly ash-based LWA activated with NaOH concentration of 6 molars (FA 6M LWA) delivered a similar strength to a mortar containing expanded clay LWA (EC LWA).

In order to screen suitable alkali activated LWAs as a bacterial protector, waste products besides fly ash such as municipal solid waste incinerator bottom ash (MSWI BA) and Sidoarjo volcanic mud (Lusi) were also employed as an alternative binder in the production of alkali activated LWA. Sodium silicate was mixed with sodium hydroxide with the concentration of 6 molars at a weight ratio of 1.5 and was used as alkali activator in the LWA production. The results show that Lusi and fly ash-based LWA meet the requirements to be employed as a bacteria carrier. Those two LWA had a water absorption of more than 20% over 24 hours with its major pores size between 6 to 10 µm. When those two novel aggregates were incorporated into the mortar with replacement rate of 16%, a comparable compressive strength to mortar containing EC LWA was achieved. Moreover, increasing the aggregate replacement rate up to 30% did not drastically decrease the properties of the resulting mortar. In contrast, with the same aggregate replacing rate, mortar containing MSWI BA suffered from expansion. A preceding treatment to remove metallic aluminium would be needed here, before using the MSWI BA for making LWA. The metallic aluminium in

MSWI BA LWA seems to be toxic to the *B. sphaericus* cells. Only limited amount of urea could be decomposed by bacteria after encapsulation into MSWI BA LWA. On the other hand, no issues occurred when bacteria were encapsulated into EC, FA 6M and Lusi 6M LWA.

By replacing 16 % of fine aggregate with FA 6M LWA in mortar production, a comparable chloride migration coefficient and capillary water uptake in the mortar were observed as for mortar containing EC LWA and for a reference mortar without LWA. Furthermore, the carbonation resistance of mortar containing FA 6M LWA was comparable to mortar containing EC LWA. A denser interfacial zone between EC LWA and FA 6M LWA with the cement paste contributed to acceptable durability performance in their resulting mortar.

In the production of bacteria-based self-healing concrete, bio-agents such as nutrients, urea, and calcium sources are needed to support the MICP process, which uses the urea hydrolysis pathway. The problem is that the yeast extract needed for bacteria spores to germinate into vegetative cells was reported to have a negative effect on the mechanical properties of the resulting mortar. This research introduced three yeast extract concentrations of 0, 2, and 5 g/l in mortar production. The results allow to recommend a yeast extract concentration of 2 g/l in mortar when the presence of yeast extract is mandatory. The compressive strength of the resulting mortar was decreased by about 16% compared to that of the reference sample. While in the sample with 5 g/l yeast extract, the compressive strength could decrease up to 50% compared to the reference sample. When vegetative cells were used as a healing agent, omitting yeast from the mortar mix is possible. The absence of yeast only decreased the workability of fresh mortar but did not disturb the casting process. Thus, no decrease in bulk density and compressive strength compared to reference mortar was observed when yeast extract was omitted from the mortar mix.

The following research phase applied FA 6M LWA and Lusi 6M LWA as vegetative cells carriers. The result show that cells inside the FA 6M LWA still survived even when cracks were fabricated at the age of 90 days. In the crack width range of 0.3-0.4 mm, the healing ratio of mortar which used FA 6M LWA as bacteria carrier, was slightly better than that when EC LWA was used. The average healing ratio in a crack width range of 0.3-0.4 mm for the FA 6M LWA sample after being subjected to wet-dry cycle curing for 30 days was 54%, while it was 47 % in the EC LWA sample. Even though the crack healing ratio at the crack mouth observed in all LWA carriers was relatively low, the sealing efficiency of the mortar containing immobilized cells in EC and FA 6M LWA could reach up to 100%. Through the crack observation on the sides of the sample, some precipitation was observed in the bacteria samples. However, this precipitation was not sufficient to reach the top surface where the crack closure monitoring was performed. Nevertheless, it was sufficient to prevent water from penetrating through the crack. At the same time, bacteria encapsulated in Lusi 6M LWA did not provide good healing performance. The high pH of Lusi 6M LWA may have damaged the bacteria cells inside the LWA's pores. This resulted in either a limited amount of healing product or no healing at all in the Lusi 6M LWA samples.

When cracks were fabricated at the age of 28 days, the role of LWA as internal curing agent makes the reference sample deliver the same healing performance or, in some cases, even better than for the bacteria-based samples. This condition makes it difficult to see the effect of adding immobilized bacteria into LWA. The sealing efficiency results of samples cracked at the age of 28 days is also not convincing.

The high leakage that occurred after bacteria were encapsulated into the LWA was one of the major issues to be overcome to improve the healing performance of mortar, when using LWA as a bacteria carrier. Thus, suitable coatings that could prevent bacteria leakage were screened. Among three coating agents applied on the EC and FA 6M LWA, bacteria inside LWA's pores only survived when sodium alginate coating was applied. The urease activity of bacteria inside LWA's pores after being coated with sodium alginate was lower compared to that in the uncoated samples. However, the cells inside LWA's pores survived and were able to actively decompose the urea. In contrast, no urea could be decomposed by the bacteria impregnated LWA coated with sodium silicate or polyvinyl alcohol (PVA). The leakage of bacteria also decreased after a sodium alginate coating was applied. Without the coating application, the bacteria leakage could reach 31%, while the bacteria leakage was not more than 7% after the coating application.

The last stage in this research investigated the performance of the mortar after applying sodium alginate coating on EC and FA 6M LWA. In this part, spores and cells from *B. sphaericus* were used as healing agents. In the samples containing vegetative cells, yeast extract was omitted from the mixture, while in the spore containing samples, yeast extract with a concentration of 2 g/l was added to support the germination process of spores. The results show that sodium alginate coating has a negative effect on the compressive strength. The compressive strength of the resulting mortar decreased up to 33% relative to the reference sample. Regarding healing performance, in the FA 6M LWA sample group, the sodium alginate coating only slightly improved the healing capability when spores were employed as a healing agent, while there was no significant improvement due to the sodium alginate application in the vegetative cells group. In contrast, for EC LWA carriers, sodium alginate coating tends to slightly decrease the healing capability of the resulting mortar both when using cells or spores.

In conclusion, this thesis successfully investigated the feasibility of using waste materials such as fly ash, Lusi and MSWI BA as artificial lightweight aggregate. Among others, fly ash-based alkali activated lightweight aggregate proved to deliver comparable properties with commercial expanded clay LWA when employed as fine aggregate replacement in mortar production. The durability performance delivered by mortar containing fly-ash based LWA was also comparable to mortar containing EC LWA. This novel LWA was providing excellent autogenous crack healing. Fly ash-based LWA provided sufficient protection for the vegetative cells of *B. sphaericus* to heal the cracks at later age (90d). Even though the healing performance provided by this fly ash-based LWA is not as excellent as for EC LWA, this finding could pave the way for further improvements to move towards the use of artificial aggregate from waste material as bacterial carrier in the production of self-healing concrete.

Samenvatting

Beton is wereldwijd het meest gebruikte bouwmateriaal, omdat het sterk, duurzaam en betaalbaar is. De lange levensduur van beton kan echter drastisch afnemen door het ontstaan van onvermijdelijke scheuren. De aanwezigheid van scheuren groter dan 0,3 mm in betonconstructies kan de levensduur verkorten, omdat scheuren ervoor zorgen dat chloride, water en CO_2 het beton binnendringen en corrosie veroorzaken van de ingebedde stalen wapeningstaven. Betonreparatie wordt dus een noodzakelijke maatregel om verdere schade aan betonconstructies te voorkomen wanneer scheuren optreden. Helaas zijn de kosten van betonreparatie vrij hoog. In Europa kunnen de geraamde reparatiekosten oplopen tot de helft van het bouwbudget. Om deze aanstaande hoge onderhoudskosten, die naar verwachting nog zullen stijgen naarmate het betonverbruik toeneemt, te beperken, is zelfhelend beton een nieuw materiaal dat dit duurzaamheidsprobleem zou kunnen oplossen.

Van de ontwikkelde zelfhelende technieken werd gemeld dat zelfhelend beton op basis van bacteriën met microbieel geïnduceerde calciumcarbonaat precipitatie (MICP) uitstekende prestaties levert voor het helen van scheuren in beton. Het basisprincipe van deze techniek is dat micro-organismen een lokaal micromilieu creëren met omstandigheden die de neerslag van calciumcarbonaten mogelijk maken, waardoor de scheur kan worden geheeld.

Het hydratatieproces in beton dat leidt tot afnemende poriëngrootte van het verharde materiaal zou de bacteriën kunnen verpletteren, en de hoge afschuifkrachten tijdens het mengen van beton zouden de bacteriën in het beton kunnen schaden. Er is dus behoefte aan een drager die de bacteriën beschermt totdat er scheuren ontstaan. Poreuze granulaten lijken geschikte dragers te zijn, omdat ze compatibel zijn met de betonmatrix en betaalbaar zijn. Eerder onderzoek heeft aangetoond dat door het inkapselen van sporen of cellen van *B. sphaericus, B. cohnii, B. alkalinitrilicus, S. pasteurii, B. pseudofirmus, Diaphorobacter nitroreducens en Pseudomonas aeruginosa* in verschillende types poreuze granulaten, via de metabolische routes van ureum hydrolyse, denitrificatie, of omzetting van organische verbindingen, na onderdompeling in water tot 100 dagen, scheuren met een breedte tussen 0,20 en 0,79 mm volledig konden worden geheeld. Vanuit milieu-oogpunt zijn gewone poreuze granulaten die op de markt verkrijgbaar zijn, zoals geëxpandeerde kleikorrels, echter niet zo milieuvriendelijk, omdat zij bij de productie een hoge temperatuur vereisen.

Wil een lichtgewicht granulaat (LWA) geschikt zijn als bacteriedrager, dan moet aan twee belangrijke eigenschappen worden voldaan. Ten eerste moet het LWA poriën hebben met een grootte van 2 tot 5 maal de grootte van de bacterie. Het moet ook een hoge porositeit hebben zodat meer bacteriecellen in de poriën kunnen doordringen. De tweede vereiste is dat het sterk genoeg moet zijn om het mengen van beton te overleven. Als we alle basisvereisten van een poreuze drager opnieuw bekijken, zou met alkali geactiveerd LWA een geschikte kandidaat-bacteriebeschermer kunnen zijn. Het zou een hoge waterabsorptie hebben en voldoende weerstand tegen verbrijzelen. Vanuit milieuoogpunt kan het gebruik van alkaligeactiveerde LWA het gebruik van een hoge sintertemperatuur vermijden, die nodig is om commerciële poreuze LWA zoals geëxpandeerde klei te produceren.

Het eerste aspect dat moet worden onderzocht bij de productie van alkali geactiveerde LWA is de concentratie van NaOH als de primaire alkali-activator naast natriumsilicaat. Drie NaOH-concentraties van 4, 6, en 8 molair werden getest om vliegas te activeren bij de productie van alkali geactiveerde LWA in de eerste fase. Voor de productie van LWA werd een relatief lage NaOH-concentratie gekozen, omdat een hoge NaOH-concentratie de chemische reactie te veel zou versnellen, hetgeen het agglomeratieproces bij de LWA-productie zou kunnen verstoren. Gebaseerd op de resultaten bij het onderzoeken van de eigenschappen van alkali geactiveerd LWA op basis van vliegas en de resulterende mortel, is een NaOH concentratie van 6 molair voldoende voor de LWA productie. Een significante afname van de hoeveelheid macroporiën werd verkregen met een NaOH concentratie van 6 molair. Bovendien had het grootste aantal poriën in deze LWA een grootte waarin bacteriën kunnen doordringen (6-15 µm). In morteltoepassingen leverde het vervangen van 16 volume-% van de fijne toeslagmaterialen door LWA op basis van vliegas geactiveerd met een NaOH concentratie van 6 molair (FA 6M LWA) een vergelijkbare sterkte op als een mortel met geëxpandeerde klei (EC LWA).

Om geschikte alkaligeactiveerde LWA's als bacteriënbeschermer te screenen, werden naast vliegas ook afvalproducten zoals bodemassen van verbrandingsovens voor gemeentelijk vast afval (MSWI BA) en vulkanisch slib van Sidoarjo (Lusi) gebruikt als alternatief bindmiddel bij de productie van alkaligeactiveerde LWA. Natriumsilicaat werd gemengd met natriumhydroxide met een concentratie van 6 molair in een gewichtsverhouding van 1,5 en werd gebruikt als alkali-activator bij de productie van LWA. De resultaten tonen aan dat LWA op basis van Lusi en vliegas voldoen aan de eisen om te worden gebruikt als bacteriedrager. Deze twee LWA hadden een waterabsorptie van meer dan 20% na 24 uur met de grootste poriëngrootte tussen 6 en 10 µm. Wanneer deze twee nieuwe granulaten in de mortel werden opgenomen, werd een druksterkte bereikt die vergelijkbaar was met die van mortel met EC LWA. Bovendien deed een verhoging van het granulaatvervangingspercentage tot 30% de eigenschappen van de resulterende mortel niet drastisch afnemen. Bij hetzelfde percentage granulaatvervanging had mortel met MSWI BA daarentegen te lijden onder expansie. Een voorafgaande behandeling om metallisch aluminium te verwijderen zou hier nodig zijn, voordat de bodemassen worden gebruikt voor het maken van LWA. Het metallisch aluminium in LWA van MSWI BA schijnt toxisch te zijn voor de cellen van *B. sphaericus.* Slechts een beperkte hoeveelheid ureum kon door bacteriën worden afgebroken na inkapseling in MSWI BA LWA. Anderzijds deden zich geen problemen voor wanneer de bacteriën werden ingekapseld in EC, FA 6M en Lusi 6M LWA.

Door 16 % van het fijne toeslagmateriaal te vervangen door FA 6M LWA bij de mortelproductie, werden een vergelijkbare chloridemigratiecoëfficiënt en capillaire wateropname in de mortel waargenomen als voor mortel met EC LWA en voor een referentiemortel zonder LWA. Bovendien was de carbonatatieweerstand van mortel met FA 6M LWA vergelijkbaar met mortel met EC LWA. Een dichtere transitiezone tussen EC LWA of FA 6M LWA en de cementpasta droeg bij tot aanvaardbare duurzaamheidsprestaties in de resulterende mortel.

Bij de productie van zelfhelend beton op basis van bacteriën zijn bio-agenten zoals nutriënten, ureum en calciumbronnen nodig ter ondersteuning van het MICP-proces, dat gebruik maakt van de ureumhydrolyse-route. Het probleem is dat het gistextract dat nodig is om bacteriesporen te laten ontkiemen tot vegetatieve cellen naar verluidt een negatief effect heeft op de mechanische eigenschappen van de resulterende mortel. Dit onderzoek introduceerde drie gistextractconcentraties van 0, 2, en 5 g/l bij de mortelproductie. De resultaten tonen aan dat een gistextractconcentratie van 2 g/l in mortel aanbevolen kan worden wanneer de aanwezigheid van gistextract onontbeerlijk is. De druksterkte van de resulterende mortel was met ongeveer 16% gedaald ten opzichte van die van het referentiemonster. Dit terwijl in het monster met 5 g/l gistextract de druksterkte tot 50% kon afnemen ten opzichte van het referentiemonster. Wanneer vegetatieve cellen werden gebruikt voor de heling, is het weglaten van gist uit het mortelmengsel mogelijk. De afwezigheid van gist verminderde alleen de verwerkbaarheid van verse mortel, maar verstoorde het gietproces niet. Er werd dus geen afname van de dichtheid en de druksterkte ten opzichte van de referentiemortel waargenomen wanneer gistextract uit het mortelmengsel werd weggelaten.

In de volgende onderzoeksfase werden FA 6M LWA en Lusi 6M LWA toegepast als vegetatieve celdragers. Het resultaat toont aan dat cellen binnenin de FA 6M LWA nog steeds overleefden, zelfs wanneer scheuren werden gefabriceerd op de leeftijd van 90 dagen. In het scheurwijdtebereik van 0,3-0,4 mm was de helingsratio van mortel die FA 6M LWA als bacteriedrager gebruikte, iets beter dan die wanneer EC LWA werd gebruikt. De gemiddelde helingsratio bij een scheurwijdte van 0,3-0,4 mm voor het FA 6M LWA monster na 30 dagen heling in een nat-droog cyclus was 54%, terwijl dit 47% was bij het EC LWA monster. Hoewel de scheurhelingsratio aan de scheurmond waargenomen voor alle LWA dragers relatief laag was, kon de afdichtingsefficiëntie van de mortel met geïmmobiliseerde cellen in EC en FA 6M LWA oplopen tot 100%. Bij de waarneming van de scheur aan de zijkanten van het monster werd enige neerslag waargenomen in de mortel met bacteriën. Deze neerslag was echter niet voldoende om het bovenoppervlak te bereiken waar de meting van de scheurdichting werd uitgevoerd. Niettemin was het voldoende om te voorkomen dat water door de scheur zou binnendringen. Tegelijkertijd leverden de in Lusi 6M LWA ingekapselde bacteriën geen goede helingsprestaties. De hoge pH van Lusi 6M LWA kan de bacteriecellen in de poriën van het LWA beschadigd hebben. Dit resulteerde in een beperkte hoeveelheid helend product of helemaal geen heling in de Lusi 6M LWA monsters.

Bij scheurcreatie op een ouderdom van 28 dagen, zorgde de rol van LWA bij interne nabehandeling ervoor dat het referentiemonster dezelfde helingsprestaties leverde of, in sommige gevallen, zelfs beter dan de op bacteriën gebaseerde monsters. Deze omstandigheid maakt het moeilijk om het effect te zien van de toevoeging van geïmmobiliseerde bacteriën aan LWA. De resultaten van de afdichtingsefficiëntie van monsters die op de leeftijd van 28 dagen werden gescheurd, zijn ook niet overtuigend.

De grote uitloging van bacteriën die optrad na inkapseling in de LWA was een van de belangrijkste problemen die moeten worden opgelost om de heling van de mortel te verbeteren, wanneer LWA wordt gebruikt als bacteriedrager. Daarom werden geschikte coatings gescreend die het uitlogen van bacteriën konden voorkomen. Van de drie types coating die werden aangebracht op de EC en FA 6M LWA, overleefden de bacteriën binnen de poriën van LWA alleen wanneer een natriumalginaatcoating werd aangebracht. De urease-activiteit van de bacteriën in de poriën van de LWA's na bekleding met natriumalginaat was lager dan die in de niet-gecoate monsters. De cellen binnen de poriën van LWA overleefden echter en waren in staat het ureum actief af te breken. Daarentegen kon geen ureum worden afgebroken door de bacteriën die geïmpregneerd waren in LWA gecoat met natriumsilicaat of polyvinylalcohol (PVA). De uitloging van bacteriën nam ook af nadat een natriumalginaatcoating was aangebracht. Zonder het aanbrengen van de coating kon de bacterielekkage oplopen tot 31%, terwijl het verlies aan bacteriën na het aanbrengen van de coating niet meer dan 7% bedroeg.

In de laatste fase van dit onderzoek werden de prestaties van de mortel onderzocht na het aanbrengen van een natriumalginaatcoating op EC en FA 6M LWA. In dit deel werden sporen en cellen van *B. sphaericus* gebruikt als helende middelen. In de monsters die vegetatieve cellen bevatten, werd gistextract uit het mengsel weggelaten, terwijl in de monsters die sporen bevatten, gistextract met een concentratie van 2 g/l werd toegevoegd om het kiemproces van de sporen te ondersteunen. Uit de resultaten blijkt dat de natriumalginaatcoating een negatief effect heeft op de druksterkte. De druksterkte van de resulterende mortel daalde tot 33% ten opzichte van het referentiemonster. Wat betreft de helingsprestaties, verbeterde in de FA 6M LWA-monstergroep de natriumalginaatcoating het helend vermogen slechts in geringe mate wanneer sporen werden gebruikt, terwijl er geen significante verbetering was als gevolg van de natriumalginaattoepassing in de vegetatieve cellengroep. Bij de EC LWA dragers daarentegen had de natriumalginaatcoating de neiging het helend vermogen van de resulterende mortel licht te verminderen, zowel bij gebruik van cellen als van sporen.

Concluderend kan worden gesteld dat in dit proefschrift met succes de haalbaarheid is onderzocht van het gebruik van industriële bijproducten zoals vliegas, Lusi en bodemassen als kunstmatig lichtgewicht toeslagmateriaal. Op vliegas gebaseerde alkali-geactiveerde lichtgewicht toeslagmaterialen bleken vergelijkbare eigenschappen te leveren als commerciële geëxpandeerde klei LWA wanneer ze werden gebruikt ter vervanging van fijn toeslagmateriaal bij de productie van mortel. De duurzaamheidsprestaties van mortel met LWA op basis van vliegas was ook vergelijkbaar met mortel met EC LWA. Deze nieuwe LWA zorgde voor een uitstekende autogene scheurheling. LWA op basis van vliegas bood voldoende bescherming voor de vegetatieve cellen van *B. sphaericus* om scheuren gevormd op latere leeftijd (90 dagen) te helen. Hoewel de helingsprestatie van dit LWA op basis van vliegas niet zo uitstekend was als die van EC LWA, kunnen deze bevindingen de weg effenen voor verdere verbeteringen op vlak van het gebruik van kunstmatig granulaten uit afvalmateriaal als bacteriedrager bij de productie van zelfhelend beton

Table of content

Chapter 1. General Introduction

This page is Intentionally blank.

1.1 Cracks in Concrete

Concrete is the most used construction material worldwide as it is strong, durable, and affordable. However, the long life span of concrete could decrease drastically due to unavoidable cracks. Many conditions could induce cracks, such as overloading or shrinkage due to chemical effects, drying, or large temperature changes during the hydration process. But it is pretty challenging to determine precisely which condition caused the crack as it is usually caused by more than one reason. Thus, Klemczak categorized the type of crack based on the concrete age and the condition that possibly induced it (Klemczak and Knoppik-Wróbel, 2011) (see **Table 1.1**). The reasons cracking occurs at early age are volume or moisture change due to the hydration process, drying and thermal gradient such as when casting a massive concrete slab (Klemczak and Knoppik-Wróbel, 2011). While in mature concrete, cracks usually occur due to fatigue and overload (ACI, 2001). The physical and chemical aspects such as drying shrinkage and temperature stress usually induce smaller cracks (ACI, 2001). The cracks might also occur due to deterioration processes and the loss of material durability (AL-Ameeri et al., 2021).

Table 1.1. Causes of Cracks in Concrete Structures (Klemczak and Knoppik-Wróbel, 2011)

Type of Cracks		
Fresh Concrete	Hardened Concrete	
	Early age	Mature
Formwork movement Subgrade movement Plastic shrinkage Plastic settlement Autogenous shrinkage Frost damage	Volume change Autogenous and drying shrinkage Changing in temperature due to hydration	Design load/accidental overload Fatigue Drying shrinkage Temperature stress Corrosion of the reinforcement bars Freeze-thaw cycling Alkali aggregate reactions Concrete carbonation

Crack widths above a certain threshold could shorten the service life span of concrete structures, especially if exposed to a harsh environment. Therefore, EN NBN 1992-1-1 provides guidelines on the acceptable crack limit in each exposure condition (**Table 1.2**). Overall, when concrete structures are subjected to quasi-permanent load in a wet condition, the maximum allowable crack width is 0.3 mm. When cracks larger than 0.3 mm occur and no repair action is taken, the structure's service life could decrease dramatically (AL-Ameeri et al., 2021; Park et al., 2012). Park et al. found that the chloride diffusion coefficient of concrete containing a crack larger than 0.4 mm, could be 145 times higher when compared to an uncracked sample, and 24 times higher when compared to concrete with a crack width less than 0.1 mm (Park et al., 2012).

Table 1.2. Permissible Crack Width for Reinforced Concrete in Each Exposure Condition According to EN NBN 1992-1-1 Standard

Corrosion types	Exposure Class	Quasi-permanent load	Frequent load
Induced by carbonation	Dry or permanently wet	0.4 mm	0.2 mm
	Wet, rarely dry	0.3 mm	0.2 mm
	Moderate humidity	0.3 mm	0.2 mm
	Cyclic wet and dry	0.3 mm	0.2 mm
Induced by chlorides	Moderate humidity	0.3 mm	0.2 mm
	Wet, rarely dry	0.3 mm	0.2 mm
	Cyclic wet and dry	0.3 mm	0.2 mm
Induced by chlorides from seawater	Exposed to airborne salt	0.3 mm	0.2 mm
	permanently submerged	0.3 mm	0.2 mm
	tidal zones	0.3 mm	0.2 mm

Therefore, repairing the cracks becomes vital for maintaining the service life of the concrete structure. So far, injection methods are the most used methods for repairing cracked concrete. However, as the basic principle of this method involves manually introducing new material to fill in the cracks, the chance of failure is relatively high since it involves human intervention.

Based on a cement consumption report, in 2018, 179.8 million tons of cement were consumed in European countries and the consumption was predicted to increase by 2.2 % per year (Cembureau, 2020). This European consumption is only representing 4.4 % of the total world consumption, which is dominated by China which accounted for more than 50% of total world consumption (Cembureau, 2020). With the growth of concrete production indicated by the growing cement consumption, maintenance costs for structural concrete repair are also expected to increase. In the US, in 2005, 18-21 billion US dollars were spent on repairing concrete (International Concrete Repair Institute, 2006). To mitigate these forthcoming high maintenance costs, which are expected to increase even further with increasing concrete consumption, a new material that could solve this durability issue is presented: self-healing concrete.

1.2 Autogenous vs Autonomous Healing

As mentioned before, cracks wider than 0.3 mm can accelerate the concrete degradation and shorten its service life. Literally, concrete has an autogenous healing ability that was reported to effectively close the crack width in the range of 0.1-0.15 mm (De Belie et al., 2018). Mainly, four factors contributed to the autogenous healing mechanism in concrete: 1) The swelling of calcium silicate hydrate (C-S-H) at the crack's walls, (2) The continued hydration of unhydrated cement particles, (3) The formation of calcium carbonate due to the carbonation process of portlandite and (4) The clogging of the crack mouth by loose concrete particles or from debris coming from intruding water (M. De Rooij, K. Van Tittelboom, N. De Belie, 2013).

Besides, autogenous healing has limitations in terms of crack width that could be healed; this healing mechanism is also difficult to control and hardly predictable (De Belie et al., 2018; Yusuf Çağatay Erşan, 2016). Thus another healing mechanism named encapsulated autonomous healing was introduced. This healing mechanism relies on encapsulated healing agents added into the concrete mixture to provide a self-healing function (De Belie et al., 2018).

In general, there are four types of encapsulated autonomous self-healing methodologies: (1) microencapsulation, (2) macro encapsulation, (3) vascular healing, and (4) self-healing bio-concrete (De Belie et al., 2018). In the microencapsulation mechanism, microcapsules loaded with the healing agent embedded in the mortar matrix. When cracks occur, the healing agent will leak out and react with a catalyst available in the mortar matrix and heal the crack (White et al., 2001). In the literature, crack widths up to 0.97 mm could be entirely closed when spores of *B. sphaericus* were loaded into microcapsules (Wang et al., 2012). When microcapsules with sodium silicate as a core were implemented into the mortar, the average healing ratio for a crack width of 0.25 mm was 40 %. This value was achieved after the sample was cured for 28 days in a chamber with a relative humidity of 98% (Litina and Al-Tabbaa, 2020). Besides, while microcapsules may provide excellent healing performance in some cases, they tend to decrease the mechanical performance in mortar or cement paste (De Belie et al., 2018).

The most used capsules for macro-encapsulation are made of polypropylene, glass, or cement-based materials. In the literature, when expansive minerals and water were encapsulated into a two compartment glass tube, a crack width of 0.4 mm could be almost completely sealed after being immersed in water for 56 days (Qureshi et al., 2016). The major drawback of this system is that most of the capsules are expensive, and when glass capsules were used, a possible alkali-silica reaction could occur. To avoid this drawback, cement-based capsules were implemented. Loaded with spores of *B. sphaericus*, crack widths of 0.3 mm could completely heal after being subjected to water immersion for 7 days (Anglani et al., 2020).

In the vascular healing system, the availability of healing agents in the matrix could be guaranteed. Thus, theoretically, excellent healing performance could be achieved. Minebo et al, injected polyurethane liquid into various vascular systems generated from various materials (ceramic, cementitious composites, starch, and polymethylmethacrylate). The result shows that mechanical repair generally occurred in all samples, proving that the healing mechanism was successful (Minnebo et al., 2017). However, more improvement still needs to be obtained in the vascular healing systems, especially minimizing human intervention during the healing process (De Belie et al., 2018).

The last system is self-healing bio-concrete or bacteria-based self-healing concrete. In this system, an alkali-resistant bacteria strain that could induce calcium carbonate production, which later on could seal the cracks, was used as a healing agent. The healing performance of this system was excellent. A crack up to 0.97 mm could be completely healed in relatively short time by microcapsules loaded with *B. sphaericus* spores (Wang et al., 2012). When porous carriers were loaded with spores of *B. alkalinitrilicus* a crack width of 0.46 could also be healed (Wiktor and Jonkers, 2011). Compared to other healing methods aforementioned, it seems that bacteria-based healing provided better healing performance. Thus this thesis will focus on utilizing bacteria-based self-healing method.

1.3 Bacteria Based Self-healing Concrete

Bacteria-based self-healing concrete is one of the promising construction materials that heals concrete cracks using bacteria through a microbially-induced calcium carbonate precipitation (MICP) process. Based on literature, MICP occurs when the microorganism forms a local micro-environment, with conditions that allow precipitation of carbonates (Hamilton, 2003). The basic principle of MICP is that within a saturated aqueous solution, even with limited dissolution of CO_2 from air, the metabolic activity of bacteria will lead to an increase in CO_3^{2-} concentration, so that with the presence of Ca^{2+} in the solution, calcium carbonate will be precipitated (Yusuf Çağatay Erșan, 2016). This calcium carbonate can then close the crack mouth.

MICP can not only heal a concrete crack, this technique can also improve soil consolidation (Achal and Pan, 2014) and be applied as surface treatment for stones (De Muynck et al., 2008). The alkali-resistant bacteria strains that can form spores such as *S. pasteurii, B. alkalinitrilicus, B. sphaericus, B subtilis, and B. cohnii* have been used successfully as microorganism sources in the MICP process (Bayati and Saadabadi, 2021; Feng et al., 2021; Wang et al., 2017; Wiktor and Jonkers, 2011; Zhang et al., 2017).

Several bacterial metabolic pathways were chosen to promote calcium carbonate precipitation (Mondal and Ghosh, 2019). The urea hydrolysis pathway is the most frequently used mechanism to promote rapid calcium carbonate precipitation (Erșan, 2016; Mondal and Ghosh, 2019). By applying this pathway, *B. sphaericus* encapsulated into microcapsules can rapidly heal cracks up to 0.97 mm after being subjected to wet-dry cycle curing in water for 56 days. The hydrolysis pathway is presented in **Figure 1.1**. However, the ammonia produced during the hydrolysis process becomes a major drawback for this pathway from an environmental point of view.

On the other hand, Jonkers and Schlangen used *B. alkalinitrilicus* as a healing agent and reported an excellent healing performance when applying metabolic conversion of organic compounds (Jonkers and Schlangen, 2009). This pathway was claimed to overcome the drawback of ammonia produced by the urea hydrolysis pathway. However, it took around 100 days for the system to close a 0.46 mm crack, which is relatively slow compared to the urea hydrolysis pathway (Wiktor and Jonkers, 2011).

The hydration process in concrete that leads to decreasing pore sizes of the hardened material could crush the bacteria, and the high shear forces during concrete mixing could harm the bacteria inside concrete (Jonkers and Schlangen, 2009). Thus, some researchers encapsulated the bacteria into various carriers to prolong the viability of bacteria until the cracks occurred (**Table 1.3**). The basic principle is, that when cracks occur and break the carrier, the bacteria will leak out and start healing the cracks. When cracks occur, the concrete pH near the crack walls will drop to a favorable condition due to carbonation. An excellent healing performance was reported when spores of *B. cohnii* were encapsulated into expanded perlite and then coated with metakaolin-based geopolymer coating. A crack wider than 0.5 mm could be closed after the samples were immersed in water for 28 days (J. Zhang et al., 2017). In other literature, using the denitrification pathway, the maximum crack width that could be closed by encapsulated bacteria cells of *Diaphorobacter nitroreducens* and *Pseudomonas aeruginosa* into porous carriers was 0.47 mm (Yusuf Çağatay Erşan et al., 2016).

From the healing performance point of view indeed porous carriers may not provide an excellent healing as hydrogel or microcapsules carriers. However, the presence of porous carriers in the mortar matrix which usually replaces partially the natural aggregate, does not significantly decrease the strength of resulting mortar. A strength reduction of 12 % relative to the reference sample was achieved when 16% volume of natural aggregate was replaced with expanded clay (Risdanareni et al., 2020). At the same time, the addition 5% by cement weight of microcapsules was reported to decrease the mortar strength up to 50 % relative to the reference samples (Wang et al., 2012). Besides, the cost needed to produce advance carrier technologies such as hydrogel and microcapsules is also relatively high compared to the price of porous carriers.

Considering all the advantages and disadvantages of each carrier, utilizing porous carriers could be an option from a practical point of view. This porous carrier is more affordable, compatible with mortar or concrete matrix and provided acceptable healing performance when employed as bacterial carrier. However, some carriers such as expanded clay or expanded perlite need to be sintered at a high temperature (approximately 1200°C). Thus it would be a significant improvement if a similar porous bacteria carrier that needs less energy during its production can be manufactured.

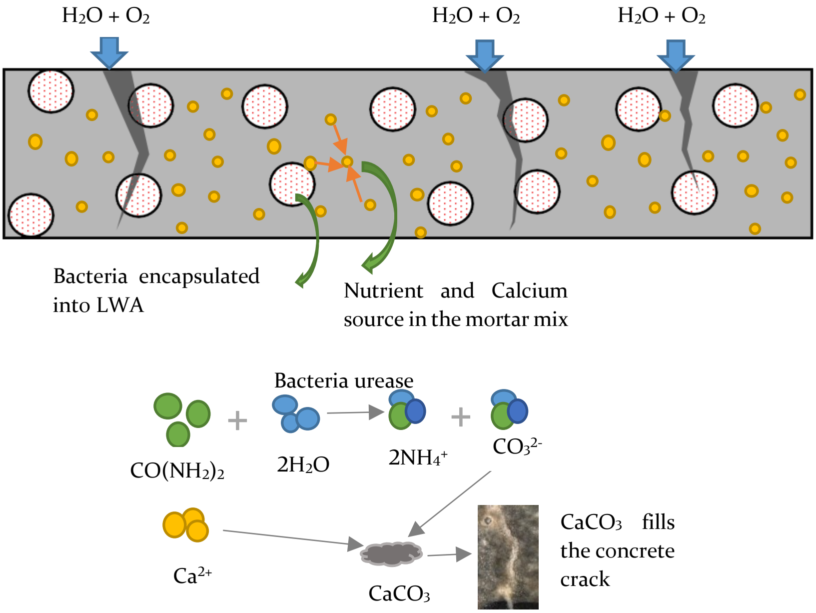

Figure 1.1. Illustration on the healing mechanism (urea hydrolysis) provided by bacteria in the porous carrier.

Table 1.3. The healing performance of bacteria encapsulated in various carriers.

Types of Carrier	Bacteria strain	Pathway	Curing Regime	Curing time (days)	Max. crack closed (mm)	Ref
Expanded Clay	*B. alkalinitrilicus*	conversion of organic compound	Immersed in water	100	0.46	(Wiktor and Jonkers, 2011)
Expanded clay	*B. pseudofirmus*	conversion of organic compound	Immersed in water	56	0.2	(Jakubovskis et al., 2021)
Expanded perlite	*B. pseudofirmus*	conversion of organic compound	Humid chamber	165	0.3	(Alazhari et al., 2018)
Expanded Perlite	*B. cohnii*	conversion of organic compound	Immersed in water	28	0.79	(J. Zhang et al., 2017)
Chitosan-Based Hydrogel	*B. sphaericus*	urea hydrolysis	Wet-dry cycle in water	28	0.25	(Wang et al., 2018)
Hydrogel	*B. sphaericus*	urea hydrolysis	Wet-dry cycle in water	7	0.5	(Wang et al., 2014)
Extruded capsule	*B. sphaericus*	urea hydrolysis	Immersed in demi water	7	0.3	(Anglani et al., 2020)
Ceramsite	*S. pasteurii*	urea hydrolysis	Immersed in water	120	0.45	(J. Xu et al., 2020)
Microcapsule	*B. sphaericus*	urea hydrolysis	Wet-dry cycle in water	56	0.97	(Wang et al., 2012)
Biochar	*B. sphaericus*	urea hydrolysis	Wet-dry cycle in water	14	0.2	(Kua et al., 2019)
Diatomaceous Earth	*B. sphaericus*	urea hydrolysis	Immersed in DM	40	0.17	(Wang et al., 2012)

Expanded clay	*Diaphorobacter nitroreducens andPseudomonas aeruginosa*	denitrification	Immersed in water	28	0.35	(Yusuf Çağatay Erşan et al., 2016)
Activated carbon	*Diaphorobacter nitroreducens andPseudomonas aeruginosa*	denitrification	Immersed in water	56	0.47	(Yusuf Çağatay Erşan et al., 2016)

*DM deposition medium (urea and $Ca(NO_3)_2$, 0.2 M)

1.4 Alkali Activated LWA as an Alternative Bacteria Carrier

Since current porous bacterial carriers require high energy levels during their production, an attempt to produce more green and eco-friendly porous carriers becomes an attractive research field. Samonin and Elikova mentioned two important properties that porous bacteria carriers should meet to provide an ideal environment for bacteria (Samonin and Elikova, 2004). The first one is a high ability to absorb liquid, which means that the carrier must have a high open porosity to retain a large amount of liquid. The second one is the pore size. The pore size of the carrier should be 2 to 5 times the bacteria size. If it is too small, the bacteria could not penetrate inside, and when it is too big, the bacteria could easily leak out. Another requirement that the bacteria carrier should have is sufficient strength. The carrier should be the weakest part in the matrix in order to attract concrete cracks that should rupture the carrier and allow self-healing to occur, but not so weak that it breaks during the concrete mixing process.

Artificial lightweight aggregate (LWA) made of waste materials such as fly ash and waste from municipal solid waste incinerators have been recently developed due to the numerous advantages (Gesoğlu et al., 2007; Tang et al., 2017; Thomas and Harilal, 2015). From a performance point of view, this LWA was proved to deliver adequate strength and acceptable durability performance (Güneyisi et al., 2013). From an environmental point of view, by replacing the aggregate, which takes up to 70% of the concrete mixture, recycling of a significant amount of waste material would be expected. If this method were to be upscaled, replacing natural aggregate with the waste-based LWA will also reduce the risk of over-mining natural aggregate and harming the environment. Moreover, this LWA does not need a sintering process to be hardened; a cold bonded hardening method would be sufficient.

In available literature, most researchers used cement-based binder LWA that were hardened with a cold bonded curing method (Geetha and Ramamurthy, 2013; Gu, 2000; Güneyisi et al., 2013; Tang et al., 2017). In this method cement was added with the waste material such as fly ash, municipal solid waste incinerator bottom ash (MSWI BA) or slag to produce artificial lightweight aggregate through agglomeration technique (Balapour et al., 2020; Gesoğlu et al., 2007; Xiao yu Shang and Li, 2020; Tang et al., 2017). The properties of this cement-based LWA were quite acceptable, the water absorption over 24 hours was in the range of 21-25 % and the crushing strength of LWA with particle size below 6 mm was around 100 N (Gesoğlu et al., 2007; Tang et al., 2017). In concrete application, the compressive strength of resulting concrete decreased by 18%, when 30% of natural aggregate was replaced by cold bonded fly ash-based LWA (Gesoğlu et al., 2007).

Although the cement-based LWA provides acceptable properties when added into concrete, it still needs cement as a binder, which has a negative effect on the environment due to its high carbon footprint during production. The cement could be avoided if an alkali activated binder system was applied in the production of LWA. However, the use of an alkali activated binder system to produce LWA is scarcely reported in literature. One study by Illikainen et al. reported that fly ash-based alkali activated LWA could deliver comparable strength to the cement-based LWA that is commonly used in other studies (Colangelo et al., 2015; Illikainen et al, 2017). The water absorption of those fly ash-based LWA is still high (more than 20%), but it has a higher crushing strength than a commercial expanded clay (Illikainen et al., 2017).

Revisiting the requirements for the bacterial carrier, alkali activated LWA could be a suitable candidate. It was reported to have a high water absorption that corresponds with high porosity, and enough strength, in the same range as the commercial expanded clay. Moreover, it has been reported that the pH of alkali activated material decreased with curing time. The initial pH of cement-based concrete was 13, while in alkali activated material, the initial pH could reach 14. However, the pH of the pore solution tends to increase with curing time in cement-based material, while a lower final pH was observed in alkali activated material compared to the cement-based materials (Paudel et al., 2020). Thus alkali activated LWA might also provide a better environment for bacteria to survive.

1.5 The Potential Use of Vegetative Cells as Healing Agent

In previous investigations, more researchers chose spores over vegetative cells as a healing agent. Spores are suitable as they will stay dormant in the concrete until a crack occurs (Jonkers and Schlangen, 2009; Wang et al., 2017). However, some problems might occur during the germination process; either the pH of the environment is not favorable or there are difficulties for the spores to reach the nutrient (Setlow, 2013). Moreover, yeast extract, commonly used as the main nutrient for germination, was also reported to decrease the concrete strength (Zeynep Basaran Bundur et al., 2015).

On the other hand, a pilot study on encapsulating vegetative cells of *B. sphaericus* into diatomaceous earth was reported to deliver satisfying healing performance. Crack widths up to 0.17 mm could completely close after being cured in a deposition medium (DM) for 40 days, while no healing was observed in the control sample (Wang et al., 2012). Applying the vegetative cells of *B. sphaericus* also proven to deliver rapid healing and a higher healing ratio than encapsulated spores (Intarasoontron et al., 2021). Crack widths up to 0.3 mm were 97 % healed in the vegetative cells group, while the spores group achieved a healing ratio of 84 % (Intarasoontron et al., 2021).

However, as the vegetative cells are active cells, the chance of this microorganism still being available for a long period is scarce. It has been reported that a self-protected nitrate-reducing culture still can seal the cracks in 6 months old mortar. But, those cultures are already protected with nutrients to keep them viable for a long period (Ersan et al., 2015). Bundur et al. found that the cells of *S. pasteurii* were still viable in cement paste after one year, but no further test on its healing performance was performed (Bundur et al., 2015). Based on the available literature, the use of vegetative cells as a healing agent is suitable for rapid healing in a young age concrete. Spores would still become a suitable healing agent when the healing needs to be done at a later age.

1.6 Up to Date Research Needs

Considering the current findings in the development of bacteria-based self-healing concrete, several research needs could be pursued. The first one is the need for affordable and more eco-friendly bacterial carriers to make the use of self-healing technology in the concrete industry more feasible. The second one is to investigate the feasibility of using vegetative cells instead of spores to achieve rapid healing at relatively young ages and not hamper the concrete's mechanical properties by omitting the organic nutrients (for instance yeast extract).

1.7 Scope of the Thesis

This thesis aims to manufacture alkali activated LWA that could become the carrier for vegetative cells and spores in the production of bacteria-based self-healing concrete. The study was divided into five parts: (1) Optimization of LWA Production; (2) Investigating the Properties and the Durability of mortar containing alkali activated LWA; (3) Optimizing the use of yeast extract for bacteria based self-healing; (4) Optimization of the bacteria-based self-healing, and (5) Evaluation of result achievements.

After the general introduction (Chapter 1), the following chapters are outlined as follows :

Part 1 Optimization of LWA Production

Chapter 2: Finding Suitable NaOH Concentration for Manufacturing Alkali Activated LWA

The main goal of this chapter is to find the minimum concentration of NaOH that could activate the binder in LWA production. NaOH with 4, 6, and 8 molar concentrations was applied to produce fly ash-based LWA.

Outcome: The NaOH concentration of 6 molars was sufficient to activate the fly ash in LWA production. This NaOH concentration delivered satisfactory properties that are comparable with the commercial expanded clay LWA. This NaOH concentration might then be also suitable to activate other materials that are rich in silica and alumina like fly ash.

Part 2 Investigation of the Properties and Durability of Mortar Containing Alkali activated LWA

Chapter 3: Properties of Alkali Activated Lightweight Aggregate Generated from Sidoarjo Volcanic Mud (Lusi), Fly Ash and Municipal Solid Waste Incineration Bottom Ash

In this chapter, the properties of alkali activated LWA generated from fly ash (FA), municipal solid waste incinerator bottom ash (MSWI BA), and Sidoarjo volcanic mud (Lusi) are investigated.

The main goal was to characterize the properties of all alkali activated LWA, such as water absorption, porosity, crushing strength, and compressive strength when the LWA was incorporated into mortar. By characterizing the LWA properties, it allows us to select the most suitable LWA that could be used as bacterial carrier.

Outcome: fly ash-based LWA, and Lusi LWA had acceptable mechanical properties. They had a high enough porosity which makes them ideal as a bacteria carrier. The ureolytic activity of bacteria after encapsulated into those LWA was also comparable with those encapsulation into EC LWA. On the other hand, further pretreatment on MSWI BA is needed to use MSWI BA 6M LWA as a bacteria carrier. The metallic aluminum in MSWI BA seems to be toxic for *B. sphaericus* cells, as only limited urea could be decomposed when cells were encapsulated into MSWI BA 6M LWA.

Chapter 4: Durability of Mortar Containing Fly Ash-Based Alkali activated Lightweight Aggregate

In this chapter the durability of mortar containing fly ash-based LWA is investigated. This is important as the addition of porous LWA might shorten the life span of the resulting mortar or concrete as it is more permeable for CO_2 and water to penetrate.

The main goal is to determine the feasibility of using alkali activated LWA in a mortar mixture by measuring the durability performance of the resulting mortar.

Outcome: The presence of alkali activated LWA did not negatively affect the durability performance of the resulting mortar. Instead, the mortar containing fly ash-based LWA tends to improve the resistance of mortar against carbonation due to the dense ITZ formed between LWA and cement paste.

Part 3 Optimizing the Use of Yeast Extract

Chapter 5: Suitable Yeast Extract Concentration for the Production of Self-Healing Concrete with Expanded Clay as Bacterial Carrier.

Here the focus is on finding the minimum dosage of yeast extract that could be added into the mortar mixture, which would minimize the strength decrease in mortar when the presence of yeast extract in the mix is mandatory e.g. for germination of bacterial spores.

The main goal is to be able to produce bio-concrete that has efficient self-healing properties without scarifying mechanical properties.

Outcome: When yeast extract is needed in the mixture, a concentration of 2 g/l mortar is recommended as it did not significantly decrease the strength of the resulting mortar. On the other hand, when yeast extract is not mandatory, omitting the yeast from the mixture could maintain the strength of the resulting mortar.

Part 4 Optimization of the Bacteria-Based Self-Healing

Chapter 6 : Alkali Activated LWA as Bacterial Carrier in Manufacturing Self-Healing Mortar

In the development of bacteria-based self-healing concrete, first there is a need to screen bio-compatible alkali activated LWA as bacterial carrier in the production of self-healing concrete and to examine the possibility of using vegetative cells as a healing agent.

The main goal is to select an alkali activated LWA that delivers acceptable healing performance when employed as a vegetative cells carrier. Fly ash-based LWA and Lusi-based alkali activated LWA were chosen as the bacteria carrier candidates.

Outcome: Fly ash-based LWA delivered comparable or even better healing performance compared to expanded clay (EC) LWA when cracks were fabricated at the age of 90 days.

Chapter 7: Screening Suitable Coating for Lightweight Aggregates as Bacteria Carrier for Manufacturing Self-Healing Concrete

There is a need for screening suitable coating materials to mitigate bacteria leakage to improve the healing performance of the resulting mortar.

The main goal is to find a bio-compatible coating to effectively reduce bacteria leakage. Three kinds of coating, sodium alginate, sodium silicate, and polyvinyl alcohol (PVA) coating, were chosen as coating candidates.

Outcome: The vegetative cells of *B. sphaericus* only survived in sodium alginate coated LWA, and the leakage value of bacteria from LWA coated with sodium alginate decreased significantly.

Chapter 8: Performance of Self-Healing Mortar Containing Bacteria Immobilized In Alginate Coated Alkali Activated Lightweight Aggregate

As a next step, the effect of applying the sodium alginate coating on LWA with vegetative cells or spores as a healing agent, on the healing performance of the resulting mortar was investigated.

The main goal was to obtain an improvement in healing performance by applying sodium alginate coating.

Outcome: No significant improvement in the healing performance was observed by the application of the coating, neither for the EC LWA samples, nor for the fly ash-based LWA samples. However, the vegetative cells group proved to deliver better healing performance compared to the spores group.

Part 5. Evaluation of the Results

Chapter 9 General Conclusion and Future Perspectives

All results were evaluated in terms of allowing alkali activated LWAs to be accepted as a bacterial carrier in self-healing production and final recommendations were formulated.

Chapter 2. Finding Suitable NaOH Concentration for Manufacturing Alkali Activated LWA

This chapter was redrafted after:

Risdanareni, P., Schollbach, K., Wang, J., De Belie, N. (2020). *Effect of NaOH concentration on the mechanical and physical properties of alkali activated fly ash-based artificial lightweight aggregate*. Construction and building materials, 259, 119832, 8 p.
doi: https://doi.org/10.1016/j.conbuildmat.2020.119832

2.1 Introduction

The global consumption of construction aggregate exceeded 48.3 billion tons per year in 2015 and is expected to increase by 5.2% annually (Freedonia, 2012). On the other hand, by 2010 the global production of fly ash around the world was around 780 million metric ton and is expected to increase by 1.6% annually (Heidrich et al., 2013). Based on the same report, around 53% of this ash is used as supplementary material in cement production. Furthermore, as around 70% of the concrete mixture is made up by the aggregate, reducing natural aggregate consumption by replacing it with artificial aggregate generated from waste material such fly ash will be an effective way to reduce the amount of non-renewable material consumption.

Several investigations on employing fly ash as raw material to produce pelletized lightweight aggregate (LWA) with cement, glass powder or clay as a binder have already been conducted (Gesoğlu et al., 2007; Güneyisi et al., 2013; Kourti and Cheeseman, 2010). Researchers also reported that several aspects such as curing method and pelletizing procedure affected the properties of pelletized LWA (Gu, 2000; Güneyisi et al., 2013; Manikandan and Ramamurthy, 2008). However, almost all the reports are focused on optimizing the properties of LWA in which clay or cement was used as a binder (Gesoğlu et al., 2007; Gu, 2000; Güneyisi et al., 2013; Kourti and Cheeseman, 2010; Manikandan and Ramamurthy, 2008). Only limited studies can be found on alkali activation of fly ash for producing LWA, although this technique can improve the mechanical and physical properties of pelletized aggregate (Geetha and Ramamurthy, 2013; Shivaprasad and Das, 2018).

According to literature, the alkali activator solution plays an important role in geopolymerization as a silica and alumina solvent (H. Xu and Deventer, 2000). The type of alkali solution (H. Xu and Deventer, 2000), the concentration of alkali activator (Hamidi et al., 2016; Hardjito, 2005; Rattanasak and Chindaprasirt, 2009), the ratio between binder and solution (Cheng et al., 2015; Heah et al., 2012; Silva et al., 2011), and the curing regime (Hardjito, 2005) significantly affect the geopolymerization. NaOH with a concentration range of 8-12 Molars gives optimal mechanical properties in concrete and mortar application (Görhan and Kürklü, 2014a; Hamidi et al., 2016; Hardjito, 2005). Geetha and Ramamurthy found that the minimum concentration of NaOH needed to synthesize geopolymer LWA is 8 molar (Geetha and Ramamurthy, 2013), while Gorhan and Kurklu found that the optimum NaOH concentration for fly ash-based geopolymer is 6 molar (Görhan and Kürklü, 2014). Increasing the molarity of NaOH proved to reduce water absorption and increases the strength of LWA. However, a higher concentration of NaOH caused workability issues of fresh concrete that lead to a decrease in the mechanical properties (Hamidi et al., 2016; Risdanareni et al., 2015). Although efforts have been made to determine the most suitable NaOH concentration for manufacturing geopolymer paste or LWA, no clear guidelines regarding the minimum NaOH concentration to synthesize alkali activated LWA exist.

Comparing fly ash LWA with commercial LWA is necessary to have an idea about the ability of fly ash-based LWA to compete in the market. In this study, expanded clay LWA (Argex NV) was chosen for comparative analysis because of its wide availability and its high strength. However, a high sintering temperature of 1100°C is needed during the production of expanded clay LWA. Reducing the energy needed by choosing cold bonding instead of sintering in the production of fly ash-based LWA is expected to decrease the environmental impact and has a positive effect on the market acceptance of this LWA.

Summarizing, the aim of this part of the study is to find a suitable NaOH concentration to produce alkali activated LWA that meets the requirement to be used as a bacteria protector and is compatible with mortar matrix. In order to avoid the workability problems resulting from a high concentration of NaOH, a low concentration of NaOH in the range of 4 to 8 molars was chosen in this study, which also has the advantage of keeping the production costs low. The water absorption, the pore characterization, and the crushing strength, as the main properties needed for bacteria carriers, were investigated. The other supporting LWA's properties, such as mineralogy and particle size distribution were also tested. Furthermore, the LWA with the fraction of 2-4 mm was applied in mortar as a natural fine aggregate replacement to investigate its effect on the mechanical properties of the resulting mortar. The properties of LWA generated from expanded clay have also been investigated in this research for comparison.

2.2 Materials and methods

2.2.1 Materials

Fly ash class F (FA) from a thermal power plant in the Netherlands was used as a precursor to produce lightweight aggregate (LWA). The chemical composition of fly ash was determined with XRF measurements. The tests were carried out on a loose powder sample using a Rigaku NeXCG equipment.

The particle size distribution of fly ash was measured using laser diffraction (Malvern mastersizer 2000). Isopropanol (VWR International Bvba) was used as dispersant in this test.

A liquid form of sodium silicate (Na_2SiO_3) (VWR International Bvba) which contains 26.3% silica, 7.9% sodium oxide, and 65.8% water and a powder form of sodium hydroxide (NaOH) (VWR International Bvba) with a purity of 97-98% was used as the alkali activator (AA). In order to obtain the desired NaOH concentration, the NaOH was dissolved in demineralized water until reaching the concentrations of 4, 6, and 8 Molar, respectively. Later on, sodium silicate and sodium hydroxide with the desired concentration were mixed with a weight ratio of 1.5. Subsequently, the mixed alkali activator was left at room temperature conditions for at least 24 hours before use.

For mortar application, cement type I 52.5 N from Holcim was used as a binder while river sand with a size of 0/4 mm was used as the fine aggregate.

Commercial sintered expanded clay from Argex NV Belgium with the fraction of 0/4 for structural use was studied for comparison. This LWA was produced by sintering natural clay in a rotating kiln at a temperature of 1100°C.

2.2.2 Pelletizing Method

The Production Process of LWA is illustrated in **Figure 2.1.** The Production Process of LWA. LWA was produced by agglomeration technique using a stainless steel pan granulator with a diameter of 500 mm and a depth of 95 mm. The pan granulator parameters were chosen based on research by Baykal, et al., and were a speed of 60 rpm, a slope of 48° and pelletizing time of 20 minutes (Baykal et al., 2000). The agglomeration method was chosen in this research as it proved to provide LWA with sufficient strength, high water absorption which allows it to act as internal curing agent in concrete or mortar (Balapour et al., 2020; Bentz, 2009) and enhances the durability of resulting concrete and mortar (Hamidi et al., 2016). Casting a paste in moulds and crushing it into aggregates would give higher aggregate strength and reduce the high water absorption, but the aggregates would not meet the requirements for lightweight aggregate (Shon et al., 2013).

The weight ratio between alkali activator and fly ash of 0.25 was used based on previous research (Kockal and Ozturan, 2011; Shivaprasad and Das, 2018; Tang et al., 2017). Firstly, fly ash was added into the pan, followed by adding alkali activator by means of spraying for about 10 minutes. During the pelletizing process, the powder form of fly ash turned into granules after being bonded with alkali activator liquid. Finally, due to gravity and the movement of the pan, the granules that had reached a stable form fell out from the pan. After that, wet granules were dried in a curing room at a temperature of 20ºC and relative humidity of 95 ±5 % for 24 hours. This curing regime was chosen based on a previous report stating that geopolymer LWA cured at ambient temperature has similar properties with LWA cured at elevated temperature (Geetha & Ramamurthy, 2013). Dried LWA were sieved using a 2 mm sieve to remove the dust and finer particles. Later on, the sieved LWA with a particle size bigger than 2 mm were stored in a sealed plastic bag in the curing room for 28 days before being used.

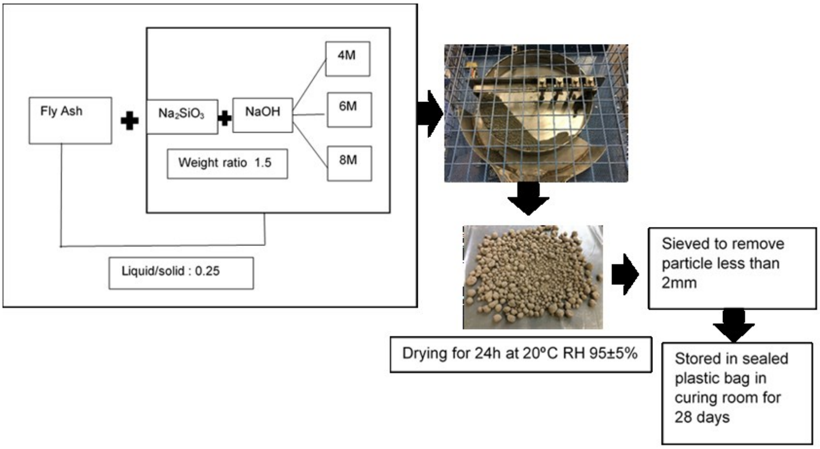

Figure 2.1. The Production Process of LWA

2.2.3 Physical Properties Testing of LWA

The water absorption over 24 hours (WA24) of all LWA was measured by following the guidelines of NBN EN 1097-6. The apparent particle density ρ_a (kg/dm^3), the saturated surface dry (SSD) density ρ_{SSD} (kg/dm^3) and the relative oven dried density ρ_{rd} (kg/dm^3) were measured according to the same standard.

Mercury Intrusion Porosimetry (MIP) was performed to investigate the pore size distribution of LWA. In order to dry the samples without damaging the microstructure of the sample, freeze-drying was applied. Dry LWA was immersed in liquid nitrogen for 5 minutes and then was put in the vacuum freeze dryer with a pressure of 0.1 Pa for two weeks until constant mass had been achieved. Afterwards, around 1.7 gram LWA was brought into the dilatometer of the MIP (Pascal 140 and 440 series, Thermo Fisher Scientific Inc) to be tested.

Particle size distribution of all LWA was determined according to Belgian standard NBN EN 12620. The standardized sieves column with the sizes of 63, 45, 40, 31.5, 22.4, 20, 16, 14, 12.5, 10, 8, 6.3, 4, 2, 1, 0.5, 0.25, 0.125 and 0.063 mm was used. The data obtained for the cumulative percentage of material passing through each sieve were analysed and plotted to a particle size distribution curve.

The strength of aggregates can be measured from its crushing resistance value. This test was performed by following Belgian standard NBN B11-205. Firstly, the dried aggregate sample was added into a metal cylinder mould with an inner diameter of 150 mm. After that, the no-friction plunger was put into the mould which was then loaded with 400 kN in 4 min and the load was maintained for 2 minutes before unloading.

Finally, the crushed aggregates were sieved with a 2 mm sieve. The crushing resistance value of the aggregate was the mass ratio between the crushed aggregate, which has a size bigger than 2 mm and the initial sample before loading.

X-ray diffraction (XRD) was used to determine the mineralogy of LWA and fly ash powder while quantitative XRD (QXRD) was performed using Rietveld analysis. Firstly, the LWA samples were oven dried at 105°C for 24 hours and pre-crushed. After that, around 10 wt% internal standard, in this case ZnO, was added to the pre-crushed aggregate samples. Then, the mixed pre-crushed aggregate and ZnO were ground in a Mc Crone mill (Retsch) to a size of around 50 microns. The XRD measurement was done with a D4 (Bruker) using a Co-Tube and equipped with a Lynx Eye detector. The settings were fixed divergence slits (0.5°), 0.04 rad Soller slits and a step size of 0.02.

The properties of sintered expanded clay (EC) LWA such as density and water absorption, were determined the same way as for the fly ash-based LWA for comparison.

2.2.4 Mortar Application

Mortar specimens were produced according to NBN EN 196 standard. The material needed for producing three mortar prisms with the size of 40x40x160 mm^3 is presented in **Table 2.1** Mix Design of Mortar Prisms. In this research, LWA with the fraction of 2/4 was used as a natural fine aggregate replacement in producing mortar. 16 % of the total volume of fine aggregate was replaced with LWA, while a water to cement ratio of 0.5 was used. This aggregate replacement percentage was chosen as the river sand used has a particle size distribution in which 16% belongs to the fraction 2 to 4 mm.

As LWA has high water absorption, LWA were treated to achieve SSD condition before use in order to limit the water absorption during mixing. Hence, the mass of LWA in oven dried condition (OD) and entrained water needed to achieve SSD condition of LWA are presented in Table 1. The mass of LWA OD needed in each mixture differs because the replacement rate used in this paper is based on volume and the densities of each LWA are different.

Table 2.1 Mix Design of Mortar Prisms.

Type	LWA OD 2/4 (g)	Entrained water (g)	Sand 2/4 (g)	Sand 0/2 (g)	Cement (g)	Water (g)
Reference	0	0	220	1130	450	225
FA 4M	120	34	0	1196	450	225
FA 6M	122	32	0	1196	450	225
FA 8M	125	29	0	1196	450	225
EC LWA	82	17	0	1251	450	225

Note: EC (Expanded Clay); OD (Oven Dried)

The fresh mortar samples were cured in a curing room at 20±2 ºC and a relative humidity (RH) of 95±5% for 24 hours before being demolded. The compressive strength and the bending strength of the mortar prisms were determined according to the standard NBN EN 196. This test was conducted after 7, 14 and 28 days of curing at 20±2 ºC and RH of 95±5%. The compressive strength was determined by averaging the value of 3 replicate samples.

2.3 Results and Discussion

2.3.1 Fly Ash Characteristics

Based on XRF test results, the fly ash used in this research could be categorized as fly ash class F as it contains more than 70 wt% silica, alumina, and iron oxide (**Table 2.2**). Furthermore, XRD quantification results also confirmed that the fly ash contains of 80.4% amorphous phase (**Table 2.3**). Previous research reported that fly ash with an amorphous content over 70% could form sufficient geopolymer gel in geopolymer paste production [25]. Thus, based on the XRF and XRD characterization of fly ash, this material meets the requirement to be employed as precursor in manufacturing alkali activated fly ash-based LWA.

Based on data displayed in **Figure 2.2**, the d_{50} of fly ash is 6.20 μm while its surface area is 0.83 m^2/g, which is sufficient for a geopolymer precursor.

Table 2.2 Chemical Composition of Fly Ash.

Compound	CaO	SiO_2	Al_2O_3	Fe_2O_3	K_2O	MgO	CuO	ZnO	SO_3	P_2O_5	TiO_2	LOI
% by Mass	3.79	57.40	26.16	5.98	1.88	1.43	0.02	0.02	0.98	0.88	1.13	0.32

Table 2.3 QXRD of Fly Ash.

Mineral	Mulite	Magnetite	Anhydrite	Perovskite	Sodalite	Amorphous
% Wt	11.1	2.9	0.3	0.3	0.4	80.4

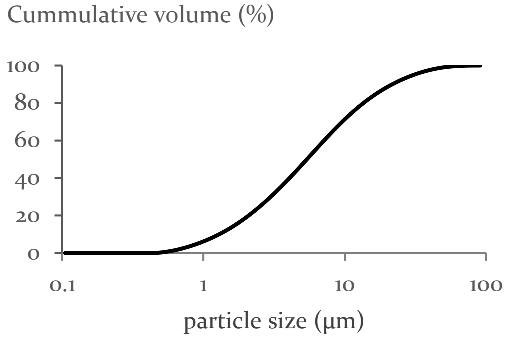

Figure 2.2. Particle size distribution of fly ash powder

2.3.2 Mass Density and Water Absorption

Based on data presented in **Table 2.4** it can be seen that the lightweight aggregates denominated as FA 8M have the highest apparent, oven dried and SSD density followed by FA 6M and FA 4M. The apparent density of LWA was in the range of 2.22-2.27 g/cm^3, oven dried density was in the range of 1.45 to 1.51 g/cm^3 and SSD density was in the range of 1.8 to 1.85 g/cm3. It can be noted that in the literature artificial aggregate that uses cement as a binder has an apparent density in the range of 2.0-2.3 g/cm^3, and 1.6-1.7 g/cm^3 for sintered fly ash-based geopolymer LWA (Görhan and Kürklü, 2014; Shivaprasad and Das, 2018)

The difference between apparent density and oven dried density indicated the porosity of the material. The open porosity of all samples is in the range of 33-34 %; which is similar to the research by Baykal et al. which reports open porosity in the range of 31-34 % for cold bonded fly ash LWA (Baykal et al., 2000)

The water absorption of all samples is in the range of 22-23 %. This result is similar to previous literature that uses cement as a binder which results in lightweight aggregates with a water absorption in the range of 18-47% (Gesoğlu et al., 2013; Gomathi and Sivakumar, 2015; Baykal et al., 2000). Compared to geopolymer LWA with a size fraction of 2/8, generated from mine tailings and fly ash class C , the water absorption obtained in this research is lower (Illikainen et al., 2017). Compared to expanded clay (EC) LWA, fly ash-based LWA in this research has a bit higher water absorption.

Based on the results of the density and water absorption test of LWA, it can be concluded that increasing NaOH concentration proved to slightly reduce the water absorption and the open porosity of LWA and increase its density. The decrease of water absorption in LWA is one indication that the amount of unreacted fly ash in LWA has decreased and more geopolymer gel has formed. It is reasonable as the alkali solution acts as silica and alumina dissolvent of fly ash during the geopolymer reaction, thus with a higher amount of OH^- in the highly concentrated NaOH, a more stable geopolymer gel can be formed (H. Xu and Deventer, 2000).

One way ANOVA was chosen to see the significant difference between different NaOH concentrations regarding the apparent density, oven-dried density, SSD particle density, porosity and water absorption of fly ash-based LWA. A confidence level of 95 % was applied. Based on the result it can be seen that increasing NaOH concentration only has a significant effect on the oven-dried and SSD density as for those variables an effective significance level (F-value) of less than 0.05 is found (**Table 2.5**).

Table 2.4 Mass Density and Water Absorption of LWA (n=3)

Test	FA 4M	FA 6M	FA 8M	EC LWA
ρ_a (g/cm^3)	2.22 ±0.02	2.23 ± 0.01	2.27 ± 0.01	1.25 ± 0.01
ρ_{rd} (g/cm^3)	1.45±0.01	1.47 ± 0.01	1.51 ± 0.01	0.99 ± 0.01
ρ_{ssd} (g/cm^3)	1.80±0.01	1.81 ± 0.02	1.85 ± 0.07	1.19 ± 0.01
Porosity (%)	34.66 ±2.14	34.12 ± 0.75	33.42 ± 0.21	20.85 ± 0.09
WA_{24} (%)	23.92±1.79	23.23 ± 1.14	22.08 ± 0.26	21.14 ± 0.3

Table 2.5 The Result of ANOVA test regarding the effect of NaOH concentration on the properties of LWA

Property of LWA	F-value
Apparent particle density (ρ_a)	0.14
Oven Dried Density (ρ_{rd})	0.003
SSD particle density (ρ_{ssd})	0.001
Porosity	0.544
Water absorption	0.199

2.3.3 Porosity

The MIP intrusion curves for all the LWA have two major peaks located at a pore size between 0.01 to 0.2 µm and at the pore size between 2 to 15 µm (**Figure 2.3**a). The highest intensity of dV/dLog(d) occurred for FA 8M followed by FA 4M and FA 6M. Based on **Figure 2.3** it can be seen that all the LWA have a threshold diameter in the range of 10-15 µm, but there is a difference in intruded volume. FA 4M shows the highest intruded volume followed by FA 6M and FA 8M. Only a small difference can be found in the intruded volume of FA 6M and FA 8M. The IUPAC guidelines were used to classify the pore size of LWA into mesopores (2-50 nm) and macropores (bigger than 50 nm) (IUPAC Commission on Colloid and Surface Chemistry, 1990). It can be seen in **Figure 2.3** that the amount of macropores in the FA 4M sample is higher compared to the other LWA. The highest amount of mesopores and the lowest volume of macropores occurred in FA 6M. Moreover, there is only a negligible difference between the pore types of the FA 6M and FA 8M samples.

The MIP results show a similar trend as water absorption and open porosity data presented in **Table 2.4**. Increasing NaOH concentration proved to decrease the water absorption and the open porosity of LWA. However, the differences in porosity obtained from the water saturation test were not as significant as the differences obtained from MIP. This presumably is because, under the high pressure, mercury could break the LWA's fragile pore walls and could penetrate into the closed pores which resulted in high porosity measurements.

The high intruded volume and high amount of macropores in FA 4M indicated that FA 4M is more porous and fragile. The fragile structure of FA 4M could occur due to the uncompleted geopolymer reaction. Thus there was some unreacted fly ash in the FA 4M sample which usually made it fragile and containing many voids. Xu et al (2000) also mentioned that sufficient amount of OH^- is needed in order to dissolve aluminium and silica in fly ash into alumina silica gel.

The appearance of numerous peaks in the pore size distribution curve of the LWA is typical for a porous material. In previous research Tziviloglou also found similar pore distribution pattern for expanded clay aggregate called Liapor (Tziviloglou, 2018). The multiple peaks in the pore distribution curve indicated that there is random micro-cracking due to the pressure when mercury penetrates into the pores (Cook and Hover, 1999).

Compared to sintered LWA that was generated from fly ash and sintered expanded clay in the literature, the threshold diameter obtained in this study is larger (Kockal and Ozturan, 2011; Korat, Ducman, Legat, and Mirtič, 2013; Tziviloglou, 2018). This could be expected as the sintering process will close the pores (Kockal and Ozturan, 2011).

In summary, based on the MIP test it can be concluded that a significant decrease in porosity only occurs when the concentration of NaOH is increased from 4M to 6M. Increasing the NaOH concentration from 6M to 8M did not provide a significant difference in the pore properties of the resulting LWA.

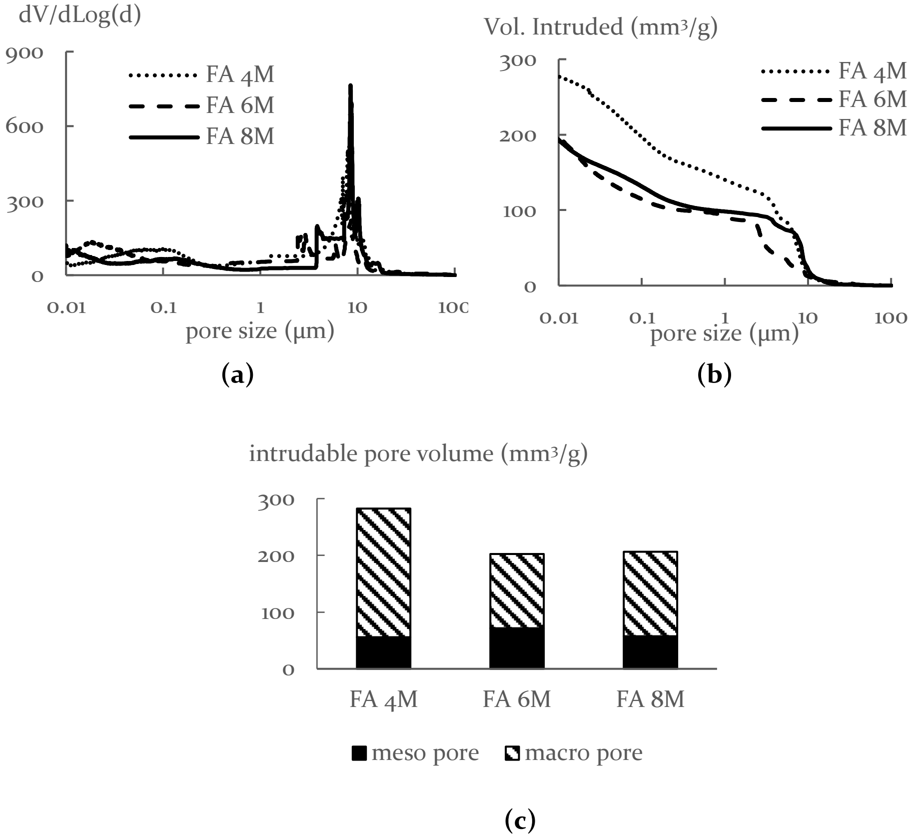

(a) (b)

(c)

Figure 2.3. Pore size distribution of LWA, (b) cumulative intruded volume of LWA, (c) types of pore

2.3.4 Particle Size Distribution

Based on particle size distribution data that are displayed in **Figure 2.4**, FA 6M has more fine particles compared to the others. The FA 6M sample has approximately 9% pellets that have a diameter of less than 2 mm, while FA 8M has 6% and FA 4M has 2%. For all samples, less than 5% of pellets have a particle size bigger than 10 mm. These big pellets usually have an irregular shape because they are not perfectly compacted or sticking to each other during the pelletizing process. This result is quite similar to previous research by Tang et al. in which approximately 7% of pellets were obtained with a diameter of less than 2 mm and 5% pellets with a diameter bigger than 10 mm for cold bonded bottom ash aggregate (Tang et al., 2017).

There is only a slight difference between the curves of FA 6M and 8M samples. However, according to NBN EN 12620 about the definition of minimum and maximum aggregate size, FA 8M and FA 4M meet the requirements of an aggregate 2/10, while FA 6M is classified as aggregate 2/8. Moreover, it can also be noted that all of the LWA have a larger content of big particles compared to natural aggregate with the fraction of 2/8.

From the result above, it can be concluded that NaOH concentration has only a small effect on the pellets' size according to the similarity of the particle size distribution of all LWA. This result is in good agreement with previous research by Shivaprasad and Das who found that the formation of geopolymer pellets depends more on liquid content rather than the Na_2O content (Shivaprasad and Das, 2018). This is expected, as the early stage of pelletization is primarily a physical process and the amount of liquid plays an important role in the pellet formation. The chemical reaction of the binder will influence the later strength development stage of the pellets. If the NaOH concentration in the liquid is very high, it will react with fly ash quite quickly and chemically binds the material together before proper pellets can be formed leading to problems in the manufacturing.

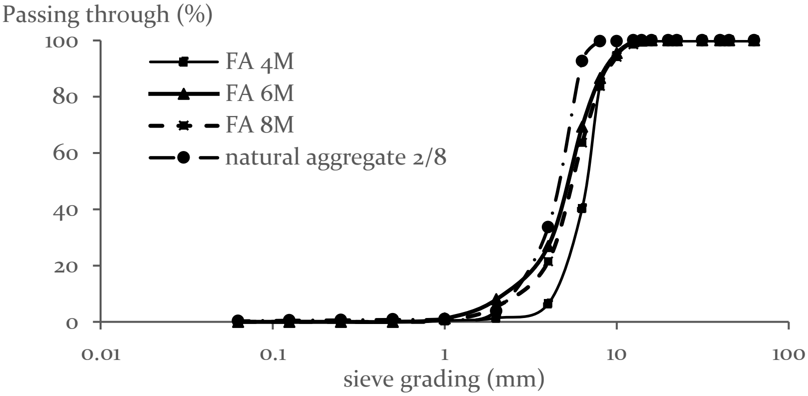

Figure 2.4. Particle size distribution of LWA

2.3.5 Crushing Resistance Value

Based on the results presented in **Table 2.6**, it can be concluded that increasing the molarity of NaOH up to 6 Molars brought a positive impact to aggregate strength. However, there is only less than 3% difference in crushing resistance value among all samples. This result is entirely unexpected, as a higher concentration of NaOH was expected to give a higher crushing value. This slight difference was presumably due to a difference in the particle size of LWA. Furthermore, as some of the LWA were compacted after being tested and formed bigger particles that could not be broken up by sieving, it is quite difficult to determine its crushing value. Based on the literature, it can be noted that the crushing strength of LWA increases with the increase of particle size (Gesoğlu et al., 2013). However, LWA in this research has a very small size compared to LWA in the literature which mostly has a fraction of 4/16 (Gesoğlu et al., 2007; Güneyisi et al., 2013). Hence, it could be concluded that the crushing resistance test that was applied in this research is not so suitable for LWA of small particle size.

Compared to bottom ash and limestone aggregate, the crushing resistance value of this LWA is almost equal to limestone aggregate which has a particle size of 2/6 and a crushing strength of 63.8% (Van den Heede et al., 2016). Compared to sintered expanded clay LWA, fly ash LWA in this research has a higher crushing resistance. Due to the different standard methods that have been used to determine the strength of aggregates in literature, it is quite difficult to compare the results obtained in this research with other crushing resistance values for LWA in the literature.

Table 2.6. Crushing Resistance (CR) value of LWA (n=3)

Type	**CR Value (%)**
FA 4M	61.4 ± 0.2
FA 6M	62.8 ± 0.7
FA 8M	60.0 ± 0.9
EC LWA	23.6 ± 1.7

2.3.6 Mineralogy of LWA

Based on Quantitative X-Ray Diffraction (QXRD) analysis results presented in **Table 2.7**, the main phases in LWA are Amorphous (82-83%), Quartz (3.6-4%), Mullite (6.2-6.9%), Magnesioferrite (2.1-2.2%), Gaylussite (1-2.2%), and Hematite (1-1.2%).

There is no significant difference in the quantities of amorphous and crystalline phases among the LWA samples. This result is not in accordance with the initial expectation that increasing the concentration of NaOH in the mixture will lead to an increase of the amorphous phase in LWA as there will be more OH^- to react with fly ash to form alumina-silica gel (H. Xu and Deventer, 2000). However, a similar result was also obtained in the literature which investigated the microstructural properties of dry mixed geopolymer with low alkali activator concentration (Chen et al., 2018). The reason for this behaviour is likely the fact that both the fly ash as well as the alumino-silicate (N-A-S-H) gel that forms are X-ray amorphous and cannot be differentiated with the Rietveld method. It is likely that the amount of gel increases with an increase in NaOH concentration, while the amount of unreacted fly ash is reduced. But since both phases are X-ray amorphous the total amount of amorphous content that is measured remains unchanged.

It is also possible that higher concentrations of NaOH only change the composition of the N-A-S-H gel and do not generate more geopolymer. Other methods such as SEM/EDS should be used to gain more insight into the composition.

Table 2.7. XRD Quantification of Fly ash-based LWA

Mineral	FA 4M	FA 6M	FA 8M
Quartz	3.6	4.0	4.0
Mullite	6.2	6.9	6.5
Magnesioferrite	2.2	2.2	2.1
Calcite	0.3	0.7	0.4
Gaylussite	2.2	1.7	1.0
Sodalite	0.1	0.8	0.2
Gupeiite	0.1	0.1	0.1
Sillimanite	1.0	1.0	1.0
$AlFe_3$	0.2	0.2	0.2
Hematite	1.0	1.2	1.1
Amorphous	83.0	82.0	83.5

2.3.7 Properties of Resulting Mortar

Based on mortar compressive strength data displayed in **Figure 2.5**, FA 8M provided the highest compressive strength at an age of 28 days followed by FA 6M and FA 4M. Until the age of 14 days, the mortar with FA 8M did not tend to have the highest compressive strength, but its compressive strength increased more rapidly when approaching the age of 28 days. It can also be noted that the compressive strength of all mortar containing fly ash LWA is developing slower compared to the reference sample.

Replacing 16% by volume of fine natural aggregate with fly ash LWA caused a reduction in compressive strength of the resulting mortar. The sample containing FA 8M LWA had the lowest compressive strength reduction. It has less than 5% reduction of strength at 28 d with 16% replacement ratio.

The bulk density of mortar at 28 days of age had a directly proportional relationship with its 28 days age compressive strength result (**Figure 2.6**). It is also observed that the FA 8M sample had the highest bulk density compared to the other samples with LWA. A quite significant difference in the average bulk density of FA 6M and FA 8M occurred. However, the standard deviation of sample FA 6M is quite high, and its upper limit was almost similar to the upper limit for the FA 8M sample's bulk density.

The compressive strength and bulk density result of mortar containing LWA is not well correlated with the properties of the LWA such as water absorption, porosity and XRD results. Samples containing FA 6M were expected to have similar compressive strength as samples containing FA 8M, as the used LWA has similar properties. Surprisingly, mortar containing FA 8M has higher 28 days compressive strength. The FA 8M LWA has slightly lower water absorption relative to the FA 6M LWA. It corresponds to lower amount of entrained water was added during the mortar production. The lower amount of water entrained could lead to higher bulk density and higher compressive strength of the resulting mortar.

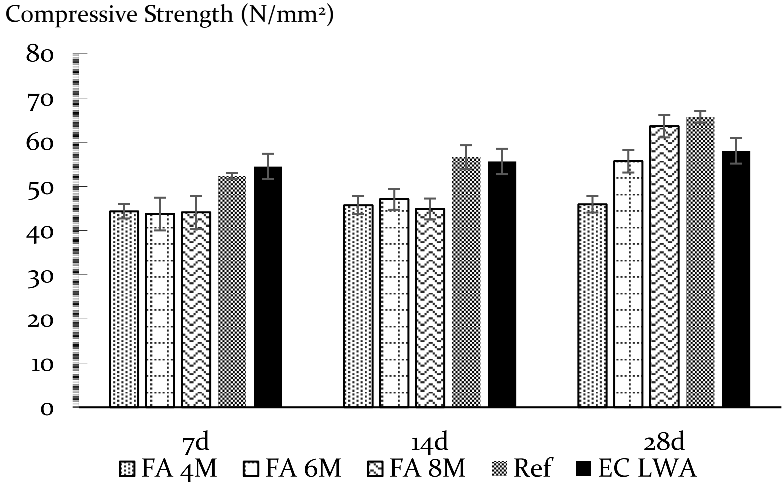

Figure 2.5. Compressive Strength of Resulting Mortar (n=9)

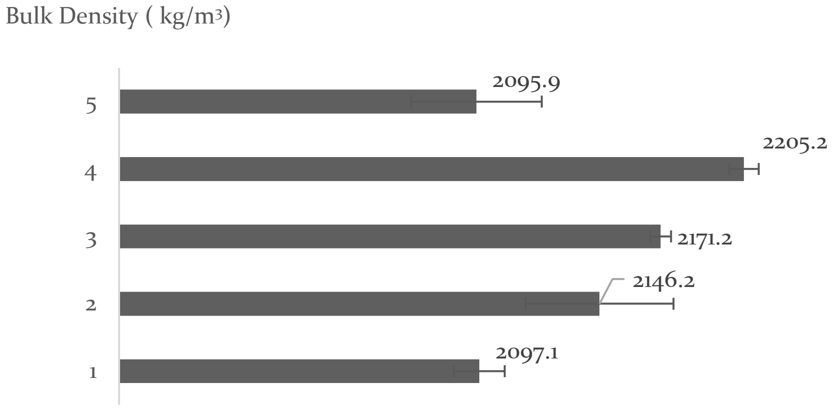

Figure 2.6. Bulk Density of 28d old Mortar (n=3)

2.3.8 Comparison with Sintered Expanded Clay Based LWA

Based on data presented in **Table 2.4**, it can be seen that the apparent, oven-dried and SSD particle density of the expanded clay LWA is lower than the fly ash-based LWA. However, expanded clay LWA has a slightly lower water absorption value compared to fly ash LWAs. In addition, expanded clay LWA has lower crushing strength compared to fly ash LWAs (Table 4). No significant strength improvement with age was observed in EC LWA mortar samples. The compressive strength of 7 days old mortar was almost the same with the 28 days' compressive strength. Furthermore, with the same replacement ratio, the 28 days compressive strength of mortar containing expanded clay LWA is a bit higher than the compressive strength of mortar containing FA 6M LWA (**Figure 2.6**). The entrained water inside the pores of fly ash-based LWA and the unreacted fly ash attached to its surface could induce hydration at a later age. This mechanism could be the reason behind the gradual strength increasing in fly ash-based LWA at the age of 28 days.

The fact that expanded clay aggregate leads to high compressive strength when applied in the mortar even though it has a low crushing strength could be due to its low open porosity. The open porosity of expanded clay LWA is 21 %. It is lower compared to fly ash-based LWA. Indeed, expanded clay LWA was produced with a sintering process that increases the amount of closed pores, which improved the mechanical strength of its resulting mortar (Kockal and Ozturan, 2011).

Comparing to expanded clay LWA, fly ash-based LWA produced in this research has adequate strength. Fly ash-based LWA has a bit higher density and water absorption, but when it was applied in the mortar, it delivers similar compressive strength with the one containing expanded clay LWA (**Figure 2.6**). The low bulk density but high compressive strength of the resulting mortar containing EC LWA is an indication of the appearance of closed pores resulting from the sintering process in the production of EC LWA which could enhance the mechanical properties (Güneyisi et al., 2013). Indeed mortar containing EC LWA delivers slightly better properties compared to fly ash-based LWA. But, one should also take into account that more energy is needed to sinter the expanded clay LWA during its production compared to the production process of fly ash LWA.

2.4 Conclusions

This chapter presents the effect of NaOH concentration on mechanical and physical properties of fly ash-based alkali activated LWA. With increasing NaOH concentration, the mass density of LWA slightly increased while the water absorption slightly reduced. Increasing the NaOH up to 6M also proved to decrease the intruded volume measured by MIP, the amount of macropores and the total porosity of LWA. Irrespective of the NaOH concentration, all LWA had similar critical pore diameter in the range of 10-15 µm. The concentration of NaOH only had a small effect on the particle size distribution of LWA. There is some unexpected trend occurring in crushing resistance strength, FA 6M has a higher CR value than FA 8M. The difficulties to determine the real crushed part of the rather fine LWA after the CR test might be the cause, which indicates that other strength testing methods should be found.

A maximum compressive strength of 64 N/mm^2 at 28 days and a strength reduction of less than 5% in comparison with a mortar with natural sand could be achieved by mortar containing 16 Vol.-% of LWA 8M in the sand fraction. It can be suggested that the minimum NaOH concentration to produce fly ash-based LWA with good properties is 6M. The properties of fly ash-based LWA activated with NaOH 6M also meet the requirement to become a bacteria protector. It has a pore size in the range that bacteria could penetrate (10-15µm), sufficient water absorption higher than 20 %, and when applied into the mortar, the strength decrease caused by this LWA is at an acceptable level.

Compared to the properties of commercial expanded clay LWA, fly ash-based LWA generated in this research had acceptable properties and could be a viable alternative, because less energy is needed for their production.

Chapter 3. Properties of Alkali Activated Lightweight Aggregate Generated from Sidoarjo Volcanic Mud (Lusi), Fly Ash and Municipal Solid Waste Incineration Bottom Ash

This chapter was redrafted after:

Risdanareni, P., Villagran, Y., Schollbach, K., Wang, J., De Belie, N. (2020). *Properties of Alkali Activated Lightweight Aggregate Generated from Sidoarjo Volcanic Mud (Lusi), Fly Ash and Municipal Solid Waste Incineration Bottom Ash.* Materials, 13, 2528
Doi : https://doi.org/10.3390/ma13112528

3.1 Introduction

As mentioned in Chapter 2, beneficiating waste material in the production alkali activated lightweight aggregates could become an alternative way to up scale the consumption of waste material. In this chapter two alternative waste materials besides fly ash named Sidoarjo volcanic mud (Lusi) and municipal solid waste incinerator bottom ash (MSWI BA) were chosen as binder candidates to produce alkali activated LWA.

Sidoarjo volcanic mud (Lusi) is an indigenous Indonesian material resulting from a volcanic eruption at Sidoarjo city, East Java, Indonesia on May 2006. Until now, as much as 50 million m^3 of this mud has been placed in a giant embankment with an area of 640 ha. This eruption caused a massive loss of habitable land at Sidoarjo and was recognized as a national disaster in Indonesia (Deguchi, 2009). Therefore, the Indonesian government has been looking for a suitable solution to utilize this abundant material. Since 2007 several attempts have been made by Indonesian researchers to utilize Lusi as a construction material, e.g., as a cement substitute or precursor for geopolymer material due to its high silica and alumina content (Ekaputri, 2015; Hardjito et al., 2012; Triwulan and Ekaputri, 2015). It is reported that cement production in Indonesia reached 63 million tons in 2019 (Cembureau, 2017). If the maximum replacement rate of cement by Lusi was 40 %, around 25 million ton Lusi could be used in this application (Hardjito et al., 2012). On the other hand, beneficiating Lusi for use in LWA would be an alternative option. Indeed the global production of LWA is low compared to cement production. It only reaches 1% of the total aggregate demand, which is less than 1 billion ton per year (Freedonia, 2012). However, the global demand of LWA will grow quite rapidly along with the increasing demand of lightweight structural concrete, which is expected to have an annual increase of 7.1% (Freedonia, 2012).

Other abundant raw material sources are coal combustion fly ash and municipal solid waste incineration bottom ash. In 2015, it was reported that the global production of coal combustion products (CCP) such as fly ash was around 780 million metric ton which is expected to increase with 1.6% each year (Heidrich et al., 2013). Although more than 50% of those CCP was successfully utilized, there is still a huge amount of fly ash available. On the other hand, around 130 million ton municipal solid waste (MSW) are generated each year around the world (Joseph et al., 2018). Most of the non-hazardous fraction of this MSW is co-incinerated, with the heat produced being converted into electrical energy. The largest portion of incineration plant by-products is bottom ash. This is mostly landfilled, which is not a good option as it can result in ground water pollution due to its heavy metal content (Oehmig et al., 2015). It is also reported that treated MSWI bottom ash which is rich in silica and alumina could be a potential alternative supplementary cementitious material in concrete production (Joseph et al., 2018). Combining fly ash and MSWI bottom ash as precursor in geopolymer production was also proven to improve the properties of resulting geopolymer concrete (Wongsa et al., 2017). Hence, Lusi, fly ash, and MSWI bottom ash are interesting candidates to mass produce LWA.

Transforming fly ash (FA), municipal solid waste incineration bottom ash (MSWI BA), and Lusi into artificial lightweight aggregate is not a new technique. However, most of the research was focused on sintering and cold bonding with cement (Gesoğlu et al., 2007; Gomathi and Sivakumar, 2015; Tang and Brouwers, 2017; Tang et al., 2017). There are limited studies on applying alkali activation to produce LWA even though this binding system can improve the properties of the resulting LWA (Görhan and Kürklü, 2014a; Shivaprasad and Das, 2018).

In an alkali activated binder system, the type of alkali activator (H. Xu and Deventer, 2000), the concentration (Chindaprasirt et al., 2009; Görhan and Kürklü, 2014; Heah et al., 2012), the curing regime (Hardjito, 2005; Salman et al., 2014), and the type of precursors (González-corrochano et al., 2016; Tang and Brouwers, 2017; Thomas and Harilal, 2015) were reported as important parameters for the properties of the resulting geopolymer products such as paste, mortar, concrete and LWA. Based on literature, the dissolution rate of material which is rich in silica and alumina is higher in NaOH than in KOH solution (H. Xu and Deventer, 2000). As Lusi, fly ash, and bottom ash are known for their high silica and alumina content, NaOH was chosen as alkali activator in this study. In the literature, the ideal concentration of NaOH for producing geopolymer paste is reported to be in the range of 8-12 M (Hamidi et al., 2016; Hardjito, 2005; Heah et al., 2012). On the other hand, Gorhan et al. showed that the optimum concentration of NaOH for better properties of fly ash geopolymer paste is 6M (Görhan and Kürklü, 2014a). The weight ratio between liquid/solid in the current study is lower compared to geopolymer paste, as in LWA production the mixture should be a bit drier so that the granule can roll and would not stick to the pan granulator. A lower concentration of NaOH was also required to avoid workability issues during the pelletization process. In the previous chapter, NaOH with the concentration of 6 molars together with sodium silicate was recommended as suitable alkali activator in the production of fly ash-based LWA. Regarding the similar chemical compounds of Lusi and MSWI BA, rich in alumina and silica like fly ash, the NaOH concentration of 6 molars was also chosen to produce LWA with Lusi and MSWI BA as binder.

Summarizing, the objective of this part of the research is to find an alternative binder to produce alkali activated LWA besides fly ash for later use as bacterial carrier in self-healing concrete production. Several properties were investigated, such as water absorption, density, particle size distribution, heat evolution of the precursor during reaction with the activator, pore size distribution, crushing resistance, mineralogical composition and morphology. In order to see the feasibility of using this novel LWA as bacterial carrier in self-healing concrete production, the viability of *Bacillus sphaericus* cells after encapsulation into LWA was also monitored.

The LWA was also applied in mortar as natural fine aggregate substitution. The compressive strength and the bulk density of mortar containing LWA were determined. In the end, the properties of LWA and mortar containing LWA were compared to commercial expanded clay LWA in order to show the possibility of applying this novel LWA in the construction industry.

3.2 Materials and Methods

3.2.1 Materials

Fly ash, MSWI bottom ash, and Sidoarjo Mud (Lusi) were utilized as a binder. The fly ash (FA) used were the same as mentioned in section 2.2.1. MSWI BA with a fraction of 2-6 m obtained from a municipal solid waste incinerator (Indaver, Belgium), had been pre-treated at the plant with magnetic and eddy current separation treatment to remove its ferrous content. The MSWI BA were then dried for 24 hours at 105°C and ground into powder using a ball mill. In order to remove the elemental aluminum, the MSWI BA ashes were then slowly grinded and particles larger than 142.5 µm were removed by means of sieving. Lusi, an indigenous volcanic mud from Indonesia was oven-dried for 24 hours at 105°C, ground into powder, and then calcined at 800°C for 6 hours to activate the silica and alumina oxide in the Lusi.

The powder form of sodium hydroxide (NaOH) with purity of 98% (VWR International Belgium Bvba) and liquid form of sodium silicate (Na_2SiO_3)

(VWR International Belgium Bvba) which contains 26.3% silica, 7.9% sodium oxide, and 65.8% water were used as an alkali activator in this research. NaOH solution with a concentration of 6 M was obtained by dissolving 240 g of NaOH powder in 1 liter of distilled water one day before use. Later on Na_2SiO_3 was mixed with the NaOH 6M solution with a weight ratio of 1.5. Finally, the mixed alkali activator was left at room temperature for one day prior to use.

Vegetative cells of *Bacillus sphaericus* LMG 22257 (Belgian Co-ordinated Collections of Micro-organisms, Ghent) were used as healing agent. The cells were cultured in sterile urea yeast extract (UYE) medium with concentration of 20 g/l for 24 hours on an incubator shaking table (speed 120 rpm, temperature 28°C). The cells pellets were separated from the medium by centrifuging the mature culture in a centrifuge machine for 7 minutes with the speed of 15050 g. Finally the cells pellets were re-suspended in 5 g/l yeast extract solution. The final concentration of cell suspension was 2×10^9 cells/ml.

Commercial expanded clay (EC) based LWA (Argex NV) was used as reference. This LWA was produced by sintering natural clay at a temperature of 1100°C in a rotating kiln. The nominal size of EC LWA is 0/4.

A Portland cement type I 52.5 (Holcim) was used as binder in mortar application while standard river sand with the fraction of 0/4 was used as fine aggregate.

3.2.2 Pelletizing Method

The values for the parameters in LWA manufacturing, such as the diameter, the slope angle, and the speed of the rotating pan, were chosen based on previous research by Baykal (Baykal, 2000). The pan granulator (EIRICH, TR04) had a diameter of 80 cm, the slope of the pan was set to 48°, and the speed of 60 rpm was applied.

Around 5 kg of dry binder powder was added into the rotating pan followed by spraying alkali activator liquid continuously. After approximately 20 minutes, the wet pellets that formed fell out of the pan automatically (**Figure 3.1**). The wet pellets were dried for 24 hours in a curing room which had a temperature of 20±2 ºC and a relative humidity of 95 ±5 %. They were then stored in a sealed plastic bag until the testing date.

The amount of alkali activator liquid that was added to the mixture was varied, depending on the type of raw material used as binder. The amount of liquid needed was determined experimentally for each raw material based on its water absorption and the pellets consistency. The mixture proportion of each LWA is presented in **Table 3.1**, while the illustration of the granulation process using a pan granulator is displayed in **Figure 3.1**.

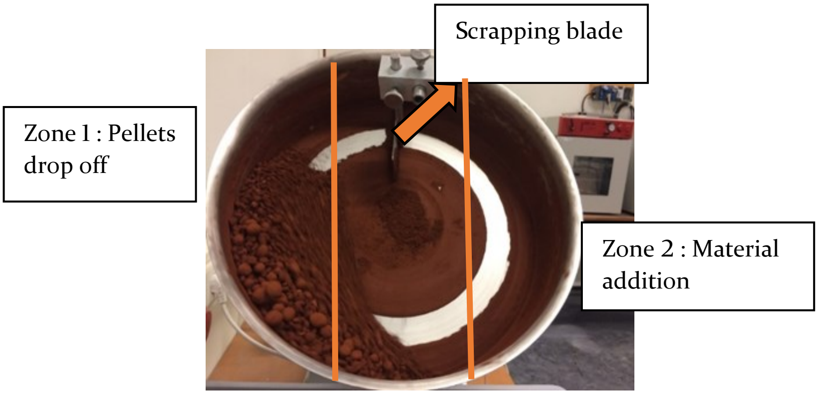

Figure 3.1. The Production Process of LWA.

Table 3.1. Liquid/solid weight ratio of LWA (n=5).

Sample Codes	**liquid/solid**
FA 6M	0.25 ± 0.01
Lusi 6M	0.51 ± 0.01
MSWI BA 6M	0.26 ± 0.01

3.2.3 Characterization of Sample

A laser diffraction apparatus (Malvern mastersizer 2000) was used to measure the particle size distribution of all the binder powders after dispersion in isopropanol (VWR International Bvba). The absorption index of all raw materials was 0.1, while the refractive indexes for fly ash, MSWI bottom ash and Lusi were 1.67, 1.70 and 1.57, respectively. For FA and MSWI BA the refraction index was obtained from the databased available in the software. The refraction index of Lusi was assumed to be similar with materials with high silica oxide content that are available in data base. The obscuration level was maintained between 12 and 15. During the measurements, the dispersant and the sample were stirred with the speed of 800 rpm. The d_{50} values were obtained as the average value of 6 measurements.

The leaching of potential heavy metal in raw materials powder was examined according to EN 12457-2. Fly ash, MSWI BA and Lusi powder were put in a falcon tube and immersed in demineralized water with liquid to solid ratio of 10/1. The mixtures were then left on a shaking table with speed of 120 rpm for 24 hours. Afterwards, the samples were filtrated and mixed with nitric acid 10 mol/l (Merck KGaA, Germany)). Finally these filtrates were analyzed for elemental composition with ICP-OES (inductively coupled plasma-optical emission spectrometer; Spectroblue from Sysmex).

The particle size distribution of LWA was determined using standard sieves according to NBN EN 12620. A sieves column with standardized sieves with sieve openings of 63, 45, 40, 31.5, 22.4, 20, 16, 14, 12.5, 10, 8, 6.3, 4, 2, 1, 0.5, 0.25, 0.125 and 0.063 mm was used. The cumulative mass percentage of LWA passing through each sieve was measured and then plotted in the particle size distribution graph.

The chemical composition of the binders was determined by X-ray Fluorescence (XRF) measurements. These tests were carried out using a Rigaku NeXCG equipment on a loose powder sample. The excitation is provided by a close-coupled 50 KV/50 W Pd-anode end-window X-ray tube. The tube was fitted with a shutter to maintain its stability and durability. Finally, the spectra from the sample were recorded by a silicon drift detector (SDD). The chemical compositions of raw materials were obtained as the average of three measurements.

Heat evolution of fresh LWA was monitored using an isothermal calorimeter (Tam Air instruments). All raw materials were put in the climate room with a temperature of 20 ± 2 ºC one day before use. Around 10-15 g of precursor was mixed with alkali activator in a glass ampoule. The weight ratio between liquid and solid of FA 6M, Lusi 6M and MSWI BA 6M was 0.25, 0.51 and 0.26, respectively, like for the LWA as shown in Table 1. The ampoules filled with paste samples were then placed into a TAM Air isothermal calorimeter and measured at 20ºC for 7 days.

The apparent density (ρ_a), the oven dried density (ρ_{OD}), the water saturated surface-dry density (ρ_{SSD}), and water absorption over 24 hours (WA_{24}) were determined by following the NBN EN 1097-6 (2013) standard. Around 500 gram dried LWA were immersed in water in a calibrated flask. After that, the flask was stacked in a water bath for 24 hours and was weighed (M_2). Later on the LWAs were dried until reaching saturated surface dry condition and were weighed (M_1). The SSD LWA then were dried in an oven with temperature of 110±5°C until reaching a constant mass and were weighed again (M_4). Meanwhile, the flask was refilled with water to the same volume as before and was weighed (M_3). Finally, the apparent density (ρ_a), the oven dried density (ρ_{OD}), the water saturated surface-dry density (ρ_{SSD}), and water absorption over 24 hours (WA_{24}) were calculated using Equation 3.1-3.4 .

$$\rho_a = \rho_w \frac{M_4}{M_4-(M_2-M_3)} \qquad \text{(Equation 3.1)}$$

$$\rho_{od} = \rho_w \frac{M_4}{M_1-(M_2-M_3)} \qquad \text{(Equation 3.2)}$$

$$\rho_{SSD} = \rho_w \frac{M_1}{M_1-(M_2-M_3)} \qquad \text{(Equation 3.3)}$$

$$WA_{24} = \frac{100\times(M_1-M_4)}{M_4} \qquad \text{(Equation 3.4)}$$

Where ρ_w is the density of water measured at 20°C which is 998 kg/m^3. The values reported for density and water absorption are the average values from three replicates, while the standard deviation on individual values was calculated as well.

Mercury Intrusion Porosimetry (MIP) was performed to analyze the pore size distribution of LWA. In order to dry the samples without damaging the microstructure, freeze-drying was applied (Snoeck et al., 2014). LWA was immersed in liquid nitrogen for 5 minutes and put in the freeze dryer vacuum chamber with a pressure of 0.1 Pa for two weeks until constant mass was achieved. Afterwards, around 1.7 g LWA was filled into the dilatometer and was tested in a Pascal 140 and Pascal 440 machine. The pressure was then increased with the speed of 5-17 MPa/min. Finally, the pressure needed for mercury to penetrate into the pores of the sample is expressed in Equation 3.5 (Washburn, 1921).

$$p = -4\gamma\cos(\theta)/d \qquad \text{(Equation 3.5)}$$

P is the pressure needed, γ is the surface energy of mercury (483 mN/m), θ is the contact angle (142º) and d is the pore diameter of the sample. In order to avoid damaging the microstructure of the sample, the maximum pressure was limited to 200 MPa.

The mechanical properties of LWA were assessed by performing a crushing resistance test according to NBN B11-205. A cylindrical steel container with a diameter of 75 mm was filled with oven-dried LWA. After that, the no-friction plunger was put on the top of the container and was forced down with a speed of 0.42 kN/s until 100 kN was reached. This load was maintained for 2 minutes. Later on, the crushed aggregates which had a diameter larger than 2 mm were separated by means of sieving. Finally, the crushing resistance value of the aggregates was the mass ratio between the crushed aggregate with a fraction bigger than 2 mm over the initial weight of the sample.

The mineralogy of LWA was assessed by X-ray diffraction (XRD). For the quantitative XRD (QXRD), the Rietveld method with zinc oxide (ZnO) as an internal standard was used. Firstly, the LWA sample was pre-ground, then mixed with ZnO (10% wt). The pre-ground LWA and ZnO mix was ground all together in a Mc Crone mill (Retsch) until a size of about 50 microns was reached. A D4 (Bruker) with a Co-Tube ($K\alpha_1$ 1.7901 Å, $K\alpha_2$ 1.7929 Å) and Lynx eye detector was used for the measurement. The settings were fixed to divergence slits (0.5°), 0.04 rad Soller slits, and a step rate of 0.02 °2θ/s.

LWA granules were observed by SEM. The granules were immersed in methanol to stop the hydration followed by drying in a 40°C oven for 24 hours or until they reached constant weight. The dried LWA were then impregnated in epoxy solution under vacuum condition. The impregnated samples were then dried in an oven at a temperature of 40°C for 24 hours. Finally epoxy impregnated samples were polished with SiC paper from coarser to finer (320, 500, 1200 and 2400) for approximately 1.5 minutes each, followed by polishing with diamond paste 3 and 1 µm for 4 minutes each. The polished samples were then dried in a 40°C oven for 24 hours. The preparation step was completed by applying carbon coating.

The back scattered electron (BSE) images of LWA were obtained with Jeol JSM-7600F Field Emission Scanning Electron Microscope (FESEM) equipped with AZtecEnergy software [Oxford Instruments (2014)] for EDS mapping. EDS mapping and point analysis was performed for following elements: Ca, Na, Al, Fe and Si. In each sample mapping was performed in 3 different locations, by taking at least 16 point at each location to be analyzed.

3.2.4 Activity of Bacteria after Encapsulation Into LWA

The viability of bacteria after encapsulation was monitored by performing Total Ammonium Nitrogen (TAN) Nessler test (Fujita et al., 2000). During the urea hydrolysis, bacteria could decompose urea into 2 mols ammonium ions and 2 mols of carbonate. This carbonate will, later on, react with calcium and form calcium carbonate that can heal the concrete crack. Thus measuring the ammonium produced by bacteria after encapsulation is considered as an indirect method to measure the calcium carbonate precipitation.

The first step of the encapsulation procedure is introducing pressure -0.8 bar to the sterile LWA sealed in a penicillin bottle. The cells suspension were then injected into the bottle under vacuum condition. The vacuum condition was maintained for 30 minutes. The amount of cells injected depends on the water absorption of the LWA. The next step is introducing pressure of +1 bar into the bottle. The pressure was maintained for 24 hours. After 24 hours, the LWA was transferred into a sterile flask and immersed in urea solution 20 g/l (15 g LWA into 50 ml urea solution). The pH and the TAN of immersed LWA in urea solution were then monitored for 6 hours. The decomposed urea was calculated based on Equation 3.6 (J. Wang, Jonkers, et al., 2017)

$$DU = TAN \times dilution \times Mr \frac{Urea\ (\frac{60g}{mol})}{2Nitrogen\ (2x14\frac{g}{mol})} \qquad \text{(Equation 3.6)}$$

Where DU is the decomposed urea (g/l), Mr is the relative molecule mass, TAN is measured with a spectrometer at wavelength 425 nm, while the dilution used is 2.5.

3.2.5 Application of LWA in the Mortar

In this research, sand with a fraction of 2/4 was substituted by volume with LWA of the same fraction to produce mortars. In order to avoid detrimental effects of the high water adsorption of LWA during the mortar production, LWA was treated to obtain saturated surface dry condition before it was added into the mortar mixture. Two aggregate replacement rates were applied in this part (16% and 30%) . The mix design of each mortar including the amount of LWA in oven-dried condition and the absorbed water needed to achieve SSD condition, are presented in **Table 3.2**. In general, the weight ratio composition between sand and LWA 2-4 mm was corresponding to the apparent density of LWA 2-4 mm or sand 2-4 mm for the reference sample. The apparent density of sand 2-4 mm, Lusi 6M LWA, FA 6M LWA, MSWI BA LWA, and EC LWA was 2.63, 2.6, 2.23, 2.61, and 1.25 g/cm^3, respectively. After the volume replacement of LWA 2-4 mm was set to 16 % and 30%, this volume was converted into mass based on their apparent density value. By keeping the total weight of fine aggregate to 1350 g/batch, the weight of sand could be determined.

The mortar was molded into prisms with a dimension of 40 x 40 x 160 mm^3. The workability of fresh mortars was tested according to NBN-EN-1015-3 (1999). After demolding, the mortar prisms were cured until the age of 28 days in a room with temperature of 20±2 ºC and relative humidity of 95±5%. The mechanical properties of the mortars were assessed by measuring flexural and compressive strength in accordance with EN NBN 196. First the dimension and the mass of the prism were measured. After that, the prism was tested in an apparatus for three-point bending (Walter + Bai 250/15). The load was increased smoothly with the rate of 2400±200 N/s. Later on, the halves of the broken prisms from the flexural test were subjected to a uniformly distributed load to measure compressive strength.

Table 3.2. Mix design of mortar with replacing rate of 16 and 30 vol-% of sand 0/4 with LWA

Type	Sand 2-4 (g)	LWA_{OD}[1] 2-4 (g)	Absorbed water (g)	Sand 0-2 (g)	Cement (g)	Water (g)
Reference 16%	220	0	0	1130	450	225
Lusi 6M 16%	0	116	37	1196	450	225
FA 6M 16%	0	122	32	1196	450	225
MSWI BA 6M 16%	0	132	23	1195	450	225
EC LWA 16%	0	82	17	1251	450	225
Reference 30%	395	0	0	955	450	225
Lusi 6M 30 %	0	290	72	1060	450	225
FA 6M 30 %	0	282	53	1068	450	225
EC LWA 30%	0	186	32	1164	450	225
MSWI BA 6M 30 %	0	308	61	1042	450	225

[1] OD : oven dried

3.3 Results and Discussion

3.3.1 Properties of Raw Materials

The characterization data obtained on fly ash raw material such as the chemical composition, particle size distribution, and mineralogy are the same as presented in chapter 2. In this chapter, the results are shown once again as a comparison.

Table 3.3 shows the chemical composition of the binders determined by XRF. It can be seen that MSWI BA has the lowest amount of SiO_2, Al_2O_3, and Fe_2O_3 but has the highest amount of CaO. FA and Lusi have similar amounts of SiO_2, Al_2O_3, Fe_2O_3, and CaO. It is also shown that Lusi has the highest loss on ignition (LOI), followed by FA and MSWI BA. The specific density of Lusi and MSWI BA are similar, while FA has the lowest specific density.

Figure 3.2 displays the particle size distribution (PSD) of all the powders (FA, Lusi, and MSWI BA). It can be seen that FA and MSWI BA have a very similar size distribution, while the PSD curve of Lusi indicates that it contains a higher content of large particles (**Figure 3.2**). The d_{50} of Lusi, FA, and MSWI BA are 10.5 μm, 6.2 μm, and 5.4 μm, respectively (**Figure 3.2**). The surface area of Lusi, FA and MSWI BA are 0.51 m^2/g, 0.83 m^2/g, and 0.65 m^2/g, respectively.

The mineralogy of raw materials shows that Lusi has the lowest amorphous content followed by MSWI BA and FA (**Table 3.4**). The amount of amorphous phase in MSWI BA is quite high, but this value is similar to the value reported earlier for fresh MSWI BA obtained from the Belgian incinerator, being 73% (Santos et al., 2013). The major crystalline phases are quartz, mullite, and calcite. Lusi has the highest quartz content followed by MSWI BA and FA, while calcite is only content detected in MSWI BA and Lusi.

The XRD pattern of raw materials shows that FA has less crystalline phase compared to Lusi and MSWI BA (**Figure 3.3**). A small broad hump in the region of 21-31° was clearly observed in FA, indicating its high amorphous phase content. Quartz could be detected in all the raw materials, while mullite was only detected in FA and Lusi.

The leaching behavior of raw materials obtained in a one batch leaching test compared to the Dutch legal limit are presented in **Table 3.5**. The leaching of Copper (Cu) in MSWI is higher than the legal threshold value, which commonly occurs in MSWI BA (Alam et al., 2019). The leaching of chromium (Cr) and molybdenum (Mo) in fly ash was also higher than the legal thresh-hold value. Similar behavior was found in the fly ash generated from a cogeneration plant in Sweden (Nordmark and Lagerkvist, 2018). pH stabilization by means of carbonation of the fly ash was claimed to effectively reduce the leaching of Cr and Mo in washed fly ash (Nordmark and Lagerkvist, 2018). In contrast, Lusi has no issue regarding leaching of heavy metals, it has quite a high sulfate leakage. However, it was still within the accepted legal limits (Rijkswaterstaat, 2007).

Table 3.3. Chemical Composition of the Binders Determined via XRF

Composition (%)	**MSWI BA**	**FA**	**Lusi**
Cl	0.37	-	0.15
CaO	16.80	3.79	2.27
SiO_2	48.40	57.40	52.90
Al_2O_3	10.10	26.17	22.20
Fe_2O_3	7.69	5.99	7.64
K_2O	1.13	1.88	1.59
Na_2O	6.43	-	-
MgO	2.98	1.43	2.52
CuO	0.25	0.02	0.01
ZnO	0.47	0.02	0.01
SO_3	2.06	0.98	1.83
P_2O_5	1.91	0.88	-
TiO_2	1.27	1.13	0.81
LOI	0.15	0.32	8.08
Specific Density (g/cm^3)	2.61	1.99	2.75

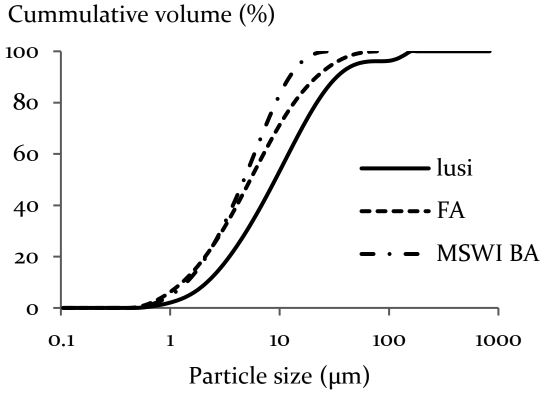

Figure 3.2. Particle size distribution of raw material

Table 3.4. QXRD of Municipal Solid Waste Incineration Bottom Ash (MSWI BA), Fly Ash (FA) and Lusi

Mineral	**MSWI BA**	**FA**	**Lusi**
akermanite	2.1	-	-
quartz	5.3	4.6	8.0
mullite	3.8	11.1	-
calcite	2.3	-	0.4
anhydrite	-	0.3	1.0
magnetite	0.6	3.0	-
wuestite	0.4	-	-
sodalite	-	0.4	-
iron	0.4	-	-
cristobalite	0.1	-	-
MgAlSiO	0.7	-	-
feldspar	2.8	-	16.3
hematite	1.0	-	4.1
vermiculite	-	-	1.7
anatase	-	-	0.6
corundum	1.9	-	-
apatite	2.2	-	-
(Na,K)Cl	1.4	-	-
periclase	1.4	-	-
perovskite	-	0.3	-
dolomite	0.9	-	-
susannite	0.1	-	-
amorphous	72.8	80.4	67.9

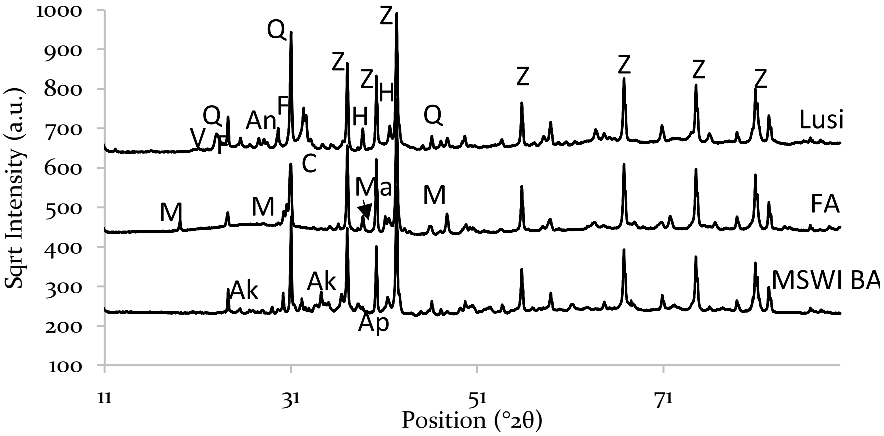

Figure 3.3. XRD Pattern of Raw Materials, showing the square root of intensity versus the 2θ position, where Q is Quartz; F is Feldspar ; Z is ZnO; Ak is Akermanite ; A is Anhydrite; V is Vermiculite ; C is Calcite; M is Mullite ; Ap is Apatite and Ma is Magnetite

Table 3.5. Leaching of heavy metals using one batch leaching test and the comparison with acceptable leaching limits from Dutch legislation (Rijkswaterstaat, 2007)

Sample	Ba mg/ kg	Cr mg/ kg	Cu mg/ kg	Ni mg/ kg	V mg/ kg	Zn mg/ kg	Mo mg/ kg	Cl mg/ kg	SO4 mg/ kg
FA	9.89	3	b.d.	0.09	0.92	0.46	6.76	b.d.	3.47
MSWI BA	0.61	0.06	2.46	0.1	b.d.	1.39	0.93	1.8	5.7
Lusi	0.39	0.07	b.d.	b.d.	1.14	0.36	b.d.	0.79	13.44
Legal Limit	22	0,63	0,9	0,44	1,8	4,5	1	616	1730

b.d. : below detection

3.3.2 Heat Evolution

Based on the heat evolution shown in **Figure 3.4**, it can be seen that all the LWA have low reactivity indicated by the absence of a significant heat flow after the initial mixing. The cumulative heat of all LWA was also quite low with MSWI BA 6M releasing the highest heat followed by FA 6M and Lusi 6M. Similar behavior was also observed in the hydration kinetics of untreated MSWI BA, this high heat released in MSWI BA can be partially related to the reaction of residual metallic aluminium in MSWI BA (Joseph et al., 2020). The total released heat of MSWI BA 6M, FA 6M, and Lusi 6M after 7 days amounted to 40.47 J/g, 25.97 J/g and 19.03 J/g respectively. This result is also influenced by the different average particle size of the 3 materials. The total heat released is inversely proportional to the particle size of raw material.

The absence of a heat flow following the initial heat release that occurs directly after mixing was also observed while activating fly ash, slag, and metakaolin with NaOH at ambient temperatures (Chithiraputhiran and Neithalath, 2013; Kang et al., 2019; Nath and Kumar, 2019). As the NaOH concentration increases, more energy (higher temperature) is required to initiate and forward the reaction (Nath and Kumar, 2019). Therefore, it makes sense that samples which were cured at room temperature have a single peak pattern. There was not enough energy to initiate further geopolymerization and the alkali solution produced a slow reaction with fly ash and caused difficulties to observe all the possible peaks.

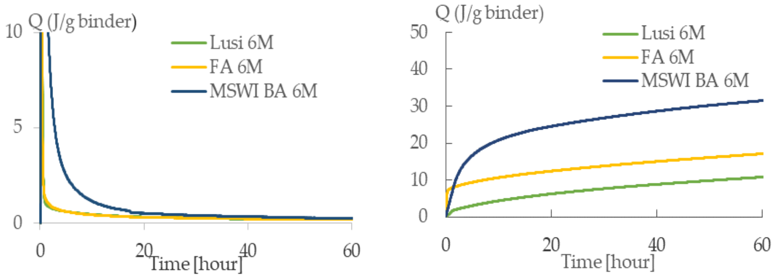

(a) **(b)**

Figure 3.4 (a) Heat evolution of LWA (b) Heat cumulative of LWA

3.3.3 Density and Water Absorption

The density and water absorption data of FA 6M LWA in this chapter are the same as presented in chapter 2. In this chapter, the results are shown once again as a comparison.

Based on data presented in **Table 3.6**, it can be seen that the pellets of MSWI BA 6M have the highest apparent density, saturated surface dry (SSD) density and oven-dried (OD) density. Lusi 6M has the lowest OD density but one of the highest apparent densities as well. All the LWA have water absorption of more than 20%. Lusi 6M has the highest water absorption and porosity values followed by MSWI BA 6M and FA 6M.

In general, water absorption and porosity of LWA have inverse relationships with density (Tang et al., 2017). In contrast, in this research, it is quite difficult to draw that conclusion. The apparent density, the oven-dried (OD) density, and the SSD density of all the LWAs show no single trend. The results for water absorption and density for FA 6M and MSWI BA 6M are not fully consistent. Whereas MSWI BA 6M has the highest OD density, it would be expected that it also had the lowest water absorption. However, the lowest water absorption was the one from FA 6M, with a difference of less than 2% compared to the water absorption of MSWI BA 6M. The main explanation for this inconsistency seems to be the microstructure of the different LWAs that will be further discussed later in this chapter.

Compared to bottom ash geopolymeric LWA, produced with 8M concentration NaOH and $Ca(OH)_2$ admixture, the water absorption of the LWA in this study is higher (Geetha and Ramamurthy, 2013). It is reasonable, as the increased NaOH concentration and the addition of calcium enhance the geopolymer reaction. An insufficient amount of calcium and alkali activator reduces the reactivity of the geopolymer and increases the amount of unreacted phase in the resulting LWA. Moreover, unreacted phases in LWA cause an increase in the open porosity. The denser structure of FA 6M and MSWI BA 6M, made with binders with high calcium contents, supports this hypothesis. Furthermore, Gesoglu et al. explain that the particle size of LWA has a proportional relationship with its strength and density (Gesoğlu et al., 2007). Thus, another possible explanation for the high water absorption of LWAs in the present research is their smaller particle size fraction compared to LWA in the literature.

Table 3.6. Mass Density and Water Absorption of the resulting LWA (n=3).

Test	Lusi 6M	FA 6M	MSWI BA 6M	EC LWA
Apparent particle density ρ_a (g/cm^3)	2.60 ± 0.09	2.23 ± 0.01	2.61 ± 0.03	1.25 ± 0.01
Oven Dried Density ρ_{rd} (g/cm^3)	1.40 ± 0.02	1.47 ± 0.01	1.59 ± 0.01	0.99 ± 0.01
SSD particle density ρ_{ssd} (g/cm^3)	1.86 ± 0.03	1.81 ± 0.00	1.98 ± 0.01	1.19 ± 0.01
Water absorption (%)	32.8 ± 0.28	23.23 ± 1.14	24.80 ± 0.56	21.14 ± 0.30
Porosity (%)	45.98 ± 0.96	34.12 ± 0.75	39.32 ± 0.78	20.85 ± 0.09

3.3.4 Particle Size Distribution

The particle size distribution data of FA 6M LWA in this chapter are the same as presented in chapter 2. In this chapter, the results are shown once again as a comparison.

Figure 3.5 shows that all samples have a very small content of fine particles of less than 2 mm. Lusi 6M has the least steep curve, and a higher fraction of fine particles compared to the other LWAs. According to NBN EN 12620 Lusi 6M and MSWI BA 6M LWA meet the requirement for the 2/8 fraction, while FA 6M is a fraction of 2/10. Thus, it can be noted that the types of raw materials did not affect the particle size distribution of LWA in any significant way. Based on the literature, it is mainly the setup of the pan granulator such as the slope, the speed and the duration of pelletizing that affect the particle size of the resulting LWA (Gu, 2000).

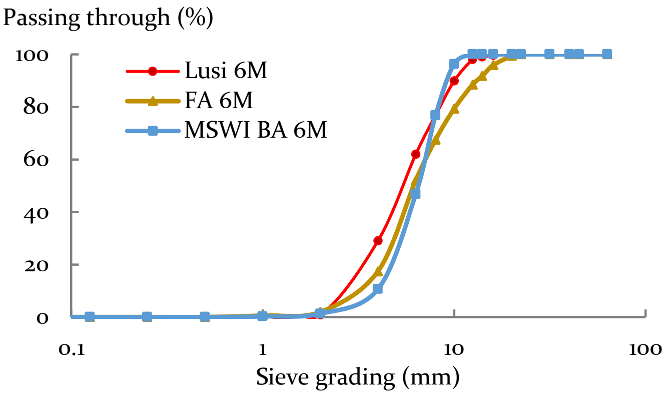

Figure 3.5 Particle Size Distribution of LWA

3.3.5 Crushing Resistance Test

The crushing resistance data of FA 6M LWA in this chapter was the same as presented in chapter 2. In this chapter, the results are shown once again as a comparison

Based on **Figure 3.6**, Lusi 6M has the highest crushing resistance (CR) followed by FA 6M and MSWI BA 6M. This result is unexpected as Lusi 6M has the highest water absorption among the 3 LWA. In general, the CR value of aggregates has an inverse relationship with its water absorption (Gesoğlu et al., 2013; Heidrich et al., 2013; Illikainen, 2017)

MSWI BA 6M showed low strength even though it had high reactivity. This is likely due to the appearance of micro cracks on the surface of the aggregates (**Figure 3.7**). This could occur due to the metallic Al in the bottom ash which reacts at a high pH and generates hydrogen gas that leads to expansion. Based on previous research, the aluminum content in the MSWI BA was 0.80% (Vandeputte, 2018). Furthermore, the result of the MIP test also confirmed that MSWI BA 6M contains a high amount of macro-pores compared to the other LWA, because, even without the influence of metallic Al, the porosity of MSWI BA fines tends to be very high (Caprai et al., 2018). The CR result is also not well correlated with the calorimetry test (Fig. 3), MSWI BA 6M which showed the highest cumulative heat did not possess the highest CR. However, this high heat released in MSWI BA was mostly due to the reaction of metallic aluminum (Joseph et al., 2020). Previous research reported that NaOH activation of fly ash is more temperature dependent, observing the reactivity of this paste in 20°C environment will not provide enough information for understanding the whole kinetics of the reaction that occurred (Sun and Vollpracht, 2018).

It was observed during the test that all types of LWA were agglomerated and stuck to each other forming bigger granules once the load for the crushing test had been applied. Thus, it was quite difficult to accurately determine the crushed part of the LWA with the method applied in this research.

Due to the different standard that was used, the CR value of the LWA in this research can only be compared with limited sets of data on LWA in the literature. Compared to crushed LWA generated from bottom ash and from limestone in the literature, the CR value of LWA in this research is quite similar to limestone aggregate (Van den Heede et al., 2016). Besides, the fact that the LWAs produced in this study had similar CR value compared to those LWAs in literature is quite promising considering that the former have a much lower density and a higher water absorption than the latter.

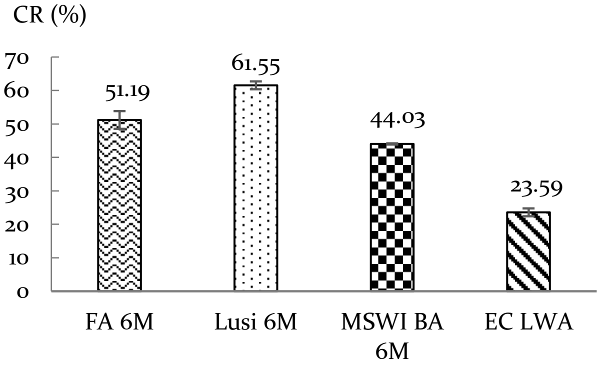

Figure 3.6 Crushing Resistance (CR) value of LWA (n=3).

(a) **(b)** **(c)**

Figure 3.7 The appearance of (a) MSWI BA 6M, (b) Lusi 6M, (c) FA 6M LWA

3.3.6 Porosity

The porosity data of FA 6M LWA in this chapter are the same as presented in chapter 2. In this chapter, the results were shown once again as a comparison

Figure 3.8 show the pore size distribution and cumulative intruded volume, respectively, of the LWAs determined by Mercury Intrusion Porosimetry (MIP). **Figure 3.8**a shows that Lusi 6M and FA 6M have two major peak regions. The first region is located between 0.1-1 μm while the second peak region is located between 3-10 μm. In contrast, MSWI BA 6M only shows one major peak region which is located between 3-10 μm. As a consequence, two threshold pore diameters are observed in **Figure 3.8b** for FA 6M and Lusi 6M, while only one is observed for MSWI BA 6M. The threshold pore diameters (d_{th}) are 18 μm for MSWI BA 6M, 0.06 μm and 6 μm for Lusi 6M, and 0.1 μm and 6 μm for FA 6M. In addition, **Figure 3.8c** also shows that MSWI BA 6M and Lusi 6M have almost the same intruded volume of 238 mm^3/g, while FA 6M has a lower intruded volume of 200 mm^3/g.

The porosity in the LWA samples can be categorized into two groups based on their size range, mesopores (2-50 nm) and macropores (larger than 50 nm) (Chemistry, 2001). As shown in **Figure 3.8** MSWI BA 6M has the lowest volume of mesopores followed by FA 6M and Lusi 6M. The relative volumes of mesopores in MSWI BA 6M, FA 6M, and Lusi 6M are, respectively, 3.48%, 28.03%, and 40.31% of the total porosity.

Tziviloglou found multiple peaks for the pore size distribution curve of expanded clay LWA Liapor (Tziviloglou, 2018). Other studies on the characterization of the pore structure of LWA also found multiple peaks in their pore size distribution curves (Korat, Ducman, Legat, and Mirtic, 2013). This condition presumably occurs due to the fracture of the pore walls when pressure is applied in order to force mercury into the pores. Compared to sintered fly ash aggregate which used bentonite and glass powder as binder, a larger critical pore size diameter was obtained in this research. It seems logical as during the sintering process the voids are better closed by the binders.

The appearance of a sharp peak at the mesopores range for FA 6M and Lusi 6M indicates the presence of ink-bottle pores. Indeed, this is a common criticism made to the MIP technique. Whereas it is intended to measure the connected open pore volume, misleading information regarding the pore size distribution may be obtained due to the presence of ink-bottle pores

(Korat, Ducman, Legat, and Mirtic, 2013). In this case, when large pores are connected by small channels, high pressure is needed to force the mercury through the small channel into the large pore, so that a large volume of small pores shows up in the pore size distribution instead of the large pores that are actually present.

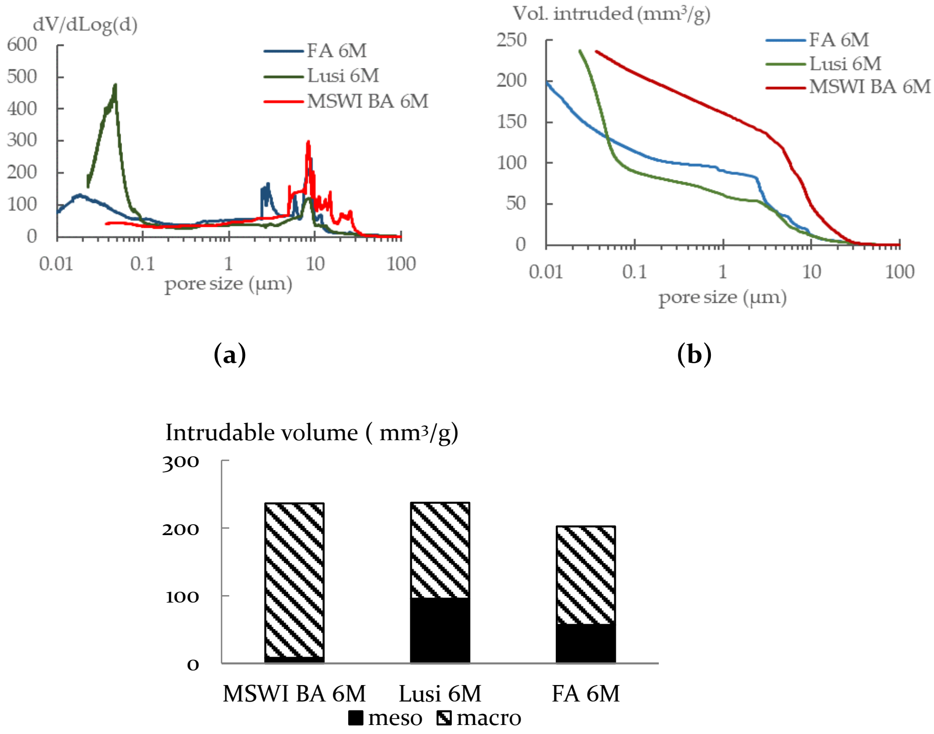

(a) (b)

(c)

Figure 3.8. (a) Pore size distribution of LWA; (b) Cumulative intruded volume of LWA; (c) Types of pores present in the LWA

3.3.7 Minerology of LWA

The minerology data of FA 6M LWA in this chapter are the same as presented in chapter 2. In this chapter, the results are shown once again as a comparison

In all types of LWA, the amount of crystalline phases such as quartz and mullite were decreased or not detected anymore after geopolymerization (**Table 3.7**). These minerals are not typically reactive in a geopolymer, so their decrease is due to the amount of alkali activator added into the mixture which was quite high (around 25% for FA and MSWI BA LWA and 51 % for Lusi LWA), which effectively dilutes the mineral content. Based on the XRD pattern in **Figure 3.9**, the broad hump of the amorphous phase was detected in the region 25-35°. The location of the broad hump in resulting LWA was shifted, compared to in raw materials (**Figure 3.3**). The same shifting phenomenon also occurred in a previous study as an indication of aluminosilicate gel formation (Bhagath Singh and Subramaniam, 2016).

The amorphous phase contents from the quantitative XRD correlates well with the compressive strength of mortars containing these LWAs. Reports in the literature, indicate that the amorphous phase content in alkali activated paste has directly proportional relationship with its compressive strength (Bhagath Singh and Subramaniam, 2016; Chen et al., 2018). FA 6M LWA had a high content of amorphous phase and high mortar compressive strength as well. On its own, Lusi 6M LWA showed the highest increase in the amorphous phase content due to its high alkali activator content, but the contribution of the aggregate to the compressive strength of mortar was lower.

Table 3.7. Mineralogy of MSWI BA 6M, FA 6M and Lusi 6M LWA

Mineral	MSWI BA 6M	FA 6M	Lusi 6M
akermanite	1.8	-	-
quartz	3.9	4.0	5.7
mullite	-	6.9	-
calcite	5.0	0.7	0.4
magnetite	2.4	-	-
wuestite	0.3	-	-
AlFe3	-	0.2	-
silimanite	-	1.0	-
gupeiite	-	0.1	-
gaylusite	-	1.7	-
sodalite	-	0.2	-
magnesioferrite	-	2.2	-
iron	0.3	-	-
cristobalite	0.2	-	-
MgAlSiO	0.1	-	-
feldspar	1.8	-	10.8
hematite	0.3	1.2	2.6

vermiculite	-	-	1.0
ulvoespinel	-	-	1.3
anatase	-	-	0.5
corundum	0.9	-	-
apatite	0.3	-	-
(Na,K)Cl	0.7	-	-
tobermorite 11 a	3.7	-	-
perovskite	1.9	-	-
ankerite	0.9	-	-
amorphous	75.3	82.0	77.6

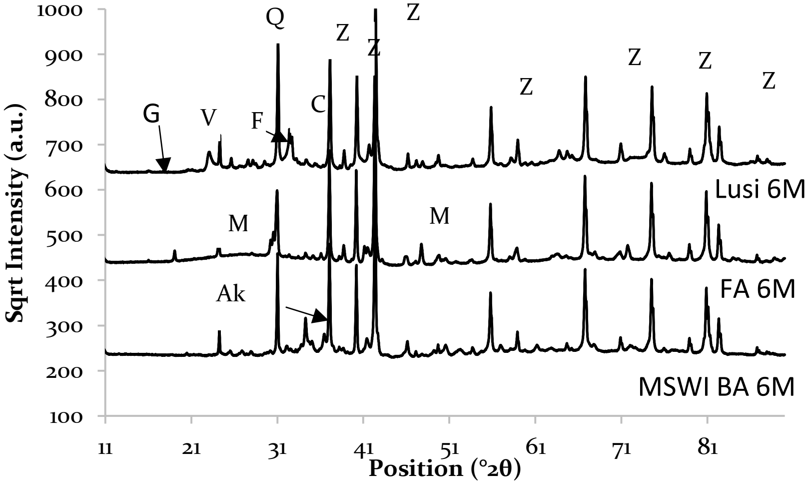

Figure 3.9. XRD Pattern of Resulting LWA, showing the square root of intensity versus the 2θ position, where Q is Quartz; F is Feldspar; Z is ZnO; Ak is Akermanite; A is Anhydrite; V is Vermiculite; C is Calcite; M is Mullite; and G is Glass

3.3.8 Morphology and chemical composition of LWA

The back scattered electron (BSE) image of LWA with its EDS layered image is displayed in **Figure 3.10**. In FA 6M LWA samples, the rounded shape of fly ash particles surrounded by gel products was observed. In Lusi 6M LWA sample, most of the area was covered with gel products with an embedded silica crystal in some spots. A large area in MSWI BA 6M sample was occupied by crystalline shapes of silica, alumina and ferro. Gel products were observed in between those crystals' shapes.

The gel area in FA 6M LWA was observed to be more heterogeneous compared to the other LWAs. Some black spots were detected inside the fly ash particles and also in the gel products. Different fly ash particles surrounded by pores may indicate the unfinished reaction of the fly ash particles (Ismail et al., 2014). A more wide area of gel product was observed in Lusi 6M LWA sample. Some spots of unreacted particles such as silica, ferro and alumina were detected sporadically. A noticeable amount of pores was observed between the gel product and unreacted particles, indicating that unfinished reactions are present in this sample. In MSWI BA 6M samples, a high amount of unreacted crystals such as silica, ferro, calcium and alumina were observed. These crystals occupied more space compared to the gel product. It is an indication that MSWI BA reacts slower with the alkali activator compared to Lusi and fly ash.

The results obtained by EDS point analysis on three different locations of LWA is presented in **Figure 3.11** and **Figure 3.12**. The proportion ratio between Na, Si, Al, and Ca could become a tool to predict the existence of N-A-S-H, C-A-S-H, and (C)-N-A-S-H gel. In the literature, the N-A-S-H has a ratio of Na/Si or Al/Si in the range of 0.3 to 0.8 and has a ratio of Ca/Si below 0.2 (Lee and Lee, 2015). C-A-S-H gel has been indicated to occur when the ratios of Ca/Si and Al/Si are higher than 0.4. The mediocre between those two ranges could be the (C)-N-A-S-H gel. It can be seen that only a few points which belong to FA 6M and Lusi 6M LWA samples consist of C-A-S-H gel, while (C)-N-A-S-H and N-A-S-H gel were detected in all LWA samples. The low amount of C-A-S-H detected in Lusi 6M and FA 6M sample correspond well with the chemical composition of its raw materials, which contain a small amount of CaO. More C-A-S-H gel was expected in MSWI BA 6M sample, as the raw materials of this LWA contain a high amount of CaO. However, it seems that the CaO content in MSWI BA did not fully react with silica and the alkali activator made the gel product in this mixture shift to (C)-N-A-S-H instead of C-A-S-H. A similar morphology pattern was also reported in the study focusing on optimizing silica content in MSWI BA-based alkali activated paste. The poor polymerization of CaO and the lack of active silica in MSWI BA attributed to the high amount of unreacted crystals in resulting paste and a failure of the system to produce C-A-S-H (Huang et al., 2019)

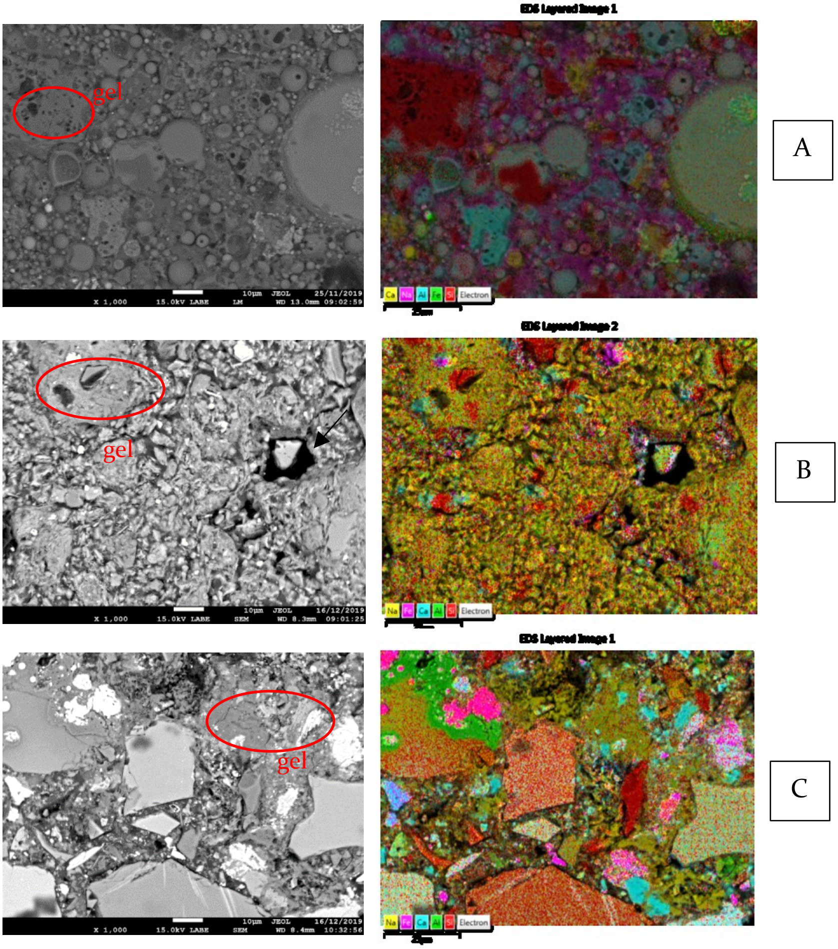

Figure 3.10. BSE SEM image (scale bar = 10 μm) and EDS layered image (scale bar = 25 μm) of (A) FA 6M LWA where yellow colour stand for Ca, magenta for Na, blue for Al, green for Fe and red for Si , (B) Lusi 6M LWA where yellow colour stand for Na, magenta for Fe, blue for Ca, green for Al and Red for Si; and (C) MSWI BA 6M LWA where yellow colour stand for Na, magenta for Fe, blue for Ca, green for Al and red for Si.

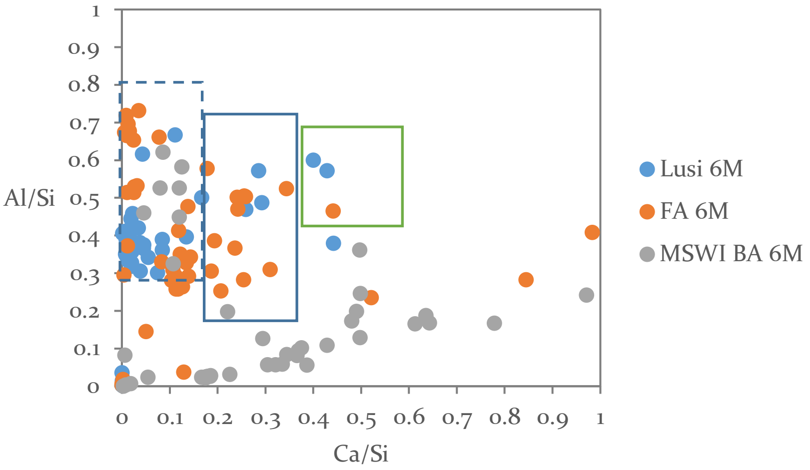

Figure 3.11. The ratio between Al/Si versus Ca/Si obtained from EDS point analysis on Lusi 6M, FA 6M and MSWI BA 6M LWA. The dashed blue box corresponds with N-A-S-H, the blue box corresponds to (C)-N-A-S-H, and the green box corresponds to C-A-S-H.

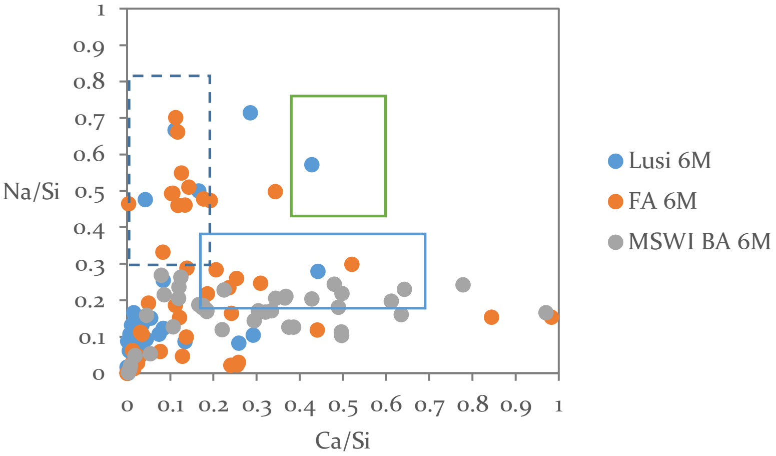

Figure 3.12. The ratio between Na/Si versus Ca/Si obtained from EDS point analysis on Lusi 6M, FA 6M and MSWI BA 6M LWA. The dashed blue box corresponds with N-A-S-H, the blue box corresponds to (C)-N-A-S-H, and the green box corresponds to C-A-S-H.

3.3.9 Viability of Bacteria after Encapsulated in LWA

In all samples, the final solution pH was below 10, which is a favorable condition for bacteria to actively decomposed urea (**Figure 3.13**) (Wang, Jonkers, et al., 2017). However, a huge difference in the urea decomposition of cells encapsulated in MSWI BA 6M was observed (**Figure 3.13**). In EC, FA 6M, and Lusi 6M sample, more than 80% of urea was fully decomposed in 6 hours, while in MSWI BA LWA, only around 30% urea was decomposed in 6 hours. The remaining metallic aluminum content in MSWI BA might be toxic to the bacteria. The aluminum could bond to DNA, membranes, or cell walls which is considered to be the main toxic effect of this metal on bacteria (Piña and Cervantes, 1996). Thus, further treatment on removing the aluminum metal in the MSWI BA should be performed to make MSWI BA 6M LWA suitable as bacteria carriers.

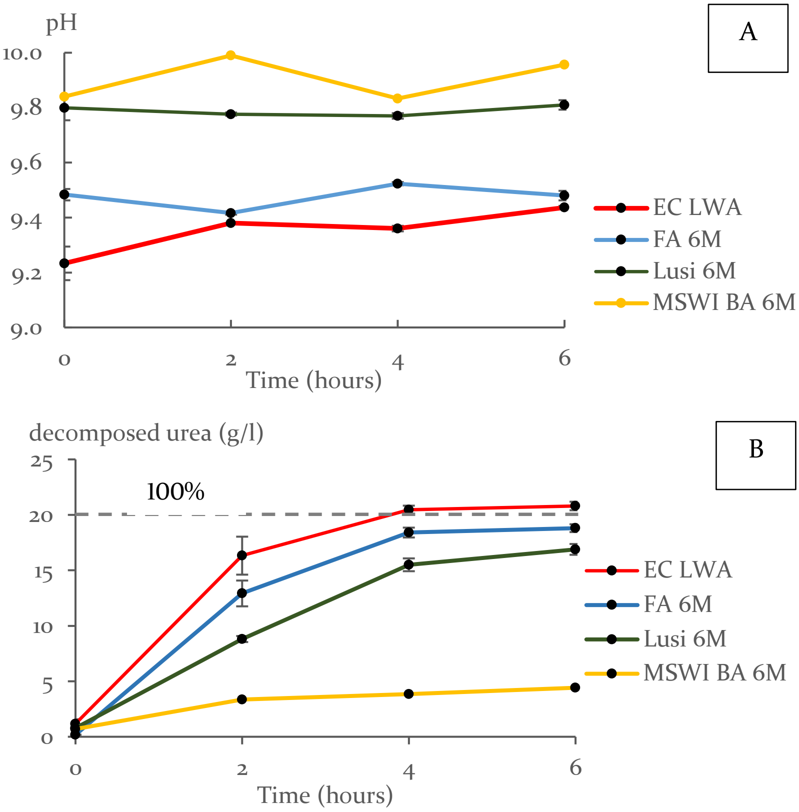

Figure 3.13. (a) The pH evolution, (b) the decomposed urea evolution of immersed LWA in urea solution (n=3).

3.3.10 Properties of Resulting Mortar

The compressive strength and bulk density result of mortar containing FA 6M and EC LWA with replacing rate of 16% by volume presented in this chapter are the same as presented in chapter 2. In this chapter, the results are shown once again as a comparison

Based on the flow value of fresh mortar presented in **Figure 3.14**, increasing the replacing rate of sand by LWA up to 30 % did not significantly affect the workability of fresh mortar. The type of aggregate was also not affecting the flow value of the fresh mortar. In general, incorporating LWA into mortar mixtures slightly decreased the flow value compared to reference samples (without LWA).

Figure 3.15 shows the bulk density of mortars made with the LWAs. In samples with replacement rate (RR) of 16%, the reference sample has the highest volume density, followed by MSWI BA 6M, Lusi 6M and FA 6M. As expected, replacing natural aggregate in a mortar matrix by LWA effectively reduces the volume density of mortar. Specifically, replacing 16% of natural aggregate can reduce the volume density up to 6%. The volume density of mortar incorporating LWA has no correlation with the density of the LWA. In terms of the OD density of LWA, Lusi 6M was supposed to produce the lightest mortar, followed by FA 6M and MSWI BA 6M. However, MSWI BA 6M generated the lightest mortar in correspondence with its highest macro-pore content among the LWAs. A significant reduction of bulk density occurred in MSWI BA 6M samples, when the LWA replacement rate was increased from 16 to 30%. Based on the cross section picture of mortar with MSWI 6M replacement rate of 30%, a significant expansion could be observed (**Figure 3.17**). The reaction of high amount of aluminum metal in MSWI BA 6M LWA with cement that release hydrogen gas could be the main cause of this behavior. It is also important to note that a significant expansion did not occur when the replacement rate of MSWI BA 6M LWA was kept to 16%. On the other hand, when the LWA replacement rate was increased to 30 %, the reduction in bulk density of the samples with Lusi 6M and FA 6M was slightly decreased by not more than 3% .In the group of samples with 16 % LWA replacement rate, mortars containing FA 6M LWA had the highest compressive strength followed by Lusi 6M and MSWI BA 6M (**Figure 3.12**). The strength reduction compared to the reference sample of FA 6M, Lusi 6M, and MSWI BA 6M was 15 %, 28%, and 29%, respectively.

On the other hand, there was no significant strength difference in mortar with different particle size distribution of the sand fraction (Ref 16% and Ref

30%). In mortar containing LWA, increasing the LWA replacement rate from 16 % to 30 % delivers a reduction in strength of 29%, 20%, 48% and 29% in mortar containing FA 6M, EC, MSWI BA and Lusi 6M LWA, respectively (**Figure 3.16**) . It also can be seen that the compressive strength obtained for LWA containing mortar was well correlated with its bulk density and the porosity value of LWAs (**Figure 3.15** and **Figure 3.16**).

In contrast, the compressive strength of the resulting mortar does not correlate well with the crushing strength of the constituting LWA. Lusi 6M, which has the highest CR value, apparently did not deliver the highest compressive strength when it was applied in mortar. Besides the difficulties with accurately determining the crushed part of LWA during the test, the reactivity of fly ash in FA 6M LWA with the cement paste could also be the reason why FA 6M mortar has the highest compressive strength. In general, all the LWA have a round shape covered with unreacted raw material powder. In mortar containing FA 6M LWA, the unreacted fly ash in the aggregate could later react with the cement in the mortar mixture, create a bond and close porosity and increase the density. Lusi seems to have less reactivity compared to fly ash when applied into concrete or mortar. In the literature, a replacement level of 20% of cement by Lusi in concrete proved to decrease the strength activity index (SAI) up to 20% (Hardjito et al., 2012). Previous research also indicated that fly ash LWA have pozzolanic reactivity when applied in mortar or concrete, especially at advanced ages (Kong et al., 2014). The same reasoning might be used to explain why mortar containing FA 6M also has higher volume density, as the chemical reaction between the LWA and cement paste may have helped the mortar to become denser.

Compared to previous research by Illikainen et al., who replaced 21% of fine aggregate in mortar by FA-based LWA, the compressive strength of mortar in this study which replaced 30% of fine aggregate with FA 6M LWA is 38% higher (Illikainen et al., 2017). Comparison with the results reported by Gesoglu et al, who substituted 25 % of fine aggregate with a cement-bound fly ash LWA in mortar, shows that the decrease in strength in comparison with the respective reference mortar is also lower in the present research (Gesoğlu et al., 2007). Whereas Gesoglu et al. obtained a reduction of 46% in the compressive strength at 28 days with 25% replacement, the results of FA 6M mortar with replacement rate of 30% in our research show a reduction of 40%.

In general, LWAs produced in this study are comparable to other lightweight aggregates generated from similar waste products, and mortar produced with them resulted in better mechanical properties than usually reported in the literature. Moreover, increasing the replacement rate up to 30% is still feasible for FA 6M and Lusi 6M LWA, as the properties of the resulting mortar are still acceptable. While additional pretreatment for mitigating expansion of MSWI BA could be taken into consideration for future research.

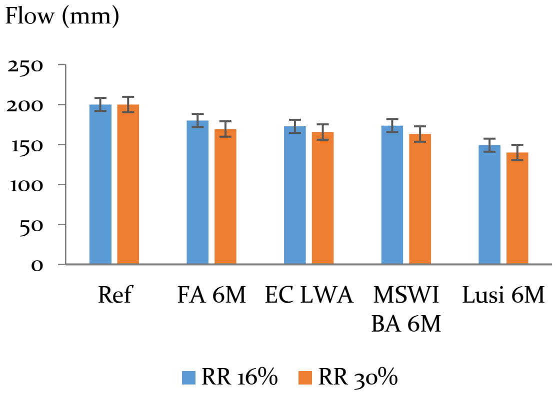

Figure 3.14. Workability of fresh mortar with LWA replacement rate of 16 and 30% (n=3).

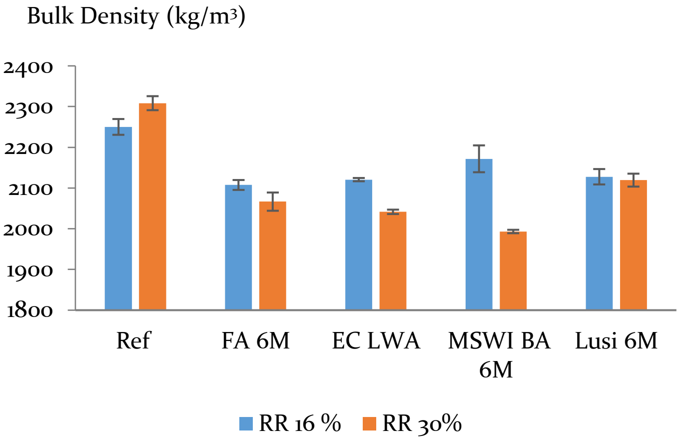

Figure 3.15. Bulk density of resulting mortar with LWA replacement rate (n=3).

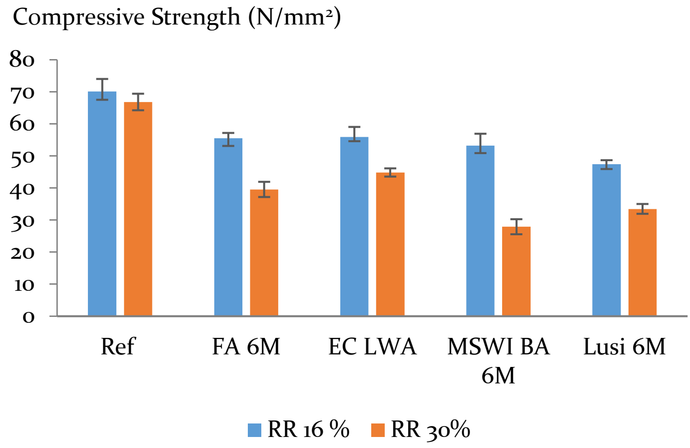

Figure 3.16. Compressive strength of resulting mortar with LWA replacement rate of 16 and 30% (n=3).

Figure 3.17. With high replacement rate, MSWI BA 6M LWA could induce expansion in the mortar matrix.

3.3.11 Comparison with Commercial LWA

For practical validation, the LWAs produced in the present research were compared to commercial aggregate generated from sintered expanded clay (EC). The fraction of EC LWA that was used in this research is 0/4 and its manufacturer states that this material is suitable for use in structural concrete. **Table 2.4** shows that the oven-dried density of EC LWA is much lower than for all the LWAs produced in this research. Moreover, water absorption of EC LWA is 8% lower than the one of FA 6M LWA, which shows the lowest water absorption among the LWAs that were produced. However, the CR value of this commercial LWA is 46% lower than the

MSWI BA 6M LWA which had the lowest CR value among the produced LWAs (**Figure 3.7**). Surprisingly, with lower density and lower CR value, EC LWA demonstrated a better performance when applied into mortar. Only slight flow value reduction was observed in fresh mortar containing EC LWA, even with high replacement rate of 30%. With a 16% replacing rate, mortar containing EC LWA only has 20% strength decrease, while increasing the replacement rate to 30%, decreased the strength of mortar by 33% compared to the reference mortar (**Figure 3.16**). The volume density of mortar containing EC LWA is almost similar to mortar containing MSWI BA 6M but it has better mechanical properties (**Figure 3.15**).

The sintering process is more efficient than geopolymerization in producing a convenient microstructure for LWA. This is the main explanation for the improved mechanical performance of EC LWA compared to the geopolymer LWA when applied in mortar. Previous reports on sintered fly ash-based LWA revealed that the sintering process is effective in closing pores as the molten material forms a solid body (Eva, 2016; Gomathi and Sivakumar, 2015). Upon this processing, the volume of closed porosity increases at the expense of the open porosity that is blocked, with a consequential decrease in water absorption and improvement of the mechanical properties.

Summarizing, compared to EC LWA, the properties of LWA in this study are still acceptable. The properties of EC LWA are slightly better than those of LWAs in this research. However, the sintering process is energetically expensive, as temperatures of up to 1100 ºC are required to produce the full volume of aggregate. In this sense, a reduced demand of energy may compensate for the moderate performance of geopolymer LWA. This aspect should be considered in future research for appropriate comparison.

3.4 Conclusions

Based on the results of the experiment, the following conclusions could be drawn:

1. The types of raw materials used affected the water absorption and the density of resulting LWAs. Fly ash and bottom ash contain more calcium and have a lower LOI than Lusi, so they delivered LWAs with a lower water absorption and denser structure compared to LWA generated from Lusi.
2. The type of raw materials had no significant effect on the particle size distribution of resulting LWA, the fraction size of MSWI BA 6M and Lusi 6M LWA was 2/8 mm, while for FA 6M LWA it was 2/10.

3. Based on the heavy metal leaching test, the leaching of copper in MSWI BA still exceeds the limits set by Dutch Legislation, while no issues were found in the leaching test of Lusi and FA raw materials.
4. The MIP test results revealed that LWA generated from fly ash and Lusi had two threshold diameters (d_{th}). FA 6M LWA had a d_{th} of 0.1 μm and 6 μm while Lusi had d_{th} of 0.06 μm and 6 μm. The largest d_{th} was measured for MSWI BA 6M, which had a d_{th} of 18 μm. MSWI BA 6M contained large amounts of macropores. The appearance of micro-cracks on the surface of MSWI BA 6M due to the metallic Al reaction could be the reason for the high amount of measured macropores in MSWI BA 6M samples.
5. There is an unexpected result obtained from the crushing resistance test, where Lusi 6M showed the highest crushing strength followed by FA 6M and MSWI BA 6M. It seems that the crushing resistance test is not suitable to determine the strength of LWA which has small particle size.
6. The ureolytic activity of bacteria after encapsulation into MSWI BA LWA was low compared to when encapsulated into EC, FA 6M or Lusi LWA. The metallic aluminum content in MSWI BA might be toxic to the bacteria.
7. Increasing the replacement rate up to 30% did not significantly affect the flow value of resulting fresh mortar. The decrease of compressive strength of resulting mortar containing FA 6M and Lusi 6M LWA produced in this study are also comparable and even better compared to other lightweight aggregates generated from geopolymerization of similar waste products.
8. A significant expansion resulting in a decrease in strength and bulk density occurred when the replacement rate of MSWI BA 6M LWA in mortar was increased to 30%.
9. Despite of the fact that the properties of mortar made with EC LWA are slightly better than for mortar made with LWAs in this research, the fact that more energy is required during the sintering process of EC LWA should also become a consideration.

Chapter 4. Durability of Mortar Containing Fly Ash-Based Alkali activated Lightweight Aggregate

This chapter was redrafted after:

Risdanareni, P.; Van den Heede, P.; Wang, J.; De Belie, N. The Durability of Mortar Containing Alkali Activated Fly Ash-Based Lightweight Aggregate. *Materials* **2021**, 14 ,3741

4.1 Introduction

In chapter 2, the results have shown that the suitable NaOH concentration for producing alkali activated lightweight aggregate with fly ash as a binder was 6 Molars. In chapter 3, the feasibility of utilizing other raw materials besides fly ash to produce alkali activated LWA named Lusi and MSWI BA were investigated. The result shows that fly ash-based alkali activated LWA has comparable properties to commercial LWA. Incorporating those LWA into mortar as fine aggregate replacement (up to 30% by volume) also did not significantly alter the compressive strength of resulting mortar. Although the mortar containing alkali activated LWA has an acceptable mechanical performance, a study of the durability is needed as this novel LWA is porous and could contribute to an increased amount of pores in the resulting mortar.

A previous study on incorporating commercial LWA into mortar mixtures as sand replacement revealed that even though the resulting mortar becomes more permeable for water or gas compared to a mortar with river sand, it has better resistance against chloride penetration (Bentz, 2009; Kou and Poon, 2010; C. Liu et al., 2020; X. Liu et al., 2011). The reduction of pore percolation at the interfacial transition zone (ITZ) and the penetration of hydration products into the LWA's open pores was the reason for this improvement (Bentz, 2009). However, most researchers only focused on the durability of lightweight concrete incorporating commercial LWA aggregate. Limited studies could be found on the performance of mortar incorporating pelletized alkali activated artificial aggregate. Illikainen et al. replaced 21% volume of sand with alkali activated fly ash-based LWA into the mortar mixture, and found that the compressive strength of resulting mortar containing fly ash LWA was higher than mortar containing LECA LWA (Illikainen, 2017).

The main goal of this thesis is to extend the service life of the concrete by applying the self-healing method. Thus, it would be necessary to investigate whether the alkali activated LWA, which will be used as the bacteria carrier, is compatible with the mortar matrix and has no negative impact on the durability of the resulting mortar. Therefore, in this part, the durability of mortar incorporating alkali activated fly ash-based LWA was investigated, by use of tests such as compressive strength, water absorption under vacuum, bulk density, capillary water uptake, chloride migration, and carbonation resistance. The ITZ morphology between LWA and cement paste was also investigated. In the end, the results obtained were compared to mortar incorporating expanded clay LWA and natural river sand in order to figure out the potential of employing alkali activated fly ash-based LWA in the construction industry.

4.2 Materials And Methods

4.2.1 Materials

The fly ash (FA) used to produce the LWA in this part is the same as the fly ash used in chapter 2. More detail on the chemical composition of fly ash has been presented in **Table 2.2**. More details on the particle density testing procedure and results were presented in **Figure 3.1**.

The type and the composition of alkali activator used to activate fly ash in this chapter was also the same as described in section 3.2.1.

The standard river sand 0/4 and expanded clay LWA aggregate used in this chapter were the same as mentioned in section 3.2.1.

4.2.2 The Production Process and the Properties of Fly ash-based LWA

Fly ash-based LWA was produced with the agglomeration technique using a pan granulator with a diameter of 500 mm and a depth of 95 mm. The slope of the pan granulator was set at 48° while the speed was set at 60 rpm. This set up was chosen based on previous research by Baykal et al., which reported optimal LWA properties for these parameter settings (Gu, 2000). The liquid/solid ratio of 0.25 was applied based on previous research (Kockal and Ozturan, 2011; Shivaprasad and Das, 2018; Tang et al., 2017). The LWA production was initiated by adding fly ash powder into the pan, followed by spraying the required amount of mixed alkali activator continuously. During that time, the fly ash powder will bond with the alkali activator and form granules. After being rotated for approximately 20 min, due to the gravity movement, the compacted pellets will fall out through the side of the pan (**Figure 3.1**). Later on, the wet granules were dried in a curing chamber with a temperature of 20 ± 2 °C and humidity of 95 ± 5% for 24 h. Then, the dried LWAs were sieved with a 2 mm sieve in order to remove dust and the finer fraction of LWA. Finally, dried sieved LWAs were moved into a sealed plastic bag and further cured in the same chamber for 28 days before being applied into a mortar. An illustration regarding the LWA production can be found in **Figure 2.1** .

The physical properties of LWA such as apparent density, oven dried density, saturated surface dry (SSD) density, and water absorption over 24 h were tested according to the NBN EN 1097-6 standard and the values are displayed in **Table 4.1**. The particle size distribution of aggregates was determined in accordance with the Belgian standard NBN EN 12620 and the values are presented at **Figure 3.5** . The IUPAC guidelines were used to characterize the LWA's pores derived from mercury intrusion porosimetry (MIP) (**Figure 3.8**). Mesopores are defined as having a size of 2–50 nm, while macropores have a diameter above 50 nm (IUPAC Commission on Colloid and Surface Chemistry, 1990). More detailed data on the pore structure of LWA using MIP were reported in Chapter 2. The other properties of fly-ash based LWA such as crushing strength resistance and mineralogy were presented in Chapter 3.

Table 4.1. Physical properties of EC LWA, FA 6M LWA and sand with the size of 2–4 mm (n=3).

Test	**EC LWA**	**FA 6M LWA**	**Sand 2–4 mm**
Apparent particle density (AD) (g/cm^3)	1.25 ± 0.01	2.23 ± 0.01	2.63 ± 0.04
Oven dried density (OD) (g/cm^3)	0.99 ± 0.01	1.47 ± 0.01	2.48 ± 0.03
SSD particle density (SSD) (g/cm^3)	1.19 ± 0.01	1.81 ± 0.00	2.54 ± 0.03
Water absorption 24 h (WA_{24h}) (%)	20.85 ± 0.09	23.69 ± 0.63	2.19 ± 0.14

4.2.3 Mortar Production

All mortar specimens were produced by following the guidelines from the NBN EN 196-1 standard. Prisms with a dimension of 40 × 40 × 160 mm^3 were used for testing compressive strength, capillary water absorption and carbonation. Cylinders with a diameter of 100 mm and a height of 200 mm were used for the water absorption under vacuum and the chloride migration test.

The material needed to manufacture three mortar prisms is presented in **Table 4.2**. Cement type I 52.5 from Holcim was used as binder while river sand with fraction of 0/4 was used as fine aggregate. The volume of river sand with a size of 2–4 mm was replaced with the LWA. The particle sizes to be replaced with LWA were chosen in the range of 2–4 mm, as LWA with granules smaller than 2 mm are more fragile. This implies that 16% of the total volume of 0/4 mm sand was replaced with LWA to maintain the distribution of fine aggregates. However, some literature mentions a higher replacement rate of LWA up to 21% by volume, and no workability issues were reported (Illikainen, 2017). The corresponding weight ratio was calculated based on the apparent density. In order to avoid workability issues during mortar production due to the high water absorption of LWA, a certain amount of extra water (entrained water) was added based on LWA's water absorption value for the LWA to reach saturated surface dry (SSD) condition. Finally, the total amount of fine aggregate (LWA SSD condition and sand 0–2) in the mixture was kept at 1350 g/batch.

After being cast, all mortar specimens were covered with plastic film to avoid evaporation and were cured in a curing chamber which has a temperature of 20 ± 2 °C and humidity of 95 ± 5% for 24 h. After 24 h, the specimens were demolded and were left in the same chamber for 28 days before being tested.

Table 4.2. Mix design of three mortar prisms.

Type	LWA OD[1] 2–4 (g)	Entrained water (g)	Sand 2–4 (g)	Sand 0–2(g)	Cement (g)	Water (g)
Reference	0	0	220	1130	450	225
FA 6M	122	32	0	1196	450	225
EC LWA	82	17	0	1251	450	225

[1] OD: Oven Dried.

4.2.4 Physical Properties of Resulting Mortar

The tested physical properties of the resulting mortar were compressive strength, water absorption, apparent density, and the amount of open porosity. The compressive strength of the mortar was determined as an average value of three replicate samples according to the NBN EN 196-1 standard. The test was conducted on prismatic specimens, which had been cured for 28 days in a room with a temperature of 20 ± 2 °C and humidity of 95 ± 5%.

The water absorption (WA), apparent density (AD), and the amount of open porosity (OP) of mortar were determined on three cylindrical specimens with a diameter of 100 mm and a height of 50 mm by following the guidelines from EN 1936 standard. These cylinders were obtained by cutting the cast cylinder specimens, which had a diameter of 100 mm and a height of 200 mm into 3 slices. The top 25 mm and bottom 25 mm of the cylinder were removed.

First, the samples were left in a sealed desiccator. Vacuum pressure was then applied for 2 h. After that, water was let into the desiccator until all the samples were fully immersed. After being immersed in the water for 24 h, samples were taken out and weighed. This weight was denoted as a saturated mass in the air (m_{sa}). Later on, samples were weighed in water. This mass was denoted as a saturated mass in water (m_{sw}). After that, samples were dried in the oven with a temperature of 105 °C until constant mass was reached. The weight of the dried samples was then denoted as the dry mass (m_d). Finally, the water absorption (WA), the apparent density (AD), and the open porosity (OP) were calculated using Equations 4.1–4.3, respectively. The values shown, represent the average value of three replicate samples, with the standard deviation on the mean presented by the error bars.

$$WA = \frac{m_{sa} - m_d}{m_d} \qquad \text{Equation 4.1}$$

$$AD = \frac{m_d}{m_{sw} - m_d} x\ \rho_{water} \qquad \text{Equation 4.2}$$

$$OP = \frac{m_{sa} - m_d}{m_{sa} - m_{sw}} \qquad \text{Equation 4.3}$$

where ρ_{water} is the density of water at 20 °C which is 998 kg/m^3

4.2.5 Chloride Migration

The chloride migration test was conducted on six mortar cylinders, which have a diameter of 100 mm and a height of 50 mm. This test was performed according to the NT Build 492 practical guidelines.

First, samples were put in a sealed desiccator, and vacuum pressure was introduced and was maintained for 3 hours. Under the vacuum condition, $Ca(OH)_2$ solution with a concentration of 4 g/L was added until all the specimens were immersed. After that, the vacuum condition was maintained for another hour. Finally, the vacuum was released, and the specimens were left immersed for 18 ± 2 hours.

Afterwards, the samples were fixed into rubber sleeves with an anolyte solution (3M NaOH) poured on the top. The bottom parts of the samples were in contact with the catholyte solution (NaCl 10%). An external electrical potential of 30 V was applied axially across the specimens to force the chloride ions to migrate into the specimen. After 24 h, the samples were removed and split axially. Later on, a 0.1 N silver nitrate solution was sprayed on the split surface of the sample. After a white layer of precipitated silver nitrate became clearly visible, the penetration depth was measured with intervals of 10 mm.

Finally, the chloride migration coefficient (D_{nssm}) was calculated using Equation 4.4.

$$D_{nssm} = \frac{0.0239(273+T)L}{(U-2)t}\left(x_d - 0.0238\sqrt{\frac{(273+T)L\,X_d}{U-2}}\right) \qquad \text{(Equation 4.4)}$$

where D_{nssm} is the non-steady migration coefficient (10^{-12} m^2/s), U is the absolute voltage applied (V), T is an average value of initial and final temperature in anode solution (°C), L is the thickness of the sample (mm), X_d is an average value of penetration depth (mm) and t is test duration (hour).

4.2.6 Capillary Water Uptake

The capillary water uptake test was performed on three mortar prisms with the dimension of 40 × 40 × 160 mm^3, following the guidelines from EN 1015-10. First, 28 days old mortar samples were further cured in a conditioned room with a temperature of 20 ± 2 °C and relative humidity of 60 ± 5% for another 28 days. One day before the test, the side surfaces of the prisms were fully covered with aluminum tape and the samples were weighed. Later on, the mortar prisms were put on metal supports in a water-filled container with an immersion depth of 3 ± 1 mm **Figure 4.1**. The weight change of the samples was monitored after 0.5 h, 1 h, 2 h, 3 h, 4 h, 5 h, 6 h, 24 h, and then every 24 h for one week.

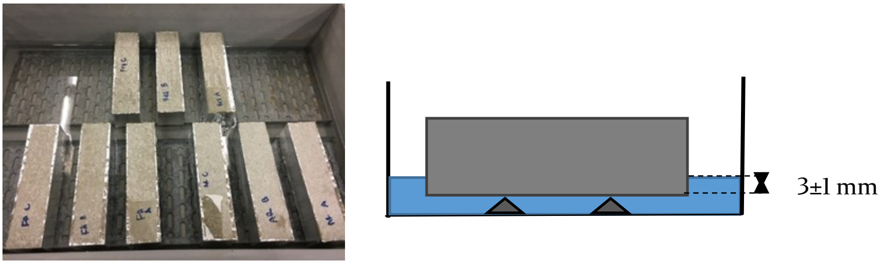

Figure 4.1. Capillary water uptake test setup.

4.2.7 Carbonation Resistance

The carbonation test was performed on prismatic mortar samples in accordance with the Belgian standard NBN B15-100. The 28 days old samples were moved from the curing room with a temperature of 20 ± 2 °C and humidity of 95 ± 5% to a conditioned room with lower humidity (60 ± 5%) for another 28 days. After that, 4 sides of the samples were covered with aluminum tape, leaving the bottom and top surface exposed. Furthermore, the samples were placed in the carbonation chamber at 1% CO_2, a temperature of 20 °C and a relative humidity of 60% with the not-covered surfaces upwards. After being exposed for 4, 12, and 16 weeks, the mortar bars were split perpendicular to the exposed surface and the split surfaces were sprayed with 1% phenolphthalein solution, for colorimetric carbonation assessment.

4.2.8 Morphology of the ITZ

Sample Preparation

The mortar samples were cut to slices with a thickness of 2 mm using a diamond saw cutter. These samples were broken until they fit in a cylindrical mold with a diameter of 30 mm. These pieces of mortar then were immersed in methanol to stop the hydration. Next, they were dried in an oven at 40°C until they reached constant weight.

The next step was sample impregnation with epoxy. The samples were subjected to vacuum pressure (0.8 bar) for 2 h. After that, the vacuum was released slowly to allow epoxy solution to penetrate into the sample. The impregnated samples were then left in an oven at 40 °C for 24 h until the epoxy had hardened.

Finally, the samples were polished with a SiC paper with a grit size of 320, 500, 1200, and 2400 (coarser to finer) for approximately 1.5 min each, followed by polishing with diamond paste with a grit size of 3 and 1 μm for 4 min. The polished samples were dried in the oven at 40 °C for 24 h. A carbon coating was then applied as the final stage of sample preparation.

Image Acquisition and Elemental Analysis

Back scattered electron (BSE) images were taken with a Jeol JSM-7600F Field Emission Scanning Electron Microscope (FESEM) equipped with AZtecEnergy software from Oxford Instruments for EDS mapping. EDS mapping was performed for Ca, Si, Fe, and Al elements.

4.3 Results and Discussion

4.3.1 Physical Properties of Resulting Mortar

The compressive strength and flexural strength results displayed in **Figure 4.2** are the same as presented in section 3.3.10. The one-way ANOVA post hoc Tuckey test shows that there was no significant difference in compressive strength and flexural strength between mortar containing EC LWA and FA 6M LWA as the p-values obtained are greater than 0.05 (**Figure 4.2**). Compared to the reference sample, a compressive strength reduction of 21% was observed. In the literature, it was found that mortar containing geopolymer mine tailing LWA with replacement rate of 21% for the fraction of 2–4 mm and using cement type II 32.5 N had a compressive strength of 25 MPa (Illikainen, 2017). With 5% lower replacement rate but higher content of Portland cement (cement type I), the compressive strength of mortar containing FA 6M LWA in this study is much higher compared to the literature results for mortar incorporated with mine tailing fly ash LWA.

A statistical analysis by one-way ANOVA post hoc Tuckey test showed a significant difference with p-value less than 0.05 on the apparent density between EC LWA and FA 6M samples compared to Reference samples (**Figure 4.2**). This result is well correlated with the LWA's apparent density value (**Table 4.1**). Even though FA 6M LWA has a higher porosity compared to EC LWA, FA 6M LWA has a higher apparent density. The small amount of open pores and high amount of closed pores in mortar with EC LWA could be the reason for the results for compressive strength and apparent density (**Figure 4.2**). A similar result was also reported in Chapter 2 revealing that the compressive strength of mortar incorporating EC LWA had higher compressive strength but lower bulk density compared with mortar incorporating FA 6M LWA. The sintering process during the production of EC LWA, which developed a closed pore system, can be related to the improvement in compressive strength of the resulting mortar (Güneyisi et al., 2013). Based on the pore structure characterization through MIP testing, EC LWA mostly contains macropores that could lead to the decrease in apparent density of the resulting mortar compared to the reference mortar (**Figure 3.8**). The denser ITZ could also contribute to the strength improvement in EC LWA samples. As LWA aggregate could act as an internal curing agent in the mortar matrix, remaining water in the pores of LWA could react with unhydrated cement and develop a denser layer at the ITZ between the cement paste and the LWA that could improve the compressive strength of the resulting mortar. This hypothesis was confirmed by the ITZ morphology observations presented further on in this paper.

In FA 6M LWA, high water absorption due to the high amount of open pores is still an issue to be solved. However, when FA 6M LWA was incorporated into a mortar matrix, the resulting mortar did not have such an extremely high-water absorption (**Figure 4.2**). It is also observed that the addition of LWA slightly reduces the flow value of fresh mortar (**Figure 4.2**). The reduction in workability in the EC LWA mortar is an indication that this LWA could absorb the water faster than FA 6M LWA. Even though FA 6M LWA has higher water absorption over 24 h (**Table 4.1**), the water seems to penetrate into the pores more slowly. The pore structure of FA 6M LWA that has smaller pore sizes could contribute to this slower rate of water absorption (**Figure 3.8**).

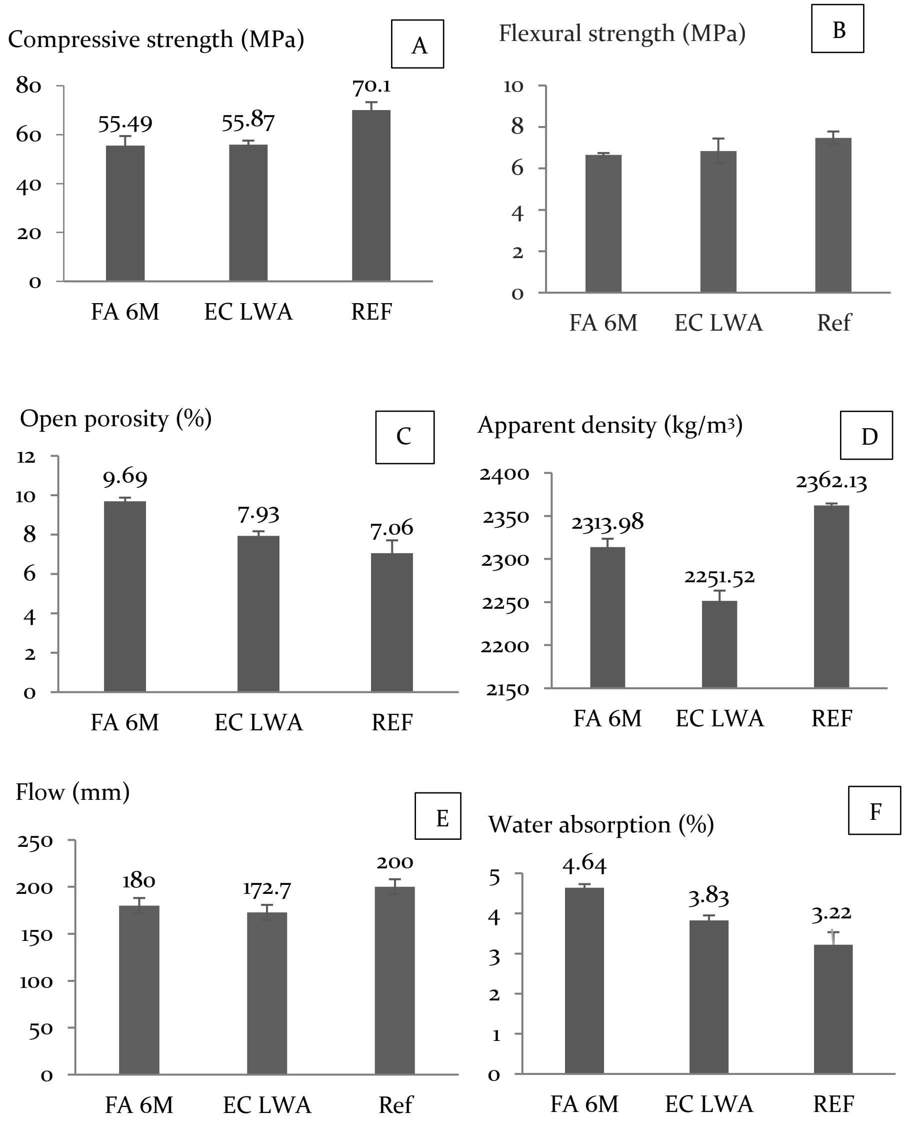

Figure 4.2. Physical properties of resulting mortar (n=3): (**A**) the compressive strength; (**B**) Flexural strength; (**C**) Flow value of fresh mortar; (**D**) Apparent density; (**E**) Open porosity and (**F**) Water absorption over 24 h.

4.3.2 Chloride Migration

Based on data of the non-steady-state migration coefficient (D_{nssm}), incorporating LWA into mortar tends to improve the chloride migration resistance. The reference mortar samples have the highest D_{nssm} value, followed by FA 6M samples and EC LWA samples (**Figure 4.3**). A statistical analysis by one-way ANOVA showed that only between Ref samples and EC LWA samples a significant difference occurred, while there was no significant difference between Ref samples and FA 6M samples.

It was expected that FA 6M LWA which has high volume of open porosity could provide internal curing, making the ITZ denser due to the additional hydration products (Bentz, 2009). However, since this LWA does seem to absorb water less fast than EC LWA; it may be that water absorption is not complete before mortar setting, and part of the additional water could just be considered as mixing water, making the resulting mortar more porous. Hence it could be that with proper water adjustment, the FA 6M mortar sample would have a similar performance regarding chloride migration as the EC LWA mortar sample (instead of being comparable to the reference sample that has no internal curing agent).

EC LWA with its faster water absorption might be more efficient to induce internal curing in mortar. However, the LWA content is insufficient to provoke a strong effect of internal curing on the chloride migration. In literature, a decrease in chloride migration in mortar by the replacement of 53% of the sand by LWA has been described (Bentz, 2009; C. Liu et al., 2020). The effect of higher replacement ratios of EC LWA and FA 6M LWA on chloride migration could be considered a topic for further research.

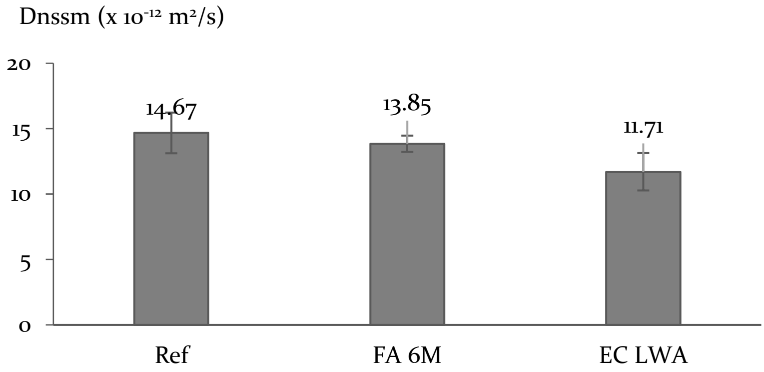

Figure 4.3 Non steady state chloride migration coefficient of the studied mortar types (n=3).

4.3.3 Capillary Water Uptake

In this research we have decided to present the capillary absorption as a function of $T^{0.25}$ instead of $T^{0.5}$ as this recently has been reported to give a better linear correlation (Villagrán Zaccardi et al., 2017). The capillary water uptake was observed over a time period of 168 h. All the data were then used to determine the capillary absorption rate by means of linear regression analysis. The results indeed show that the evolution of capillary water uptake has a linear correlation with $T^{0.25}$, indicated by the R^2 values of all the series being higher than 0.994 (**Figure 4.4**). Similar R^2 values were also reported in the literature when plotting water uptake as a function of $T^{0.25}$ (Alderete et al., 2019; Van Belleghem et al., 2016; Villagrán Zaccardi et al., 2017). In all series, in the first 24 h, around 0.2 g/cm² water was absorbed by the mortar. This value covered almost 50% of total water uptake by mortar in the total observation period (168 h). It seems that a primary capillary imbibition occurs in this period. From 24 h until 120 h immersion, the rate of water uptake was slightly slower compared to the first 24 h. A slower water uptake could be a first indication that most of the pores are filled with water. From 120 h until the end of the observation period, only small changes in water uptake could be observed. This is an indication that the mortar samples are saturated, and the water penetration into the samples was not driven by capillary force but by diffusion (Alderete et al., 2019)

No significant difference could be observed among all series. The FA 6M series had an almost overlapping capillary uptake pattern with the reference series, while a slight improvement was noticed in the EC LWA series. Similar results were also reported in previous research in which capillary absorption of structural lightweight aggregate concrete was studied (Bogas et al., 2015; Bogas et al., 2019). It was reported that the usage of LWA did not significantly affect the capillary absorption behavior of the resulting concrete.

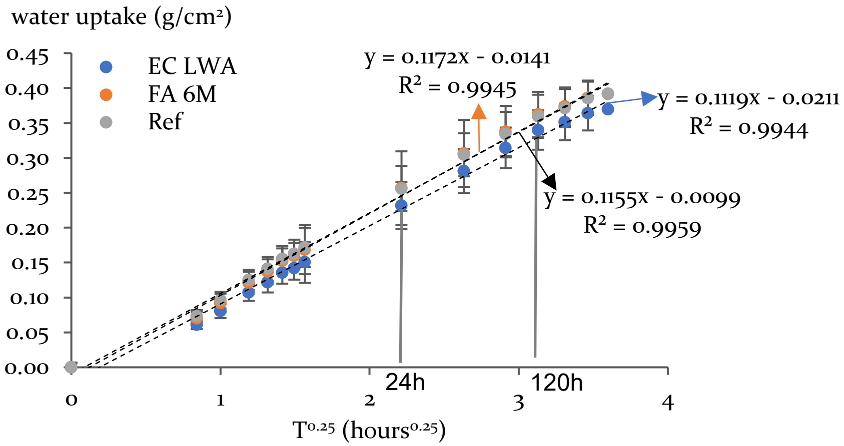

Figure 4.4 Capillary water uptake of the studied mortar plotted as a function of the fourth root of time (n=3). The dashed line refers to linear regression of each series.

4.3.4 Carbonation Resistance

No good linear correlation was noticed between the carbonation depth and the square root of time for the mortar samples with LWA (**Figure 4.5**). The R^2 for the linear regression of FA 6M mortar was quite low, followed by EC LWA and reference mortar. It seems that less linearity occurred between the carbonation depth and square root of time for mortar containing FA 6M LWA compared to other mortar types. For the mortar with FA 6M LWA, carbonation depths of the samples that were exposed for 4 weeks showed no significant difference with samples that were exposed for 16 weeks, but at 20 weeks there was a clear increase (**Figure 4.5**). In contrast, mortar containing EC LWA showed a significant increase of carbonation depth after being exposed for 16 weeks. After 20 weeks of exposure, similar carbonation depths of around 6.5 mm were observed for the samples with EC LWA and FA 6M LWA. Meanwhile, the carbonation depth for the reference samples was relatively low and showed a lower variability compared to the samples with LWA. High standard deviations were observed for samples with EC and FA 6M LWA. Based on the visual observation of the split sample sprayed with phenolphthalein, it was clear that due to the high porosity of LWA, CO_2 could penetrate through the LWA causing high variation on the carbonation depth (**Figure 4.6**). Similar results have been reported in previous research on using porous Leca aggregate as aggregate substitution in mortar production (Bogas et al., 2019).

The rapid increase in carbonation depth for samples containing LWA in the first 4 weeks was mostly due to the high volume of open porosity in the LWA. This is in agreement with literature, stating that the porosity of LWA has a great influence on the carbonation resistance of its resulting concrete or mortar (Bogas et al., 2019). At 4 weeks of exposure, samples containing EC LWA have slightly lower carbonation depth compared to the FA 6M sample. This is understandable as EC LWA has more closed pores that might be difficult to be penetrated by CO_2 compared to FA 6M LWA. However, a significant increase of carbonation depth was observed for the EC LWA sample after being exposed to CO_2 for 16 weeks. Similar behaviour occurs for the FA 6M samples after 20 weeks of exposure. Since Figure 4 shows that the EC LWA only has macropores, while FA 6M LWA still has around 20% mesopores, it could be reasonably expected that in samples with EC LWA, the significant increase in carbonation depth occurs faster than for the FA 6M samples as CO_2 will penetrate faster through bigger pores.

In the final weeks of observation, samples containing FA 6M LWA have a slightly better carbonation resistance compared to EC LWA samples. In the FA 6M LWA samples, the excess of sodium hydroxide in the aggregate might react with CO_2 and form sodium carbonate. Unreacted calcium in fly ash could also react with CO_2 and form $CaCO_3$. It has been also reported in the literature that in fly ash-based alkali activated paste, the C-A-S-H gel will mostly decalcify during accelerated carbonation and lead to the precipitation of $CaCO_3$ (Bernal et al., 2013). Those extra precipitation products could make the matrix around the aggregate denser which can deliver better carbonation resistance. A noticeable improvement in carbonation resistance was also observed when recycled aggregate was incorporated in MSWI bottom ash-based alkali activated systems rather than in control samples (cement based system) (Casanova et al., 2021). Similar to the observation of carbonated C-A-S-H gel, the enhancing of the carbonation resistance in this system is also due to the decalcification of Ca-bearing phases followed by the precipitation of $CaCO_3$, as well as the reaction of Na^+ with CO_2 in the pore solution forming sodium carbonates (Casanova et al., 2021).

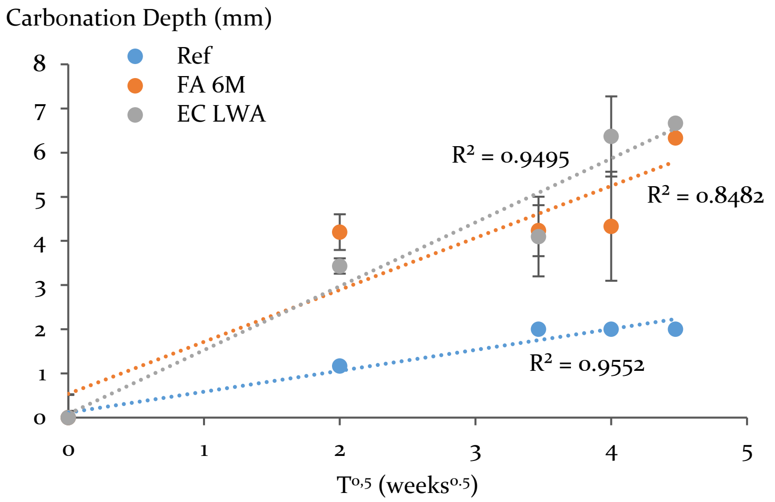

Figure 4.5 The evolution of the carbonation depth of the studied mortars. The linear regression is presented in dashed line (n=3).

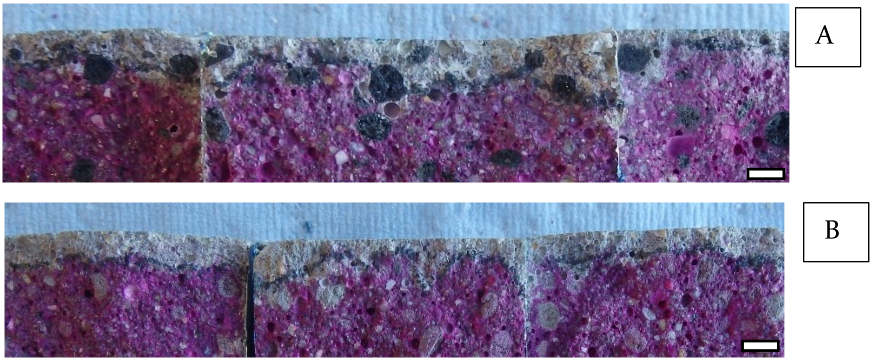

Figure 4.6 The variability on carbonation depth in (**A**) EC LWA and (**B**) FA 6M LWA mortar samples after being sprayed with phenolphthalein 1%. The scale bars represent 1 cm.

4.3.5 The Characterization of the Interfacial Transition Zone (ITZ)

The ITZ of the EC LWA sample was denser, indicated with the bright whitish line (**Figure** 4.7). In the sample containing FA 6M LWA, the ITZ could not be well observed due to the excess FA on the surface of LWA that might be mixed with cement paste (**Figure** 4.7). On the other hand, a clear gap between aggregate and cement paste was observed in the reference sample (**Figure** 4.7).

The denser ITZ in mortar containing EC LWA is in good agreement with its better performance in chloride migration and capillary water uptake. A dense morphology of the ITZ was also reported for mortar incorporating modified surface slag LWA (L. Zhang et al., 2017). The role of LWA as internal curing agent retaining water for release later to react with unhydrated cement and form hydration products that block the ITZ gap could be clearly noticed for EC LWA. Based on EDS analysis, the amount of calcium and aluminum detected in the ITZ of EC LWA sample was higher compared to the reference samples (**Table 4.3**). The ratio between Ca/Si detected in the ITZ of EC samples is 1.1 (**Table 4.3**). This ratio is in the range for C-S-H that is usually observed in cement paste, which is between 0.66 to 2.1 (Nonat, 2004; Pelisser et al., 2012; Tajuelo Rodriguez et al., 2017). As the ratio of Ca/Si detected in the ITZ of EC LWA is less than 1.5, the crystal structure of this C-S-H could be jennite (Kapeluszna et al., 2017; Taylor, 1993). Similar patterns were also found in the literature on incorporating slag-based LWA into mortar. Through backscattered electron imaging with the magnification of 1000×, it was found that the calcium rich hydration products in the denser ITZ were C-S-H (L. Zhang et al., 2017).

In the ITZ between FA 6M LWA and cement paste, pores filled with gel and round unreacted fly ash particles could be sporadically observed (Figure 11B,B1). In literature, clear pictures of gel formation have been taken (with the magnification of 20,000×) in the ITZ of fly ash-based geopolymer (Luo et al., 2021). The gel form probably was C-A-S-H or N-A-S-H, indicated by the high silica and alumina content in the ITZ (Figure 10B). A high Al/Si ratio (above 0.2) in samples that have lower Ca/Si ratio (lower than 1) was reported to deliver a very weak gel formation of C-A-S-H due to the less reactive alumina in fly ash compared to aluminum in cement clinker (Kapeluszna et al., 2017). Thus, it is reasonable that a less clear gel formation was observed in the ITZ between FA 6M LWA and cement paste, as the ratio of Ca/Si detected in this area is quite low (below 1), while the Al/Si ratio was high (above 0.2) (**Table 4.3**).

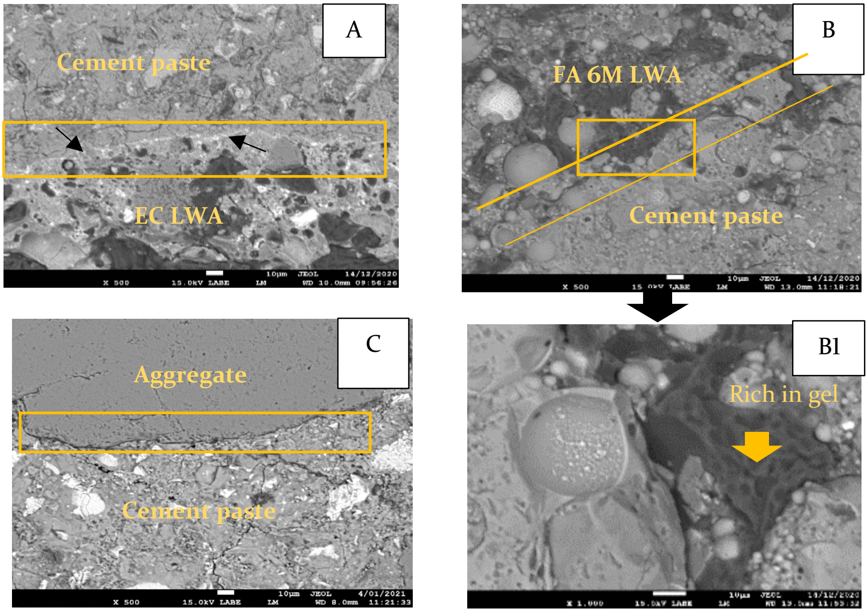

Figure 4.7 BSE SEM image of the Interfacial Transition Zone with scale bar of 10 µm (**A**) EC LWA; (**B**) FA 6M LWA; and (**C**) normal aggregate with cement paste. (**B1**) magnification of selected area in (**B**) to confirm the presence of gel in the ITZ between FA LWA and cement paste.

Table 4.3 Resume of EDS mapping analysis on the amount of Ca, Si and Al in ITZ between cement paste and aggregate.

Type	Ca (%)	Si (%)	Al (%)	Ratio Ca/Si	Ratio Al/Si
EC LWA	40.8	36.8	9	1.11	0.24
FA LWA	34	47.3	13.3	0.72	0.28
Ref	32.3	63.3	2	0.51	0.03

4.4 Conclusions

This chapter presents the physical properties and durability aspects of mortar containing fly ash-based alkali activated lightweight aggregate. The results show that the properties of hardened mortar containing FA 6M LWA are acceptable compared to a reference without LWA and a mortar with commercial expanded clay (EC) LWA. FA 6M mortar and EC LWA mortar have similar compressive strength, while high water absorption is still an issue that needs to be improved for FA 6M mortar. Exposing the FA 6M LWA to CO_2 to induce the calcification of unreacted fly ash attached on the surface of LWA is a consideration for further research. With that pretreatment the open pores on the surface of LWA are expected to be closed, which could decrease the water absorption.

Overall, the FA 6M mortar has comparable durability performance as the reference and the EC LWA mortar sample. FA 6M mortar has a slightly higher chloride migration coefficient, but has slightly better carbonation resistance compared to the EC LWA samples (differences being insignificant). Moreover, the capillary water uptake performance of FA 6M mortar is similar with reference mortar. A denser ITZ was observed both in EC LWA and FA 6M LWA samples. Summarizing, replacing a limited amount of fine aggregate in the mortar with FA 6M LWA could be an alternative solution for increasing the consumption of industrial by-products, as it gives acceptable properties and durability performance and can be further used as a bacteria carrier in self-healing concrete production.

Chapter 5. Suitable Yeast Extract Concentration for the Production of Self-Healing Concrete with Expanded Clay as Bacterial Carrier

This chapter contains results obtained in collaboration with a supervised master thesis student:

Lipeng, Ma. “Effect of Bio-agent On Self-Healing Concrete with Lightweight Aggregate as Bacteria Carrier”. Master Dissertation. Ghent University, 2021.

5.1 Introduction

Bacteria-based self-healing is reported to provide adequate healing performance to concrete (Jonkers & Schlangen, 2009; Wang et al., 2017). It was reported that spores of *B. alkanitrilicus* that had been encapsulated into expanded clay LWA could seal a crack width up to 0.46 after 30 days curing in water (Wiktor & Jonkers, 2011). In other literature, it was revealed that by encapsulating *B. sphaericus* into microcapsule, a crack width of 0.97 mm could be completely healed after subjecting the samples to wet-dry cycle curing for 21 days (Wang et al., 2012). When *B. sphaericus* was encapsulated into hydrogel, after subjecting to wet-dry cycle curing for 7 days, cracks with the width of 0.5 mm were completely closed (Wang, Snoeck, et al., 2014). While when cells of *Diaphorobacter nitroreducens* and *Pseudomonas aeruginosa* were incapsulated into expanded clay, they could seal a crack with the width of 0.35 mm after immersion into water for 28 days (Yusuf Çağatay Erşan et al., 2016).

Several alkali-tolerant bacteria strains such as *Bacillus sphaericus*, *Bacillus subtilis*, and *Bacillus alkalinitrilicus*, *Diaphorobacter nitroreducens* and *Pseudomonas aeruginosa* were successfully employed as a healing agent (Yusuf Çağatay Erşan et al., 2016; Feng et al., 2021; J. Wang, Jonkers, et al., 2017; Wiktor & Jonkers, 2011). *Bacillus sphaericus* that can induce calcium carbonate precipitation to heal concrete cracks through urea hydrolysis (Wang et al., 2017), and has been proven to deliver more dense calcium carbonate precipitation, was chosen as healing agent in this research .

In bacteria-based self-healing systems, carriers are mostly needed to protect the bacteria from the harsh environment of fresh concrete. Various carriers such as lightweight aggregate (LWA), hydrogel and microcapsules have been applied (Lucas et al., 2018; Wang et al., 2018; Wang et al., 2012; Wang, Soens, et al., 2014). In this research expanded clay lightweight aggregate (EC LWA) was prepared to become the bacteria carrier, as it has been reported to have good compatibility with the mortar matrix and also delivers excellent healing performance (Wiktor & Jonkers, 2011).

For the mechanism of bacteria-based healing, called microbially induced calcium carbonate precipitation (MICP), bioagents such as nutrients, urea, and calcium source are needed to complete the reaction. A nutrient obtained from yeast extract is needed to induce germination of spores and keep the viability of bacteria. At the same time, urea is needed to complete the metabolic pathway (De Muynck et al., 2010). With the help of the bacterial urease enzyme, the urea can be decomposed to ammonium and carbonate as described in Equation 5.1:

$CO(NH_2)_2 + 2H_2O \rightarrow 2NH_4^+ + CO_3^{2-}$ (Equation 5.1)

With sufficient amount of calcium ions in the solution, the carbonate can react and form calcium carbonate according to Equation 5.2:

$CO_3^{2-} + Ca^{2+} \leftrightarrow CaCO_3$ (Equation 5.2)

Several studies on screening calcium sources reported that different calcium sources mainly affect the morphology of the healing products, and different bacteria strains could induce different reactions (Achal and Pan, 2014; De Muynck et al., 2010; Y. Zhang et al., 2015). Thus in this research, calcium nitrate was chosen as a calcium source as it has been reported to deliver sufficient amount of calcium carbonate precipitation when *Bacillus sphaericus* is employed as a healing agent (Wang et al., 2017). Furthermore, it would not provoke a risk of rebar corrosion in reinforced concrete structures, as would be the case if calcium chloride were used.

However, bioagents, especially yeast, could negatively affect the properties of resulting mortar or concrete (Zeynep Basaran Bundur et al., 2015). The presence of yeast extract tends to delay the hydration process, and due to its autolysis, hydrogen gas is released in contact with water that later on could induce the formation of pores in concrete (Bolobova and Kondrashchenko, 2000). With the presence of extra pores in concrete, concrete's mechanical properties could decrease to an unacceptable level. Vandervoort et al. also found a 49% strength decrease relative to the reference sample when yeast extract with the concentration of 5 g/l mortar was added into mortar mixture (Vandervoort, 2019).

Regarding the function of yeast extract as germination agent for spores, in a previous study by Wang et al. in which the outgrowth of *B. sphaericus* spores, the minimum yeast extract concentration that allowed spores to significantly grow was 5 g/l (Wang et al., 2017). However, through the Nessler test, it was found that the urea decomposition rates of spores cultivated in medium containing 2 g/l or 5 g/l yeast extract were similar (Wang et al., 2017). Still from the same literature, by omitting the yeast from the culture medium, spores still can slowly decompose the urea. For comparison, when spores were cultivated in yeast extract solution 2 g/l and 5 g/l, the amount of urea decomposed was 20 g/l, while it was less than 5 g/l urea that could be decomposed in no-yeast extract samples in a time span of 72 hours.

Considering previous findings in utilizing yeast extract, when the presence of yeast is compulsory in the mortar, yeast with concentration of 2 g/l and 5 g/l would be enough for spores to germinate (Wang et al., 2017). However, the properties of bio-mortar containing those two yeast concentrations still needs to be further investigated. At the same time, the feasibility of omitting yeast from the matrix should also be investigated for self-healing concrete that employs vegetative cells as a healing agent.

To summarize, this part of the study aims to find suitable yeast concentrations that have a less negative effect on the properties of lightweight mortar prepared for bacteria-based self-healing concrete. The possibility of omitting yeast from the mortar matrix was also studied. The setting time, workability, and heat evolution of fresh mortar were studied. In the hardened state, the compressive strength, bulk density, and porosity determined by mercury intrusion porosimetry (MIP) were investigated.

5.2 Materials and Methods

5.2.1 Materials

Cement type I 52.5 from Holcim was used as binder. An Expanded Clay Lightweight Aggregate (EC LWA) with a size of 2-4 mm was used as fine aggregate replacement. This fraction was obtained by sieving the 0/4 fraction of commercial EC LWA from Argex Nv. A river sand with a size of 0-2 mm was used as fine aggregate. This fraction was obtained by sieving the 0/4 river sand. Based on the particle size distribution of river sand 0/4, the volume of sand with particle size larger than 2 mm was 16% (**Figure 5.1**). Thus, in this research the whole volume of river sand with the size of 2-4 mm was replaced with EC LWA. Extra water equal to its water absorption value was added into EC LWA, in order to bring the aggregates in SSD condition. Pre-conditioning of EC LWA before mixing was performed to avoid the EC LWA to absorb water during mixing. The properties of EC LWA and river sand are presented in **Table 5.1**, while the mix design of mortar is displayed in **Table 5.2**.

Yeast extract, urea and calcium nitrate tetrahydrate were utilized as bio-agent in this research. A powder form of yeast extract with purity of 99% (Carl Roth Belgium) was used as bacterial nutrient, while calcium nitrate tetrahydrate with a purity of 99% (Carl Roth Belgium) was used as calcium source needed for bacteria-based self-healing. Urea with a purity of 98 % was added as substrate for bacteria's metabolism into mixture as well. The amount of urea and calcium nitrate was kept constant while the amount of yeast was varied and set at 0, 2 g/l and 5 g/l (Vandervoort, 2019; Wang et al., 2017) (Table 2). The mass ratio between yeast extract and calcium nitrate in samples NY0, NY2, and NY5 was 0, 0.04, and 0.11 respectively. In order to keep the water/cement ratio of 0.5, the mixing water of samples with calcium nitrate was reduced to accommodate the excess water released from calcium nitrate tetrahydrate (4 H_2O molecules). The chosen concentration of urea and calcium nitrate was reported to deliver good healing capacity in self-healing concrete (Wang et al., 2018).

Table 5.1. Physical properties of EC LWA and river sand with the size of 2-4 mm (n=3).

Test	EC LWA	Sand 2-4 mm
Apparent particle density (AD) (g/cm^3)	1.25 ± 0.01	2.63 ± 0.04
Oven dried density (OD) (g/cm^3)	0.99 ± 0.01	2.48 ± 0.03
SSD particle density (SSD) (g/cm^3)	1.19 ± 0.01	2.54 ± 0,03
Water absorption 24 hours (WA_{24h}) (%)	20.85 ± 0.09	2.19 ± 0.14
Open Porosity (OP) (%)	21.14 ± 0.3	2.15±0,14

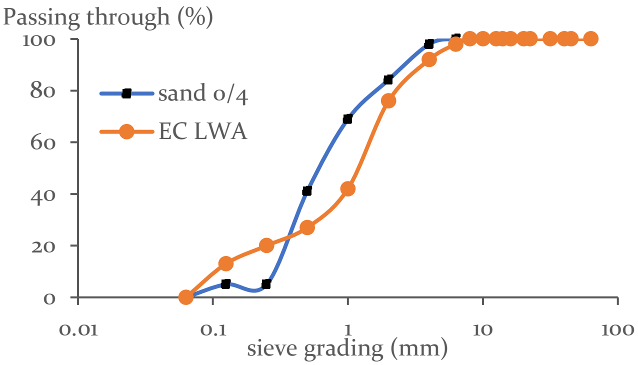

Figure 5.1 Particle size distribution of sand 0/4 and EC LWA 0/4

Table 5.2. Mix Design of Mortar

Type	Sand 0-2 (g)	LWA 2-4 (g)	Cement (g)	Entrained water (g)	Water (g)	Yeast Extract (g)	Urea (g)	Calcium Nitrate (g)
Ref	1251	82	450	17	225	0	0	0
NY0	1251	82	450	17	214	0	18	36
NY2	1251	82	450	17	214	1.53	18	36
NY5	1251	82	450	17	214	3.83	18	36

5.2.2 Fresh Properties

The setting time of paste was tested according to NBN EN 196-3. The paste containing cement, water and bio-agents (yeast extract, urea and calcium nitrate) was mixed and cast into a conical mould with a height of 400 mm, an upper diameter of 65 mm and a bottom diameter of 75 mm. The paste was then tested with a Vicatronic E044N by Matest. The initial setting time was determined when the penetration depth of the needle from the top of the mould was recorded as 34 ± 3 mm, while the final setting time was determined when the needle could not penetrate into paste, indicated by the penetration depth of 5 mm.

The heat evolution of the paste was monitored using an isothermal calorimeter (TA instrument, TAM Air) at the temperature of 20ºC. In order to keep all the materials at the same temperature, all the raw materials were kept in the curing chamber at 20 ± 2 °C one day prior the test. The yeast extract, urea and calcium nitrate were dissolved into the water required to obtain a water/cement ratio of 0.5.

Workability of fresh mortar was determined by a flow table test. This test was performed following the guidance from NBN EN 1015-3 (1999). A fresh mortar was poured gradually (2 layers) into a conical mould on the shaking table. The mixture was compacted by stroking each layer 10 times with a small stick . Finally the mould was removed, and the table was jolted for 10 times. The flow value was then determined by measuring the diameter of the spread-out mortar.

5.2.3 Hardened State Properties

The mortar mixtures were cast into prismatic moulds with the dimension of 40x40x160 mm^3. Immediately after being cast, the mortar samples were covered with plastic film to avoid evaporation and cured in a curing chamber with temperature of 20±2ºC and relative humidity of 95±5% for 24 hours. After curing for 24 hours, samples were demolded and covered with plastic film and cured in the same chamber until reaching the age of 28 days.

The bulk density and the compressive strength of 28 days old mortar were tested according to EN 196-1 standard. After the dimensions and the weight of samples were recorded, the mortar samples were tested in a machine for three point bending (Walter bai) which has a loading speed of 2400±200 N/s. Half of the broken prisms from the bending test was then subjected to uniform load to determine the compressive strength.

The pore structure of mortar was studied by Mercury Intrusion Porosimetry (MIP) test. The 28 days old mortar was broken into pieces with a diameter of more or less 20 mm, not containing EC LWA. The hydration was stopped by immersing the samples into iso-propanol, and shaking it on a shaking table with the speed of 70 rpm for 15 minutes. The procedure was repeated twice followed by drying the samples in an oven at 40ºC for 24 hours. The samples were further dried in a vacuum chamber with the pressure of -0.8 bar for approximately 2 weeks until reaching constant mass.

5.3 Results and Discussion

5.3.1 Setting Time

In general, samples containing bio-agents showed a shorter setting time compared to the reference sample (**Table 5.3**); although initial setting was delayed, final setting was reached earlier in time. Indeed there were three elements interacting in the nutrient sample. The urea and yeast extract were expected to act as a retarder that delays the setting time, while calcium has been reported to accelerate the hydration process (Bolobova and Kondrashchenko, 2000; Ogunbode and Hassan, 2011; Shaaban Mwaiuwinga, 1997). For the compositions applied in this research, it seems that calcium successfully repressed the retarding effect provoked by yeast extract and urea. In previous research by Vandervoort, the final setting time of samples only containing yeast extract 5 g/l mortar reached almost 650 minutes (Vandervoort, 2019). In comparison, with the same amount of yeast extract but with the addition of calcium nitrate and urea, the final setting time of NY5 sample which has ratio between YE and calcium nitrate of 0.11 was 80 minutes faster.

Without the addition of yeast in the mixture, the final setting time of NY0 decreased, while the initial setting time increased. A slight retardation due to the presence of urea in the NY0 sample might occur. But this was less dominant compared to the acceleration effect contributed by calcium coming from the addition of calcium nitrate into the mixture. As the calcium element (in alite) tends to dominate the early hydration process, the extra addition of calcium could accelerate the main hydration process and even lead to flash setting of the paste (Bullard et al., 2011). A flash setting of paste was also reported in literature when calcium nitrate was used as plasticizer (Ogunbode and Hassan, 2011). Still from the same literature, by adding a calcium nitrate at a dosage of 10% of cement weight, the final setting time occurred 25 minutes faster than the reference sample.

A clear delay in setting time was observed in the sample containing yeast extract, compared to a no-yeast sample containing only the calcium source and urea (NY0). Increasing the yeast extract concentration up to 5 g/l mortar delayed the final setting time for 75 minutes compared to the no-yeast sample (NY0). A slight delay in setting due to the addition of nutrient medium containing yeast was also reported in the literature (Bundur et al., 2015; Joshi et al., 2018). The presence of carbohydrates and proteins in yeast could contribute to this behaviour. It is reported that sugars could stimulate the dissolution of calcium in cement clinker and form a sucrose half-salt. The absorption of this product at the surface of C-S-H gel could inhibit the formation of stable C-S-H precipitation which mainly occurs in the early hydration process (Thomas and Birchall, 1983).

Table 5.3. The effect of nutrient to the setting time of paste

Sample	Initial setting time (minutes)	Final setting time (minutes)
Ref	135	660
NY0	225	495
NY2	330	555
NY5	390	570

5.3.2 Heat Evolution

Significant differences in the heat evolution were observed among samples (**Figure 5.2**). The nutrient sample shows a steeper curve compared to the reference sample. So even though the induction periods of all the samples were similar, the reference sample needed longer time to set. It was also observed that the second peak, which corresponds to the formation of ettringite by dissolution of tri-calcium aluminate disappeared in samples with nutrient (Bullard et al., 2011). It seems that the addition of nutrient oppressed the hydration of aluminates. Bundur et al. also obtained a single hydration peak by adding yeast extract at 0.67 % of the paste weight (Bundur et al., 2015).

When increasing the concentration of yeast (in combination with calcium source and urea), a significant retarder effect was not observed in this research. The first hydration peak of the reference sample and the nutrient samples were similar. It seems that, the role of calcium as accelerator was more dominant than the retarder effect of yeast. The effect of urea in the mixture, that was expected to delay the hydration process, might occur but not enough to shift the hydration peak location to later times.

No significant difference was observed in the cumulative heat release obtained by all samples monitored for 140 hours (**Figure 5.3**). A sharper hydration peak in the nutrient samples due to a fast heat release followed by a quick decrease makes that the final cumulative heat release obtained in nutrient samples are not as high as expected. The total heat release after 140 h obtained in the Ref, NY0, NY2 and NY5 sample was 335, 345, 329 and 334 J/g. Compared to the heat release obtained with only calcium nitrate, the heat release obtained in the NY0 sample was 13% lower (Wang et al., 2018). The presence of urea seems to slightly repress the heat release in the NY0 sample.

In addition, more heat release was observed in the nutrient sample, and this was higher when yeast was not present (**Figure 5.3**). This behaviour was also attributed to the heat released by the dissolution of C_3S, which is accelerated by the addition of extra calcium in the matrix (Bullard et al., 2011). An increase of heat release was also reported for the heat evolution of paste with a higher C_3S content (Kipkemboi et al., 2020).

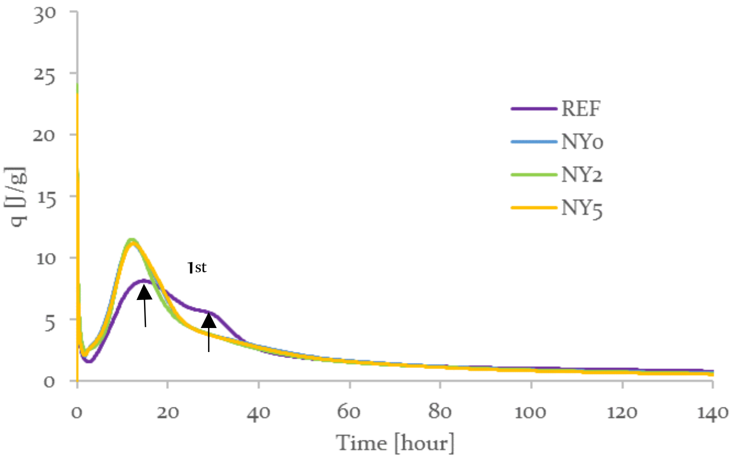

Figure 5.2 Heat evolution of paste with various yeast extract concentration

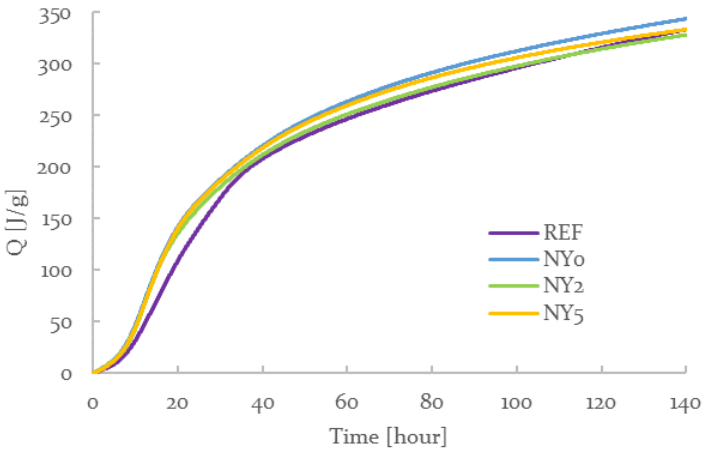

Figure 5.3 Cumulative heat release of paste with various yeast extract concentrations

5.3.3 Workability of Fresh Mortar

It can be seen that the workability of fresh mortar was increased as the concentration of yeast extract increased (**Figure 5.4**). The flow value was increased by 3% and 19% by adding yeast extract up to 2 g/l and 5 g/L, respectively, compared to that of the reference sample . The formation of hydrogen as a result of yeast autolysis reaction could explain the increase of workability observed in nutrient samples containing yeast (Martínez-

Rodríguez and Polo, 2000). The presence of gas has a lubricating effect and the slurry texture of the mixture leads to the increase of flowability of fresh mortar.

The role of calcium that is widely used as accelerator could be seen in the no-yeast sample. The mixture became more stiff in a short period of time. Without the presence of yeast extract in the mixture, the flowability of fresh mortar dropped up to 25% compared to the reference sample. The stiff fresh mortar of NY0 is well correlated with the fast setting of its paste (**Table 5.3**).

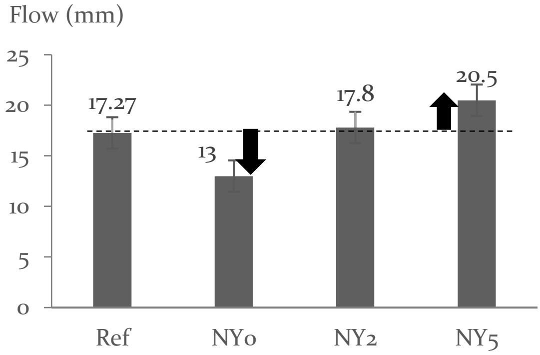

Figure 5.4 The Effect of yeast extract concentration on the flowability of fresh lightweight mortar. The dashed line corresponds to the average value of the reference sample, while the error bar represents the standard deviation on the mean (n=3).

5.3.4 Porosity

It can be seen that increasing the concentration of yeast extract increased the cumulative volume of mercury intruded into the pores of mortar (**Figure 5.5**). A higher cumulative volume intruded into mortar pores is an indication that the mortar sample has high porosity. The results were then confirmed with the characterization of the pores presented in **Figure 5.5**. Sample NY5 which has a high level of yeast extract possessed a high amount of macropores. The number of macropores decreased with the decreasing yeast extract concentration in the mixture. The gas which was released due to the hydrolysis of protein in yeast created bubbles that remained as pores when the mortar hardens (Martínez-Rodríguez and Polo, 2000).

A noticeable change in pore size was observed between the reference sample and NY5. Increasing the yeast extract concentration up to 5 g/l shifted the major pore size from 0.06 μm to 1 μm. While sample NY0 and NY2 with lower yeast extract concentration, had two threshold pore sizes. The first threshold has a similar value as the reference sample, while the other has a similar value as NY5. The threshold pore diameter in the mesopore zone occurring in NY2 and NY0 could be due to the ink bottle effect. NY5 has a limited number of small pores, which makes that the ink bottle effect could not be clearly observed. The presence of small pores connected to a large pore leads to a high pressure needed for mercury to penetrate through the small pores into the larger pore (Korat, Ducman, Legat, and Mirtič, 2013). It results in the machine recording a high amount of small pores instead of the large pores that are actually present.

Summarizing, adding yeast extract with the concentration of 5 g/l significantly changes the pore properties of the hardened mortar. Indeed, the appearance of gas bubbles could improve the flowability of fresh concrete, which was disturbed by the addition of calcium. However, when the water in the mortar mixture evaporates, the entrapped gas bubbles will become pores, that could decrease the bulk density of the resulting mortar. The presence of high amount of pores was confirmed with the low bulk density of hardened mortar with high yeast extract concentration that will need further discussion in the next section.

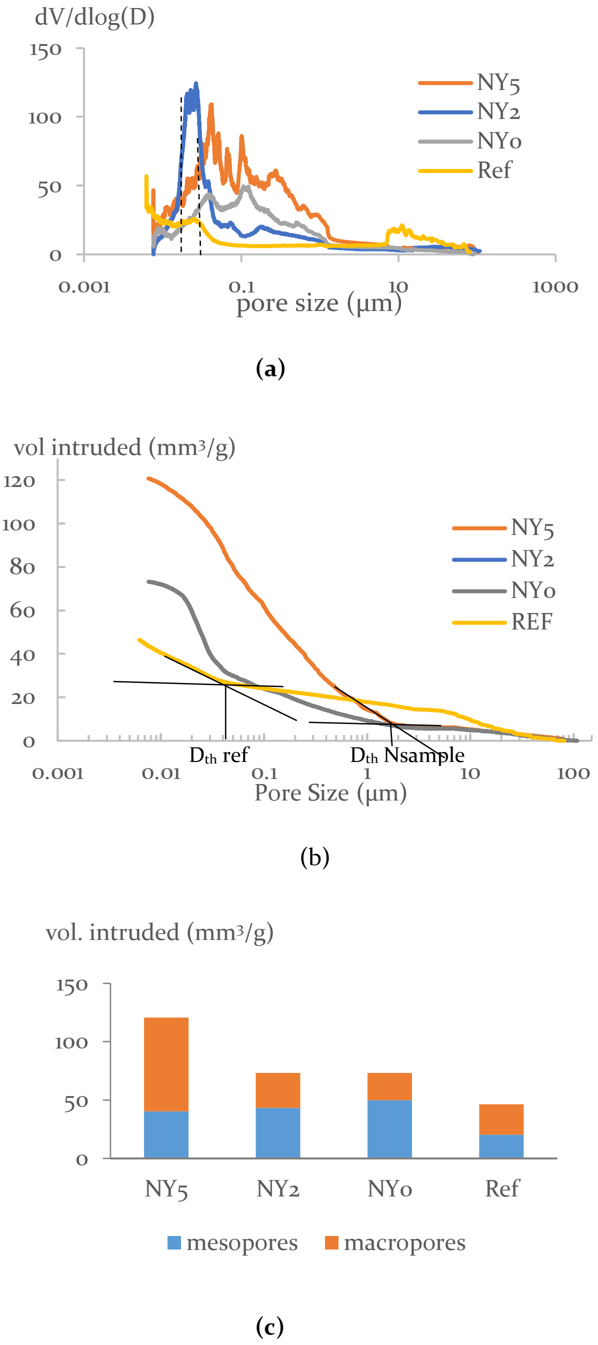

Figure 5.5. (a) Pore size distribution of mortar; (b) Cumulative intruded volume of mortar; (c) Types of pores in mortar

5.3.5 Bulk Density and Compressive Strength

The bulk density of resulting mortar was well correlated with its 28 days compressive strength (**Figure 5.6**). Increasing the yeast extract concentration proved to decrease the bulk density and the compressive strength of resulting mortar. Introducing 5 g/l yeast extract into mixture decreased the compressive strength of resulting mortar for almost 50% compared to reference sample. The strength was decreased for about 16% when the yeast extract level was decreased to 2 g/l and no significant effect could be seen when yeast extract was omitted from the mixture but calcium source and urea were still present.

The low workability of NY0 did not lead to a significant decrease of the strength and density. It seems that the presence of calcium in NY0 that should improve the strength was neutralised by the present of urea. The urea was reported to decrease the hydration heat in the system and slow down the hydration reaction (Vandervoort, 2019). The urea and calcium have an opposite role in the hydration process, which could neutralize their effects when combined in hardened mortar.

The mechanical properties of hardened mortar were also correlated with its pore characterization data generated from MIP. The sample with a high yeast extract concentration (NY5) delivers a high porosity, a low bulk density and compressive strength. The slightly larger number of mesopores and lower amount of macropores in NY0 leads to a higher compressive strength in resulting mortar compared to NY2.

In the literature, the addition of urea yeast extract medium (YE 0.63% of paste weight) into cement paste leads to 26% strength decrease of paste relative to the reference sample (Bundur et al., 2015). In concrete application, adding treated aggregate with NBU medium (yeast extract, peptone, urea, sodium chloride and calcium chloride) proved to decrease the 28 days concrete compressive strength up to 15% (Joshi et al., 2018). Compared to results obtained in concrete application by Joshi et al. the strength reduction of NY2 mortar is still comparable.

The decrease in bulk density due to the pore formation from protein hydrolysis of yeast extract was the main reason of the strength decrease in the mortar samples with high concentration of yeast extract.

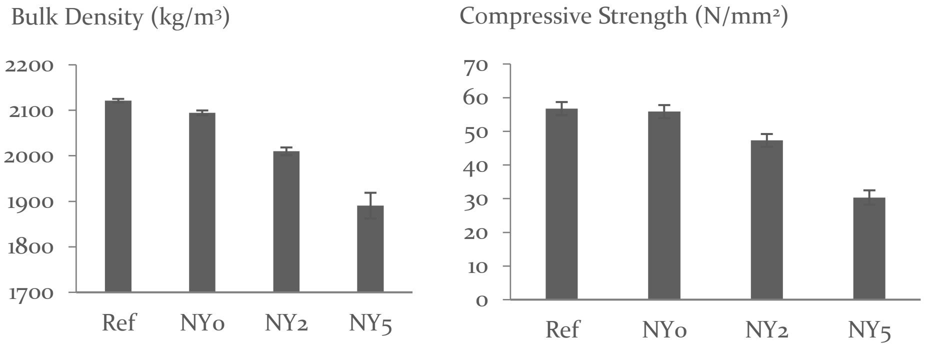

(a) **(b)**

Figure 5.6 The effect of yeast extract concentration on the (a) bulk density and (b) compressive strength of lightweight mortar (n=3). The dashed line corresponds to the average value of the reference sample, while the error bars represent the standard deviation of the mean value.

5.4 Conclusions

The presence of yeast extract significantly affected the properties of hardened bio-mortar. The number of macropores was significantly increased by adding 5 g/l yeast extract into solution. The increase in macropores content consequently decreased the density of 28 days old mortar which leads to the decrease of the compressive strength.

Due to the presence of calcium in the mixture composition, the retarder effect of yeast extract was alleviated. There is a slight delay in setting time when the yeast extract concentration was increased compared to a no-yeast extract sample. However, compared to the reference samples without calcium nitrate and urea, samples containing yeast extract still had a shorter setting time. This was corresponding well with the hydration kinetic results. The hydration peak of samples with yeast extract was similar to that of the reference sample. More heat was released in the sample with addition of calcium source and urea, compared to that of the reference sample.

A workability issue was found in the no-yeast extract samples containing only calcium nitrate and urea. With the absence of yeast extract which induced the formation of bubbles during its hydrolysis, the workability of no-yeast extract samples dropped up to 25%.

Summarizing, if spores were used as the healing agent, where yeast extract is required for the germination process, 2 g/l yeast extract into the mixture could be an option, as the properties of resulting mortar decreased to an acceptable level. However, in the condition where the presence of yeast extract is not mandatory, for example when vegetative cells were employed as healing agent, omitting yeast extract from mixture is feasible as the presence of only calcium nitrate and urea did not significantly affect the properties of resulting mortar.

This page is Intentionally blank.

Chapter 6. Alkali Activated LWA as Bacterial Carrier in Manufacturing Self-Healing Mortar

This chapter was redrafted after:

Risdanareni, P., Wang, J. and De Belie, N. 2021. "Expanded Clay as Bacteria Cells Protector in Manufacturing Self-Healing Mortar: the Possibility of Adding Less Nutrient to Maintain the Mechanical Properties of Mortar." Proceedings of the *75th Rilem Week and International Conference on Advances in Sustainable Construction Materials and Structures, Merida, México, August 29th to September 3rd, 2021,* (in press).

6.1 Introduction

Bacteria based self-healing concrete has previously demonstrated excellent healing performance (Jonkers and Schlangen, 2007; Wang et al., 2018). Several types of bacterial strains which can survive in alkaline environment, such as *Bacillus sphaericus*, *Sporosarcina pasteurii*, *Bacillus subtillis* and *Bacillus alkalinitrilicus* are used as healing agents (Feng et al., 2021; Jadhav et al., 2018; Jonkers and Schlangen, 2009; Wang, Jonkers, et al., 2017). In this research, a strain of *Bacillus sphaericus (BS)* was selected as a healing agent as it has been reported to deliver satisfying healing performance when encapsulated into various carriers (Wang et al., 2018; Wang et al., 2017; Wang et al., 2012, 2014). To protect the bacteria from harsh environment, cells need to be encapsulated into carriers such as hydrogel, porous material, microcapsules etc. (Jonkers and Schlangen, 2009; Wang et al., 2018; Wang et al., 2014). An expanded clay aggregate (EC LWA) that has been reported to have ability to protect bacteria in concrete and heal large crack widths up to 0.46 mm (Alazhari et al., 2018; Jonkers and Schlangen, 2009; Lucas et al., 2018; Zhang et al., 2017) was also used in this research as a comparison. As this lightweight aggregate is an open carrier, bacteria could leak out which could decrease the healing ability. A study investigating suitable encapsulation methods with expanded clay as a carrier suggested the application of vacuum and pressure treatment to push the bacteria deep into the pores of EC LWA (Ersan et al., 2015) to mitigate a high bacteria leakage in a porous carrier.

Researchers are mostly working with the spore form of bacteria, as it is less sensitive to the harsh environment of fresh concrete (Jadhav et al., 2018; Jonkers and Schlangen, 2007; Wang et al., 2018). However, spores need to germinate into vegetative cells first before they could actively heal the crack. Unfortunately, yeast extract that is usually employed as a germination agent negatively affects the resulting concrete or mortar (Bolobova and Kondrashchenko, 2000; Bundur et al., 2015; Vandervoort, 2019). Thus directly applying vegetative cells as a healing agent that will not require yeast for germinating processes could be an option to maintain the mechanical properties of the self-healing concrete matrix. Several articles on employing vegetative cells as a healing agent reported that encapsulated vegetative cells may remain viable inside the concrete matrix for a relatively long time and are capable to heal the cracks (Bundur et al., 2015; Bundur et al., 2017; Ersan et al., 2015; Wang et al., 2012b).

In summary, this chapter investigated the effect of nutrients and bacteria encapsulated into various porous carriers on the properties of resulting mortar. Alkali activated lightweight aggregate generated from fly ash and Sidoarjo mud (Lusi) was selected as the bacterial carrier as it is compatible with the mortar matrix. The healing ability of mortar containing encapsulated cells in various carriers was observed under an optical microscope, while the healing product formed was characterized using scanning electron microscopy. The sealing ability was measured by means of a water flow test. Finally, a recommendation on the feasibility of using alkali activated lightweight aggregate as bacteria carrier could be drawn.

6.2 Materials and Methods

6.2.1 Materials

Fly ash (FA) type F from a Dutch power plant and a treated Sidoarjo volcanic mud (Lusi) was employed as a binder in the production of lightweight aggregate (LWA). The oven-dried Lusi was treated by means of sintering at the temperature of 800°C for 6 hours. The average particle size of fly ash and Lusi powder were 6.2 μm and 10.1 μm, respectively. The major constituents of fly ash and Lusi powder determined by X-ray Fluorescence test were SiO_2, Al_3O_2, Fe_2O_3, and CaO (table 3, chapter 3). The binders were activated with Na_2SiO_3 and NaOH 6M (VWR, Belgium) with a weight ratio of 1.5 as explained in chapter 3.

Cement type I 52.5 (Holcim) was used as a binder in mortar production. River sand with the size of 0-2 mm was used as fine aggregate. This particle size was obtained from sieving river sand fraction 0/4. A commercial expanded clay aggregate (EC LWA) with the particle size of 2-4 mm from Argex nv was used as a comparison LWA. The specific particle size used was derived from sieving EC LWA with fraction 0/4.

Vegetative cells of *Bacillus sphaericus* LMG 22257 (Belgian Co-ordinated Collections of Micro-organisms, Ghent) were used as a healing agent (Fig 1). The liquid sterile medium to cultivate the cells consisted of yeast extract and urea (Carl Roth, Belgium). The yeast extract solution with the concentration of 20g/l was autoclaved for 20 minutes at a temperature of 120°C. The sterilized urea was then introduced to the medium by means of filtration using a sterile 0.22 μm millipore filter (Millipore, USA). The final concentration of yeast extract and urea in the medium was 20 g/l. The cells were inoculated into the medium under sterile conditions. Later on, the medium containing bacteria was incubated on a shaking table with the speed of 120 rpm in a 28°C room for 24 hours. Finally, the vegetative cells were harvested by centrifuging the 24h old culture (15050 g, 7 minutes). The bacterial pellets were then re-suspended in sterile yeast extract solution with concentration of 5 g/l. The final concentration of resuspended cells was 2 x 10^9 cells/ml.

Calcium nitrate tetrahydrate and urea (Carl Roth Belgium) with a purity of 99% were used as bioagents in the mortar. The concentration of calcium nitrate and urea in the mortar was the same as described in chapter 5, which was 47 g/l and 23 g/l mortar, respectively. This concentration was chosen as it delivers adequate mortar performance (Wang et al., 2018). In mortar production, the amount of water was reduced to accommodate excess water released from calcium nitrate tetrahydrate ($4H_2O$).

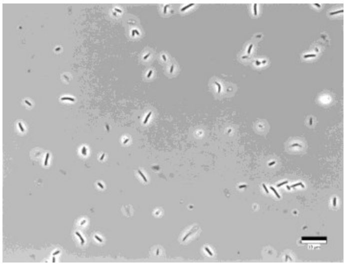

Figure 6.1. Vegetative cells of *B. sphaericus*, image taken with a magnification of 1000x, the size of scale bar is 10 μm.

6.2.2 The Production and Characterization of LWA

The production process of fly ash and Lusi-based LWA was the same as explained in Chapter 3. The fly ash and Lusi-based LWA were produced in a pan granulator with a diameter of 500 mm and 95 mm depth. The slope of the pan was set to 48° and the pan rotated with a speed of 60 rpm. The binders (FA or Lusi) were put in the pan, and the alkali activator was sprayed into the pan. The liquid/ solid ratio of fly ash LWA and Lusi LWA was 0.25 and 0.51, respectively. The pan was run for approximately 20 minutes until the compact granules fell from the side of the pan.

The fresh granules were dried in the curing room with a temperature of 20±2°C and humidity of 95±5 % for 24 hours. The dried granules were sieved to obtained granules with a particle size of 2-4 mm. Finally, the sieved granules were sealed in a plastic bag and kept in the same curing room for 28 days.

The water absorption over 24 hours and the density of 28d old LWA was determined according to NBN EN 1097-6 (**Table 3.6**). This data was later on needed to calculate the amount of extra water for LWA during the mortar production

6.2.3 Viability and Leakage of the Bacteria after Encapsulation

The viability of bacteria was tested to ensure that the bacteria are still alive after the encapsulation process. A Nessler test was performed to determine the ureolytic activity of bacteria. The urease enzyme in the bacterial cells can decompose the urea into two ammonium molecules and one carbonate molecule. Thus by measuring the total ammonium formed, the amount of urea decomposed could be calculated (Equation 6.1)

$$DU \ = TAN \ \times dilution \ \times Mr \frac{Urea \ (\frac{60g}{mol})}{2Nitrogen \ (2x14\frac{g}{mol})} \qquad \text{(Equation 6.1)}$$

Where DU is decomposed urea (g/l), TAN (g/l) is total ammonium nitrogen recorded with a spectrometer at wavelength 425 nm. The dilution used in this research was 2.5. The relative molecular mass (Mr) of urea and two nitrogen molecules were 60g and 28g, respectively.

First, a certain amount of dried LWA was put into a penicillin bottle with a rubber stop and sterilized by autoclaving for 20 minutes at a temperature of 120 °C. A vacuum pressure (-0.8 bar) was introduced to the sealed bottles, followed by adding the vegetative cells suspension. The vacuum pressure was kept for 30 minutes. After that, the pressure of +1 bar was introduced and maintained for 24 hours in a room with a temperature of 28°C. The amount of bacteria (B) encapsulated into the LWA depends on its water absorption over 24h (Equation 6.2). The illustration of the encapsulation procedure is presented in **Figure 6.2**.

$$B = M_{lwa} \ \times WA_{24}/100 \qquad \text{(Equation 6.2)}$$

Where B is the amount of cells suspension needed, M_{lwa} is the weight of LWA and WA_{24} is the water absorption of LWA over 24 hours.

After 24 hours, the encapsulated LWA were rinsed in demineralized water. Half of the samples (around 7 g LWA) were immersed into 30 ml of sterile urea solution of 20 g/l for ureolytic activity test, and the other half were immersed in demineralized water for the leakage test. The ureolytic activity determined by decomposed urea and pH evolution of encapsulated LWA was checked at 0 ,2, 4, 6, 24 and 72 hours. For the leakage test, the samples were put on a shaking table (120 rpm) for one hour. After 1 hour, one milliliter sample was taken from the immersion water. A serial dilution was conducted on a sample, and the bacteria concentration was measured using a flow cytometer (BD Accury 6+).

Before cell suspensions were injected into LWA, the concentration of the cells was measured. This number will become the initial cell number. This initial cell number was then converted from cells/ml into cells/g LWA by dividing the cell number by the amount of LWA (A1). The same converting was also done in the leakage cell number (A2). Thus the leakage percentage could be calculated with Equation 6.3.

$$\%\,Leakage = \frac{A2\ (\frac{cells}{g})}{A1\ (\frac{cells}{g})} \times 100 \qquad \text{(Equation 6.3)}$$

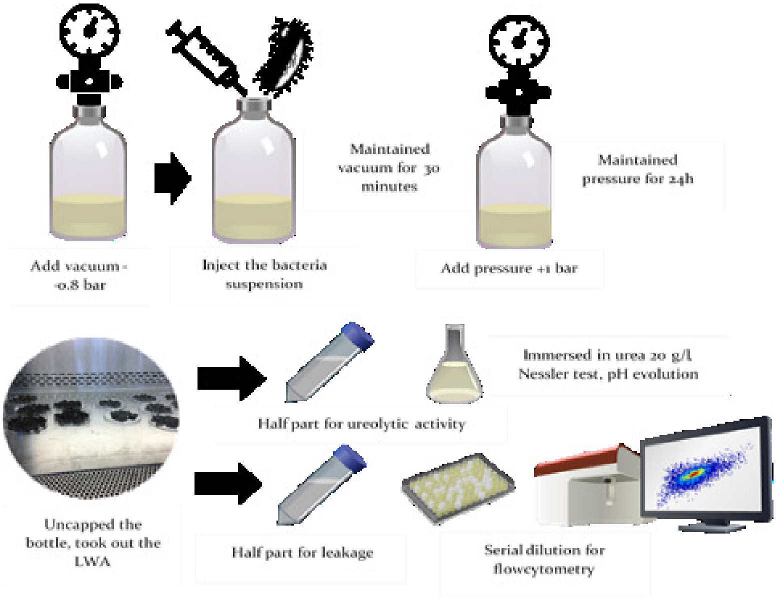

Figure 6.2. Illustration of the encapsulation procedure

6.2.4 Mortar Preparation

The mortar samples were manufactured following the guidelines of EN NBN 196. The fine aggregate with the size of 2-4 mm were replaced with LWA, resulting in a replacement rate of 30% by volume. In the previous chapter, LWA replacement rate of 16 Vol.-% was used. However, without the presence of yeast in the mixture, the healing performance obtained with

LWA replacement rate of 16% was limited (Risdanareni et al., 2021). Thus in order to increase the amount of cells into the matrix, the healing ratio was increased to 30% in this chapter. In literature, it also stated that by increasing the aggregate replacement rate up to 30%, satisfactory healing was obtained in a crack width range up to 0.2 mm (Tziviloglou, 2018). A certain amount of extra water based on the water absorption value of LWA was added before it was mixed into the mortar mixture. For a sample with bacteria, the amount of bacterial suspension needed is equal to the amount of extra water, hence only the bacterial suspension was added to the LWA before introducing into the mortar mix. The nutrients were introduced into the mixture by addition into the mixing water.

The list of samples and the material needed to manufacture three mortar prisms with dimensions of 40x40x 160 mm^3 are presented in **Table 6.1**. There are four series in each LWA's group: Ref, N, NB, and NBE. A control sample that has no LWA content was also produced. A Ref sample is a sample without bacteria and nutrients but still containing LWA. N samples contain nutrients without bacteria. NB samples contain nutrients and bacteria, but no encapsulation procedure was applied. NBE samples contain nutrients and the bacteria were introduced into LWA using vacuum and pressure treatment.

The workability of fresh mortar was measured according to NBN-EN-1015-3 (1999) standard before it was cast into the mold. After being cast, the mortar was cured in a curing chamber with a temperature of 20±2°C and humidity of 95±5 %. The mortar was demoulded after being cured for 24 hours. The one-day-old mortar samples were then covered with plastic film and were cured in a curing room with a temperature of 20°C and relative humidity of 60% until they reached the testing age of 28 days and 90 days. The compressive strength and bulk density were tested on 28 days and 90 days old mortar according to EN NBN 196 standard.

Table 6.1. Mix design of three mortar prisms with dimensions of 40x40x160 mm³

Type	LWA (g)	BS* (ml)	extra water (g)	Sand (g)	Cement (g)	Water (g)	Cal* (g)	Urea (g)
Control	0	0	0	1350	450	225	0	0
EC Ref	186	0	32	1164	450	225	0	0
EC N	186	0	32	1164	450	214	36	18
EC NB	186	32	0	1164	450	214	36	18
EC NBE	186	32	0	1164	450	214	36	18
FA 6M Ref	282	0	53	1068	450	225	0	0
FA 6M N	282	0	53	1068	450	214	36	18
FA 6M NB	282	53	0	1068	450	214	36	18
FA 6M NBE	282	53	0	1068	450	214	36	18
Lusi 6M Ref	290	0	72	1060	450	225	0	0
Lusi 6M N	290	0	72	1060	450	214	36	18
Lusi 6M NB	290	72	0	1060	450	214	36	18
Lusi 6M NBE	290	72	0	1060	450	214	36	18

*BS : *B. sphaericus*

*Cal : calcium nitrate tetrahydrate

6.2.5 Crack Closure Observation

Samples for crack closure observation were prisms with dimensions of 30x30x360 mm³ with a 6 mm diameter reinforcing bar. The length of the reinforcement bar was 600 mm. Cracks were fabricated at the age of 28 days and 90 days. The central rebar was clamped at the ends and the prisms were subjected to tensile load using an Instron universal testing machine (UTM) (**Figure 6.3**) with the load rate of 0.01 mm/s. The displacement of the crack was monitored after the specimen was in the plastic zone. The loading was stopped when the average displacement in each crack reached between 0.4-0.5 mm. Per sample the average number of cracks obtained was between 5-9 cracks.

After cracks were fabricated, the initial crack width was measured under an optical microscope (Leica DMC 2900). The prims were then subjected to wet-dry curing in tap water with the cycle of 4 hours wet and 4 hours dry. The crack closure was monitored under the microscope after the samples had been cured for 10, 20 and 30 days. For the crack closure monitoring, the top side surface cracks were observed. The crack was divided into three observation zones. 4 to 5 images were taken in each zone, and the width of the crack reported in each zone was the average value of those measurements. Finally, the healing ratio (HR) was then calculated for each zone based on Equation 6.4.

$$HR = (Cwi - Cwf)/Cwi \times 100\% \qquad \text{(Equation 6.4)}$$

where HR is the healing ratio, C_{wi} was the initial crack width, and C_{wf} was the final crack width.

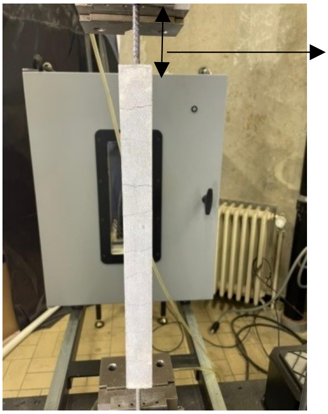
The length of the arm was 50 mm

Figure 6.3. Fabrication of Multiple Cracks using Instron UTM.

6.2.6 Sealing Efficiency

The sealing efficiency of mortar was determined by a water flow test (Gruyaert et al., 2016) . The samples for the water flow test were cast in a prismatic mould with dimension of 40x40x160 mm^3. Before casting, a smooth steel bar (Φ 5mm) coated in oil was inserted into the mould. This steel bar was placed 15 mm from the bottom of the mould. Right after the specimens were cast, a plastic film was used to cover the fresh mortar. After being cured for 24 hours in a curing chamber (20±2°C , RH 95±5 %), the samples were demoulded, and the steel bars were removed from the samples. The specimens were then covered with plastic film again and cured in the curing chamber with a temperature of 20±2°C and relative humidity of 60±5% until the testing age (28 days and 90 days). Each series contained 3 to 6 specimens.

One day prior to crack fabrication, Carbon Fiber Reinforced Polymer (CFRP) sheet with the dimension of 40x160 mm was attached to the top side of the prismatic specimens using epoxy resin (**Figure 6.4**). The hole in the specimens that was previously provided by the smooth bar was enlarged at the ends to a diameter of 6 mm by drilling. A plastic tube with a diameter of 6 mm was then inserted into the hole over a distance of ± 30 mm. The hole was then sealed with silicone on both sides (**Figure 6.4**). The modified prism samples were left at room temperature for 24 hours to allow the glue to dry.

The crack was induced via a three-point bending setup with a span of 100 mm (**Figure 6.4**). The loading speed was set to 50N/s. With the help of the CFRP sheet, the samples did not split into two parts when the maximum bending capacity was reached. However, the cracks generated from this method were too wide (± 1 mm). Thus a clamp with a screw jack was placed on the bottom side of the sample (**Figure 6.4**). The crack's width was then controlled by tightening the screw and monitoring the width of the cracks under the microscope. The crack's width was set in the range of 0.3-0.4 mm.

After a uniform crack had been obtained, the cracks on the side part were covered with aluminium tape. A piece of CFRP sheet with the size of 20x160 mm was then glued on both sides using epoxy resin. The samples were dried for 24 hours at room temperature. The next stage was to immerse the samples in tap water for 24 hours to obtain the saturated state.

The water flow test was carried out on a saturated sample in an environment with a temperature of 20°C and relative humidity of 60%. The test set up for the water flow test is illustrated in **Figure 6.4**. The tube attached to the sample was connected to a water reservoir that was placed 500 mm higher than the sample. The water would then flow through the sample for 5 minutes. The weight of the water which leaked through the cracks was measured in intervals of 1 minute. However, the water leaked in the first 30 seconds was not recorded, as during this period, air bubbles are removed. After the initial water flow test had been performed, the samples were subjected to a wet-dry curing regime (4 hours wet, 4 hours dry) for 30 days. The water flow test was performed at 0, 10, 20, and 30 days curing. Finally, the sealing efficiency was calculated with Equation 6.5.

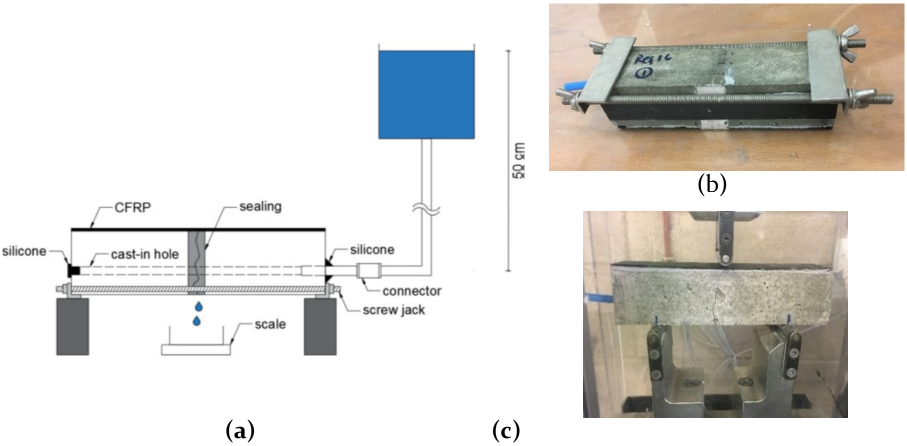

Figure 6.4. (a) Test set up for water flow (Van Mullem et al., 2019); (b) Detail of modified prism sample for water flow test; (c) Crack fabrication for water flow test.

$$SE = \left(\frac{q_{initial} - q_{healed}}{q_{initial}}\right) \times 100\% \qquad \text{(Equation 6.5)}$$

Where SE is sealing efficiency, q_{healed} was the water flow rate (g/minutes) after the healing process, and $q_{initial}$ was the water flow rate (g/minute) before the healing process.

6.2.7 Characterization of Healing Product

For SEM analysis, a piece of mortar containing a whitish healing product was collected from the crack mouth. The samples were patched on the sample holder, dried in an oven at 40ºC for 24 hours, coated with a platinum coating, and were kept in the vacuum chamber until the testing day. Finally, the morphology of the healing products was observed with Jeol JSM-7600F Field Emission Scanning Electron Microscope (FESEM) equipped with Aztec Energy software from Oxford Instruments for EDS mapping. The EDS mapping was performed for calcium, oxygen, and carbon elements.

6.3 Results and Discussion

6.3.1 The Activity and Leakage of Bacteria After Encapsulation

Based on the urea decomposition value of *B. sphaericus* encapsulated into the LWA presented in **Figure 6.5**, it seems that the cells are viable after the encapsulation process. No urea was decomposed in the control sample (**Figure 6.5**). The decomposition rate of bacteria encapsulated in FA 6M LWA that has almost similar amount bacteria in the carrier was slower compared to bacteria encapsulated into EC LWA. While more slow decomposition rate was observed in Lusi 6M LWA even though more bacteria were added into this carrier relative to EC LWA. However, after 24 hours, more than 80% urea was decomposed in all carriers. The initial solution pH of the control sample (without bacteria) of EC, FA 6M, and Lusi 6M LWA was 6.5, 10, and 11, respectively (**Figure 6.5**). The addition of bacteria affected the solution pH in all LWA carriers. After 24 hours immersion, the pH was buffered to the range of 9.5 to 9.7 (**Figure 6.5**). A similar pH value of *B. sphaericus* immersed in a medium with neutral pH was reported in a previous study (Wang et al., 2017).

The leakage of bacteria after encapsulation was in the range of 27-42% (**Figure 6.6**). EC LWA has the lowest leakage, followed by FA 6M and Lusi 6M LWA. Several aspects, such as the pore structure and size of LWA could affect the bacteria leakage. It was reported that the suitable pore size of LWA for bacterial carriers should be 2-5 times the bacteria size (Samonin and Elikova, 2004). As *B. sphaericus* has a size in the range between 2-3 µm, LWA with a high amount of macropores (<50 nm) would be a perfect shelter for the bacteria. In Chapter 3 it has been reported that the porosity of EC, FA 6M and Lusi 6M LWA obtained from MIP test was 19%, 30%, and 35%. Still, from the same chapter, all pores in EC LWA were macropores, while FA 6M LWA and Lusi 6M LWA contain 72% and 60% macropores, respectively. It seems that even though FA 6M and Lusi 6M have higher porosity compared to EC LWA, they have a smaller pore size range that might be too small for bacteria to penetrate. It was mentioned in Chapter 3 that FA 6M and Lusi 6M have two ranges of main pore sizes of 3-10 µm and 0.1-1 µm while EC LWA has various large pores (3-20 µm). The higher leakage occurring in FA 6M and Lusi 6M could be due to the high amount of the smaller pore size (0.1-1 µm).

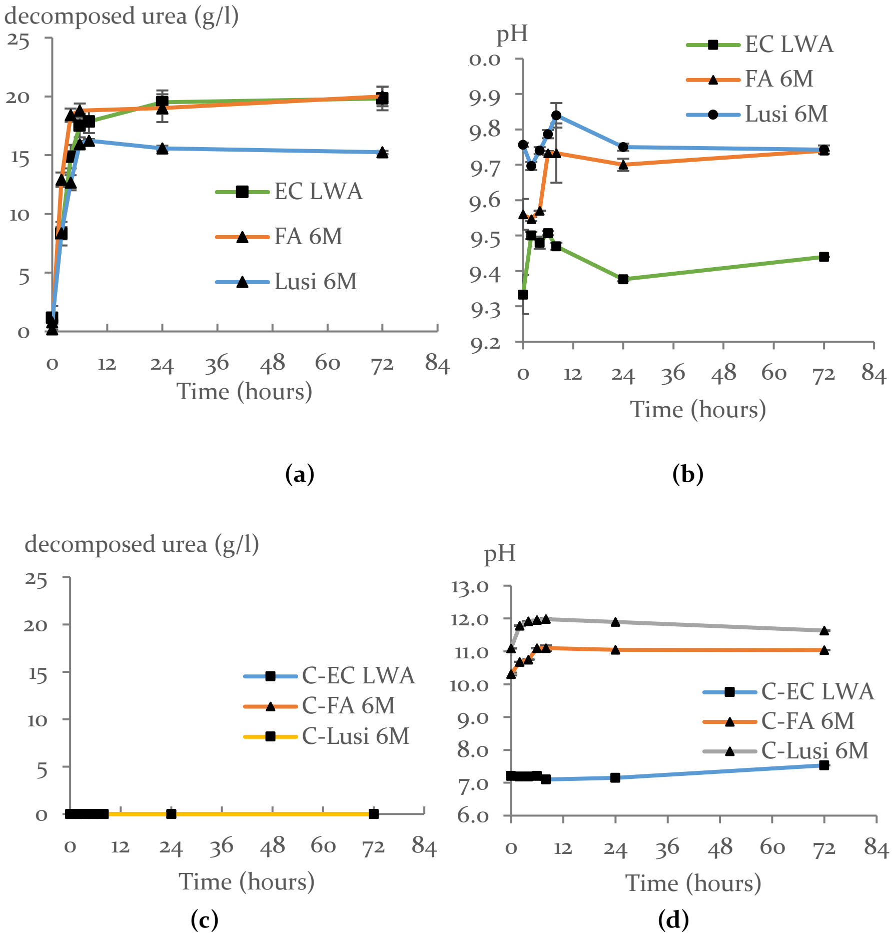

Figure 6.5. (a) The urea decomposition of *B. sphaericus* encapsulated in EC, FA 6M and Lusi 6M LWA monitored in 72 hours; (b) pH evolution of *B. sphaericus* encapsulated in EC, FA 6M and Lusi 6M LWA monitored in 72 hours; (c) The urea decomposition of control sample EC, FA 6M and Lusi 6M LWA monitored in 72 hours; (d) pH evolution of control sample EC, FA 6M, and Lusi 6M LWA monitored during 72 hours (n=3).

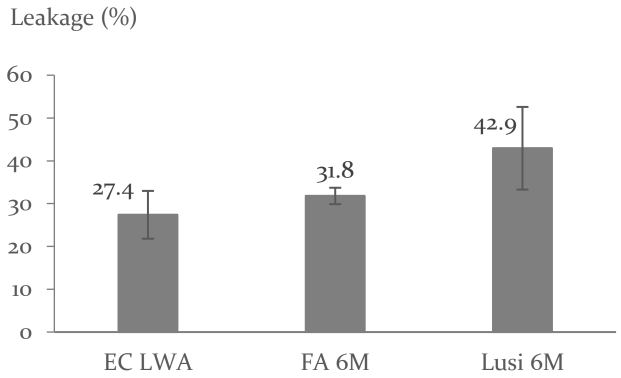

Figure 6.6. The bacterial leakage after one hour on the shaking table (n=3).

6.3.2 Mechanical Properties of Resulting Mortar

Effect of Utilizing LWA

In the EC LWA group, replacing 30% by volume of fine aggregate with EC LWA proved to decrease the compressive strength and the bulk density of mortar up to 32 % and 11%, respectively. In FA 6M LWA samples, the addition of LWA decreased the compressive strength of the resulting mortar up to 28 %, while the bulk density decreased up to 8 % compared to the control sample. The compressive strength of Lusi 6M LWA group was also decreased up to 44 %, while the bulk density decreased up to 9 %.

Compared to the results obtained in the previous batch, presented in chapter 3, with the same aggregate replacing rate of 30%, the 28 days old mortar strength decrease obtained in EC LWA and Lusi 6M LWA obtained in this batch was slightly lower. In the previous batch, the strength decrease of mortar containing EC LWA was 33%, while it was 50 % in Lusi 6M LWA sample. A significant strength improvement was obtained in a mortar containing FA 6M LWA relative to this batch. In the previous batch, the strength reduction of 41 % was obtained, while the strength reduction was 28 % in this batch. The age difference of the LWA used in each batch might cause this strength improvement. In the production of lightweight mortar reported in Chapter 2 and 3, the age of alkali activated LWA was around 1-2 month. But the alkali activated LWA used for this batch has the age of around 6 month.

There is no significant difference in the workability of samples containing EC and FA 6M LWA compared to the control sample. A slight decrease in workability was observed in Lusi 6M samples.

Effect of Nutrient and Bacteria

Overall in all sample groups, the addition of nutrients and bacteria with or without encapsulation procedure did not significantly affect the compressive strength of the resulting mortar (**Figure 6.7**). The flow value of N (nutrient samples) was decreased up to 21 % in the EC LWA samples compared to its reference sample. In FA 6M and Lusi 6M sample groups, the reduction in the flow value of the N sample was less than 10%. As discussed in Chapter 5 a decrease in the flow value is expected due to the addition of calcium, but is partly compensated by the addition of urea. The addition of calcium nitrate could accelerate the hydration process and decrease the setting time. Therefore, when the flow value was measured, the mixture would be stiffer compared to the reference sample, and a lower flow value was obtained.

The decrease in the flow value of fresh mortar did not negatively affect its hardened properties. The bulk density of N samples in EC LWA slightly decreased up to 7% compared to the Ref sample, while in FA 6M and Lusi 6M LWA, the decrease in bulk density due to the addition of nutrients was less than 5%.

In all sample groups (EC, FA 6M, and Lusi 6M LWA), bacteria did not affect the properties development of the resulting mortar (**Figure 6.7**). The compressive strength and the bulk density of the samples containing bacteria (NB and NBE series) are very similar to the nutrient samples. In conclusion, it seems that the addition of nutrients or the bacteria cells had less effect on the properties of resulting mortar than the fine aggregate replacement by LWA.

Effect of Different Testing Age

Overall the compressive strength of the resulting mortar at 90 days was higher by 5 to 8 % when compared to the 28 d strength for the reference and control sample group (**Figure 6.7**). A slightly higher compressive strength was observed in N, NB, and NBE samples (10-12 %).

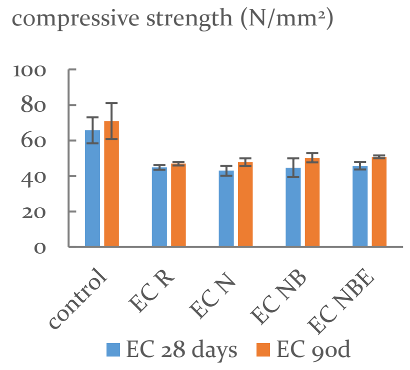
compressive strength (N/mm²)
100
80
60
40
20
0
control
EC R
EC N
EC NB
EC NBE
EC 28 days
EC 90d

(a)

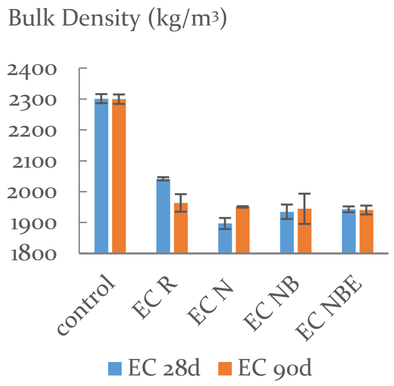
Bulk Density (kg/m³)
2400
2300
2200
2100
2000
1900
1800
control
EC R
EC N
EC NB
EC NBE
EC 28d
EC 90d

(b)

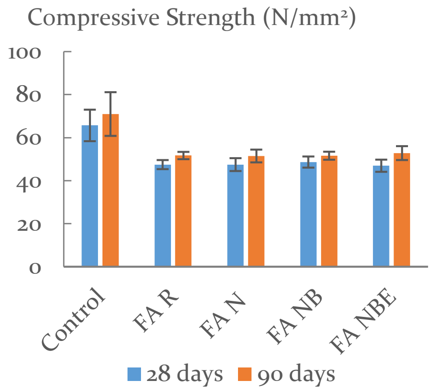
Compressive Strength (N/mm²)
100
80
60
40
20
0
Control
FA R
FA N
FA NB
FA NBE
28 days
90 days

(c)

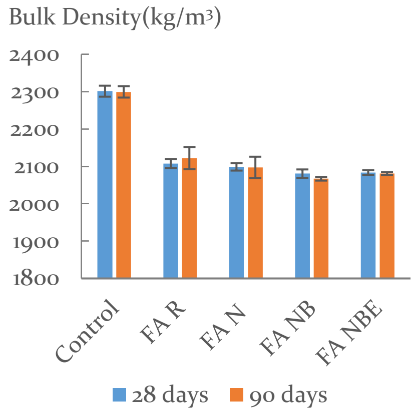
Bulk Density(kg/m³)
2400
2300
2200
2100
2000
1900
1800
Control
FA R
FA N
FA NB
FA NBE
28 days
90 days

(d)

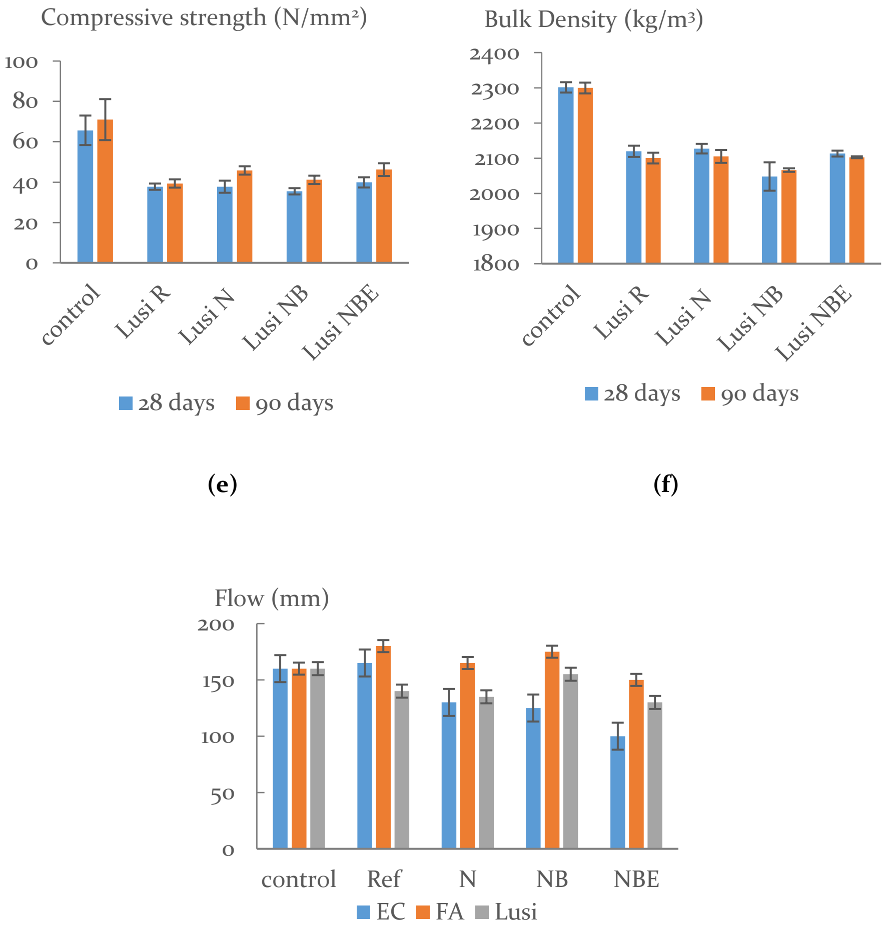

(e) **(f)**

(g)

Figure 6.7 (a) The compressive strength of EC LWA samples,(b) the bulk density of EC LWA samples, (c) the compressive strength of LWA samples,(d) the bulk density of FA 6M LWA samples, (e) the compressive strength of Lusi 6M LWA samples,(f) the bulk density of Lusi 6M LWA samples, (g) the workability of fresh mortar (n=3).

6.3.3 Crack Closure for samples cracked at 28 Days

6.3.3.1 EC LWA Sample Group

In NB and NBE samples, crack widths in the range between 0.2 to 0.3 mm were healed entirely, while in N and Ref samples, one crack of this size was partially healed, while the rest of the cracks were also completely healed. In the control sample, cracks with similar width reached 35 % healing. It could be summarized that without the addition of bacteria into the matrix, but with the presence of LWA, cracks with the range of 0.2-0.3 mm could be fully healed after 30 days being subjected to a wet-dry cycle regime. The role of LWA as internal curing agent that could release the water trapped in their pores at a later age to react with un-hydrated cement could possibly contribute to the crack healing in the Ref sample group (Paul et al., 2021). In the N sample group, calcium in the mixture could contribute to the higher amount of healed cracks compared to the reference sample.

In the Ref sample, only 1 out of 3 cracks in the width range of 0.3-0.4 mm were completely closed after being subjected to wet-dry cycle curing for 30 days (**Figure 6.8**). In the N group samples, 50% of cracks in the same width range were also completely closed. In NB and NBE group samples, more than 50% of cracks in the width range of 0.3-0.4 were completely healed. While in the control sample, no cracks in the same width range could completely heal. The average healing ratio of the control sample in that crack width range was around 33 %.

A more clear effect of the addition of bacteria into the mortar could be seen in cracks in the range of 0.4-0.5 mm. In the Ref sample group, no cracks in that range were completely healed. Only two cracks were completely healed in the N and NB sample group, while the rest had a healing ratio in the range between 27-75%. A slight improvement was observed in the NBE sample. Two cracks were completely closed, but the healing ratio of the other cracks reached 68 %. The encapsulation process seems successful in keeping the bacteria inside the LWA pores before cracks were fabricated. While in the NB sample, the bacteria were unprotected in the mortar matrix, resulting in fewer bacteria surviving at the time cracks were fabricated.

EC NBE sample's healing performance was similar as for self-healing concrete including spores of *B. alkalinitrilicus* as a healing agent and expanded clay as a carrier. For the latter, a maximum closed crack width of 0.46 mm was mentioned for samples being immersed for 100 days in tap water (Jonkers and Schlangen, 2009). In the current research, some cracks with a width of 0.49 mm could completely heal within 30 days of curing. It seems that the curing regime applied in this research also had a positive effect. A previous study reported that wet-dry cycle curing could improve the healing ability of bacteria-based self-healing mortar with expanded clay as a carrier (Tziviloglou, 2018).

The healing ability obtained in this research was better compared with a previous study that used sodium silicate encapsulated into EC LWA

(Alghamri and Kanellopoulos, 2016). The maximum crack width that could be healed by sodium silicate was 0.3 mm after being immersed in water for 28 days.

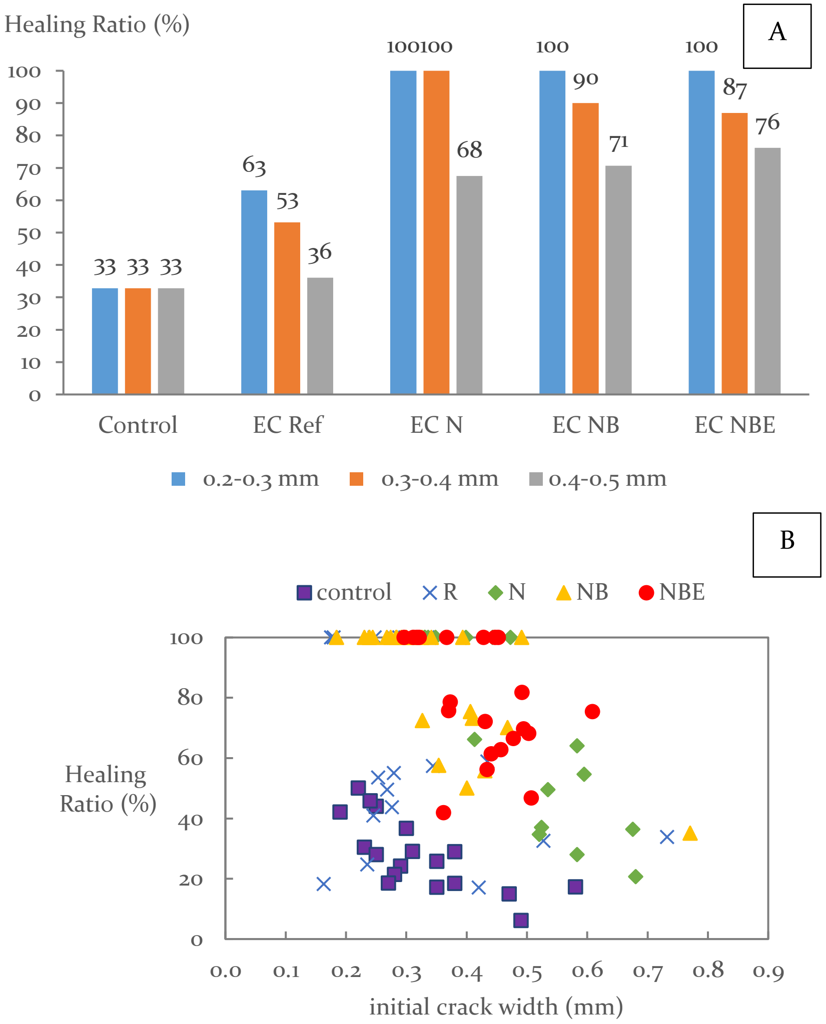

Figure 6.8 (a) Average healing ratio in all EC LWA series categorized by its crack width; (b) The healing ratio of each crack in all EC LWA series. All samples were cured for 30 days. Cracks were fabricated at the age of 28 days.

6.3.3.2 FA 6M LWA Sample Group

Almost all cracks with the width range of 0.3-0.4 mm were completely closed in sample FA 6M Ref after being cured for 30 days. Similar behaviour was also observed in the N group sample. An unexpected result was observed in NB and NBE samples. Somehow, the addition of bacteria did not improve the healing ratio of the resulting mortar (**Figure 6.9**). No crack with the width of 0.3-0.4 mm was completely healed in the NB sample. The maximum healing ratio of the sample with that crack width range was 70% for the NB sample. Only one crack in that width range was completely closed in the NBE sample, while the rest of the cracks were only 60% healed.

Compared to the EC LWA group, the healing ability of the Ref sample in the FA 6M LWA group was better. In FA 6M LWA Ref sample, all cracks with a width less than 0.4 could completely heal. While in the EC LWA ref group, the presence of LWA could only heal the crack with a width less than 0.3 mm. An excellent healing performance provided by FA 6M LWA could be due to the advancing hydration between unreacted fly ash in the LWA with the water retained inside the LWA.

In the crack width range of 0.4-0.5 mm, one crack was completely healed in the Ref sample group after being cured for 30 days, while the rest of the cracks were 70-80 % healed. In the N, NB, and NBE sample group, no crack was completely healed in this crack width range. The average healing ratio of N, NB, and NBE samples for cracks with an initial crack width in the range of 0.4-0.5 mm, was 69 %, 63 %, and 52%, respectively. It seems that some amount of bacteria in the FA 6M LWA were leaking out, which limited the still available bacteria inside the LWA. This result is in accordance with the bacteria leakage results presented in **Figure 6.6**. The viability of bacteria after being encapsulated into the FA 6M LWA was also lower compared to in EC LWA samples (**Figure 6.5**).

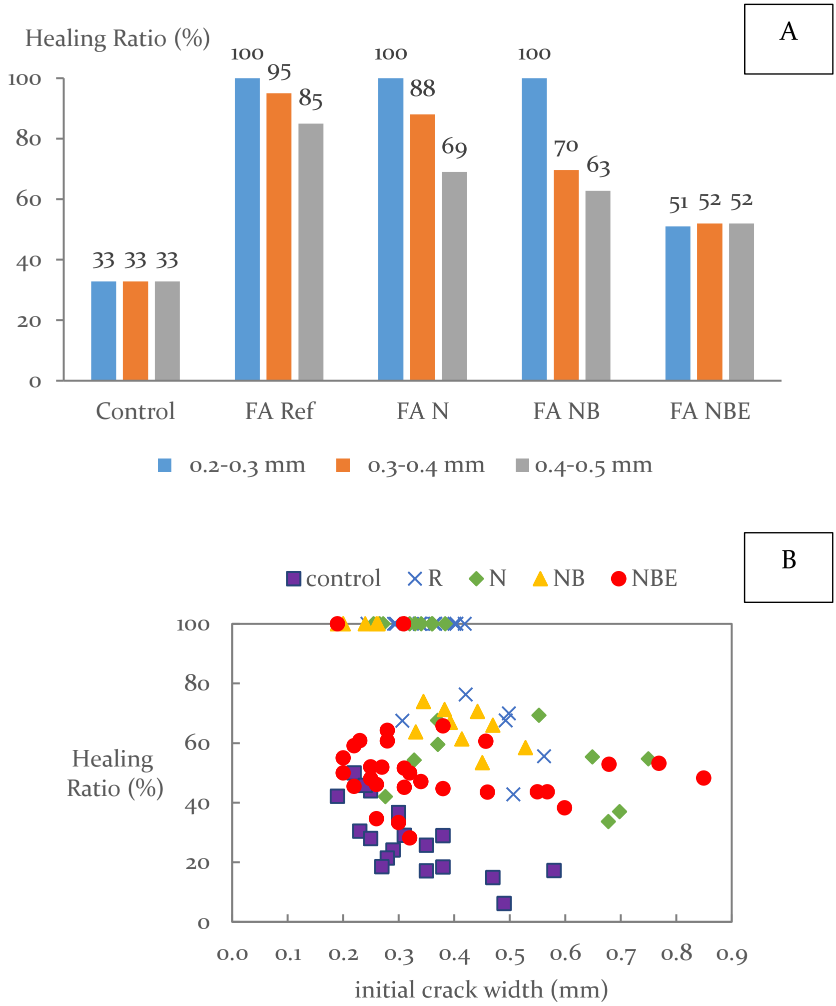

Figure 6.9 (a) Average healing ratio in all FA 6M LWA series categorized by its crack width; (b) The healing ratio of each crack in all FA 6M LWA series. All samples were cured for 30 days. All cracks were created at the age of 28 days.

6.3.3.3 Lusi 6M LWA Sample Group

Overall, the healing performance of Lusi 6M LWA samples was the lowest among all carriers. In the Ref sample, only one crack in the range of 0.3-0.4 was completely healed after being cured for 30 days, the rest of the cracks were only 60% healed (**Figure 6.10**). A better healing performance was observed in the N sample. More than 50% of cracks in the same width range were utterly healed, while the rest of the cracks were 60% healed. Two cracks were completely healed in the NB group sample, while the rest of the cracks were 65 % healed. No improvement in healing performance compared to the NB group was observed in the NBE group sample.

For initial crack widths in the range of 0.4-0.5, no cracks were completely healed in the Ref, NB, and NBE group sample. In the N sample, two cracks were fully closed in that crack width range. The average 30d healing ratio in all Lusi 6M samples is around 60%. One thing that is worth mentioning is, the healing ratio in these samples increased significantly only in the first ten days of curing. After that period, the healing ratio did not increase significantly. The healing that occurs in this group might only be due to the internal curing provided by Lusi 6M LWA. The Lusi 6M LWA with more mesopores than FA 6M LWA, leads to higher bacteria leakage (**Figure 6.6**). The high pH of Lusi 6M LWA as a result of its high alkali activator requirement during its production may be also inhibiting the viable bacteria from precipitating calcium carbonate, resulting in the lower healing ratio observed in Lusi 6M sample group.

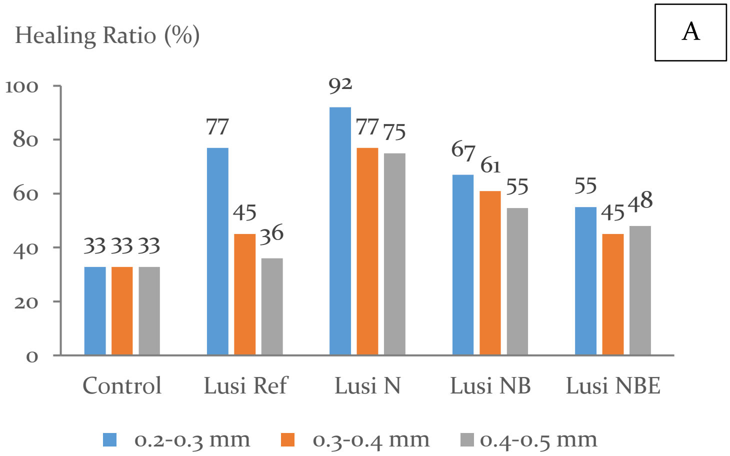

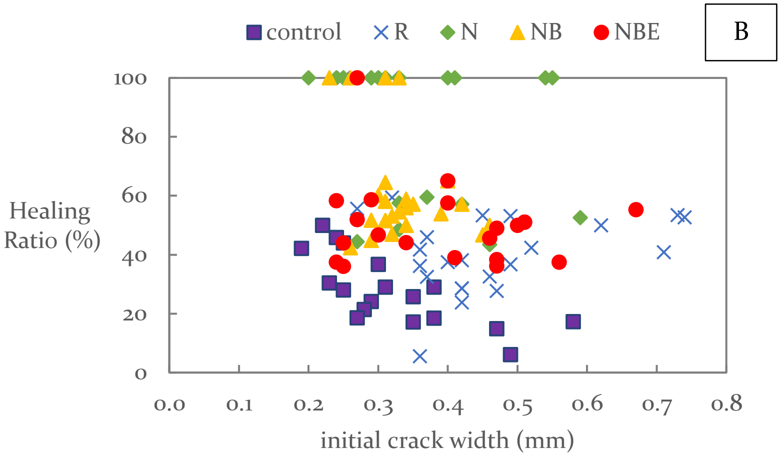

Figure 6.10 (a) Average healing ratio in all Lusi 6M LWA series categorized by its cracks width (b) The healing ratio of each crack in all Lusi 6M LWA series. All sample were cured for 30 days. Cracks were fabricated at the age of 28 days.

6.3.4 Crack Closure in the samples cracked at 90 days

6.3.4.1 EC LWA Sample Group

Overall, all samples' healing ratio was decreased when cracks were fabricated at the age of 90 days. At this age, the hydration processes must be nearly completed and the contribution of ongoing hydration to crack healing will be limited. In the initial crack width range of 0.4-0.5 mm, the average 30d healing ratio in Ref, N, NB, and NBE samples was around 17%, 23%, 39%, and 40%, respectively (**Figure 6.11**). It is quite difficult to see the improvement that was provided by the encapsulation procedure, as the average healing ratio provided by NB series was similar to the NBE series. The bacteria leakage issue after encapsulation which is still quite high (above 20%) could have contributed to this behavior.

Based on the observation, it seems that the healing product could not reach the top of the specimens, where microscopic observation was performed. While observing the side part of the NBE mortar sample prism, the cracks with a width of 0.43 were completely healed. Partial healing was observed in the NB samples with the same crack width range, while no healing product was observed in the Ref and N sample group (**Figure 6.12**). The effect of gravity could have contributed to this mechanism. During the wet-dry cycle curing, when the sample was slowly taken out from the water, the healing products that were formed would be going down and start to precipitate in the bottom part of the sample. When we look at the bottom part of the NFC sample, stalactites of calcium carbonate can be easily found (**Figure 6.13**). This result indicated that the vegetative cells are still viable after 90 days inside the mortar, as NBE and NB samples provide better healing performance than Ref and N samples. It was reported in literature that vegetative cells could survive until more than 300 days in a favorable environment (Bundur et al., 2017).

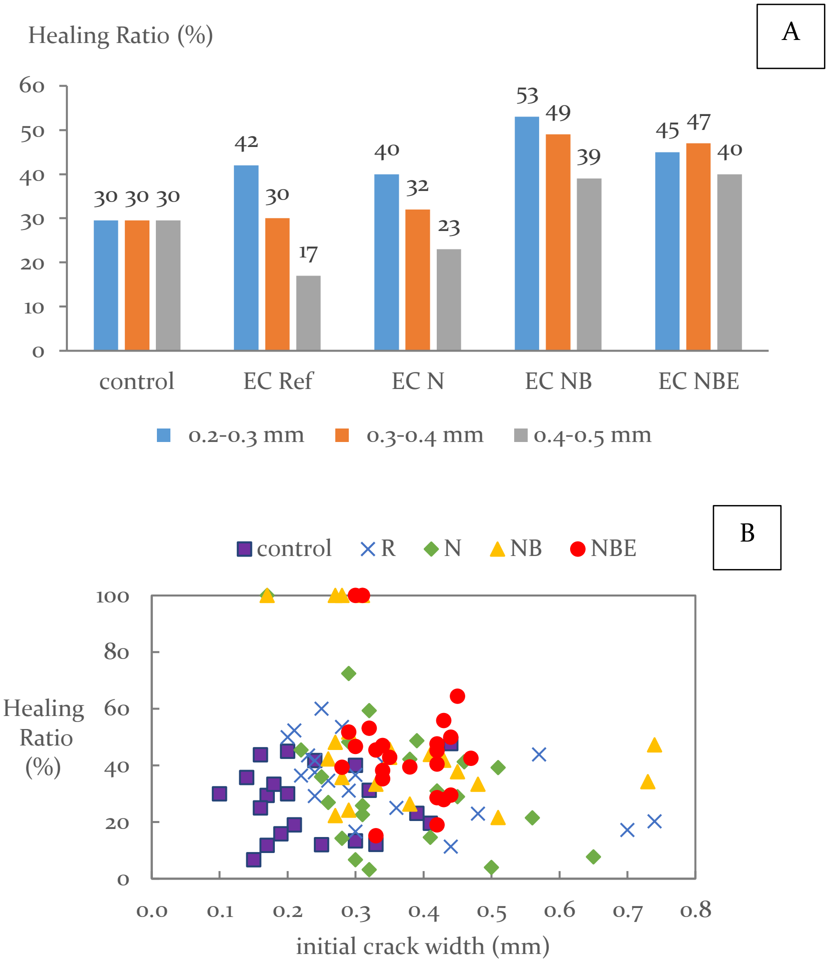

Figure 6.11 (a) Average healing ratio in all EC LWA series categorized by its crack width; (b) The healing ratio of each crack in all EC LWA series. Cracks were fabricated at the age of 90 days. All samples were cured for 30 days.

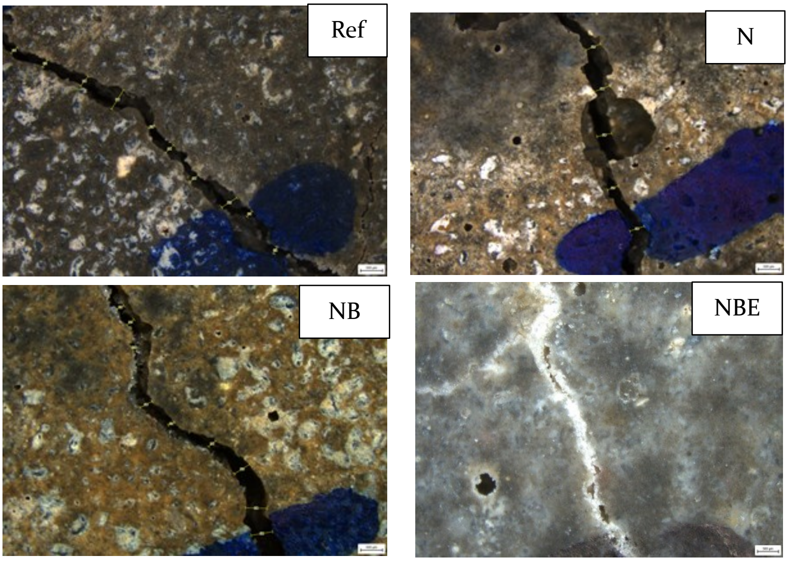

Figure 6.12 Microscope crack picture on the side part of EC LWA group sample after being cured for 30 days. Cracks were fabricated at the age of 90 days, and the average initial crack width was 0.43 mm.

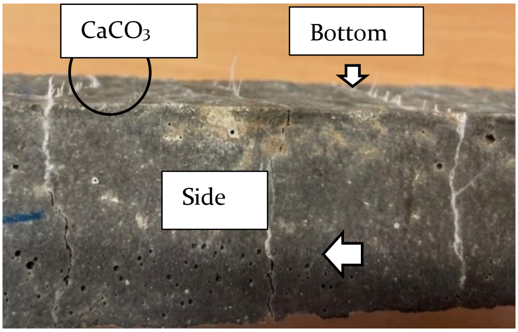

Figure 6.13 The stalactites of $CaCO_3$ observed on the bottom part of specimens of the NBE group.

6.3.4.2 FA 6M LWA Sample Group

Overall, the healing ability of a sample cracked at the age of 90 days is decreased compared to samples cracked at 28 days (**Figure 6.14**). In control, reference, and nutrient series, a significant increase in healing ratio did not occur after 10 days of curing. The healing ratio of samples cured for 10, 20, and 30 days are similar. In NB and NBE series, the prolongation in the curing duration slightly increases the healing ratio.

The average healing ratio of samples with initial crack width in the range of 0.3-0.4 mm for Ref, N, NB, and NBE samples after being cured for 30 days was 32 %, 26%, 56%, and 54%, respectively. In the crack width range of 0.2-0.3 mm, some cracks were completely closed in the NBE and NB series, while in the same crack width range, no cracks were completely closed in control, Ref, and N series samples. It seems that when the cracks were fabricated at a later age, the addition of bacteria into the matrix could improve the healing of cracks in the different crack width ranges. Nevertheless, only cracks in the crack width range of 0.2-0.3 could sometimes be completely healed. A similar result was obtained when bacteria were encapsulated into EC LWA. The effect of the encapsulation procedure might not be seen clearly in FA 6M LWA samples, as NB and NBE series have similar healing abilities in FA 6M LWA. Still, there is an improvement in healing ability when compared to the Ref and N series. This indicates that the bacteria cells in the mortar matrix are still viable and could precipitate $CaCO_3$ even after 90 days.

Compared to the healing ability of *B. sphaericus* spores encapsulated into the hydrogel, the healing ability obtained of vegetative cells encapsulated into FA 6M and EC LWA was comparable or even better. Using chitosan-based hydrogel as a carrier, for crack widths in the range of 0.3-0.4 mm, only 1 crack had a healing ratio of 60%, the rest of the cracks were 10-50% healed after being subjected to a wet-dry cycle for 10 weeks for cracks that were fabricated at the age of 28 days (Wang et al., 2018). Compared to a previous study that encapsulated cells of B. *sphaericus* into diatomaceous earth carrier, the healing ability obtained in this research is also better (Wang et al., 2012). In those studies, the maximum crack width that could be healed by cells was 0.17 mm after being immersed in a deposition medium for 40 days. But when we compared the average healing ratio provided by spores of *B. sphaericus* encapsulated into hydrogel that could completely heal the cracks with the width of 0.5 mm after being cured for 7 days, indeed healing performance provided by this current carrier system is lower (Wang et al., 2014). However, from an economical point of view, LWA carrier might become more affordable.

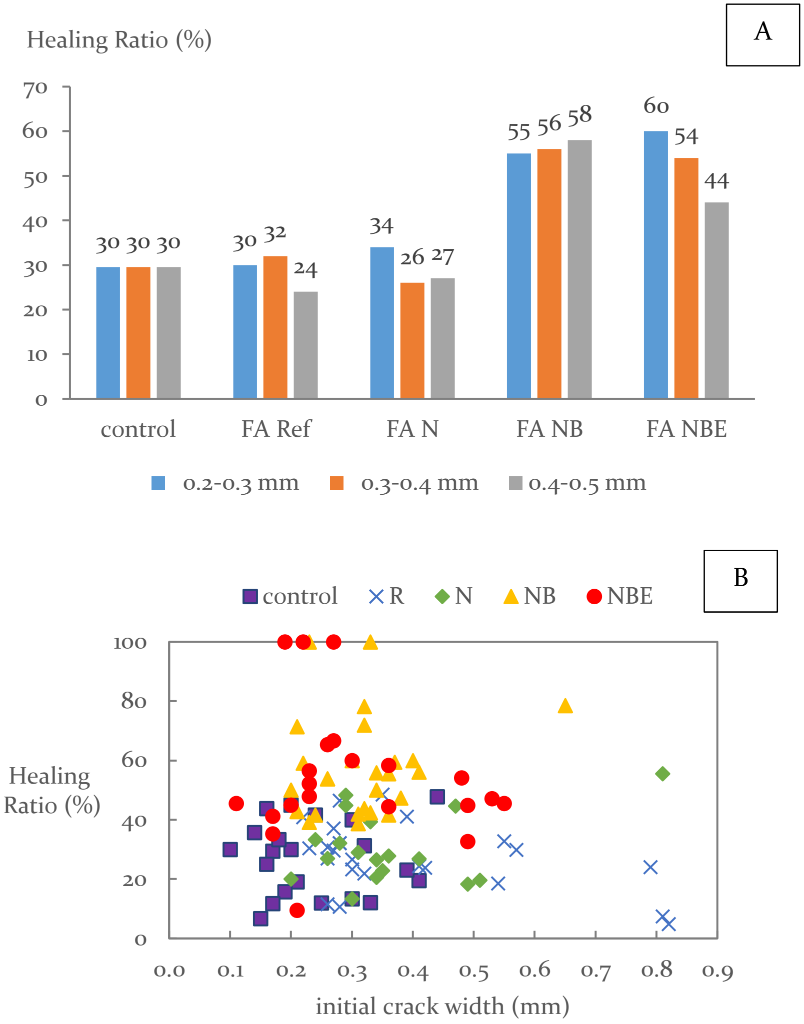

Figure 6.14 (a) Average healing ratio in all FA 6M LWA series categorized by its crack width; (b) The healing ratio of each crack in all FA 6M LWA series. Cracks were fabricated at the age of 90 days. All samples were cured for 30 days.

6.3.4.3 Lusi 6M LWA Sample Group

In the sample with the crack width range of 0.3-0.4 mm, only a slight improvement in the healing ratio was observed when bacteria were encapsulated into Lusi 6M LWA (**Figure 6.15**). Within the same crack width range, the control, reference, and nutrient sample have a healing ratio of 19-27%, while NB and NBE series (with the bacteria) have a healing ratio around 40% after being subjected to the wet-dry cycle for 30 days. When we look at a smaller crack width lower than 0.3 mm, the addition of bacteria could not improve the healing ratio. In the crack width range of 0.2-0.3 mm, the healing ratio of around 30% was achieved in all series. As this healing occurs in all series, the advanced hydration was more contributed to this healing rather than the presence of bacteria in the matrix. It also could be seen that in all series, longer curing periods do not seem to contribute to the improvement in the healing ratio. The healing ratio of samples cured for 10,20, and 30 days are similar.

Compared to the other carriers, the performance of bacteria in Lusi 6M LWA is the lowest. Reasons for this may be the high bacteria leakage due to the high amount of mesopores combined with the high initial pH of Lusi 6M resulting from the high amount of alkali activator needed during the production of Lusi 6M LWA.

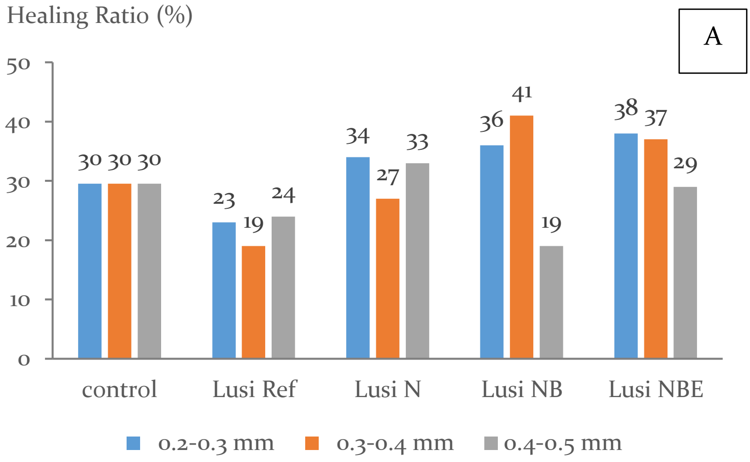

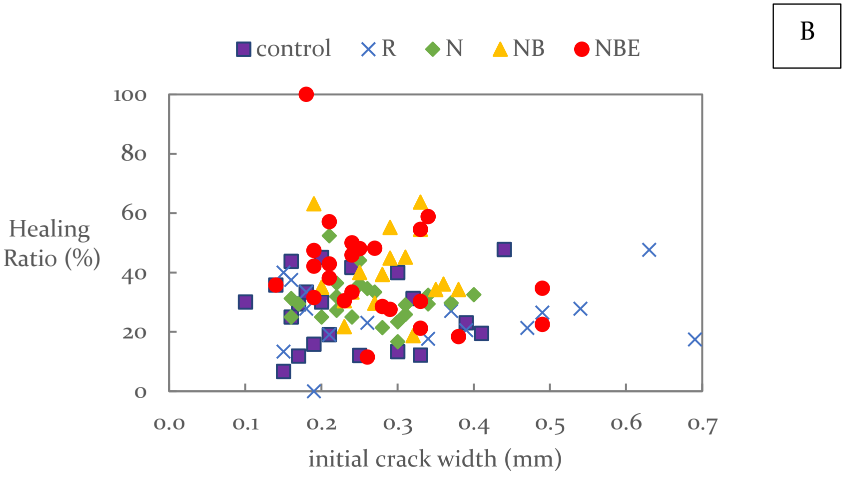

Figure 6.15 (a) Average healing ratio in all Lusi 6M LWA series categorized by its cracks width (b) The healing ratio of each crack in all Lusi 6M LWA series. Cracks were fabricated in the age of 90 days. All sample were cured for 30 days.

6.3.5 Sealing Efficiency

Several problems occurred when cracks were fabricated at the age of 28 days, especially in Lusi 6M LWA samples (**Figure 6.16**). In the Lusi 6M LWA group, no water leaked through the cracks in all series. Thus, a picture of the crack in NBE samples from all LWA series after crack healing for 30 days was taken to figure out the cause of the unexpected result in the Lusi 6M samples (**Figure 6.17**). It can be seen that the crack mouth in all samples was still open. But in Lusi 6M series, no water could penetrate those cracks (SE 100%). While in the EC LWA and FA LWA series, sealing efficiencies of 60% and 70% were observed, respectively. It could be that the Lusi 6M LWA particles crushed and blocked the hole, so the water could not flow and leaked through the crack mouth.

The reference has better sealing efficiency than the bacteria samples in FA 6M LWA and EC LWA sample groups. This result is in accordance with the crack closure result presented in **Figure 6.8** and **Figure 6.9**. The results revealed that in EC and FA 6M LWA samples, some cracks in the crack width range of 0.3-0.4 mm were completely healed after being cured for 30 days due to the internal curing provided by the LWA. A high variation in the sealing efficiency between the samples in one group was also observed. Even though the crack width was maintained in the same range (0.3-0.4 mm), significantly different water flow values between samples from the same series were observed. This was also noticed in a previous study using the active crack control method to generate the cracks. The difference in the inner crack geometry and the formation of extra cracks due to the restraining process caused this behaviour (Van Mullem et al., 2019).

A better result in the sealing efficiency was observed when cracks were fabricated at the age of 90 days. Autogenous healing due to further hydration of yet unhydrated binder particles, stimulated by internal curing water provided by the LWA was almost complete by this age. In the EC LWA sample group, the EC NBE series that contained encapsulated bacteria, obtained a sealing efficiency (SE) of 80%, while the rest of the series only had a maximum 60% sealing efficiency. Similar behaviour was also observed in FA 6M LWA samples. FA NBE series has almost 100 % sealing efficiency. One sample from the Nutrient and Reference series (FA N and FA R) also obtained 100% sealing efficiency, but the remaining samples from that series had a sealing efficiency ranging between 20-80%. In EC and FA 6M LWA samples, the NB series has similar sealing efficiency to the N and ref samples. This is an indication that without the encapsulation procedure, the bacteria could leak out to the mortar matrix and could not survive until 90 days. The blocking of the hole by Lusi particles was still an issue in Lusi 6M LWA sample group. In this sample group, the addition of encapsulated bacteria in the LWA could also not be seen clearly as the Lusi NBE series has lower sealing efficiency value than the Reference and Nutrient series.

The sealing efficiency obtained in the NBE series of EC LWA and FA LWA cracked in the age of 90 days was higher than for encapsulated spores of *B. sphaericus* in cement-based capsules that were cracked at 7 days (Anglani et al., 2020). Compared to spores of *B. sphaericus* that were encapsulated into a pH-responsive hydrogel, sealing efficiency obtained in EC NBE and FA NBE was also better. An average sealing efficiency of 80% was achieved when samples with crack width of 0.2 mm fabricated at the age of 28 days were subjected to wet-dry cycle curing for 10 weeks (Wang et al., 2018).

Based on the crack closure observation of EC NBE and FA NBE series presented in **Figure 6.11** and **Figure 6.14**, no cracks in the range between 0.3-0.4 mm were completely closed after being subjected to wet-dry cycle curing for 30 days. But within the same crack width range, the sealing efficiency of the cracks is quite high (80-100%). The healing products may have filled the crack at the intersection with the hole from where water should flow through the specimens, but this precipitation was not sufficient to close the crack mouth.

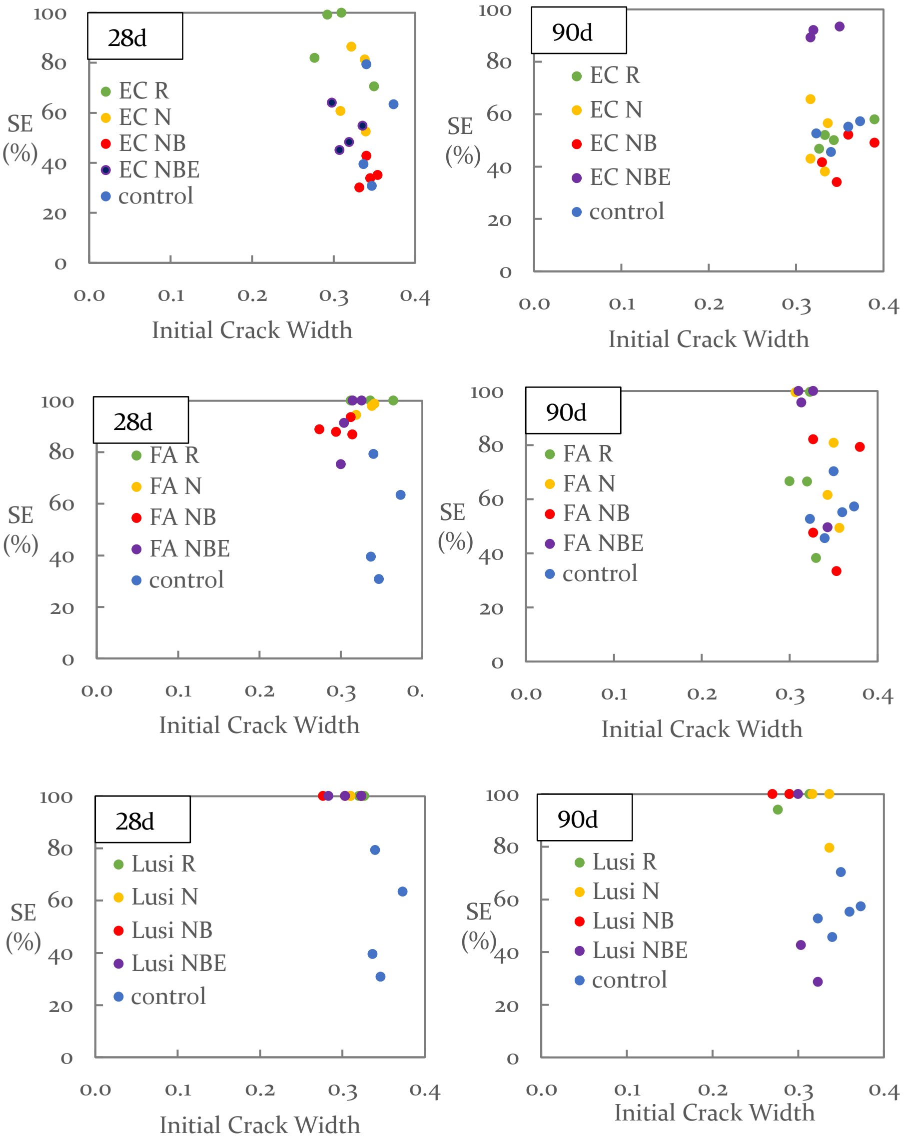

Figure 6.16 Sealing efficiency versus initial crack width of EC LWA, FA 6M LWA and Lusi 6M LWA after being cured for 30 days. Cracks were fabricated in the age of 28 and 90 days.

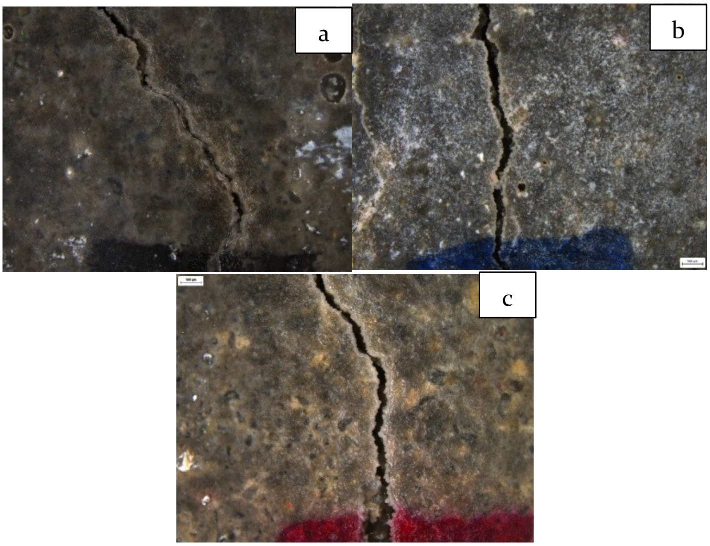

Figure 6.17 Microscope picture of crack occurring in (a) EC NBE, (b) FA NBE and, (c) Lusi NBE sample after being cured for 30 days. Cracks were fabricated at the age of 28 days.

6.3.6 Comparison of healing performance between LWA carriers

When cracks were fabricated at the age of 28 days, the EC LWA group has the highest average healing ratio (**Figure 6.18**). Cracks smaller than 0.3 mm were fully healed, while cracks larger than 0.4 still have a healing ratio higher than 70%. The performance of Lusi 6M and FA 6M LWA was quite similar. Their healing ratio in all crack width ranges was around 50%. In contrast, when cracks were fabricated at the age of 90 days, FA 6M LWA has better healing performance among other LWA carriers, followed by EC LWA and Lusi 6M LWA. The further hydration provided by fly ash in the LWA could contribute to this better performance.

The internal curing role of LWA that stands alone without addition of bacteria could provide autogenous healing in young concrete (**Figure 6.19**). It can be seen that FA 6M LWA could provide superior healing among other LWA when cracks were created at the age of 28 days. But this healing ability drastically decreased when cracks were created at the age of 90 days.

Regarding sealing efficiency, when cracks were fabricated at the age of 28 days, Lusi 6M LWA group has the highest sealing efficiency, followed by FA 6M LWA and EC LWA group (**Figure 6.19**). But, this high sealing efficiency was mostly due to the blockade of Lusi particles inside the crack and not due to the bacteria activity. More clear data were obtained when the crack was fabricated at 90 days. The FA 6M LWA group has the highest sealing efficiency followed by EC LWA and Lusi 6M LWA group.

When we connect the data obtained from crack closure observation and sealing efficiency, even though the crack mouth on the top of the sample was not completely closed, the healing product seems to have filled the inner part of the crack. Moreover, the fact that the vegetative cells were still active and able to precipitate calcium carbonate even when cracks were made at the age of 90 days, is a positive fundamental result for future research. The healing performance result obtained for the FA 6M LWA group is similar or even better than for the EC LWA group (regarding sealing efficiency and healing ratio at 90 days. A positive insight is that alkali activated lightweight aggregate generated from fly ash can be used as a bacteria carrier in self-healing mortar production.

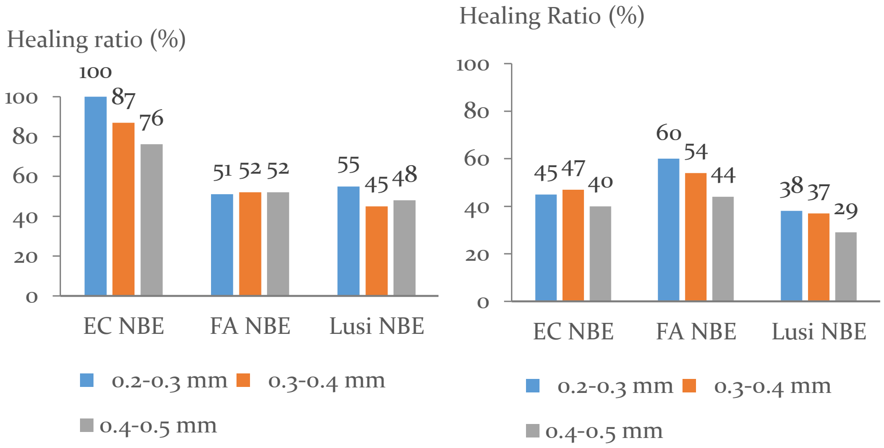

(a) (b)

Figure 6.18 Average healing ratio value among NBE series after being cured for 30 days and cracks were fabricated at (a) 28 days, (b) 90 days.

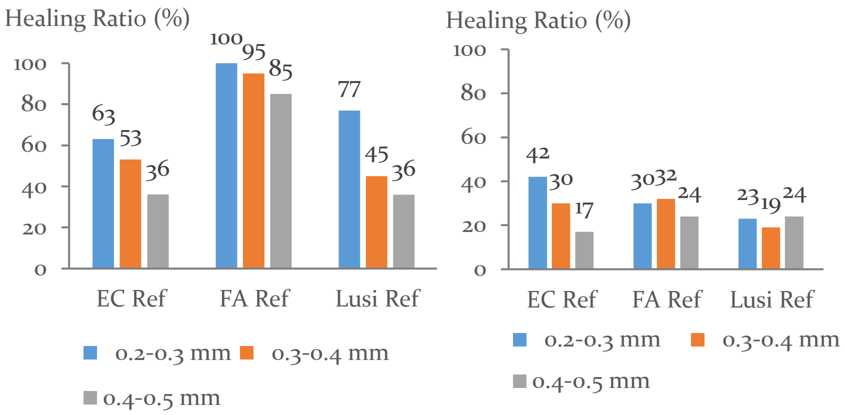

Figure 6.19 Average healing ratio value among Ref series after being cured for 30 days and cracks were fabricated at (a) 28 days, (b) 90 days.

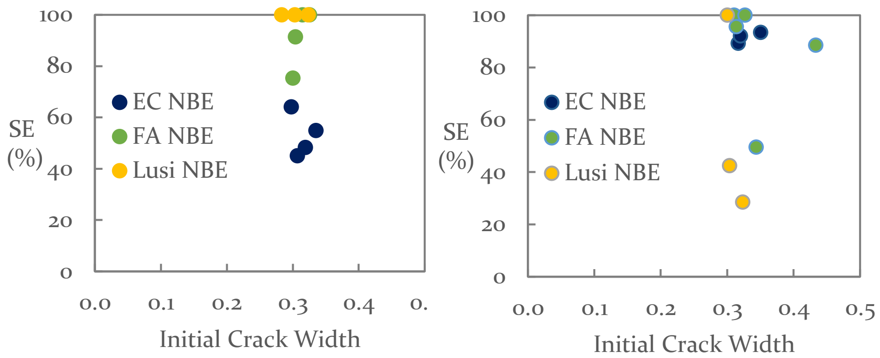

(a) (b)

Figure 6.20 Average sealing efficiency value among NBE series after being cured for 30 days and cracks were fabricated at (a) 28 days, (b) 90 days.

6.3.7 Characterization of the healing product

The cubic shape of calcium carbonate could be observed in the healing products of EC NBE, FA NBE, and Lusi NBE samples (**Figure 6.21**). However, the healing product's shape of each sample is different. A sharp-edged and triangular form was observed in the EC NBE sample, a blunt cube-like form was observed in the FA NBE sample, while a layer of rhombohedral cubes was observed in the Lusi NBE sample. A similar cube-like shape of the healing product was also observed in the literature and was confirmed as $CaCO_3$ (Li et al., 2010). It has been reported that difference in the impurities, initial saturation of the sample combined with bacterial activity contributed to the different morphology of $CaCO_3$ precipitation (De Muynck et al., 2010; Jonkers and Schlangen, 2009). The EDS mapping analysis result presented in **Table 6.2** shows that the ratio between calcium and oxygen in all samples was in the range of 0.5-0.7. EC NBE has a higher Ca/O ratio followed by FA NBE and Lusi NBE. The interaction between chemical content especially the calcium oxide in Lusi and FA LWA with the bacteria activity might cause different initial impurities and saturation levels that could cause different morphology of $CaCO_3$ precipitation in each sample.

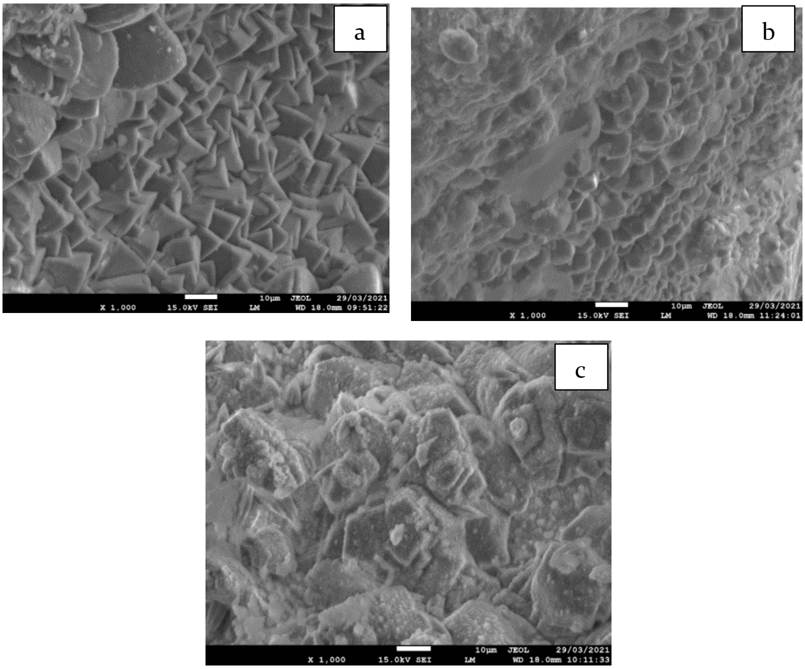

Figure 6.21. The morphology of healing product observed in (a) EC NBE, (b) FA NBE, and (c) Lusi NBE samples

Table 6.2. EDS mapping analysis on calcium, oxygen, and carbon in the healing product

Sample's name	Ca	O	C	Ca/O
EC NFC	35.9	50.2	13.7	0.7
FA NFC	25.2	43.7	26.1	0.6
Lusi NFC	28.5	53.0	17.5	0.5

6.4 Conclusions

Based on the results presented in this chapter, the following conclusions can be drawn:

1. The high initial pH of alkali activated LWA slightly inhibits the ureolytic activity of bacteria.
2. The presence of LWA had more effect on the properties development of resulting mortar rather than the addition of nutrients or bacteria.
3. In samples cracked at the age of 28 days, the role of LWA as internal curing agent could be clearly seen. Several cracks in the Reference and Nutrient series of EC, FA 6M, and Lusi 6M group with a crack width range between 0.2-0.3 mm were completely healed.
4. The vegetative cells encapsulated in the EC LWA could completely heal several cracks with the width of 0.3-0.4 after being subjected to wet-dry cycle curing for 30 days. The maximum crack width that could be healed in EC LWA group samples was 0.49 mm.
5. A decrease in the healing performance was observed in FA 6M and Lusi 6M sample groups compared to EC LWA. With the initial crack of 0.3-0.4, an 80% healing ratio was achieved by the FA NBE series, while a 60% healing ratio was obtained in the Lusi NBE series.
6. The vegetative cells encapsulated into EC LWA and FA LWA are still active, indicated by the improvement of healing performance in those sample, even when the cracks were fabricated at the age of 90 days.
7. The crack width in the range of 0.2-0.3 mm could completely heal in EC NBE and FA NBE samples cracked at 90 days. In comparison, no healing product could be found for the same crack width in Lusi NFC series.
8. The effect of the encapsulation procedure could be seen in the sealing efficiency result on the samples cracked at the age of 90

days. For EC and FA LWA carriers, samples with an encapsulation procedure (NBE) performed better regarding sealing efficiency than the other series. While a problem with particle blocking probably occurred in Lusi 6M samples. It made the sealing efficiency result obtained in Lusi 6M samples not reliable.

9. Through SEM-EDS analysis, the healing product formed in all NFC series was calcium carbonate.

In general, it can be concluded that FA 6M LWA could be considered as a bacteria carrier, as it provides similar healing and sealing performance with the commercial expanded clay (EC LWA) carrier. A further improvement, such as by application of a suitable coating, could allow to mitigate the high leakage of bacteria from the LWA carrier. By reducing the bacteria leakage, an improvement in the healing ability of the resulting mortar could be expected.

Chapter 7. Screening Suitable Coatings for Lightweight Aggregates as Bacteria Carrier for Manufacturing Self-Healing Concrete

This chapter was redrafted after:

Risdanareni, P., Wang, J., Boon, N., De Belie, N. “Screening a Suitable Coating for Expanded Clay Aggregate as Bacteria Carrier for Manufacturing Self-Healing Concrete”, in Proceeding of *RM4L 2020 International Conference,* Cambridge, 20-22 September 2021 *(accepted)*

7.1 Introduction

Bacteria-based self-healing becomes a promising autonomous self-healing method due to its compatibility with the concrete matrix. The Microbially Induced Carbonate Precipitation (MICP) method was proven to increase the durability of construction materials such as concrete and stone (De Muynck et al. 2008; 2011). The urease active bacterium from *Bacillus* genus named *Bacillus sphaericus* was selected as the bacteria healing agent in this study due to its higher carbonate production compared to others for a range of different temperatures between 10 and 37°C (De Muynck et al., 2013)

Furthermore, the bacteria need protection in order to survive in the harsh environment of fresh concrete (Thijssen et al., 2010). Several attempts on encapsulating bacteria into various carriers such as hydrogel (Wang et al. 2018), microcapsules (Wang et al. 2014), and porous aggregate (Alazhari et al., 2018; Ersan et al., 2015) have been performed. However, cheaper and easier to apply bacterial carriers are still required in order to make self-healing concrete become accepted in the construction industry sector. Thus artificial lightweight aggregate (LWA) generated from industrial by-products such as fly ash and a commercial ready-to-use expanded clay aggregate can be used as bacteria carriers. Those carriers could retain a high amount of bacterial solution into their pores and are compatible with mortar or concrete mixtures. It was also reported in Chapter 6 that the healing performance obtained by encapsulating *B.sphaericus* cells into FA 6M LWA is comparable to healing performance delivered by EC LWA carrier.

Although the LWA seems to be the ideal bacteria carrier, the leakage issue of the bacteria after encapsulation is still the main problem that needs to be solved. In previous research, vacuum treatment of LWA before encapsulation and pressure treatment afterwards had a positive impact on the encapsulation efficiency (Ersan et al., 2015). However, due to the fact that the surface of the LWA is not covered after the pressure treatment, leaking of bacteria after pressure treatment, measured in chapter 6 was still above 20%. Thus, coating the LWA surface after the bacteria encapsulation process could be a possible solution for leakage mitigation.

In this study, polyvinyl alcohol (PVA), sodium silicate, and sodium alginate were selected as a coating material. Research has shown that PVA and sodium silicate effectively sealed the pores of recycled aggregate and improved the properties of its resulting concrete (Kou and Poon, 2010). PVA has previously also been applied to seal sodium silicate into LWA for self-healing concrete production (Alghamri and Kanellopoulos, 2016). While sodium alginate crosslinked with calcium chloride was used as the core structure in manufacturing LWA aggregate (Xiaoyu Shang and Li 2020; Xiaoyu Shang, Li, and Zhan 2020). However, only limited reports could be found on applying those coatings as protection for LWA impregnated with bacteria.

Summarizing, this study aims to find a suitable coating material for protection of LWA impregnated with bacteria. The pH evolution in urea solution and ureolytic activity were tested to monitor the viability of bacteria after the encapsulation process. In the end, the leakage of bacteria after encapsulation was also examined to see the effect of coating application on preventing the bacteria leakage.

7.2 Materials and Methods

7.2.1 Materials

Alkali activated lightweight aggregate (LWA) generated from fly ash type F (Dutch Power Plant) and a commercial expanded clay (EC) LWA from Argex NV with the size of 2-4 mm was used as a porous bacterial carrier.

In the production of fly ash LWA (FA LWA), sodium silicate and sodium hydroxide solution with the concentration of 6 molars (6M) was mixed with a weight ratio of 1.5 and was employed as an alkali activator. Sodium hydroxide solution with the concentration of 6M was obtained by diluting 240 g NaOH with a purity of 99% (VWR Belgium) into 1 liter distilled water. At the same time, sodium silicate, which contained 26.3% silica, 7.9% sodium oxide, and 65.8% water, was applied. The production and storage method of FA 6M LWA was described in chapter 3, section 3.2.

The bacterial healing agent used was *Bacillus sphaericus* (BS) LMG 22257 (Belgian Co-ordinated Collection of Micro-organisms, Ghent). The bacteria were cultured in a sterile liquid medium containing yeast extract (Carl Roth Belgium) with the concentration of 20 g/l and urea (Carl Roth Belgium) with the same concentration for 24 hours on the shaking table (120 rpm) in a room with a temperature of 28ºC. The vegetative cells were harvested by centrifuging the culture solution at 15050 g for 7 minutes to get the bacteria pellets. The pellets were then resuspended in yeast extract solution (5 g/l). The final concentration of the bacteria was 2×10^9 cells/ml.

A flake form of 98% hydrolyzed polyvinyl alcohol (PVA) with a molecular weight of 146.000-186.000 from VWR was applied as the coating protection of impregnated LWA. The final concentration of PVA that was dissolved into warm distilled water (80ºC) was 8 %. At the same time, a gel form of Sodium Silicate (SIL) with a purity of 99% from Sigma Aldrich was directly applied as a coating material. In addition, a powder form of sodium alginate (SAL) from Sigma Aldrich was dissolved into distilled water with a final solution concentration of 5 g/l. While a flake form of calcium nitrate tetrahydrate of 98% (VWR) dissolved into demineralized water with the desired final concentration of 54 g/l was used as a medium to crosslink the sodium alginate into a stable coating gel

7.2.2 Methods

The water absorption over 24 hours (WA_{24}) of LWAs was determined in accordance to NBN EN 1097-6. This value is needed to determine the amount of bacterial solution (B) required to be encapsulated into LWA as described in Equation 7.1. Moreover, the required LWA and bacteria solution needed for 1 batch experiment is presented in **Table 7.1**. For each type of LWA, nine series of samples were examined. One series contained free bacteria in urea solution (EC/FA B), one series contained only the LWA (L), one series contained bacteria encapsulated into LWA (L-B), three series only contained coated LWA (L-SIL; L-PVA; L-SAL), and the last three series consisted of the bacteria encapsulated into LWA and coated with sodium silicate (L-B-SIL), PVA (L-B-PVA) or sodium alginate (L-B-SAL).

$$B = M_{lwa} \times WA_{24}/100 \qquad \text{(Equation 7.1)}$$

Where B is the amount of required bacteria M_{lwa} is the weight of LWA and WA_{24} is the water absorption value of LWA.

Table 7.1. Materials needed for encapsulation procedure's set up

Sample	M $_{LWA}$ (g)	WA24 (%)	Bacteria (ml)
EC B	0	0	3.2
EC L	15	21.1	0
EC L-B	15	21.1	3.2
EC L-SIL/PVA/SAL	15	21.1	0
EC L-B-SIL/PVA/SAL	15	21.1	3.2
FA B	0	0	3.6
FA L	15	23.7	0
FA L-B	15	23.7	3.6
FA L-SIL/PVA/SAL	15	23.7	0
FA L-B-SIL/PVA/SAL	15	23.7	3.6

The bacteria cells were injected into LWA by vacuum and pressure treatment as described in Chapter 6. The encapsulation steps were continued by transfer of the impregnated LWA from the penicillin bottle to a sterilized Petri dish. Afterward, the coatings were applied by means of dipping for 30 seconds. First, for sodium alginate coating, the impregnated LWA was immersed into sodium alginate solution for 10 minutes, followed by immersion into calcium nitrate solution for 20 minutes to get stable gel formation. The coated LWA was then dried in an incubator at 28ºC for 24 hours before being examined.

One-half of the coated impregnated LWAs were crushed and transferred to a sterilized urea (20 g/l) solution. The ureolytic activity of the bacteria was indicated by urea decomposition by using the Nessler method (Erris et al., 2003). During the urease hydrolysis process, one mole of urea was decomposed into two moles of ammonium and one mole of carbonate (Eq 2). Thus, by calorimetrically measuring the total ammonium nitrogen (TAN) in the urea solution, the total decomposed urea (g/l) could be calculated (Eq 3) (Wang et al. 2017). The ureolytic activity was monitored every 2 hours for 24 hours.

$$CO(NH_2)_2 + 2H_2O \rightarrow 2NH_4^+ + CO_3^- \qquad \text{(Equation 7.2)}$$

$$DU = TAN \times dilution \times Mr \frac{Urea\ (\frac{60g}{mol})}{2Nitrogen\ (2x14\frac{g}{mol})} \qquad \text{(Equation 7.3)}$$

where DU is the decomposed urea (g/l), and TAN (g/l) is total ammonium nitrogen recorded with a spectrometer at wavelength 425 nm. The procedure to perform TAN Nessler test was the same as described in Chapter 6.

The other half of the coated impregnated LWAs were then washed with distilled water to remove the bacteria stuck on the surface of the LWA. The washed LWA were then immersed in distilled water and were left on a shaking table with a speed of 120 rpm for 1 hour. Finally, the immersion water was taken to check the number of bacteria that leaked using the flow cytometer (BD Accury 6+). 20 µl of the sample was diluted into 180 µl sterile saline solution (NaCl 0.08%) in 96 flat-bottom plates. A serial dilution was then performed. The diluted samples were then stained with SYBR Green and were kept in an incubator at 37°C for 13 minutes. The number of bacteria counted in the plot cage needs to be in the range of 200-2000 count/cells. The bacteria leakage was measured based on equation 3 in chapter 6. Take into account that the flow cytometry test was only performed in a sample that proved to have ureolytic activity.

7.3 Results and Discussion

7.3.1 pH Evolution

There is no buffer effect detected in series of samples coated with sodium silicate (**Figure 7.1**). In the EC LWA group (**Figure 7.1**a), the pH of the urea solution bacteria impregnated in LWA and being coated (EC L-B-SIL) were submerged, was similar to coated no-bacteria samples (EC L-SIL). The final pH value after 24 hours of observation was in the range of 13-14. Thus, it seems that sodium silicate coating increases the pH in solution from 7 (EC-L) to around 13 (EC L-SIL). Moreover, applying sodium silicate on the impregnated EC LWA tends to decrease the ureolytic activity indicated by no buffering on the final pH of sample EC L-B-SIL. Compared, non-coated samples (EC L-B) and samples with free bacterial cells (EC B) have final pH in the range of 9-10, which means that the bacteria increased the pH from 7 to 9.

A similar result was also observed in the FA LWA sample group (**Figure 7.1**). The final pH value of FA L-B-SIL and FA L-SIL were in the range of 12-13. Given the initial pH of 11 (FA L) by applying sodium silicate coating, the pH increased to the range of 12-13. Moreover, the addition of bacteria in this group did not affect the final pH value as well. Compared to the non-coated group (FA L-B), bacteria could decrease the pH from 11 to 9.5.

Similar behaviour was also observed in the PVA series (**Figure 7.1**), although the PVA coating induces a lower pH than the sodium silicate coating. The final pH values of the L-B-PVA series for both LWA (EC and FA LWA) were not buffered to the pH range of 9-10 as samples without coating. In the EC LWA group, the L-B-PVA and L-PVA series' pH was in the range of 6-7. While in the FA LWA group, the L-B-PVA and L-PVA series' pH value was in the range of 11-12.

Better performance regarding the pH evolution of samples coated with sodium alginate was observed (**Figure 7.1**). In the EC LWA series, the final pH value of samples containing bacteria and coated with sodium alginate (EC L-B-SAL) were almost similar to free bacteria samples (EC B). While in the FA group, the final pH value of the FA L-B-SAL series was slightly higher than FA B but lower than FA L-SAL. It was also observed that the sodium alginate coating slightly decreased the final pH of the solution. The final pH of the FA L series decreased after sodium silicate coating was applied (FA L-SAL).

In the sodium silicate series, the pH was not buffered to the range of 9-10 due to the high initial pH of sodium silicate (13). The vegetative cells might not survive when in contact with a high pH intensively. In the PVA coating group, the alcohol content in PVA might harm the bacteria, which could not induce the decomposition of urea. Hence the pH did not increase to the range of 9-10.

Sodium alginate coating seems not to disturb the ureolytic activity of bacteria encapsulated into the LWA. A slow pH increase in the FA LWA group sample was due to the high pH of FA LWA and the introduction of calcium solution during the crosslinking process of sodium alginate coating. Monitoring the pH evolution is quite a reliable method to detect the viability of urease-positive bacteria. The ammonium ion, which forms due to the urea decomposition process, could change the environment into pH 9 due to ammonium-ammonia equilibrium (Algaifi et al., 2020). Such behaviour was also reported in a previous study, which stated that *B. sphaericus* could buffer the pH in urea solution into the range of 9-10 (Wang et al., 2017). Thus when the initial pH of the solution is neutral, the activity of bacteria could increase the pH of the solution to 9-10.

On the other hand, in the FA LWA sample group, when the initial pH of the solution was in the range of 11-12, introducing the bacteria allowed to decrease the pH to the range of 9-10. Nevertheless, when the coating was applied, this effect was reduced: the pH of FA L-B-SAL remained higher than for FA B and FA L-B.

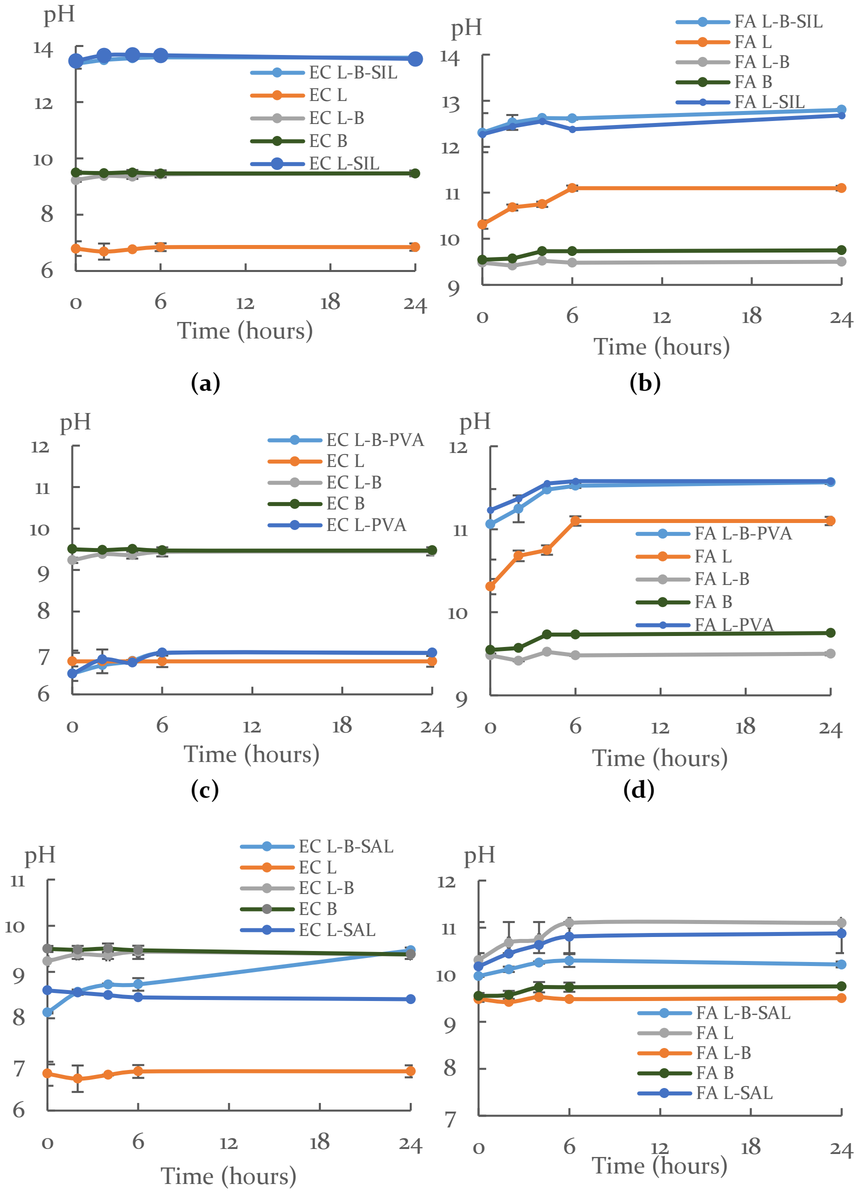

(a) **(b)**

(c) **(d)**

(e) **(f)**

Figure 7.1. pH evolution monitored for 24 hours (n=3) in (a) EC LWA coated with sodium silicate (SIL) and (b) FA LWA coated with sodium silicate (SIL) (c) EC LWA coated with PVA (d) FA LWA coated with PVA (e) EC LWA coated with sodium alginate (SAL) and (f) FA LWA coated with sodium alginate (SAL).

7.3.2 Ureolytic Activity

The ureolytic activity of bacteria was determined by the amount of urea decomposed in the solution. The concentration of urea solution in this research was 20 g/l. Thus, when the decomposed urea reached 20/g, it means that all the urea in the solution was fully decomposed. In the EC and FA LWA groups, in series without the coating application (B and L-B), the urea was fully decomposed in 6 hours (**Figure 7.2**). This shows that application of bacterial cells inside a protective carrier, being either EC or fly ash-based LWA, allows to maintain the ureolytic activity.

Once LWA with impregnated bacteria was coated with sodium silicate, no urea was decomposed after 24 hours (**Figure 7.2**). The same behaviour occurred in samples coated with PVA (**Figure 7.2**). An improvement was detected in samples coated with sodium alginate. In EC LWA coated with sodium alginate, a slow urea decomposition rate compared to uncoated samples was observed. Only 50% of urea was decomposed in 24 hours (**Figure 7.2**). Compared to the non-coated samples series (EC L-B), the urea decomposition rate in the sodium alginate coated series was slower. The increasing pH of the solution during the crosslinking process in calcium solution might slow down the bacteria activity in the EC samples group coated with sodium alginate. Compared to EC LWA coated with sodium alginate, the urea decomposition rate that occurred in the FA LWA series was slower (**Figure 7.2**). Only around 5% urea was decomposed in 24 hours. The high initial pH of FA LWA could be a factor that inhibits the ureolytic activity that occurs in the FA LWA series coated with sodium alginate.

The decomposed urea results were well correlated with the pH evolution results presented in **Figure 7.1**. Ureolytic activity was detected in samples that have a pH in the range of 9-10. It seems that the ureolytic activity was sharply decreased when the pH of the solution increases above 10 (L-B-SAL). Previous studies have shown that ureolytic activity of *B. sphaericus* was optimal when the pH of the environment was set to pH 7.5-8.5 (J. Wang, Jonkers, et al., 2017). The bacteria are still viable in a pH environment higher than 10-12, but the urea decomposition rate becomes slower. The results are in line with a previous study reporting that at the pH of 9, the ureolytic activity of *B. sphaericus* was at its peak. At the pH of 12-13, some ureolytic activity was detected, but it decreased up to 75% compared to the one at a pH of 9 (Algaifi et al., 2020).

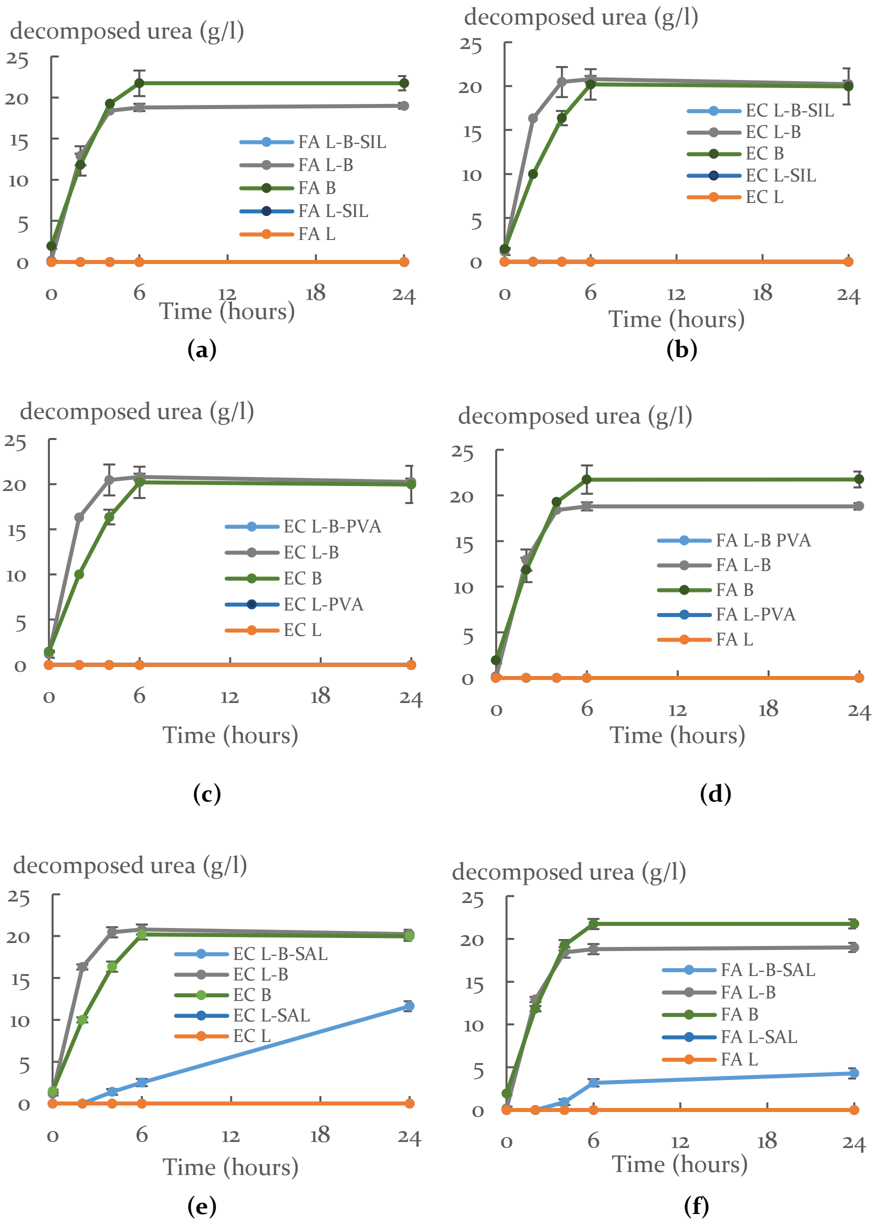

Figure 7.2 . Ureolytic activity monitored for 24 hours (n=3) in (a) EC LWA coated with sodium silicate (SIL); (b) FA LWA coated with sodium silicate (SIL); (c) EC LWA coated with PVA; (d) FA LWA coated with PVA; (e) EC LWA coated with sodium alginate (SAL) and (f) FA LWA coated with sodium alginate (SAL).

7.3.3 Leakage of Bacteria after Encapsulation

A significant decrease in bacterial leakage was observed in samples coated with sodium alginate (**Figure 7.3**). In the EC LWA sample, without coating application, 27.39% of bacteria leaked into the immersion solution after being left on a shaking table with the speed of 120 rpm for 1 hour. After the coating had been applied, only 3.34 % of bacteria were detected in the immersion solution. It means that the coating application decreased the leakage up to 87%. Similar behavior was observed in the FA LWA group samples. The leakage of bacteria could be decreased up to 80% by applying sodium alginate coating. It seems that the gel form of sodium alginate effectively blocked the pores at the surface of LWA so that the bacteria could not escape during the immersion period that was aimed to mimic the conditions during mortar production.

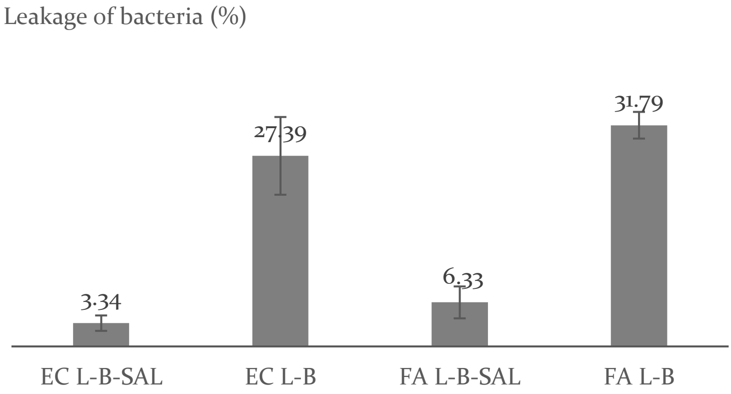

Figure 7.3. The effect of sodium alginate coating on the bacteria leakage (n=3).

7.4 Conclusions

Alkali activated LWA generated from fly ash is a suitable candidate as a bacterial carrier. Without applying a coating, bacteria were still viable in this carrier and had comparable activity with the samples where expanded clay aggregate was used as the bacterial carrier.

Among different coating applications, the bacteria only survived when the protective LWA had been coated with sodium alginate. The sodium alginate coating tended to decrease the ureolytic activity, indicated by a slower decomposition rate than for uncoated samples. However, the bacteria inside the LWA were still viable and actively decomposed the urea slowly.

The sodium alginate coating was also proven to prevent bacteria leakage. After sodium alginate coating was applied, the leakage of bacteria decreased up to 87 %. A better healing performance can be expected in the resulting concrete containing bacteria impregnated LWA coated with sodium alginate because of an improvement in the bacteria leakage issue.

Chapter 8. Performance of Self-Healing Concrete Containing Bacteria Immobilized In Alginate Coated Alkali Activated Lightweight Aggregate

This page is intentionally blank

8.1 Introduction

Revisiting previous results on the utilization of alkali activated LWA generated from Lusi and fly ash presented in Chapter 6, alkali activated LWA generated from fly ash has shown to be a feasible carrier for bacteria as it delivers comparable performance relative to EC LWA used as carrier. Due to high leakage, presumably as result of its smaller pore sizes, LWA generated from Lusi did not deliver a good healing performance when used as bacterial carrier.

Still, from results obtained in Chapter 6, the leakage of bacteria after encapsulation into an open carrier LWA becomes an issue that needs to be solved. Thus in Chapter 7, an attempt to find a suitable coating for encapsulated cells in LWA was made. Sodium alginate coating, that was also reported to not damage the bacteria, was selected above polyvinyl alcohol (PVA) and sodium silicate coating that have previously been broadly used as porous aggregate coating material (Alghamri and Kanellopoulos, 2016; Shukla et al., 2020).

Regarding healing agent selection, even though vegetative cells reported to deliver satisfying healing when encapsulated into porous carriers, the viability of the cells tends to decrease with time (Ersan et al., 2015; Intarasoontron et al., 2021). As mentioned in Chapter 6, when cracks were created at the age of 28 day, cracks with a width of 0.35 mm still could be entirely healed when cells were encapsulated into FA 6M LWA, and even crack widths of 0.49 mm when cells were encapsulated into EC LWA. However, when cracks were created at the age of 90 days, a dramatic decrease in healing performance was observed for all LWA carriers. The average healing ratio of 56 % was obtained for cracks of 0.3-0.4 mm when cells of *B. sphaericus* were encapsulated in FA 6M LWA.

Given the viability issue of vegetative cells in concrete at later age, spores would be suitable healing agent candidates. Bacterial spores have been reported to be less sensitive to the harsh concrete environment, and could be viable in concrete for long period, hence using spores could overcome the decrease of healing performance provided by vegetative cells at later ages (Jonkers and Schlangen, 2009; Wang et al., 2017).

This chapter, after immobilization of spores or vegetative cells of *B. Sphaericus* in LWA, sodium alginate was used as a coating material. The effect of coated EC LWA and FA 6M LWA on the compressive strength, crack healing performance, and sealing efficiency of the resulting mortar were investigated. Beforehand, the viability of spores and cells after the encapsulation process followed by sodium alginate coating was also examined. By applying the sodium alginate coating, the healing performance of the mortar was expected to be improved.

8.2 Materials and Methods

8.2.1 Materials

Fly ash (FA) type F from a Dutch power plant was utilized as a binder in the production of lightweight aggregate (LWA). The average particle size of fly ash was 6.2 µm. The major constituents of fly ash determined by an X-ray fluorescence test were SiO_2, Al_3O_2, Fe_2O_3, and CaO. More detailed information regarding the chemical composition of fly ash used in the production of FA 6M LWA was presented in table 2 in chapter 2. The binders were activated with Na_2SiO_3 and NaOH (VWR, Belgium) 6M with a weight ratio of 1.5.

Cement type I 52.5 (Holcim) was used as a binder in mortar production. River sand with the size of 0-2 mm was used as fine aggregates. The required particle size was obtained by sieving river sand fraction 0/4. A commercial expanded clay aggregate (EC LWA) with a particle size of 2-4 mm from Argex nv was used as a comparison LWA. The specific particle size used was derived from sieving EC LWA with fraction 0/4.

Yeast extract, calcium nitrate tetrahydrate, and urea (Carl Roth Belgium) with a purity of 99% were used as bioagents in the mortar.

Vegetative cells and spores of *Bacillus sphaericus* LMG 22257 (Belgian Co-ordinated Collections of Micro-organisms, Ghent) were used as a healing agent. A sterile liquid yeast extract medium with a concentration of 20 g/l was obtained by autoclaving the medium at a temperature of 120°C for 20 minutes. Sterilized urea with a concentration of 20 g/l was then introduced to the medium by filtration using a sterile 0.22 µm millipore filter (Millipore, USA). Thus, the final concentration of yeast extract and urea in the medium of 20 g/l was obtained. The next step was to inoculate the cells into the medium under sterile conditions. A medium containing bacteria was then incubated on a shaking table with the speed of 120 rpm in a room at 28°C for 24 hours. Finally, the vegetative cells were harvested by centrifuging the 24h old culture for 7 minutes in the centrifuge machine with a speed of 15050 g. The bacterial pellets were then re-suspended in a sterile yeast extract solution of 5 g/l. The final concentration of resuspended cells was 2 x 10^9 cells/ml.

To generate the spores, 24 hours old bacteria pellets were transferred into a sterile sporulation medium. The sporulation medium consisted of yeast extract (2 g/L), peptone (3 g/L), glucose (4 g/L), malt extract (3 g/L), K_2HPO_4 (1 g/L), $(NH_4)_2SO_4$ (4 g/L), $CaCl_2$ (0.1 g/L), $MgSO_4$ (0.8 g/L), $MnSO_4.H_2O$, (0.1 g/L), $FeSO_4.7H_2O$ (0.001 g/L), $ZnSO_4$ (0.01 g/L) and $CuSO_4.5H_2O$(0.01 g/L). The culture was then incubated on the same shaking table as mentioned earlier (120 rpm, 28°C) for 7-14 days until at least 80% of the vegetative cells turned into spores. The spores were then harvested by centrifuging (15050 g for 7 minutes). The spore pellets were resuspended into a sterile saline solution (NaCl 8.5 g/l). A pasteurization process (80°C for 20 minutes followed by 5 minutes in cold ice water) was then applied to kill the remaining vegetative cells in the spore suspension. Finally, spore suspension with a final concentration of 2x10^9 cells/ml was obtained and was kept in the fridge with a temperature of 4°C until further use.

A powder form of sodium alginate (SAL) from Sigma Aldrich was dissolved into distilled water with the final solution concentration of 5 g/l. In the meantime, a calcium nitrate tetrahydrate solution with a concentration of 54 g/l was used as a medium to crosslink the sodium alginate into a stable coating gel.

8.2.2 Germination of Spores in the Growth Media

To induce germination, the spores were introduced in a sterile liquid medium which contained 2 g/l of yeast and 20 g/l of urea. The cells' growth was monitored at 0 hours, 24 hours, and 72 hours using a Tecan plate reader (Tecan Infinite M200 Pro). The data obtained from the Tecan plate reader was the optical density of the culture measured at the wavelength of 620 nm. The optical density represents the ability of solution to block the light. The germination process was also monitored under the microscope. A few milliliters of culture sample were taken and observed under the microscope (Zeis Axioskop). The monitoring was performed on 0 hours, 24 hours and 72 hours old culture. Meanwhile, the ureolytic activity of the spore culture during the germination process was measured by the TAN Nessler method. The pH evolution was monitored as well during the germination process.

8.2.3 The Production of Alkali Activated LWA

The fly ash powder was added to the pan granulator with a diameter of 500 mm and a depth of 90 mm. The alkali activator liquid was sprayed on the fly ash at the pan's side continuously for 20 minutes while the pan was rotated at a speed of 80 rpm. Finally, the compacted fly ash granules would fall from the side of the pan. The fresh granules were then cured in a curing chamber with a temperature of 20°C and humidity of 95 % for 24 hours. After 24 hours, granules were sieved to remove particles smaller than 2 mm. The sieved granules were put in a sealed plastic bag and were stored in the same curing chamber for 28 days. The procedure for LWA production was explained in more detail in Chapter 2 and 3.

8.2.4 Encapsulation and Coating Process

The dried LWA was added into a penicillin bottle which was sealed with a rubber stop and a metal cap and then was autoclaved for 20 minutes at a temperature of 120°C. A -0.8 bar pressure was then applied to the sterile penicillin bottle, followed by adding the bacteria suspension. This pressure was maintained for 30 minutes. After that, 1 bar of pressure was applied to the penicillin bottle for 24 hours to push the bacteria (cells/spores) solution deep into the pores of the LWA. The impregnated LWA was then transferred from the penicillin bottle to a sterilized petri-dish for being coated.

The coatings were applied by dipping the LWA into a 5 g/l sodium alginate solution for 10 minutes, followed by immersion into a 54 g/l calcium nitrate solution for 20 minutes to get a stable gel formation. The coated LWA was then dried in a 28°C incubator for 24 hours before being examined.

8.2.5 Activity of Bacteria after Encapsulation

The viability of spores and vegetative cells after the sodium alginate coating application was monitored by measuring its ureolytic activity. The TAN Nessler method that measures the total ammonium in the solution was applied to monitor the ability of bacteria to decompose urea in a solution.

The coated LWA was first rinsed in distilled water to remove the cells attached to the surface of LWA. After that, the coated LWA was crushed and was immersed into the specific medium as follows. For the samples with vegetative cells, a 20 g/l sterile urea solution was used, while in the spores group, a 20 g/l sterile urea solution mixed with 2 g/l of yeast extract was used. In each group (cell and spores), 3 sample series were made. The EC/FA Sal series contained the coated samples with impregnated spores in the spores' group, while EC/FA S were the samples impregnated with spores but without alginate coating. The last series, EC/FA Cal, contained the samples with the coating but without bacteria. In the vegetative cells group, the EC/FA Val series contained the coated samples with impregnated cells. EC/FA V were the samples impregnated with cells without coating. And the last series EC/FA Cal contained the samples with the coating but without bacteria. The TAN value and pH were monitored at 0h, 2h, 4h, 6h, and 24h for the vegetative cells group and 0h, 24h, and 72h for the spores group.

8.2.6 Mortar Production

Three types of moulds were used in this research. The first one was a standard prism mould with dimensions of 40x40x160 mm^3, which was used to cast samples for bending and compressive strength tests. The second mould was a modified prism mould with dimensions of 40x40x160 mm^3 with a hole in the middle to allow a bar with a diameter of 6 mm to be inserted. These moulds were used to cast samples for the water flow test. The third mould was a prism mould with dimensions of 30x30x360 mm^3 with a hole in the middle to place a reinforcement bar with a diameter of 6 mm. This mould was used to cast samples for crack closure observation.

The mortar samples were fabricated according to EN NBN 196 standard. The mix compositions for casting three standard prims is presented in **Table 8.1**. The amount of water in a sample containing calcium nitrate tetrahydrate was reduced to compensate for extra water provided by four water molecules in calcium nitrate tetrahydrate. The fine aggregate with the size of 2-4 mm was replaced by LWA with the same size. In order to encapsulate more bacteria into the mortar matrix, the replacement rate of 30% by volume was applied.

For mortar containing LWA encapsulated bacteria, the dried LWA was placed in a sealed tube with an opening to connect to gas. The vacuum with a pressure of -0.8 bar was introduced and kept for 30 minutes. Under the vacuum condition, bacteria suspensions were added slowly into the tube, and the vacuum was maintained at the same pressure (-0.8 bar) for another 30 minutes. The 1 bar pressure was then introduced into the tube and was kept for 24 hours. The next day, the bacteria encapsulated LWA was immersed into sodium alginate solution (5 g/l) for approximately 10 minutes following by immersing in calcium nitrate solution (54 g/l) for 20 minutes.

The coated LWA was then placed in a closed container and dried in a curing chamber with a temperature of 20°C and relative humidity 60% for 24 hours.

After being cast, the fresh mortars were covered with a plastic film and were cured in a curing chamber with a temperature of 20°C and relative humidity of 95 % for 24 hours. After 24 hours, the specimens were demoulded and were covered with plastic film and stored in the curing room with a temperature of 20°C and relative humidity of 60% until the testing age.

Table 8.1. Mix Compositions of Mortar

Type	LWA (g)	BS* (ml)	extra water (g)	Sand (g)	Cement (g)	Water (g)	YE (g)	Cal (g)	urea (g)
EC Ref	186	0	32	1164	450	225	0	0	0
EC Sal	186	32	0	1164	450	214	1.53	36	18
EC S	186	32	0	1164	450	214	1.53	36	18
EC Val	186	32	0	1164	450	214	0	36	18
EC V	186	32	0	1164	450	214	0	36	18
FA Ref	282	0	53	1068	450	225	0	0	0
FA Sal	282	53	0	1068	450	214	1.53	36	18
FA S	282	53	0	1068	450	214	1.53	36	18
FA Val	282	53	0	1068	450	214	0	36	18
FA V	282	53	0	1068	450	214	0	36	18

BS : *Bacillus Sphaericus* (cells/spores)
YE: yeast extract
Cal: calcium nitrate tetrahydrate
EC/FA Ref : reference sample
EC/ FA Sal : coated LWA in spores group
EC/FA S : uncoated sample in spores group
EC/FA Val : coated sample in vegetative cells group
EC/FA V : uncoated sample in vegetative cells group

8.2.7 The Mechanical Properties of Resulting Mortar

The compressive strength of 28 days old mortar was assessed based on the guidelines from EN NBN 196 standard. The compressive strength is shown as the average value from 3 measurements, with the standard deviation represented with an error bar.

8.2.8 Crack Fabrication and Crack Closure Observation

The procedure to create multiple cracks was the same as mentioned in Chapter 6. The cracks were fabricated on the 28-day old mortar prims which have a reinforcement bar. The sample was subjected to a tensile strength test with displacement control at the speed of 0.01 mm/s (Instron Universal testing Machine). The load was stopped after the average crack width reached 0.4-0.5 mm.

The initial crack width that occurs was observed under a microscope (Leica DMC 2900). After that, the sample was subjected to wet-dry cycles (4 hours wet, 4 hours dry) in the curing room with a temperature of 20°C and relative humidity of 60% for 30 days. The evolution of crack closure was monitored every 10 days. The crack healing ratio was then calculated with Equation 8.1.

$$HR = (Cwi - Cwf)/Cwi \times 100\% \qquad \text{(Equation 8.1)}$$

Where HR is the healing ratio, C_{wi} was the initial crack width, and C_{wf} was the final crack width.

8.2.9 Crack Sealing Observation

The mortar sample for crack sealing efficiency was a modified prism sample with a dimension of 40x40x160 mm^3, as mentioned in Section 6.2.6. Before casting, a smooth steel bar with a diameter of 5 mm was attached to the mould. During the demoulding process, this steel bar was removed from the mortar sample, leaving a hole in the prims. The mortar was then cured in the curing chamber mentioned in Section 8.2.6 for 28 days. The sample preparation to conduct the water flow test, the procedure for testing the water flow, and the equation to determine the sealing efficiency ratio were also the same as mentioned in Chapter 6.

8.3 Results

8.3.1 Spore Germination in Growth Medium

Based on the results of the optical density evolution displayed in **Figure 8.1**, an optical density larger than 1 was obtained after spores were cultured in the yeast extract medium for 72 hours. This is an indication that the spores germinated into active cells and then grew in the medium. The microscope image also confirmed that the spores had germinated after 72 hours (**Figure**

8.2). The round shape endospores turned into a rod-shape after having been inoculated in the yeast extract medium for 72 hours.

To check whether the bacteria culture is urease active, the spores were inoculated in a sterile urea-yeast extract liquid medium. The results showed that the spores germinated into vegetative cells in 72 hours (**Figure 8.3**). All the urea in the solution was fully decomposed in 72 hours. For 0 until 24 hours, only limited urea could be decomposed by the bacteria, but at 72 hours, all the spores were likely germinated into vegetative cells and actively decomposed the urea.

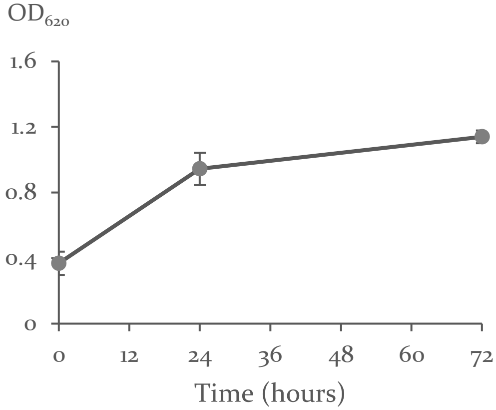

Figure 8.1. The Optical Density (OD_{620}) evolution measured during the germination period, with error bar representing the standard deviation (n=3).

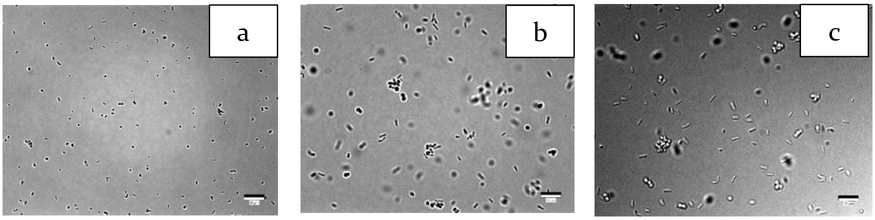

Figure 8.2. The spores evolution; the scale bar is 10μm; the pictures were taken with 1000x magnification at (a) 0 hours, (b) 24 hours and (c) 72 hours.

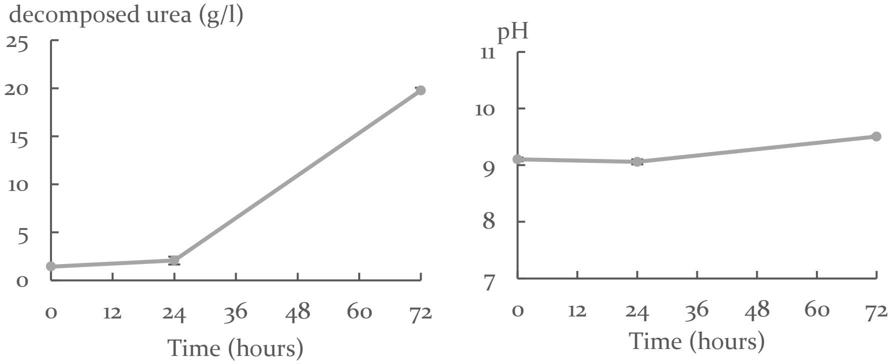

(b)

Figure 8.3. (a) The ureolytic activity and (b) the pH evolution of spore culture during the germination period (n=3).

8.3.2 Activity of Bacteria after Coating Application

The urea decomposition as a function of time by the spores and cells immobilized in the EC and FA LWA are displayed in **Figure 8.4**. In the EC LWA with spores, sodium alginate coating slightly slowed the urea decomposition rate (**Figure 8.4**). In contrast, in the vegetative cells group, the sodium alginate coating drastically slowed down the ureolytic activity (**Figure 8.4**). In the FA LWA group, the spores were difficult to germinate as only limited urea could be decomposed in 72 hours in FA S sample. Coating this sample with sodium alginate also did not improve its ureolytic activity (**Figure 8.4**). A better result was obtained in the vegetative cells group, even though the sodium alginate drastically slowed down the urea decomposition rate, a noticeable activity was still detected (**Figure 8.4**).

In FA 6M LWA series, the initial pH of the control sample (Cal) in the FA 6M carrier was more than 10, and the pH of the solution increased along with the immersion time (**Figure 8.5**). The final pH of the control sample after 72 hours immersion was almost 11. In the FA S sample, the pH stayed above 10 after 72 hours of immersion. It seems that the spores could not germinate into cells. The pH result was also well correlated with the decomposed urea result. Only a limited amount of urea could be decomposed in the FA S sample. A similar ureolytic activity pattern as for the FA S series was obtained in the FA Sal series.

In the vegetative cells group of FA 6M LWA, the pH buffering effect due to the bacterial activity could still be clearly seen in the FA Val sample. The sodium alginate coating application in the vegetative cells group also led to the decrease in the ureolytic activity of bacteria. Sample FA Val could only decompose 50 % of all the urea after being immersed in a urea solution for 72 hours. At the same time, samples without coating (FA V) could decompose all urea in solution within 24 hours.

When spores were employed as a healing agent in the EC LWA carrier, the urea decomposition was a bit delayed, but more than 80% urea was decomposed after 72 hours. It was decreased by around 5 % compared to the non-coated samples. In contrast, the spores had hardly germinated in FA 6M LWA carrier, and the sodium alginate coating did not improve the situation.

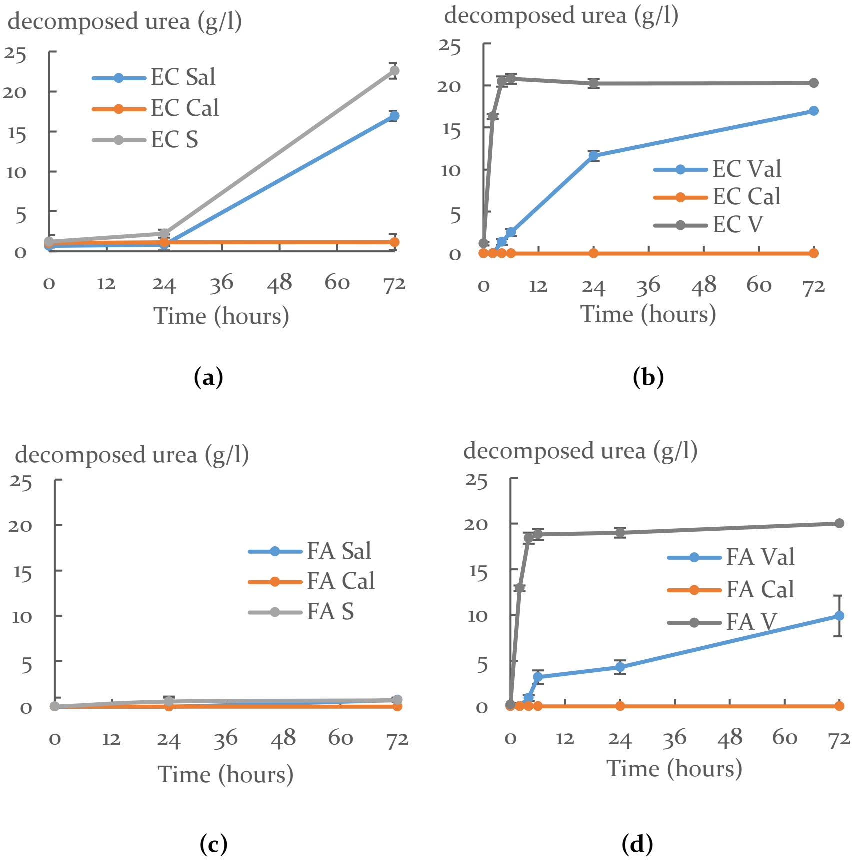

(a)

(b)

(c)

(d)

Figure 8.4 The decomposed urea as a function of time in (a) EC LWA spores group, (b) EC LWA vegetative cells group, (c) FA 6M LWA spores group and (d) FA 6M LWA vegetative cells group.

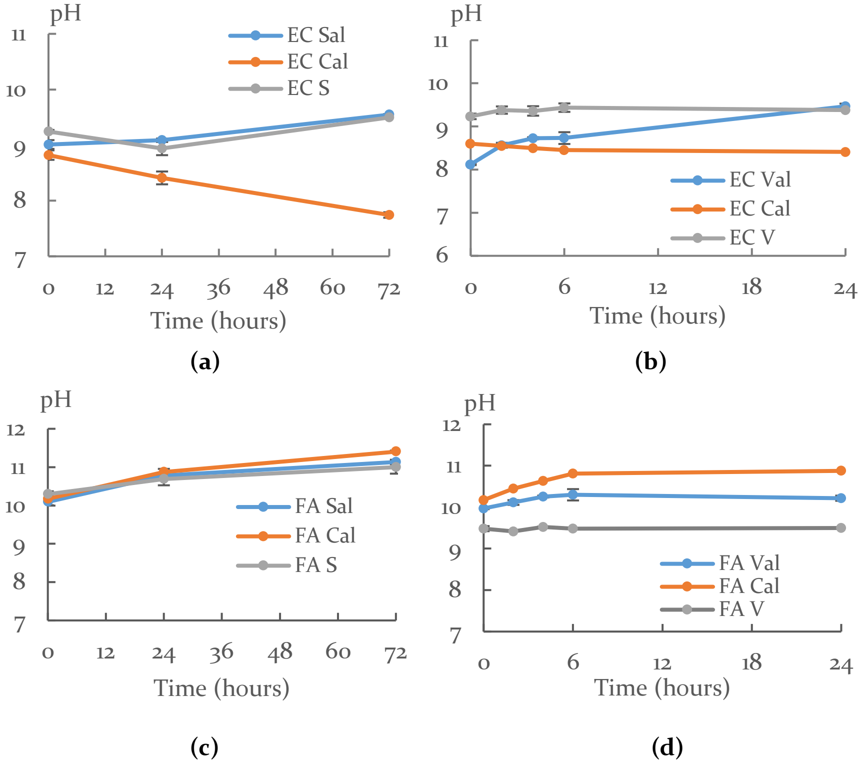

Figure 8.5 The pH in the solution as a function of time (n=3) in (a) EC LWA spores group, (b) EC LWA vegetative cells group, (c) FA 6M LWA spores group and (d) FA 6M LWA vegetative cells group.

8.3.3 Compressive Strength of Resulting Mortar

Sodium alginate coating had a negative effect on the mechanical properties of the mortar specimens. It can be seen in **Figure 8.6** that, in the vegetative cells group, compared to the samples with no coating (V series), the application of sodium alginate coating decreased the strength by 25 and 33% in FA 6M LWA and EC LWA, respectively. In the spores group, both yeast extract and sodium alginate coating decreased the strength of the resulting mortar. Due to the addition of yeast, compared to the Ref sample, the strength was decreased by 16 and 22% for EC LWA and FA 6M LWA series, respectively. After sodium alginate was applied, an additional decrease of 33 % and 22 % for EC LWA and FA 6M LWA was obtained. In total, compared to the reference samples, the strength was decreased by almost 50% in all LWA series which used spores as a healing agent. This strength reduction was too high. However, in general, the addition of sodium alginate coating delivered a slightly better performance in FA 6M LWA than in EC LWA carrier. It might be that the sodium alginate could still react with the calcium in FA 6M LWA and formed a thin dense layer that leads to a slight improvement in the compressive strength of the resulting mortar.

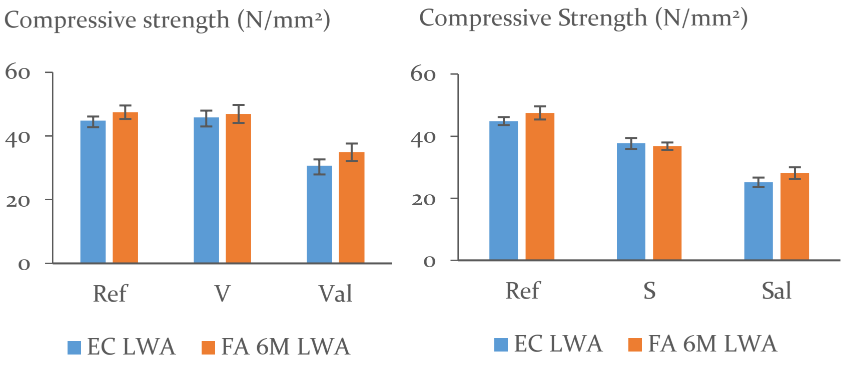

(a) (b)

Figure 8.6 Compressive strength of hardened mortar tested at the age of 28 days (n=3) for (a) vegetative cells samples and (b) spores samples.

8.3.4 Crack Healing Observation

8.3.4.1 EC LWA Carrier

After being cured for 30 days, 2 out of 6 cracks with widths between 0.3-0.4 mm were completely healed in the EC S series, while the rest of the cracks had an average healing ratio of around 50% (**Figure 8.7**). In contrast, in the EC Sal series, only one crack in that width range was healed. The rest of the cracks had an average healing ratio of around 60%. However, when the healing ratio in that crack width range is calculated, EC S has slightly better performance compared to the EC Sal sample.

A better healing performance was obtained in the vegetative cells group. Without coating, after being cured for 30 days, cracks in the width range of 0.3-0.4 have an average healing ratio of 87 %. A slight decrease in healing performance was noticed in the EC Val sample. In the same crack width range, the average healing performance of 11 cracks was 78 %. However, the healing performance obtained in all bacterial mortar samples was better compared to the Reference sample that only had an average healing performance of 60% in the same crack width range.

In conclusion, when EC LWA was employed as a carrier, the sodium alginate coating application did not improve healing performance, neither for encapsulated spores, nor for vegetative cells.

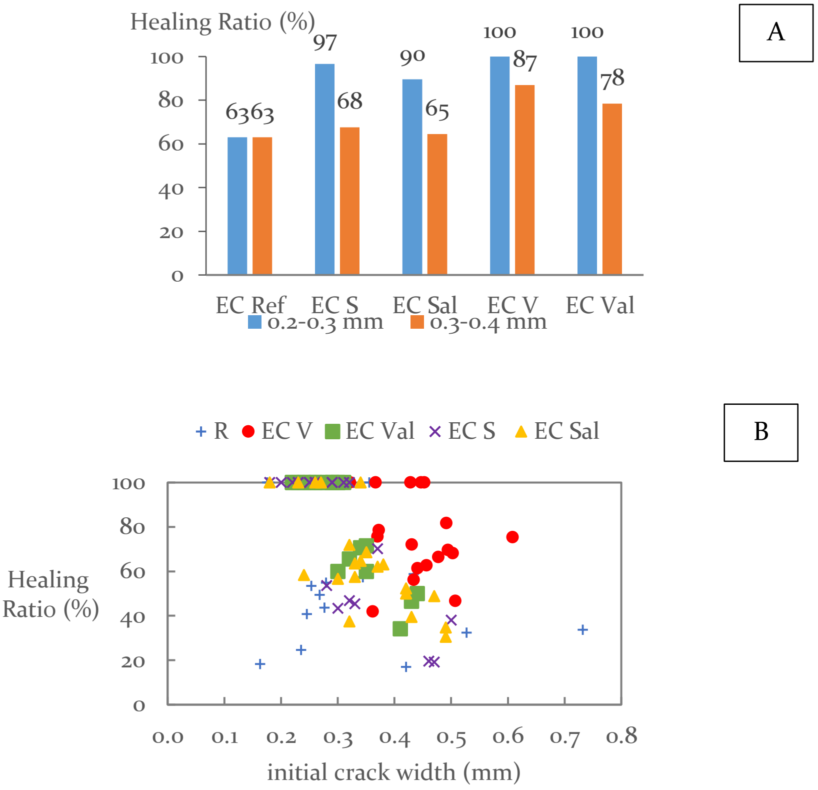

Figure 8.7 (a) The average healing ratio categorized per crack width range and (b) the healing ratio as a function of initial crack width in mortar with the EC LWA carrier cured for 30 days

8.3.4.2 FA 6M LWA Carrier

In the FA 6M group series, the reference sample already provided good autogenous healing. After being cured for 30 days, almost all the cracks in the crack width range of 0.3-0.4 mm were completely healed (see **Figure**

8.8). However, when spores or vegetative cells were added, the healing performance was decreased compared to the reference sample.

In the spores group sample, the sodium alginate coating tends to improve the healing ability of the resulting mortar. None of the cracks in the non-coated sample (FA S) with a width between 0.3-0.4 mm had a healing ratio of more than 50%, while in the coated sample (FA Sal), 3 out of 12 cracks had a healing ratio of more than 70%.

In the vegetative cells group sample, the healing performance of the sample with and without sodium alginate coating was nearly the same. In the crack width range of 0.3-0.4 mm, the average healing ratios in FA V and FA Val sample were 52 % and 53 %, respectively.

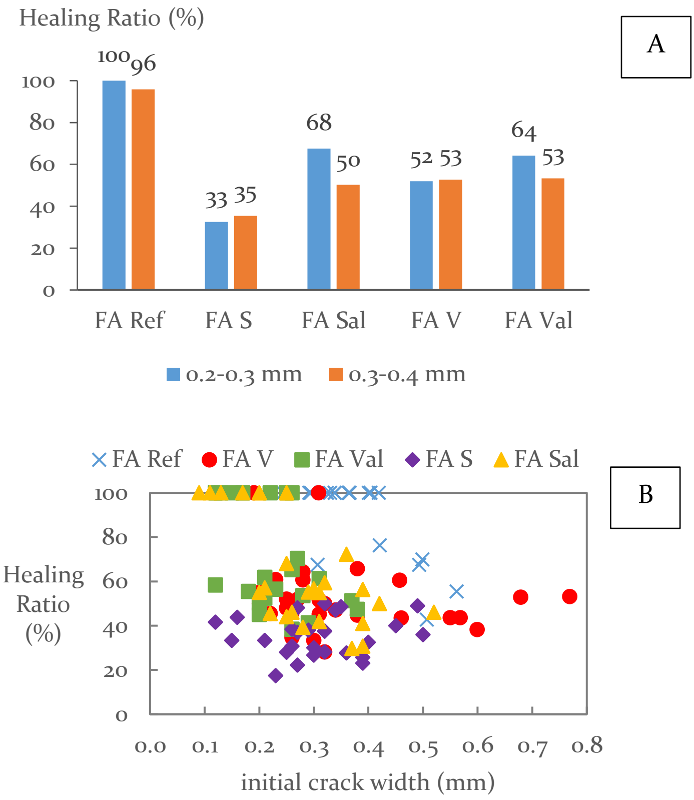

Figure 8.8 (a) The average healing ratio categorized per crack width range and (b) the healing ratio as a function of initial crack width in EC LWA carrier cured for 30 days.

8.3.5 Crack Sealing

In the EC LWA samples, where spores were used as a healing agent, it seems that sodium alginate coating slightly improved the sealing efficiency in the spores sample (**Figure 8.9**). Even though one sample in EC S has a sealing efficiency of almost 100%, the rest of the samples has a sealing efficiency of around 40%. It also can be seen that one sample from EC Sal has almost zero sealing while the rest of the samples have around a 60% sealing efficiency. High variability in sealing efficiency was also reported in previous studies. Uniform crack width did not consistently deliver uniform sealing efficiency (Anglani et al., 2020; Van Mullem et al., 2019). The internal crack geometry was reported to also contribute to this behaviour (Van Mullem et al., 2019). Still, in the EC LWA group samples, when vegetative cells were employed as healing agents, sodium alginate coating greatly improved the resulting mortar's sealing efficiency. The sealing efficiency of EC Val was more than 80%, while EC V only has around 50% sealing efficiency. In conclusion, when EC LWA was used as a bacteria carrier, sodium alginate coating could work better when vegetative cells were used as a healing agent rather than spores.

In FA 6M LWA sample, when spores were used as a healing agent, a sodium alginate application could not greatly improve the sealing efficiency. Samples without coating (FA S) had a sealing efficiency in the range of 50 to 80 %, while the sample with a coating (FA Sal) has a sealing efficiency in the range of 35-70 %. This result does not correlate with the crack closure result presented in Fig. 8, where a crack width range of 0.3-0.4 mm in the FA Sal sample has a better healing ratio than the FA S sample. The inner crack geometry combined with the fragile healing product could contribute to the unexpected result in sealing performance in the spores group sample. In the vegetative cells group sample, sodium alginate coating also did not improve the sealing efficiency of the resulting mortar. No sample in the FA Val group has a sealing efficiency higher than 60%, while in FA V sample, sealing efficiency could reach 90%.

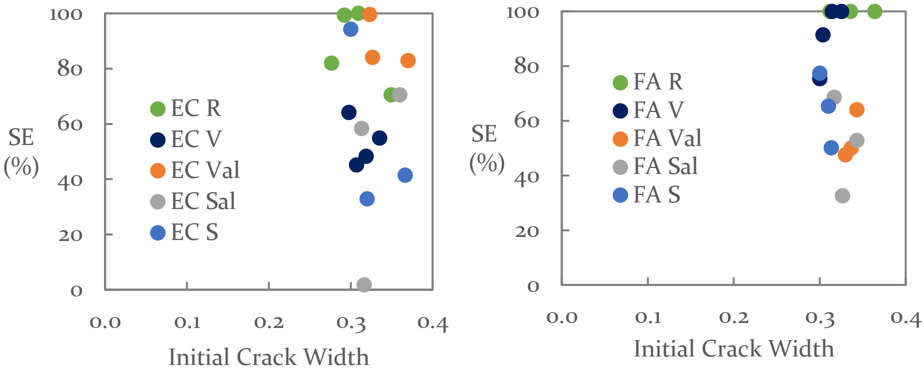

(a) (b)

Figure 8.9 The sealing efficiency as a function of initial crack width in (a) EC LWA group samples and (b) FA LWA group samples cured for 30 days.

8.4 Discussion

Effect of Sodium Alginate Coating on Ureolytic Activity of Bacteria

The yeast extract medium with a concentration of 2 g/l was sufficient to support the germination of spores into vegetative cells in 72 hours (**Figure 8.3**). This result is in line with previous findings by Wang et al., which revealed that in a medium containing 2 g/l yeast extract, spores of *Bacillus sphaericus* could germinate into urease positive cells in 3 days (Wang et al., 2017).

A similar ureolytic activity was observed when spores were encapsulated into EC LWA, and application of sodium alginate coating only slightly slowed down the urea decomposition rate (**Figure 8.4**a). But when spores were encapsulated into FA 6M LWA, with or without sodium alginate coating, spores did hardly germinate (**Figure 8.4**c). The initial pH in FA LWA which was above 10, might inhibit the spores to germinate. But actually the initial pH of FA LWA is not harmful for the bacteria, since vegetative cells that were encapsulated into FA 6M LWA had similar decomposition rate as when they were encapsulated into EC LWA (**Figure 8.4**). A slower decomposition rate was observed in all Val series (EC and FA 6M LWA, with vegetative cells and alginate coating) but still at an acceptable level.

Similar issues in the germination process have been reported before, when spores of *B. sphaericus* were encapsulated into commercial Pluronic hydrogel. Only 1 to 2 g/l of urea was decomposed after 48 hours immersion in UYE medium 20 g/l (Wang et al., 2014). Still, from the same report, when spores were encapsulated into hydrogel together with the nutrients (yeast extract, urea, and calcium nitrate), almost all urea in the solution could be fully decomposed by bacteria inside hydrogel in 3 days. It seems that several aspects besides pH could inhibit the germination process of spores. The access for bacteria to the nutrients is one of them. When spores were encapsulated into FA 6M LWA, it might be that the alginate was further reacting with the calcium in fly ash and developed an extra coating layer inside the pores, which could have entrapped the bacteria inside the pores with limited access to the nutrient.

Effect of Sodium Alginate Coating on the Mechanical Properties of Resulting Mortar

As mentioned in the results section, the sodium alginate coating tended to decrease the compressive strength of resulting mortar (**Figure 8.6**). Coated LWA with sodium alginate is a new research topic in concrete applications. Thus no literature could be found on the effect of applying LWA coated with sodium alginate on the properties of resulting mortar. A 15% strength decrease was reported when 1% by cement mass of alginate beads were used as an internal curing agent in mortar production (Mignon et al., 2016). Indeed those results in the literature are not comparable to results in this chapter. However, it seems that the presence of sodium alginate has the tendency to decrease the strength of resulting mortar. Nevertheless, the ability of sodium alginate to absorb moisture from the environment could help to retain water for internal curing.

Effect of Sodium Alginate on the Healing Performance in Bio-Mortar

When comparing the vegetative cells and spores group, in the same EC LWA carrier, with or without coating, the healing performance provided by vegetative cells was better (**Figure 8.7**). However, without any protection, the healing ability of the EC V sample dropped when cracks were fabricated in 90 days instead of 28 days old mortar (Chapter 6). Thus, in the vegetative cells sample, the effect of extra protection provided by sodium alginate coating might be obtained when cracks were fabricated at the age of 90 days.

In the FA 6M LWA sample group, despite of the expected positive effect of the bacteria and sodium alginate coating, the reference sample gave a superior healing performance (**Figure 8.8**). The sodium alginate coating had no effect when cells were used as healing agent. At the same time, an increase of healing performance was observed when spores were employed as healing agent.

In comparison to several other types of coating applied on LWA impregnated with spores, the healing performance provided by sodium alginate coating in this research was lower. As comparison, spores of *B. cohnii* encapsulated into expanded perlite and coated with metakaolin-based geopolymer could completely heal cracks with the width of 0.79 mm after being immersed in water for 28 days (Zhang et al., 2017). In another report that entrapped spores of *B. cereus* into alginate gel followed by coating with cement-based material, in the crack width range of 0.15-0.55 mm, a healing ratio of 35 % was obtained after subjecting the samples to wet-dry cycle curing in water for 21 days (Wu et al., 2020). The healing performance obtained by EC Sal and FA Sal where alginate was used as coating is better compared to when the alginate was used as the capsule core (Wu et al., 2020).

Regarding the sealing efficiency, although a better performance was observed when sodium alginate was used to coat bacteria encapsulated into EC LWA, this performance seems to be lower in comparison to the reference sample. Without addition of bacteria or sodium alginate coating, a stand-alone LWA provided almost 100% sealing efficiency. Indeed this result is not as expected, but it opens a perspective to investigate more in depth the use of LWA as a healing agent for young concrete.

In conclusion, the sodium alginate coating did not deliver a great improvement in the healing performance of resulting mortar for all tested LWA and all healing agents. A clearer impact of sodium alginate coating could be seen when cracks were fabricated at the age of 90 days. At that age, the advancing hydration provoked by LWA would be almost complete, thus the chance that the reference sample has better healing performance than the bacteria mortar would be lower.

8.5 Conclusions

Based on the results described in this chapter, the following conclusions could be drawn:

1. Spores from *B. Sphaericus* cultivated in yeast extract medium 2 g/l could fully germinate into the vegetative cells in 72 hours.

2. When spores were encapsulated into FA 6M LWA, the high initial pH in FA 6M LWA tended to inhibit the germination process, leading to limited urea decomposition in this sample. At the same time, no issues for spores germination arose when spores were encapsulated into EC LWA.
3. For all LWA carriers and all healing agent types, applying sodium alginate tended to slow down the urea decomposition rate.
4. The sodium alginate coating on LWA tended to decrease the compressive strength of the resulting mortar. More severe strength reduction was observed in the EC LWA sample group than in the EC LWA group.
5. In EC LWA carrier, sodium alginate coating tended to decrease the healing performance in all types of healing agent. In FA LWA, sodium alginate coating slightly improved the healing performance in the spores group, but no improvement was observed in the vegetative cells group.
6. The sodium alginate coating slightly improved the sealing efficiency only in the EC LWA sample group. However, the sealing efficiency results have high variability, making it difficult to draw a clear conclusion.
7. The sealing efficiency for all LWA carriers was not well correlated with their crack healing performance.

Chapter 9. General Conclusions and Future Perspectives

This page is intentionally blank

9.1 Revisiting the Research Needs

As stated in **Chapter 1**, self-healing concrete aims to prolong the service life of the concrete by avoiding external repairing when cracks occur. One promising healing technique is by leveraging the ability of alkali-resistant microorganisms to induce calcium carbonate precipitation (MICP) that could close micro-cracks in concrete. While several types of bacteria are resistant to high alkalinity, the initial pH of fresh concrete, which is around 13, would be too high for them to remain active. Furthermore, the concrete pores becoming smaller during the hydration process and the high shear forces during concrete mixing, pose additional challenges. Various attempts were completed to immobilize the bacteria to survive inside the concrete matrix. Spores from various alkali-resistant bacterial strains such as *B. sphaericus, B. cereus, B. alkalinitrilicus, and S. pasteurii* have been encapsulated into different carriers such as a hydrogels, microcapsules, macrocapsules, and porous aggregates. The porous aggregates are considered an interesting carrier, as they are more affordable yet still deliver satisfactory healing performance. However, the commercially-available lightweight aggregates needs a high sintering temperature during production. Thus, the need arises for a more eco-friendly porous aggregate as a bacterial carrier. Alkali activated lightweight aggregate (LWA) generated from waste material becomes one of the promising candidates as a bacteria carrier. Beneficiating waste material into valuable construction material such as LWA could also contribute to the sustainability of construction materials. This artificial LWA was reported to have high porosity and does not require high energy in its production.

9.2 Research Outcomes

9.2.1 Feasibility of utilizing alkali activated LWA in the construction industry as aggregate replacement

In this thesis three kinds of waste material which are rich in silica and alumina named fly ash, Sidoarjo volcanic mud and municipal solid waste incinerator bottom ash (MSWI BA) were used as raw material in LWA production. However, only fly ash was used as binder in LWA production to carry out an initial optimization regarding NaOH concentration to produce LWA. In **Chapter 2** the effect of NaOH concentration on mechanical and physical properties of fly ash-based alkali activated LWA was investigated. Three NaOH concentrations of 4, 6, and 8 molars were mixed with sodium silicate to produce the LWA. The ratio between sodium silicate and sodium hydroxide was 1.5, while the ratio between liquid/solid was 0.25.

Based on the results, in general, it can be concluded that increasing the NaOH concentration slightly increased the mass density of LWA while the water absorption slightly reduced. Increasing the NaOH concentration up to 6 molars also proved to significantly decrease the number of macropores and the total porosity of the resulting LWA measured by mercury intrusion penetration (MIP). The pore size of all LWA produced was in the range that the bacteria could penetrate (6-15 μm).

In mortar production, 16 % volume of fine aggregate was replaced with fly-ash based LWA. The results show that mortar containing fly ash-based LWA activated with 6 molar NaOH solution (FA 6M LWA) had a 28-day compressive strength of 55 MPa. This strength was nearly the same compressive strength of mortar containing commercial explanded clay (EC LWA) (58 MPa). Based on the result, it could be concluded that the minimum NaOH concentration to produce fly ash-based LWA with good properties is 6 molars.

In **Chapter 3** the properties of alkali activated lightweight aggregate generated from fly ash, Lusi, and MSWI BA, activated with NaOH 6M and sodium silicate was further investigated. Based on the results, Lusi 6M LWA had the highest water absorption, followed by MSWI BA and FA 6M LWA. Based on the pore characterization, the larger threshold pore size of Lusi and FA 6M LWA is 6 μm, while MSWI BA 6M LWA had a threshold pore size of 18 μm. According to the IUPAC classification, almost all the pores in MSWI BA 6M LWA were macropores, while in Lusi and FA 6M LWA, the amount of micropores was around 70 % of the total pore volume. FA 6M LWA had the highest amorphous phase content, that corresponds to more reacted product based on the mineralogy. Moreover, through SEM EDX point analysis, the most gel products in all LWAs were N-(C)-A-S-H. A limited amount of C-A-S-H gel was observed in FA 6M LWA. In the end *B. sphaericus* cells were encapsulated into EC, FA 6M and MSWI BA LWA to check the compatibility of those LWA as bacteria carrier. Based on the urea decomposition results, cells were able to actively decompose urea in the solution after encapsulation into EC, FA 6M and Lusi 6M LWA. On the other hand the metallic alumunium in MSWI BA seems to be toxic to the bacteria, as only limited amount of urea could be decomposed by bacteria after encapsulation into MSWI BA carrier.

Based on the characterization of LWA, so far, FA 6M LWA delivered the most satisfying properties. Moreover, the good properties of FA 6M LWA also delivered good properties to its resulting mortar. A comparable strength was obtained when 30% of fine aggregate in the mortar was replaced by FA 6M LWA or with EC LWA. In contrast, mortar containing MSWI BA 6M LWA suffered from expansion, leading to a significant decrease in strength. No expansion was observed in a mortar containing Lusi 6M LWA, but with LWA replacing rate of 30%, the 28 days mortar compressive strength of this sample was only around 30 MPa.

In conclusion, based on the LWA characterization and the properties of their resulting mortar, FA 6M and Lusi 6M LWA could be suitable candidates for bacteria carriers. Further pretreatment on the MSWI BA needs to be conducted to overcome the expansion when the resulting LWA would be applied in mortar.

The effect of applying alkali activated LWA on the durability of mortar has become a concern as this material is quite porous and permeable for gas such as CO_2 and water. As the main goal of self-healing technology is to avoid cracks that could reduce the durability of concrete, it would be ideal if the bacteria carrier candidate also contributes to making concrete more durable. Therefore in **Chapter 4,** the durability aspects of mortar containing alkali activated fly ash, such as the resistance against carbonation, chloride migration, and the capillary water uptake, were investigated. By replacing 16 % of fine aggregate with FA 6M LWA in mortar production, a comparable chloride migration coefficient and capillary water uptake in the mortar were observed as for mortar containing EC LWA and for a reference mortar without LWA. Furthermore, the carbonation resistance of mortar containing FA 6M LWA was comparable to mortar containing EC LWA. A denser ITZ was observed in both EC LWA and FA 6M LWA samples. Overall, introducing a limited amount of alkali activated fly ash LWA did not significantly decrease the durability of the resulting mortar compared to the reference sample.

9.2.2 Feasibility of utilizing alkali activated LWA as vegetative cells and spores carriers in self-healing concrete production

Yeast extract, a nutrient that is required for bacterial spores germination, is reported to have a negative impact on the properties of concrete. When spores were used as a healing agent, there is a need to find a minimal yeast extract concentration that minimizes the impact on the properties of self-healing concrete but enough for spores to germinate. Thus in **Chapter 5,** three variations of yeast extract concentration of 0, 2, and 5 g/l were applied. Urea and calcium nitrate were also added to the mixture to support the urea hydrolysis process. Based on the results, when yeast extract is mandatory in the concrete mixture, the recommended yeast extract concentration was 2 g/l. With this composition, the compressive strength was decreased by about 16 %, compared to the reference sample. This decrease in strength is lower than for a sample with a yeast extract concentration of 5 g/l which featured almost 50% strength loss. The number of macropores was also similar to the reference sample. At the same time, if the yeast extract concentration increased to 5 g/l, a significant increase in macropores compared to the reference sample was observed. The workability of a sample with 2 g/l yeast extract concentration was also comparable with the reference sample without yeast. Moreover, in previous studies, a yeast extract concentration of 2 g/l was sufficient for spores from *B. sphaericus* to germinate in 3 days (Wang et al., 2017).

However, in the condition where yeast extract is not mandatory, such as when vegetative cells were employed as healing agents, omitting yeast extract from the mixture could be an alternative option. A decrease in flow value was observed due to the addition of calcium that acted as an accelerator, but no issue in casting was experienced. Therefore, in this case, the low flow value of the fresh mortar did not cause a decrease in bulk density that would result in strength reduction.

In **Chapter 6**, vegetative cells of *B. sphaericus* were encapsulated into alkali activated LWA generated from Lusi and FA. These two LWA delivered acceptable properties when applied in the resulting mortar with an aggregate replacing rate of up to 30%. In this research, the aggregate replacing rate of 30% was applied to introduce as many cells as possible into the mortar matrix. A vacuum and pressure treatment to introduce the cells into the LWA was applied since in a previous study this method was proved to efficiently encapsulate cells into a porous aggregate (Ersan et al., 2015). The only bio-agents used were urea and calcium nitrate. Yeast extract was omitted from the mixture as cells were used as a healing agent.

Based on the total ammonium measurement test on alkali activated LWA with encapsulated cells , the ability of the cells to decompose urea decreased compared to cells encapsulated into EC LWA. The high initial pH of alkali activated LWA seemed to slightly inhibit the activity of the cells inside. The leakage of bacteria after encapsulation into LWA was also still high. In Lusi 6M LWA samples, a leakage of more than 30% was observed. Even though the alkali activated LWA had comparable water absorption to EC LWA, it had smaller pore sizes that might not be large enough for bacteria to penetrate.

The addition of vegetative cells and nutrients did not negatively affect the properties of the resulting mortar. Based on crack closure observations and sealing efficiency results, the cracking age greatly affected the resulting mortar's healing ability. When cracks were created at the age of 28 days, the LWA acted as internal curing agent that induced advanced hydration. This behaviour healed the cracks smaller than 0.3 mm in the reference sample containing LWA. In FA 6M LWA reference sample, almost all the cracks with widths between 0.3-0.4 were also healed after being subjected to wet-dry cycle curing for 30 days. The effect of the encapsulation procedure could therefore not be observed when cracks were fabricated at the age of 28 days.

In the sample containing vegetative cells with an initial crack width range of 0.3-0.4 mm, an average healing ratio of 52% and 45% was obtained when FA 6M LWA and Lusi 6M LWA were used as carriers, respectively. As a comparison, when cells were encapsulated into EC LWA, with the same initial crack width range an average healing ratio of 87% was obtained. The maximum crack width that could be healed in EC LWA NBE sample was 0.49 mm while it was 0.3 mm in FA 6M LWA NBE. In Lusi samples, none of the cracks could be healed completely. The high bacteria leakage after encapsulation into alkali activated LWA probably contributed to the decreased healing performance of the resulting mortar.

The results for sealing efficiency (reduction of water permeability) for samples cracked at the age of 28 days were not reliable, as almost all the cracks in the range of 0.3-0.4 mm were healed, especially in the Lusi 6M LWA group. The blocking of the hole by material breaking away from the crack walls combined with ongoing hydration can cause this problem.

In a sample where the cracks were fabricated at the age of 90 days, less healing was observed, but the difference in healing ratio between the different sample series was more clear. For almost all LWA groups, in the reference sample with crack width range of 0.3-0.4 mm, the healing ratio obtained after the samples were subjected to a wet-dry cycle for 30 days was only around 20-30%.

At the same time, the effect of the encapsulation procedure could be seen when crack closure on the sides of the sample was observed. In the crack width range of 0.3-0.4 mm, some complete healing was observed in the samples with encapsulation procedure (NBE), while less healing was observed in the samples without encapsulation procedure (NB). Due to the gravitation, the calcium carbonate will fill the bottom part of the crack first and gradually reach the top of the sample. When cracks were fabricated at the age of 90 days, it is likely that fewer cells survived. Thus the amount of the precipitation was not enough to pile up to the top of the sample. Thus, a clear difference in the NBE samples' healing ratio could not be obtained, since cracks were only monitored on the top side of the sample. Overall, when cracks were fabricated at the age of 90 days, in the crack width range of 0.3-0.4 mm, the average healing ratio of FA 6M LWA NBE was slightly better than EC LWA NBE. The average healing ratio in FA 6M LWA NBE was 54 % while it was 47% in EC LWA NBE samples.

The sealing efficiency results for samples cracked at the age of 90 days was more reliable than at 28 days. Samples with the encapsulation procedure in EC and FA 6M LWA achieved almost 100 % sealing efficiency even though their healing ratio was only around 50%. It seems that the calcium carbonate precipitation blocked the connection between the hole where water should flow through and the crack but was not sufficient to close the crack mouth.

In conclusion, FA 6M LWA could be employed as a vegetative cells carrier as it provides similar healing performance with EC LWA carrier. The high pH of Lusi 6M LWA due to the high amount of alkali activator required during its production made this LWA unsuitable as a bacteria carrier, and only limited healing could be found when it was used. Further improvement, such as finding a suitable coating to mitigate the high leakage of cells from the FA 6M LWA carrier, could be strived for in order to obtain a better healing performance.

Due to the need to mitigate the bacteria leakage from pores of the LWA, an attempt to coat the LWA with encapsulated cells was performed. In **chapter 7** three coating agents named sodium silicate, sodium alginate, and polyvinyl alcohol were applied on LWA with encapsulated cells. Based on the ureolytic activity observation, the vegetative cells of *B. sphaericus* encapsulated into EC and FA 6M LWA only survived when a sodium alginate coating was applied. The sodium alginate coating tends to slow down the urea decomposition rate, but does not kill the cells inside. The high pH of sodium silicate and the alcohol content in Polyvinyl Alcohol (PVA) damaged the cells inside the LWA. By applying sodium alginate coating, the leakage of bacteria after encapsulation was decreased. Without the coating application, the bacteria leakage could reach 31%, while after the coating application, the bacteria leakage was not more than 7%.

In **Chapter 8** the sodium alginate coating was applied on FA 6M and EC LWA with encapsulated cells and spores. Regarding the germination process of spores after encapsulation into LWA, the high initial pH in FA 6M LWA tends to inhibit the germination process, leading to limited urea decomposition in this sample, while no issues occurred regarding spores germination when spores were encapsulated into EC LWA. In all LWA carriers, applying the sodium alginate coating tends to slow down the urea decomposition rate. The alginate coating might block the access of bacteria to the nutrients.

Applying sodium alginate coating also tended to decrease the compressive strength of resulting mortar. When vegetative cells were used as healing agent, with an applied sodium alginate coating, the compressive strength of the resulting mortar decreased in the range of 25-33% relative to the reference sample. More severe strength decreasing was observed when spores were used as healing agent.

In the FA 6M LWA sample group, the sodium alginate coating only slightly improved the healing capability when spores were employed as a healing agent, while there was no significant improvement due to the sodium alginate application in the vegetative cells sample group. In contrast, in EC LWA carriers, sodium alginate coating both in the case of cells and spores tended to decrease the healing capability of the resulting mortar.

Regarding sealing efficiency, sodium alginate coating tends to improve the sealing efficiency of mortar in the EC LWA group sample. While no positive impact on sealing efficiency was observed when a sodium alginate coating was applied in the FA 6M LWA sample group. However, high variability in the sealing efficiency results was observed. Thus it is not easy to draw a conclusion from the obtained data.

9.3 Challenges and Future Perspectives

The possibility of utilizing alkali activated lightweight aggregate as bacterial carrier was examined in detail in this research. Even though the healing performance delivered by fly ash-based alkali activated LWA is not as good as for the commercial expanded clay carrier, this pilot research paves the way for further exploration. In the future, several improvements could be made to make alkali activated LWA become a suitable carrier for bacteria in self-healing concrete production.

Chapter 3 of this thesis investigates the properties of alkali activated LWA generated from fly ash, Lusi, and MSWI bottom ash with their resulting mortars. An expansion issue in the mortar containing MSWI bottom ash arose when the aggregate replacing rate was increased to 30%. Increasing the aggregate replacement rate is an important point, as it is a way to increase the amount of bacteria encapsulated into the LWA and increase the resulting mortar's healing performance. Thus, a pretreatment to mitigate the expansion of the MSWI bottom ash powder has to be performed to then further investigate its fitness for use as a bacteria carrier. A life cycle assessment on the production of alkali activated LWA should be performed to see the impact of using this novel LWA on the environment over an extended period of time.

In chapter 6, during the viability tests of cells after being encapsulated in fly ash and Lusi-based alkali activated LWA, it was found that the pH of alkali activated LWA in urea solution tends to inhibit cells' ability inside LWA to decompose urea. When that alkali activated LWA was incorporated into the mortar, the healing performance provided by the bacteria inside the LWA was also not as excellent as bacteria encapsulated in expanded clay LWA. Exposing alkali activated LWA to CO_2 before bacteria encapsulation could become an option to decrease the pH of alkali activated LWA as the remaining sodium and calcium at the surface of LWA could react with CO_2 and form sodium and calcium carbonate.

References

Achal, V. & Pan, X. (2014). Influence of calcium sources on microbially induced calcium carbonate precipitation by Bacillus sp. CR2. *Applied Biochemistry and Biotechnology*, *173*(1), 307–317.

ACI. (2001). Control of Cracking in Concrete Structures Reported by ACI Committee 224. ACI 224R-01. *ACI Committee 224R-01*, 1–46.

AL-Ameeri, A. S., Rafiq, M. I. & Tsioulou, O. (2021). Combined impact of carbonation and crack width on the Chloride Penetration and Corrosion Resistance of Concrete Structures. *Cement and Concrete Composites*, *115*(August 2020), 103819.

Alam, Q., Schollbach, K., Rijnders, M., van Hoek, C., van der Laan, S. & Brouwers, H. J. H. (2019). The immobilization of potentially toxic elements due to incineration and weathering of bottom ash fines. *Journal of Hazardous Materials*, *379*(December 2018), 120798.

Alazhari, M., Sharma, T., Heath, A., Cooper, R. & Paine, K. (2018). Application of expanded perlite encapsulated bacteria and growth media for self-healing concrete. *Construction and Building Materials*, *160*, 610–619.

Alderete, N. M., Villagrán Zaccardi, Y. A. & De Belie, N. (2019). Physical evidence of swelling as the cause of anomalous capillary water uptake by cementitious materials. *Cement and Concrete Research*, *120*(April), 256–266.

Alexandre Bogas, J., Gomes, M. G. & Real, S. (2015). Capillary absorption of structural lightweight aggregate concrete. *Materials and Structures/Materiaux et Constructions*, *48*(9), 2869–2883.

Alghamri, R. & Kanellopoulos, A. (2016). Impregnation and encapsulation of lightweight aggregates for self-healing concrete, *124*, 910–921.

Amer Algaifi, H., Abu Bakar, S., Rahman Mohd. Sam, A., Ismail, M., Razin Zainal Abidin, A., Shahir, S. & Ali Hamood Altowayti, W. (2020). Insight into the role of microbial calcium carbonate and the factors involved in self-healing concrete. *Construction and Building Materials*, *254*, 119258.

Anglani, G., Van Mullem, T., Zhu, X., Wang, J., Antonaci, P., De Belie, N., Tulliani, J. M. & Van Tittelboom, K. (2020). Sealing efficiency of cement-based materials containing extruded cementitious capsules.

Construction and Building Materials, *251*, 119039.

Balapour, M., Zhao, W., Garboczi, E. J., Oo, N. Y., Spatari, S., Hsuan, Y. G., Billen, P. & Farnam, Y. (2020). Potential use of lightweight aggregate (LWA) produced from bottom coal ash for internal curing of concrete systems. *Cement and Concrete Composites*, *105*(October 2019), 103428.

Basaran Bundur, Z., Kirisits, M. J. & Ferron, R. D. (2015). Biomineralized cement-based materials: Impact of inoculating vegetative bacterial cells on hydration and strength. *Cement and Concrete Research*, *67*, 237–245.

Bayati, M. & Saadabadi, L. A. (2021). Efficiency of bacteria based self-healing method in alkali-activated slag (AAS) mortars. *Journal of Building Engineering*, *42*(March).

Bentz, D. P. (2009). Cement & Concrete Composites Influence of internal curing using lightweight aggregates on interfacial transition zone percolation and chloride ingress in mortars. *Cement and Concrete Composites*, *31*(5), 285–289.

Bernal, S. A., Provis, J. L., Walkley, B., San Nicolas, R., Gehman, J. D., Brice, D. G., Kilcullen, A. R., Duxson, P. & Van Deventer, J. S. J. (2013). Gel nanostructure in alkali-activated binders based on slag and fly ash, and effects of accelerated carbonation. *Cement and Concrete Research*, *53*, 127–144.

Bhagath Singh, G. V. P. & Subramaniam, K. V. L. (2016). Quantitative XRD study of amorphous phase in alkali activated low calcium siliceous fly ash. *Construction and Building Materials*, *124*, 139–147.

Bogas, J. A., Carriço, A. & Pontes, J. (2019). Influence of cracking on the capillary absorption and carbonation of structural lightweight aggregate concrete. *Cement and Concrete Composites*, *104*(July), 103382.

Bolobova, A. V & Kondrashchenko, V. I. (2000). Use of Yeast Fermentation Waste as a Biomodifier of Concrete (Review), *36*(3), 205–214.

Bullard, J. W., Jennings, H. M., Livingston, R. A., Nonat, A., Scherer, G. W., Schweitzer, J. S., Scrivener, K. L. & Thomas, J. J. (2011). Mechanisms of cement hydration. *Cement and Concrete Research*, *41*(12), 1208–1223.

Bundur, Zeynep Basaran, Kirisits, M. J. & Ferron, R. D. (2015). Cement and

Concrete Research Biomineralized cement-based materials : Impact of inoculating vegetative bacterial cells on hydration and strength. *Cement and Concrete Research*, *67*, 237–245.

Bundur, Zeynep Başaran, Kirisits, M. J. & Ferron, R. D. (2017). Use of pre-wetted lightweight fine expanded shale aggregates as internal nutrient reservoirs for microorganisms in bio-mineralized mortar. *Cement and Concrete Composites*, *84*, 167–174.

Caprai, V., Schollbach, K. & Brouwers, H. J. H. (2018). Influence of hydrothermal treatment on the mechanical and environmental performances of mortars including MSWI bottom ash. *Waste Management*, *78*, 639–648.

Casanova, S., Silva, R. V., de Brito, J. & Pereira, M. F. C. (2021). Mortars with alkali-activated municipal solid waste incinerator bottom ash and fine recycled aggregates. *Journal of Cleaner Production*, *289*, 125707.

Cembureau. (2017). *Activity Report 2017*.

Cembureau. (2020). *Activity Report 2019*. *CEMBUREAU Committee* (Vol. 76).

Chemistry, S. (2001). international union of pure and applied chemistry division of physical chemistry manual of symbols and terminology for physicochemical quantities and units appendix ii.

Chen, Z., Li, J. S., Zhan, B. J., Sharma, U. & Poon, C. S. (2018). Compressive strength and microstructural properties of dry-mixed geopolymer pastes synthesized from GGBS and sewage sludge ash. *Construction and Building Materials*, *182*, 597–607.

Cheng, H., Lin, K., Cui, R., Hwang, C., Cheng, T. & Chang, Y. (2015). Effect of solid-to-liquid ratios on the properties of waste catalyst – metakaolin based geopolymers. *Construction and Building Materials*, *88*, 74–83.

Chindaprasirt, P., Jaturapitakkul, C., Chalee, W. & Rattanasak, U. (2009). Comparative study on the characteristics of fly ash and bottom ash geopolymers. *Waste Management*, *29*(2), 539–543.

Chithiraputhiran, S. & Neithalath, N. (2013). Isothermal reaction kinetics and temperature dependence of alkali activation of slag , fly ash and their blends. *Construction and Building Materials*, *45*, 233–242.

Colangelo, F., Messina, F. & Cioffi, R. (2015). Recycling of MSWI fly ash by means of cementitious double step cold bonding pelletization: Technological assessment for the production of lightweight artificial aggregates. *Journal of Hazardous Materials*, *299*, 181–191.

Cook, R. A. & Hover, K. C. (1999). Mercury porosimetry of hardened cement pastes. *Cement and Concrete Research*, *29*(6), 933–943.

De Belie, N., Gruyaert, E., Al-Tabbaa, A., Antonaci, P., Baera, C., Bajare, D., Darquennes, A., Davies, R., Ferrara, L., Jefferson, T., Litina, C., Miljevic, B., Otlewska, A., Ranogajec, J., Roig-Flores, M., Paine, K., Lukowski, P., … Jonkers, H. M. (2018). A Review of Self-Healing Concrete for Damage Management of Structures. *Advanced Materials Interfaces*, *5*(17), 1–28.

De Muynck, W., Cox, K., Belie, N. De & Verstraete, W. (2008). Bacterial carbonate precipitation as an alternative surface treatment for concrete. *Construction and Building Materials*, *22*(5), 875–885.

De Muynck, W., Verbeken, K., De Belie, N. & Verstraete, W. (2010). Influence of urea and calcium dosage on the effectiveness of bacterially induced carbonate precipitation on limestone. *Ecological Engineering*, *36*(2), 99–111.

Deguchi, H. A. Æ. T. (2009). Subsidence and uplift of Sidoarjo (East Java) due to the eruption of the Lusi mud volcano (2006 – present), 845–846.

Ekaputri, J. J. (2015). Lightweight Geopolymer Binder Base on Sidoarjo Mud, (April).

Erris, F. G. F., Hoenix, V. P., Ujita, Y. F. & Mith, R. W. S. (2003). Kinetics of calcite precipitation induced by ureolytic bacteria at 10 to 20 ° C in artificial groundwater, *67*(8).

Ersan, Y., Bravo, F., Silva, D., Boon, N., Verstraete, W. & Belie, N. De. (2015). Screening of bacteria and concrete compatible protection materials, *88*, 196–203.

Ersan, Y., Gruyaert, E., Louis, G., Lors, C., De Belie, N. & Boon, N. (2015). Self-protected nitrate reducing culture for intrinsic repair of concrete cracks. *Frontiers in Microbiology*, *6*(NOV).

Erşan, Yusuf Çağatay. (2016). *Microbial nitrate reduction induced autonomous self-healing in concrete.*

Erşan, Yusuf Çağatay, Hernandez-Sanabria, E., Boon, N. & De Belie, N.

(2016). Enhanced crack closure performance of microbial mortar through nitrate reduction. *Cement and Concrete Composites*, *70*, 159–170.

Eva, T. Ĥ. (2016). Effect of firing temperature on the structure of the aggregate from sintered ashes, *151*, 345–351.

Feng, J., Chen, B., Sun, W. & Wang, Y. (2021). Microbial induced calcium carbonate precipitation study using Bacillus subtilis with application to self-healing concrete preparation and characterization. *Construction and Building Materials*, *280*, 122460.

Freedonia. (2012). World Construction Aggregates - Industry Study with Forecasts for 2015 & 2020. *The Freedonia Group*, 6.

Fujita, Y., Grant Ferris, F., Daniel Lawson, R., Colwell, F. S. & Smith, R. W. (2000). Calcium carbonate precipitation by ureolytic subsurface bacteria. *Geomicrobiology Journal*, *17*(4), 305–318.

Geetha, S. & Ramamurthy, K. (2013). Properties of geopolymerised low-calcium bottom ash aggregate cured at ambient temperature. *Cement and Concrete Composites*, *43*, 20–30.

Gesoğlu, M., Güneyisi, E., Alzeebaree, R. & Mermerdaş, K. (2013). Effect of silica fume and steel fiber on the mechanical properties of the concretes produced with cold bonded fly ash aggregates. *Construction and Building Materials*, *40*, 982–990.

Gesoğlu, M., Özturan, T. & Güneyisi, E. (2007). Effects of fly ash properties on characteristics of cold-bonded fly ash lightweight aggregates. *Construction and Building Materials*, *21*(9), 1869–1878.

Gomathi, P. & Sivakumar, A. (2015). Accelerated curing effects on the mechanical performance of cold bonded and sintered fly ash aggregate concrete. *Construction and Building Materials*, *77*, 276–287.

González-corrochano, B., Alonso-azcárate, J., Rodríguez, L., Pérez, A., Fernández, M., José, J., Ramos, T., Dolores, M. & Muro, C. (2016). Valorization of washing aggregate sludge and sewage sludge for lightweight aggregates production, *116*, 252–262.

Görhan, G. & Kürklü, G. (2014a). The influence of the NaOH solution on the properties of the fly ash-based geopolymer mortar cured at different temperatures. *Composites Part B: Engineering*, *58*, 371–377.

Görhan, G. & Kürklü, G. (2014b). The influence of the NaOH solution on the properties of the fly ash-based geopolymer mortar cured at different temperatures. *Composites Part B: Engineering*, *58*, 371–377.

Gruyaert, E., Debbaut, B., Snoeck, D., Díaz, P., Arizo, A., Tziviloglou, E., Schlangen, E. & De Belie, N. (2016). Self-healing mortar with pH-sensitive superabsorbent polymers: Testing of the sealing efficiency by water flow tests. *Smart Materials and Structures*, *25*(8).

Gu, A. (2000). Utilization of fly ash by pelletization process ; theory , application areas and research results, *30*, 59–77.

Güneyisi, E., Gesoğlu, M., Pürsünlü, Ö. & Mermerdaş, K. (2013). Durability aspect of concretes composed of cold bonded and sintered fly ash lightweight aggregates. *Composites Part B: Engineering*, *53*, 258–266.

Hamidi, R. M., Man, Z. & Azizli, K. A. (2016). Concentration of NaOH and the Effect on the Properties of Fly Ash Based Geopolymer. *Procedia Engineering*, *148*, 189–193.

Hamilton, W. A. (2003). Microbially Influenced Corrosion as a Model System for the Study of Metal Microbe Interactions: A Unifying Electron Transfer Hypothesis. *Biofouling*, *19*(1), 65–76.

Hardjito, D. (2005). Studies on Fly Ash-Based Geopolymer Concrete. *Curtin University of Technology*, (November), 94.

Hardjito, D., Wibowo, G. M. & Christianto, D. (2012). Pozzolanic Activity Assessment of LUSI (LUmpur SIdoarjo) Mud in Semi High Volume Pozzolanic Mortar, *L*, 1654–1660.

Heah, C. Y., Kamarudin, H., Mustafa Al Bakri, A. M., Bnhussain, M., Luqman, M., Khairul Nizar, I., Ruzaidi, C. M. & Liew, Y. M. (2012). Study on solids-to-liquid and alkaline activator ratios on kaolin-based geopolymers. *Construction and Building Materials*, *35*, 912–922.

Heidrich, C., Feuerborn, H. & Weir, A. (2013). Coal Combustion Products : a global perspective. *World of Coal Ash Conference*, 17.

Huang, G., Ji, Y., Li, J., Zhang, L., Liu, X. & Liu, B. (2019). Effect of activated silica on polymerization mechanism and strength development of MSWI bottom ash alkali-activated mortars. *Construction and Building Materials*, *201*, 90–99.

Illikainen, Y. P. F. T. (2017). Development and incorporation of lightweight waste-based geopolymer aggregates in mortar and concrete. *Construction and Building Materials*, *131*, 784–792.

Intarasoontron, J., Pungrasmi, W., Nuaklong, P. & Jongvivatsakul, P. (2021). Comparing performances of MICP bacterial vegetative cell and microencapsulated bacterial spore methods on concrete crack healing. *Construction and Building Materials*, *302*(December 2020), 124227.

International Concrete Repair Institute. (2006). Vision 2020 : A Vision for the Concrete Repair Protection and Strengthening Industry, 1–29.

Ismail, I., Bernal, S. A., Provis, J. L., San Nicolas, R., Hamdan, S. & Van Deventer, J. S. J. (2014). Modification of phase evolution in alkali-activated blast furnace slag by the incorporation of fly ash. *Cement and Concrete Composites*, *45*, 125–135.

IUPAC Commission on Colloid and Surface Chemistry. (1990). *manual of symbols and terminology for physicochemical quantities and units appendix ii De nitions, Terminology and Symbols in Colloid and Surface Chemistry part i Adopted*. *Pure and Applied Chemistry* (Vol. 62).

Jadhav, U. U., Lahoti, M., Chen, Z., Qiu, J., Cao, B. & Yang, E. H. (2018). Viability of bacterial spores and crack healing in bacteria-containing geopolymer. *Construction and Building Materials*, *169*, 716–723.

Jakubovskis, R., Jankutė, A., Guobužaitė, S., Boris, R. & Urbonavičius, J. (2021). Prolonging bacterial viability in biological concrete: Coated expanded clay particles. *Materials*, *14*(11), 1–11.

Jonkers, H. M. & Schlangen, E. (2007). Crack Repair By Concrete-Immobilized Bacteria. *Civil Engineering*, (April), 1–7.

Jonkers, H. M. & Schlangen, E. (2009). A two component bacteria-based self-healing concrete. *Concrete Repair, Rehabilitation and Retrofitting II - Proceedings of the 2nd International Conference on Concrete Repair, Rehabilitation and Retrofitting, ICCRRR*, 119–120.

Joseph, A. M., Snellings, R., Heede, P. Van Den & Matthys, S. (2018). The Use of Municipal Solid Waste Incineration Ash in Various Building Materials : A Belgian Point of View.

Joshi, S., Goyal, S. & Reddy, M. S. (2018). Influence of nutrient components of media on structural properties of concrete during biocementation. *Construction and Building Materials*, *158*, 601–613.

Kang, S., Jeong, Y., Ook, M. & Moon, J. (2019). Pozzolanic reaction on alkali-activated Class F fly ash for ambient condition curable structural materials. *Construction and Building Materials*, *218*, 235–244.

Kapeluszna, E., Kotwica, Ł., Różycka, A. & Gołek, Ł. (2017). Incorporation of Al in C-A-S-H gels with various Ca/Si and Al/Si ratio: Microstructural and structural characteristics with DTA/TG, XRD, FTIR and TEM analysis. *Construction and Building Materials*, *155*, 643–653.

Kipkemboi, B., Zhao, T., Miyazawa, S., Sakai, E., Nito, N. & Hirao, H. (2020). Effect of C3S content of clinker on properties of fly ash cement concrete. *Construction and Building Materials*, *240*, 117840.

Klemczak, B. & Knoppik-Wróbel, A. (2011). Early age thermal and shrinkage cracks in concrete structures - description of the problem. *Architecture Civil Engineering Environment*, *4*(2), 35–48.

Kockal, N. U. & Ozturan, T. (2011). Characteristics of lightweight fly ash aggregates produced with different binders and heat treatments. *Cement and Concrete Composites*, *33*(1), 61–67.

Kong, L., Hou, L. & Du, Y. (2014). Chemical reactivity of lightweight aggregate in cement paste, *64*, 22–27.

Korat, L., Ducman, V., Legat, A. & Mirtic, B. (2013). Characterisation of the pore-forming process in lightweight aggregate based on silica sludge by means of X-ray micro-tomography (micro-CT) and mercury intrusion porosimetry (MIP), *39*, 6997–7005.

Korat, L., Ducman, V., Legat, A. & Mirtič, B. (2013). Characterisation of the pore-forming process in lightweight aggregate based on silica sludge by means of X-ray micro-tomography (micro-CT) and mercury intrusion porosimetry (MIP). *Ceramics International*.

Kou, S. & Poon, C. (2010). Cement & Concrete Composites Properties of concrete prepared with PVA-impregnated recycled concrete aggregates. *Cement and Concrete Composites*, *32*(8), 649–654.

Kourti, I. & Cheeseman, C. R. (2010). Properties and microstructure of lightweight aggregate produced from lignite coal fly ash and recycled glass. *Resources, Conservation and Recycling*, *54*(11), 769–775.

Kua, H. W., Gupta, S., Aday, A. N. & Srubar, W. V. (2019). Biochar-immobilized bacteria and superabsorbent polymers enable self-healing of fiber-reinforced concrete after multiple damage cycles. *Cement and Concrete Composites*, *100*(February), 35–52.

Lee, N. K. & Lee, H. K. (2015). Reactivity and reaction products of alkali-activated, fly ash/slag paste. *Construction and Building Materials, 81,* 303–312.

Li, W., Liu, L., Chen, W., Yu, L., Li, W. & Yu, H. (2010). Calcium carbonate precipitation and crystal morphology induced by microbial carbonic anhydrase and other biological factors. *Process Biochemistry*, *45*(6), 1017–1021.

Litina, C. & Al-Tabbaa, A. (2020). First generation microcapsule-based self-healing cementitious construction repair materials. *Construction and Building Materials*, *255*(2020), 119389.

Liu, C., Yang, L., Wang, F. & Hu, S. (2020). Enhance the durability of heat-cured mortars by internal curing and pozzolanic activity of lightweight fine aggregates. *Construction and Building Materials*, (xxxx), 121439.

Liu, X., Chia, K. S. & Zhang, M. (2011). Water absorption , permeability , and resistance to chloride-ion penetration of lightweight aggregate concrete. *Construction and Building Materials*, *25*(1), 335–343.

Lucas, S. S., Moxham, C., Tziviloglou, E. & Jonkers, H. (2018). Study of self-healing properties in concrete with bacteria encapsulated in expanded clay. *Science and Technology of Materials*, *30*, 93–98.

Luo, Z., Li, W., Wang, K., Castel, A. & Shah, S. P. (2021). Comparison on the properties of ITZs in fly ash-based geopolymer and Portland cement concretes with equivalent flowability. *Cement and Concrete Research*, *143*(February), 106392.

M. De Rooij, K. Van Tittelboom, N. De Belie, E. S. (2013). *Self-Healing Phenomena in Cement-Based Materials*. Dordrecht, The Netherlands: Springer Netherlands.

Manikandan, R. & Ramamurthy, K. (2008). Effect of curing method on characteristics of cold bonded fly ash aggregates. *Cement and Concrete Composites*, *30*(9), 848–853.

Martínez-Rodríguez, A. J. & Polo, M. C. (2000). Characterization of the nitrogen compounds released during yeast autolysis in a model wine system. *Journal of Agricultural and Food Chemistry*, *48*(4), 1081–1085.

Mary Joseph, A., Snellings, R., Nielsen, P., Matthys, S. & De Belie, N. (2020). Pre-treatment and utilisation of municipal solid waste incineration bottom ashes towards a circular economy. *Construction and Building Materials*, *260*, 120485.

Mignon, A., Snoeck, D., D’Halluin, K., Balcaen, L., Vanhaecke, F., Dubruel, P., Van Vlierberghe, S. & De Belie, N. (2016). Alginate biopolymers: Counteracting the impact of superabsorbent polymers on mortar strength. *Construction and Building Materials*, *110*, 169–174.

Minnebo, P., Thierens, G., De Valck, G., Van Tittelboom, K., Belie, N. De, Van Hemelrijck, D. & Tsangouri, E. (2017). A novel design of autonomously healed concrete: Towards a vascular healing network. *Materials*, *10*(1), 1–23.

Mondal, S. & (Dey) Ghosh, A. (2019). Review on microbial induced calcite precipitation mechanisms leading to bacterial selection for microbial concrete. *Construction and Building Materials*, *225*, 67–75.

Muynck, W. De, Debrouwer, D., Belie, N. De & Verstraete, W. (2008). Cement and Concrete Research Bacterial carbonate precipitation improves the durability of cementitious materials, *38*, 1005–1014.

Muynck, W. De, Leuridan, S., Loo, D. Van, Verbeken, K., Cnudde, V., Belie, N. De & Verstraete, W. (2011). Influence of Pore Structure on the Effectiveness of a Biogenic Carbonate Surface Treatment for Limestone Conservation □, *77*(19), 6808–6820.

N. L. Thomas and J. D. Birchall. (1983). The Retarding Action Of Sugars On Cement Hydration. *Cement And Concrete Research*, *13*(c), 830–842.

Nath, S. K. & Kumar, S. (2019). Role of alkali concentration on reaction kinetics of fly ash geopolymerization, *505*(November 2018), 241–251.

Nonat, A. (2004). The structure and stoichiometry of C-S-H. *Cement and Concrete Research*, *34*(9), 1521–1528.

Nordmark, D. & Lagerkvist, A. (2018). Controlling the mobility of chromium and molybdenum in MSWI fly ash in a washing process. *Waste Management*, *76*, 727–733.

Oehmig, W. N., Roessler, J. G., Blaisi, N. I. & Townsend, T. G. (2015). ScienceDirect Contemporary practices and findings essential to the development of effective MSWI ash reuse policy in the United States. *Environmental Science and Policy*, *51*, 304–312.

Ogunbode, E. B. & Hassan, I. O. (2011). Effect of Addition of Calcium Nitrate on Selected Properties of Concrete Containing Volcanic Ash, (19), 29–38.

Park, S. S., Kwon, S. J. & Jung, S. H. (2012). Analysis technique for chloride penetration in cracked concrete using equivalent diffusion and permeation. *Construction and Building Materials*, *29*, 183–192.

Paudel, S. R., Yang, M. & Gao, Z. (2020). pH Level of Pore Solution in Alkali-Activated Fly-Ash Geopolymer Concrete and Its Effect on ASR of Aggregates with Different Silicate Contents. *Journal of Materials in Civil Engineering*, *32*(9), 04020257.

Paul, A., Murgadas, S., Delpiano, J., Moreno-Casas, P. A., Walczak, M. & Lopez, M. (2021). The role of moisture transport mechanisms on the performance of lightweight aggregates in internal curing. *Construction and Building Materials*, *268*(xxxx).

Pelisser, F., Gleize, P. J. P. & Mikowski, A. (2012). Effect of the Ca/Si molar ratio on the micro/nanomechanical properties of synthetic C-S-H measured by nanoindentation. *Journal of Physical Chemistry C*, *116*(32), 17219–17227.

Piña, R. G. & Cervantes, C. (1996). Microbial interactions with aluminium. *Biometals*, *9*(3), 311–316.

Qureshi, T. S., Kanellopoulos, A. & Al-Tabbaa, A. (2016). Encapsulation of expansive powder minerals within a concentric glass capsule system for self-healing concrete. *Construction and Building Materials*, *121*, 629–643.

Rattanasak, U. & Chindaprasirt, P. (2009). Influence of NaOH solution on the synthesis of fly ash geopolymer. *Minerals Engineering*, *22*(12), 1073–1078.

Rijkswaterstaat. (2007). *Soil Quality Regulation*.

Risdanareni, P., Ekaputri, J. J. & Triwulan. (2015). *The influence of alkali activator concentration to mechanical properties of geopolymer concrete with trass as a filler*. *Materials Science Forum* (Vol. 803).

Risdanareni, Puput, Schollbach, K., Wang, J. & Belie, N. De. (2020). The effect of NaOH concentration on the mechanical and physical properties of alkali activated fly ash-based artificial lightweight aggregate. *Construction and Building Materials*, *259*, 119832.

Risdanareni, Puput, Wang, J. & De Belie, N. (2021). Expanded Clay as Bacteria Cells Protector in Manufac-turing Self-Healing Mortar: the Possibility of Adding Less Nutrient to Maintain the Mechanical Properties of Mor-tar. In *75th Rilem Week Conference*. Merida, Mexico.

Salman, M., Cizer, Ö., Pontikes, Y., Vandewalle, L., Blanpain, B. & Van Balen,

K. (2014). Effect of curing temperatures on the alkali activation of crystalline continuous casting stainless steel slag. *Computers and Chemical Engineering*.

Samonin, V. V. & Elikova, E. E. (2004). A study of the adsorption of bacterial cells on porous materials. *Microbiology*, *73*(6), 696–701.

Santos, R. M., Mertens, G., Salman, M., Cizer, Ö. & Gerven, T. Van. (2013). Comparative study of ageing , heat treatment and accelerated carbonation for stabilization of municipal solid waste incineration bottom ash in view of reducing regulated heavy metal / metalloid leaching. *Journal of Environmental Management*, *128*, 807–821.

Setlow, P. (2013). Summer meeting 2013 - when the sleepers wake: The germination of spores of Bacillus species. *Journal of Applied Microbiology*, *115*(6), 1251–1268.

Shaaban Mwaiuwinga, T. A. and K. S. (1997). Influence Of Urea In Concrete. *Cement and Concrete Research*, *14*(1), 121~128.

Shang, Xiao yu & Li, J. shan. (2020). Manufacturing and performance of environment-friendly lightweight aggregates with core-shell structure. *Journal of Cleaner Production*, *276*, 123157.

Shang, Xiaoyu, Li, J. & Zhan, B. (2020). Properties of sustainable cellular concrete prepared with environment-friendly capsule aggregates. *Journal of Cleaner Production*, *267*, 122018.

Shivaprasad, K. N. & Das, B. B. (2018). Determination of optimized geopolymerization factors on the properties of pelletized fly ash aggregates. *Construction and Building Materials*, *163*, 428–437.

Shon, C. S., Jung, Y. S., Saylak, D. & Mishra, S. K. (2013). Development of synthetic aggregate using off-ASTM specification ashes. *Construction and Building Materials*, *38*, 700–707.

Shukla, S., Park, J. H. & Kim, M. (2020). Efficient, safe, renewable, and industrially feasible strategy employing Bacillus subtilis with alginate bead composite for the reduction of ochratoxin A from wine. *Journal of Cleaner Production*, *242*, 118344.

Silva, A., Vargas, D., Dal, D. C. C., Vilela, A. C. F., José, F., Pavão, B. & Veit, H. (2011). Cement & Concrete Composites The effects of Na 2 O / SiO 2 molar ratio , curing temperature and age on compressive strength , morphology and microstructure of alkali-activated fly ash-based geopolymers. *Cement and Concrete Composites*, *33*(6), 653–660.

Snoeck, D., Velasco, L. F., Mignon, A., Vlierberghe, S. Van, Dubruel, P., Lodewyckx, P. & Belie, N. De. (2014). Cement and Concrete Research The in fl uence of different drying techniques on the water sorption properties of cement-based materials. *Cement and Concrete Research*, *64*, 54–62.

Sun, Z. & Vollpracht, A. (2018). Cement and Concrete Research Isothermal calorimetry and in-situ XRD study of the NaOH activated fl y ash , metakaolin and slag. *Cement and Concrete Research*, *103*(September 2017), 110–122.

Tajuelo Rodriguez, E., Garbev, K., Merz, D., Black, L. & Richardson, I. G. (2017). Thermal stability of C-S-H phases and applicability of Richardson and Groves' and Richardson C-(A)-S-H(I) models to synthetic C-S-H. *Cement and Concrete Research*, *93*, 45–56.

Tang, P. & Brouwers, H. J. H. (2017). Integral recycling of municipal solid waste incineration (MSWI) bottom ash fines (0 – 2 mm) and industrial powder wastes by cold-bonding pelletization. *Waste Management*, *62*, 125–138.

Tang, P., Florea, M. V. A. & Brouwers, H. J. H. (2017). Employing cold bonded pelletization to produce lightweight aggregates from incineration fine bottom ash. *Journal of Cleaner Production*, *165*, 1371–1384.

Taylor, H. F. W. (1993). Nanostructure of CSH: Current status. *Advanced Cement Based Materials*, *1*(1), 38–46.

Thijssen, A., Muyzer, G., Copuroglu, O. & Schlangen, E. (2010). Application of bacteria as self-healing agent for the development of sustainable concrete. *Ecological Engineering*, *36*(2), 230–235.

Thomas, J. & Harilal, B. (2015). Cement & Concrete Composites Properties of cold bonded quarry dust coarse aggregates and its use in concrete. *CEMENT AND CONCRETE COMPOSITES*, *62*, 67–75.

Triwulan, T. & Ekaputri, J. J. (2015). Sidoarjo Mud-Based Lightweight Mortar Using Foaming Agent and Aluminum, (April).

Tziviloglou, E. (2018). *BIOGENIC SELF-HEALING MORTAR*. TU Delft.

Van Belleghem, B., Montoya, R., Dewanckele, J., Van Den Steen, N., De Graeve, I., Deconinck, J., Cnudde, V., Van Tittelboom, K. & De Belie,

N. (2016). Capillary water absorption in cracked and uncracked mortar - A comparison between experimental study and finite element analysis. *Construction and Building Materials*, *110*, 154–162.

Van den Heede, P., Ringoot, N., Beirnaert, A., Van Brecht, A., Van den Brande, E., De Schutter, G. & De Belie, N. (2016). Sustainable high quality recycling of aggregates from waste-to-energy, treated in awet bottom ash processing installation, for use in concrete products. *Materials*, *9*(1), 1–24.

Van Mullem, T., Gruyaert, E., Debbaut, B., Caspeele, R. & De Belie, N. (2019). Novel active crack width control technique to reduce the variation on water permeability results for self-healing concrete. *Construction and Building Materials*, *203*, 541–551.

Vandeputte, N. (2018). *Sustainable high quality recycling of bottom ashes from waste-to-energy for use in cement-bound materials*. Ghent University, Belgium.

Vandervoort, M. (2019). *Impact of bioagents on the cementitious matrix*. Ghent University.

Villagrán Zaccardi, Y. A., Alderete, N. M. & De Belie, N. (2017). Improved model for capillary absorption in cementitious materials: Progress over the fourth root of time. *Cement and Concrete Research*, *100*(March), 153–165.

Wang, J., Boon, N. & De Belie, N. (n.d.). Paper ICACTS Jianyun Wang final 20180508. In *recent advance in concrete technology*. Beijing: American Concrete Institute.

Wang, J., Jonkers, H. M., Boon, N. & Belie, N. De. (2017). Bacillus sphaericus LMG 22257 is physiologically suitable for self-healing concrete, 5101–5114.

Wang, J., Mignon, A., Trenson, G., Vlierberghe, S. Van, Boon, N. & Belie, N. De. (2018). A chitosan based pH-responsive hydrogel for encapsulation of bacteria for self-sealing concrete. *Cement and Concrete Composites*, *93*(August), 309–322.

Wang, J., Van Tittelboom, K., De Belie, N. & Verstraete, W. (2012). Use of silica gel or polyurethane immobilized bacteria for self-healing concrete. *Construction and Building Materials*, *26*(1), 532–540.

Wang, J., Vandevyvere, B., Vanhessche, S., Schoon, J., Boon, N. & De Belie,

N. (2017). Microbial carbonate precipitation for the improvement of quality of recycled aggregates. *Journal of Cleaner Production*, *156*, 355–366.

Wang, J. Y., De Belie, N. & Verstraete, W. (2012a). Diatomaceous earth as a protective vehicle for bacteria applied for self-healing concrete. *Journal of Industrial Microbiology and Biotechnology*, *39*(4), 567–577.

Wang, J. Y., De Belie, N. & Verstraete, W. (2012b). Diatomaceous earth as a protective vehicle for bacteria applied for self-healing concrete. *Journal of Industrial Microbiology and Biotechnology*, *39*(4), 567–577.

Wang, J. Y., Snoeck, D., Van Vlierberghe, S., Verstraete, W. & De Belie, N. (2014). Application of hydrogel encapsulated carbonate precipitating bacteria for approaching a realistic self-healing in concrete. *Construction and Building Materials*, *68*, 110–119.

Wang, J. Y., Soens, H., Verstraete, W. & Belie, N. De. (2014). Cement and Concrete Research Self-healing concrete by use of microencapsulated bacterial spores. *Cement and Concrete Research*, *56*, 139–152.

Washburn, E. W. (1921). The Dynamics of Capillary Flow. *The Physical Review*, *XVII*(3), 273–283.

White, S. R., Sottos, N. R., Geubelle, P. H., Moore, J. S., Kessler, M. R., Sriram, S. R., Brown, E. N. & Viswanathan, S. (2001). Autonomic healing of polymer composites. *Nature*, *409*(6822), 794–797.

Wiktor, V. & Jonkers, H. M. (2011). Quantification of crack-healing in novel bacteria-based self-healing concrete. *Cement and Concrete Composites*, *33*(7), 763–770.

Wongsa, A., Boonserm, K., Waisurasingha, C., Sata, V. & Chindaprasirt, P. (2017). Use of municipal solid waste incinerator (MSWI) bottom ash in high calcium fl y ash geopolymer matrix. *Journal of Cleaner Production*, *148*, 49–59.

Wu, M., Hu, X., Zhang, Q., Cheng, W., Xue, D. & Zhao, Y. (2020). Application of bacterial spores coated by a green inorganic cementitious material for the self-healing of concrete cracks. *Cement and Concrete Composites*, *113*(579), 103718.

Xu, H. & Deventer, J. S. J. Van. (2000). The geopolymerisation of alumino-silicate minerals.

Xu, J., Tang, Y., Wang, X., Wang, Z. & Yao, W. (2020). Application of ureolysis-based microbial CaCO3 precipitation in self-healing of concrete and inhibition of reinforcement corrosion. *Construction and Building Materials, 265*, 120364.

Zhang, J., Liu, Y., Feng, T., Zhou, M., Zhao, L., Zhou, A. & Li, Z. (2017). Immobilizing bacteria in expanded perlite for the crack self-healing in concrete. *Construction and Building Materials, 148,* 610–617.

Zhang, L., Zhang, Y., Liu, C., Liu, L. & Tang, K. (2017). Study on microstructure and bond strength of interfacial transition zone between cement paste and high-performance lightweight aggregates prepared from ferrochromium slag. *Construction and Building Materials, 142*, 31–41.

Zhang, Y., Guo, H. X. & Cheng, X. H. (2015). Role of calcium sources in the strength and microstructure of microbial mortar. *Construction and Building Materials*, *77*, 160–167.

Curriculum Vitae

Puput Risdanareni was born in Malang 1st February 1986. She holds a master degree in Civil Engineering obtained in 2009 from *Sepuluh Nopember* Institute of Technology (ITS), Surabaya, Indonesia. She started working on her PhD in Civil Engineering at Ghent University in September 2017. During her PhD, she performed experiments at the Magnel-Vandepitte Laboratory for Structural Engineering and Building Material and Center for Microbial Ecology and Technology (CMET) to investigate the feasibility of utilizing alkali activated lightweight aggregates as a bacterial protector in the production of self-healing concrete. As an output of her research, three papers were successfully published in reputable scientific journals. During her PhD, she guided one master student investigating the effect of bio-agent on the properties of self-healing concrete. She also assisted in the Life Cycle Assessment of Materials and Structures course.

Personal Information

Name	Puput Risdanareni
Date of birth	February 1st 1986
Place of birth	Malang, East Java, Indonesia
Nationality	Indonesian
Contact	puput.risdanareni@ugent.be puput.risdanareni.ft@um.ac.id

Education

2017 – 2021	Doctorate (PhD) in Civil Engineering Faculty of Engineering and Architecture at Ghent University

Thesis:
Alkali Activated Lightweight Aggregate as Bacterial
2003 – 2007 Protector in Manufacturing Self-Healing Concrete

Bachelor in Civil Engineering
Sepuluh Nopember Institute of Technology ,
Surabaya, Indonesia

Final Project:
Mechanical Characteristic of Fly ash-based Geopolymer Concrete and Trass as Filler with Sodium Hydroxide Solution of 8 and 10 Molar as
2007 – 2009 Activator

Master in Civil Engineering (Structure)
Sepuluh Nopember Institute of Technology ,
Surabaya, Indonesia

Thesis:
Influence of Concrete Stress-Strain Relationship Variation and Building Span to the Three Dimensional Frame Structure Performance with Nonlinear Pushover Method

Work Experience

2009-2010 Structure Engineer at PT. Stadin Strukturindo, Consultant
Jakarta, Indonesia

2010-2013 Structure Engineer at PT. Hutama Karya, General Contractor
Jakarta, Indonesia

2013-present Junior Lecturer
Department of Civil Engineering, State University of Malang
Malang, Indonesia

Scientific publications

A1 publications

Risdanareni, P., Van Den Heede, P., Wang, J. and De Belie, N (2021). The Durability of Mortar Containing Alkali Activated Fly Ash-Based Lightweight Aggregate. *Materials*, *14*, 3741.

Risdanareni, P., Schollbach, K., Wang, J. and De Belie, N. (2020). The effect of NaOH concentration on the mechanical and physical properties of alkali activated fly ash-based artificial lightweight aggregate. *Construction and Building Materials*, *259*, 119832.

Risdanareni, P., Villagran, Y., Schollbach, K., Wang, J. and De Belie, N. (2020). Properties of alkali activated lightweight aggregate generated from Sidoarjo Volcanic Mud (Lusi), fly ash, and municipal solid waste incineration bottom ash. *Materials, 13*, 2528.

Book Chapter

Villagran Zaccardi, Y., Alderete, N. M., Pico-Cortés, C., Zega, C., Risdanareni, P., and De Belie, N. (2021). Effect of wastes as supplementary cementitious materials on the transport properties of concrete. In J. de Brito, C. Thomas, C. Medina, and F. Agrela (Eds.), *Waste and Byproducts in Cement-Based Materials: Innovative Sustainable Materials for a Circular Economy, Woodhead Publishing Series in Civil and Structural Engineering,* ISBN 978-0-12-820549-5, 2021, pp. 191-227. DOI: 10.1016/C2019-0-01771-2

Publications in Conferences

Risdanareni, P., Wang, J., and De Belie, N. (2019). Optimization of bacteria encapsulation in artificial lightweight aggregate for self-healing concrete. In *7th International Conference on Self-Healing Materials (ICSHM 2019), Abstracts* (pp. 1–1). Yokohama, Japan, 3-5 June 2019.

Risdanareni, P., Schollbach, K., Wang, J., and De Belie, N. (2019). The effect of NaOH concentration on the mechanical and physical properties of alkali activated fly ash-based artificial lightweight aggregate. In V. Caprai and J. Brouwers (Eds.), *Proceedings ICSBM 2019 Volume 3 - Greened materials* (pp. 96–105). Eindhoven, The Netherlands, 12-15August 2019.

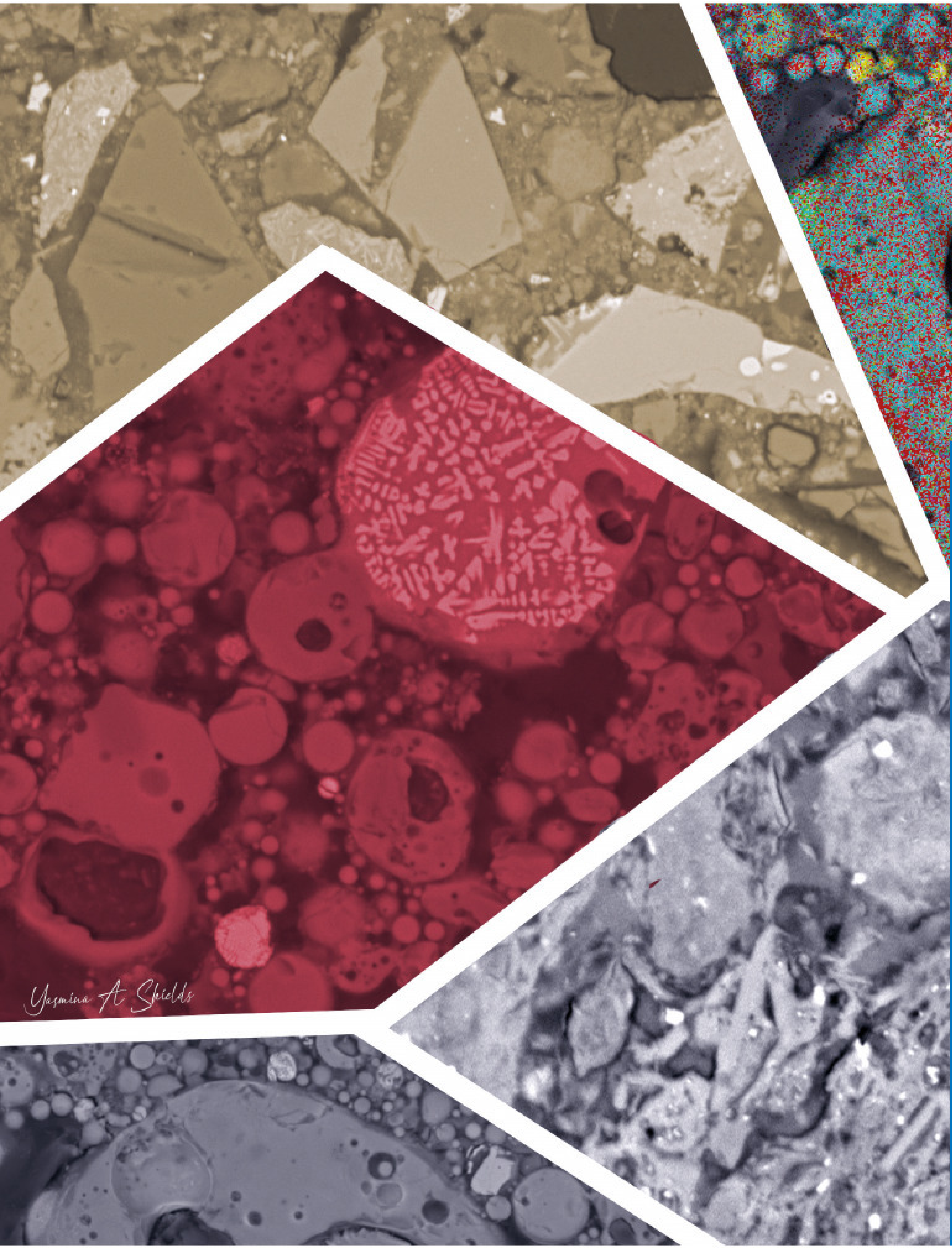

Scanning Electron Microscope Pictures of Alkali Activated Lightweight Aggregate.